METALLURGICAL ENGINEERING DEPARTMENT

QUEEN'S UNIVERSITY

KINGSTON – ONTARIO – CANADA

91-04710/

THE PLASMA PRODUCTION OF TITANIUM SILICIDES AND TITANIUM-IRON-SILICIDES

FINAL REPORT TO THE

DEPARTMENT OF SUPPLIES AND SERVICES

ON

THE PLASMA PRODUCTION OF TITANIUM SILICIDES AND TITANIUM-IRON-SILICIDES

by

C.A. Pickles
Department of Metallurgical Engineering
Queen's University
Kingston, Ontario

and

J.M. Toguri
Department of Metallurgy and Materials Science
University of Toronto
Toronto, Ontario

Contract No. 23440-7-9196/01-SS
Re: DSS File No. 55SS.23440-7-9196

MICROMEDIA

187 pp

CONTRACT SERIAL NO. 79196-01-SS
CONTRACT REQUISITION NO. 23440-7-9196
CONTRACTOR: QUEEN'S UNIVERSITY

SUMMARY

In this research the production of titanium silicide and its oxidation resistance were studied. Metallothermic and carbothermic reduction methods were investigated for the recovery of titanium and silicon. The experiments were performed in a plasma furnace. The oxidation resistance was measured by thermogravimetry and the nature of the oxide was determined by x-ray methods. In addition, growth of titanium silicide in a copper melt was studied and its subsequent extraction by leaching techniques is reported.

TABLE OF CONTENTS

Page

1. Phase Diagram Determinations 4
    - a) Fe-Ti.. 4
    - b) Ti-Si.. 30

2. Metallothermic Reduction 37
    - a) Aluminothermic................................... 49
    - b) Magnesiothermic Reduction 62
    - c) Calciothermic Reduction 76

3. Recovery of Titanium Silicide from a Copper Melt.... 83

4. Carbothermic Reduction 105

5. Comparison of Reducing Agents 108

6. Oxidation Studies 109

7. Rapid Melting and Solidification of Titanium Silicides 146

8. Research Summary 146

9. Conclusions 147

10. Personnel 150

11. Appendix - Publications Resulting from this Work ... 151

COMPUTER CALCULATION OF THE TI-FE PHASE DIAGRAM USING THE F*A*C*T FACILITY

ABSTRACT

The phase diagram of the binary system Ti-Fe was computer calculated using the F*A*C*T facility and compared to previous experimental and theoretical results. Preliminary analysis yielded a topographically correct diagram. The predicted Ti-rich eutectic of 1085°C, Fe-rich eutectic of 1275°C, peritectic of 1325°C, and congruent melting point of 1425°C agree well with previous experimental data. The relatively high predicted eutectoid temperature of 655°C, low eutectoid composition, and the absence of the γ-Fe phase are explained with the aid of free energy curves produced using the GIBBSPLOT package. Suitable corrections to system parameters are proposed, and further investigations in the thermodynamic study of the Ti-Fe system are outlined.

1. INTRODUCTION

In recent years the prediction of binary and ternary phase diagrams has been made more energy- and time-efficient by the development of computer modelling. Computer-generated binary systems can often be made very accurate and can be combined with other binary system models to generate ternary phase diagrams that are difficult to study experimentally. The computer generated models can be used either to confirm the accuracy of previously reported phase diagrams or to provide new information. In this work, the F*A*C*T (Facility for the Analysis of Chemical Thermodynamics) system is used to develop an accurate model of the Ti-Fe binary system. This binary system model will later be combined with those of Fe-Si and Ti-Si in order to model the Fe-Si-Ti ternary system, for which data are presently limited.

2. EXPERIMENTAL INVESTIGATIONS

The equilibrium phases of the Ti-Fe system (see Figure 1) are: 1) the liquid; 2) the hexagonal close-packed (hcp) solid solution (α-Ti), which exists below 882°C; 3) the body-centered cubic (bcc) solid solution, which is the equilibrium phase of β-Ti above 882°C and of α-Fe below 911°C and above 1392°C; 4) the face-centered cubic (fcc) solid solution (γ-Fe), which is the equilibrium phase of Fe between 911°C and 1392°C; 5) the compound FeTi, with the CsCl structure; and 6) the compound Fe_2Ti, the $MgZn_2$-type Laves phase. Although $FeTi_2$ was reported as an existing phase in this system[2], it has since been confirmed [3] that this phase does not in fact exist.

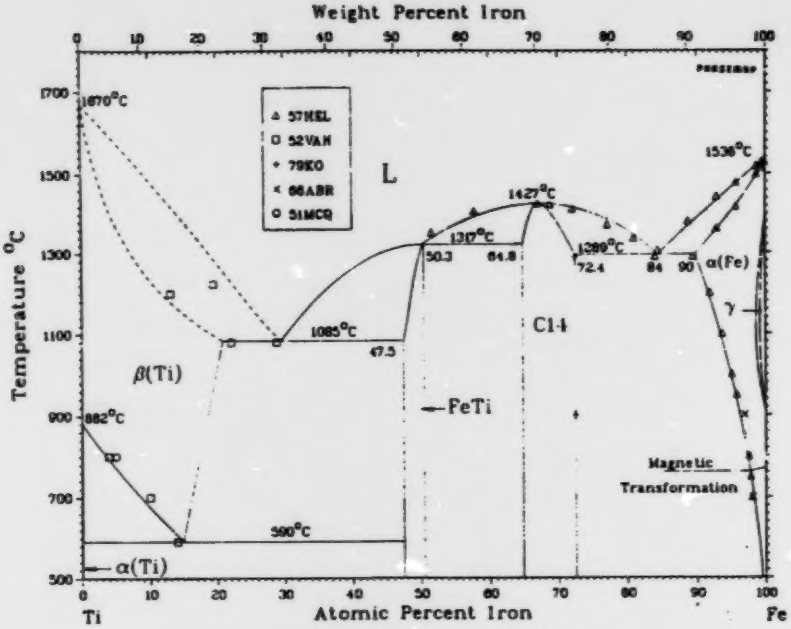

Fig. 1: Ti-Fe Phase Diagram[1]

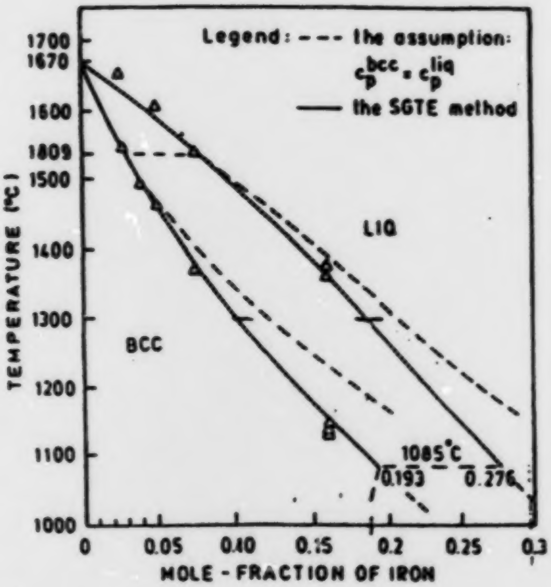

Fig. 2: The experimental solubility points and the calculated solidus and liquidus boundaries with and without the assumption of equal heat capacities of the bcc and liquid titanium[4]

2.1 Ti-Rich Solidus, Liquidus, and $\beta/(\beta+TiFe)$ Boundary

The eutectic temperature is taken as 1085°C (± 5°C), after Murray [1]. Although Murray claims solidus and liquidus compositions at 1085°C of 21 and 29.5 at % Fe, respectively, her evaluation was admittedly based on data gathered in tests using Ti of questionable purity, and her results were later shown to be inconsistent with more recent data [4] obtained with ultra-pure Ti (see Figure 2). It is now believed that the solidus and liquidus compositons at 1085°C are 19.3 and 27.6 at % Fe, respectively.

The $\beta/(\beta+TiFe)$ boundary, if drawn as a straight line between the eutectoid point at 590°C and maximum solubility at the eutectic temperature of 1085°C, is consistent with reported experimental data [1].

2.2 $\beta/(\beta+\alpha\text{-Ti})$ Boundary

According to Murray's calculations, based on several experimental investigations, the eutectoid composition is about 15-16 at.% Fe at a temperature of 590-600°C. Although the boundary does not vary strongly with values of the interaction parameters, the eutectoid temperature is dependent on the thermodynamic parameters of the FeTi phase and the α-Ti/β-Ti equilibrium.

2.3 Solubility of Fe in α-Ti

The maximum solubility of Fe in α-Ti has been reported as low as 0.04 at.% Fe and as high as 0.5 at.% Fe. Since a thermodynamic calculation [1] revealed a low solubility of only 0.045 at.% Fe in α-Ti at 700°C, this solubility was not included in present modelling of the Ti-Fe phase diagram.

2.4 The Compound TiFe

The compound TiFe, with the ordered CsCl structure, is considered to exist between 48 and 50 at.% Fe near the eutectic temperature of 1085°C. In the present evaluation it was considered to exist only as a line compound of equimolar composition. This phase forms from the liquid at 1317°C in the peritectic reaction $L + Fe_2Ti \dashrightarrow FeTi$ [1].

2.5 $TiFe_2$ Laves Compound

The compound $TiFe_2$, the Laves phase of the hexagonal $MgZn_2$ type, is considered to exist between 65 and 73 at.% Fe. The exact determination of phase boundaries of $TiFe_2$ is very difficult due to the strong reactivity of alloys near this composition. For the present evaluation this compound was assumed to be stoichiometric.

2.6 Fe-Rich Liquidus/Solidus and the Solubility of Ti in α-Fe

It is commonly accepted that the melting point of pure iron is 1536°C. Because iron is thermodynamically one of the most investigated metals [5], the position of the Fe-rich liquidus/solidus is fairly well established. The eutectic temperature and composition are 1289°C and 84 at.% Fe, respectively. The maximum solubility of Ti in α-Fe (bcc solid solution) is 10 at.% Ti at the eutectic temperature.

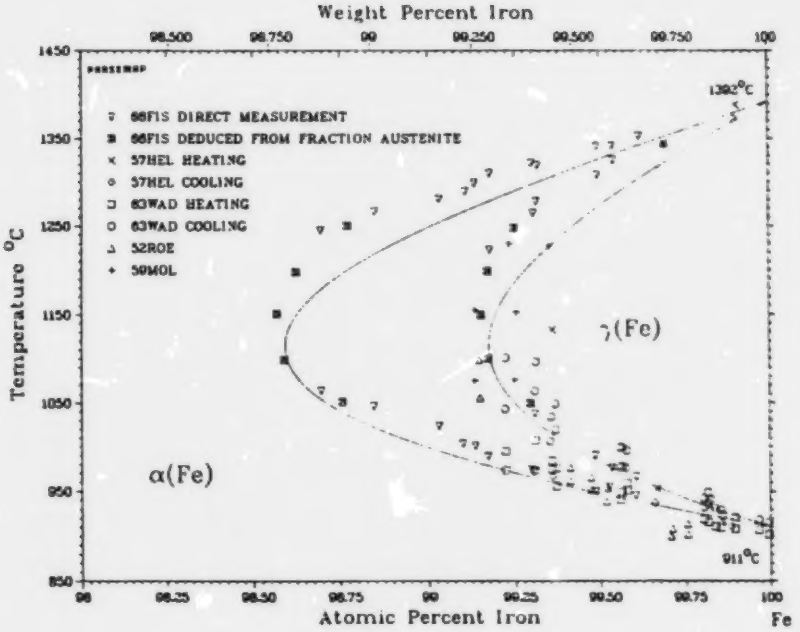

Fig. 3: Comparison of experimental data on the γ-loop to the phase boundaries of the Ti-Fe system as calculated by Murray[1]

2.7 Solubility of Ti in γ-Fe

As seen in Figure 3, the boundaries of the α-Fe and γ-Fe (fcc) phases take the form of a closed γ-loop. The maximum solubility of Ti in γ-Fe is 0.8 at.% at about 1100-1150°C, at which temperature the (α-Fe + γ-Fe) two-phase region reaches its maximum width of 0.6 at.%. The γ-Fe phase exists between 911 and 1392°C.

3. THERMODYNAMICS OF PAST AND PRESENT INVESTIGATIONS

The phase diagram generated by the present preliminary investigation using the F*A*C*T system for thermochemical analysis is presented in Figure 4. The method of analysis and the observed deviations from previous reports on Ti-Fe phase equilibria will be discussed in the following sections.

3.1 Calculation of the Phase Diagram using the F*A*C*T System

Figure 5 shows a hypothetical free energy curve for a binary system composed of the elements A and B generated by the GIBBSPLOT free energy plotting package. Three phases are present in this system: Beta (β), liquid (L), and the compound AB_2 denoted Gamma (γ). For this system, the liquid phase has been chosen as the reference phase. Thus, the free energy of pure A_L

and pure B_L is arbitrarily chosen to be zero (i.e. $G_A^{oL} = 0$, $G_B^{oL} = 0$). It can be seen that the β-phase, then, has free energies of $G_A^{o\beta} = -13{,}000$ J/mol and $G_B^{o\beta} = -5{,}000$ J/mol. These parameters are known as the "lattice stability parameters" of A and B, since

$$\Delta G_A^{oL\rightarrow\beta} = G_A^{o\beta} - G_A^{oL} = 13{,}000 \text{ J/mol}$$

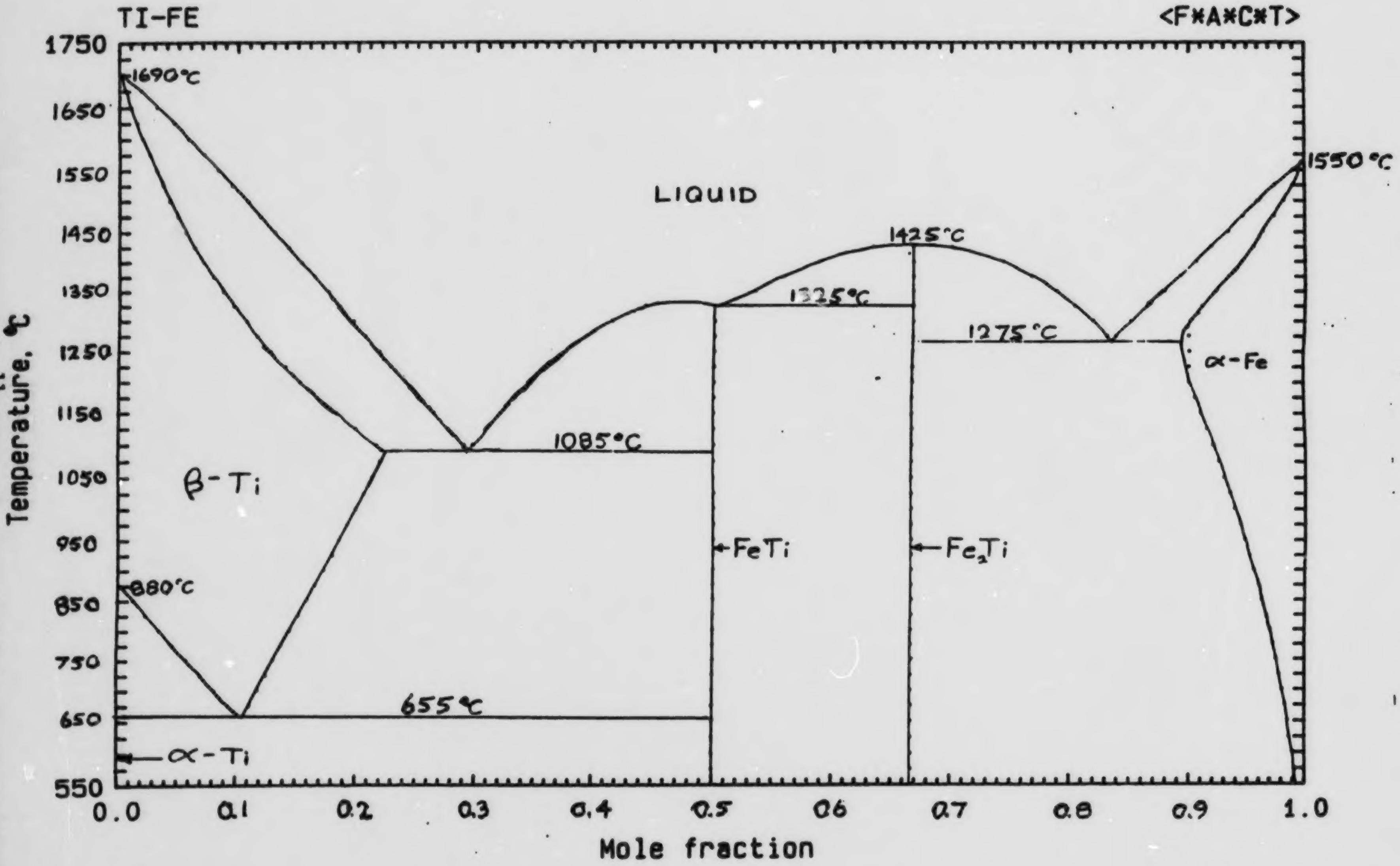

FIGURE 4: Computer Calculated Fe-Ti Phase Diagram

and $\Delta G_B^{oL\rightarrow\beta} = -5,000$ J/mol

The compound γ also has the liquid as the reference state. The lattice stability parameters are given as a function of temperature, since

$$\Delta G^o_{fusion} = \Delta H^o_{fusion} - T^o_F \Delta S^o_{fusion} \qquad (1)$$

where T^o_F is the temperature of phase transition (temperature of fusion). The above variables are defined by

$$\Delta H^o_F = \Delta H^o_F \text{ (at } T^o_F) + \int_{T^o_F}^{T} \Delta c_p dT \qquad (2)$$

$$\Delta S^o_F = \Delta S^o_F \text{ (at } T^o_F) + \int_{T^o_F}^{T} (\Delta c_p)/T\ dT \qquad (3)$$

$$\text{where } \Delta S^o_F \text{ (at } T^o_F) = \Delta H^o_F \text{ (at } T^o_F)/T^o_F$$

and Δc_p = difference in heat capacities between the two phases.

Heat capacities are usually a function of temperature. However, the heat capacities of the two phases are often taken to be the same. Equation 1 then describes the endpoints of the curves on the free energy diagram.

The ideal free energy of solution mixing of components A and B (ΔG_{ideal}, see Figure 5) is given by

$$\Delta G_{ideal} = X_A RT\ln X_A + X_B RT\ln X_B \qquad (4)$$

The total free energy change, however, is given by

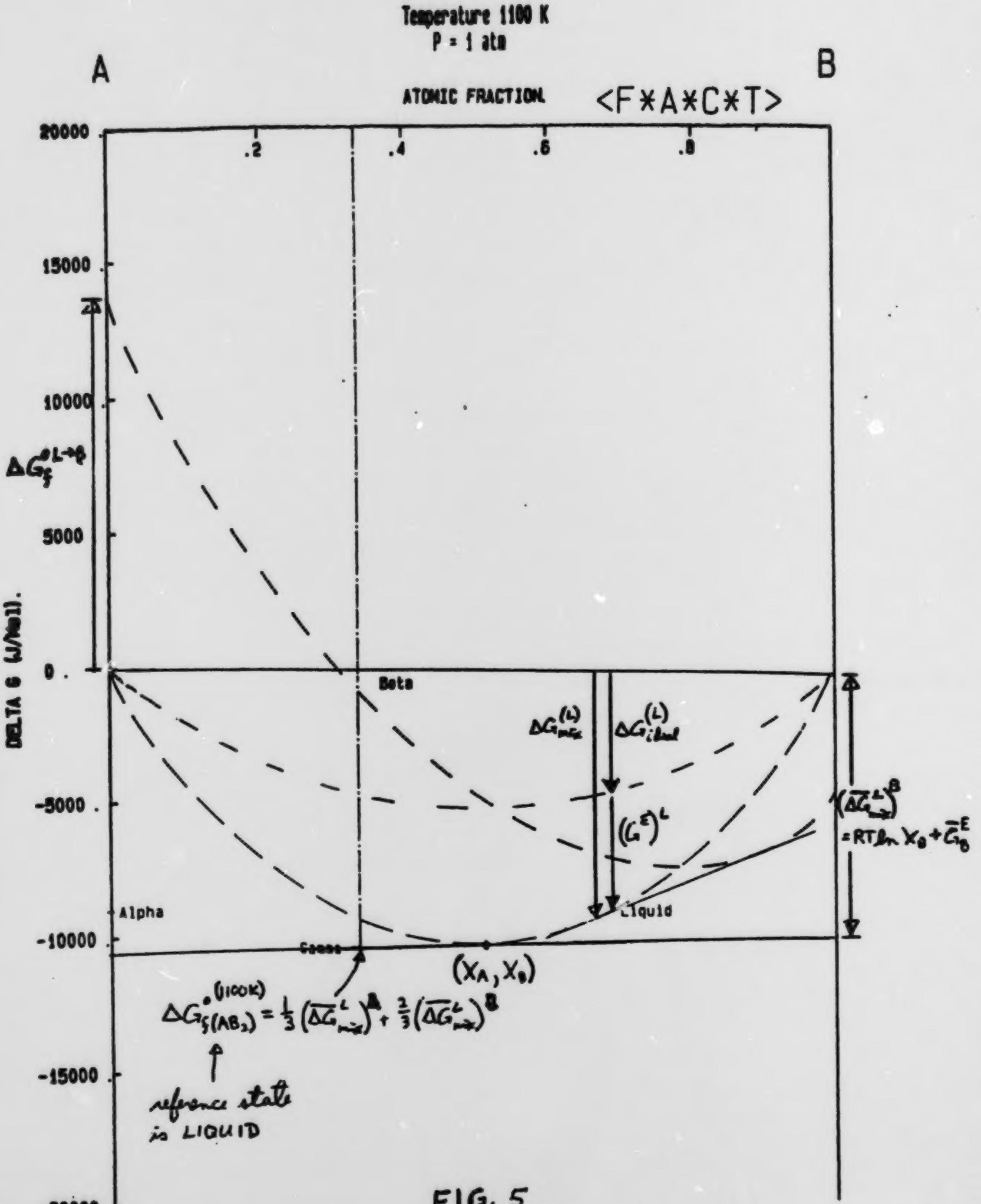

FIG. 5

GIBBSPLOT

Temperature 1100 K

$$\Delta G_{mix} = \Delta G_{ideal} + G^E \tag{5}$$

where G^E is the excess free energy. As seen in Figure 5, ΔG_{mix} describes the departure from the line joining the lattice stability of A and B for each phase. The integral excess free energy, G^E, is represented by the power series

$$G^E = X_A X_B \; (b_o + (b_1/2)X_B + (b_2/3)X_B^2 + \ldots + (b_n/(n+1))X_B^n \tag{6}$$

$$= \Delta H_{mix} - TS^E$$

where the constants, known as "interaction parameters" of the solution phase, are empirically determined and describe the extent of mixing of A and B. Note that a line drawn tangent to a curve at a point corresponding to ΔG_{mix} (X_A, X_B) intersects the A and B axis at a point whose distance from the endpoints of the free energy curve is the partial free energy of that component:

$$\Delta\bar{G}_i = RT\ln(a_i) \tag{7}$$

$$\Delta\bar{G}_i = RT\ln X_i + RT\ln\gamma_i \tag{8}$$

$$\Delta\bar{G}_i = RT\ln X_i + \bar{G}_i^E \tag{9}$$

The integral excess free energy, G^E, is related to the partial excess free energies by

$$G^E = X_A\bar{G}_A^E + X_B\bar{G}_B^E \tag{10}$$

The phase or combination of phases which provides the lowest integral free energy (ΔG_{mix}) for (X_A, X_B) at any given temperature is the equilibrium phase of the phase diagram at that temperature and composition. Thus, for example, with reference to Figure 5, at 1100K the A-B phase diagram would contain a (γ + liquid) phase between 30 and 50 at.%B. Between 60 and 90 at.% B, the most stable phase is a (liquid + β) mixture, and above 90 at.% B only the β-phase is stable. This, then, is how the phase diagram is constructed given the lattice parameters of the phases and the interaction parameters of the solutions. It can also be seen from Figure 5 how the free energy of fusion might be calculated for a given compound found in a phase diagram.

When modelling a phase diagram, it is usually best to first define the lattice stability parameters for the pure components, since the transformation temperatures (e.g. melting point of the pure solid) are usually very well known. Lattice stabilities for unusual phases of the components (eg Ti as fcc) are typically adjusted to represent solubilities, just like interaction parameters. Once these are set, the interaction parameter and free energies of fusion of compounds can be adjusted to provide adequate eutectoid, eutectic and peritectic temperatures and compositions.

3.2 Modelling the Ti-Fe System

Modelling of the Ti-Fe system has been performed previously by Murray and by Kaufman [6]. Kaufman used computer modelling, and the generated phase diagram can be found in Figure 6. Values of lattice parameters (with bcc solid as a reference state) can be found, as presented in the authors' respective papers, in Table 1. Upon evaluation of the parameters of Murray, it was immediately discovered that errors existed. The transformation temperature of Fe (bcc ---→ liquid) is predicted to be 1244°C, which is far

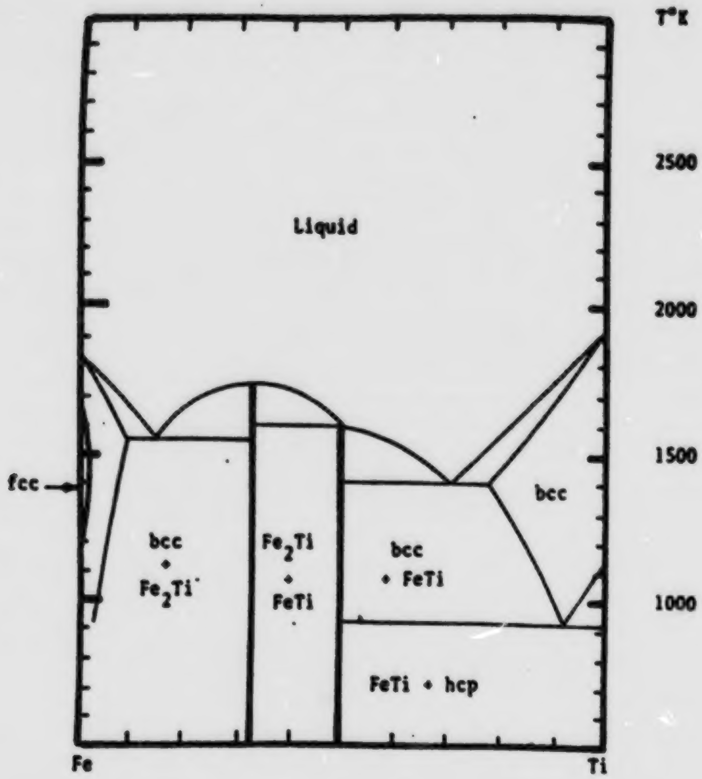
T°K
2500
2000
1500
1000
Liquid
fcc
bcc + Fe$_2$Ti
Fe$_2$Ti + FeTi
bcc + FeTi
bcc
FeTi + hcp
Fe
Ti

Fig. 6: Computer-generated Ti-Fe phase diagram of Kaufman(4)

TABLE 1 -- LATTICE STABILITIES (J/mol, T in K)

	Murray (1981)	Kaufman (1979)
$\Delta G_{Ti}^{bcc\to liq.}$	$16234 - 8.368T$	$16234 - 8.368T$
$\Delta G_{Fe}^{bcc\to liq.}$	$14644 - 9.653T$	$13807 - 7.632T$
$\Delta G_{Ti}^{bcc\to cph}$	$-4351 + 3.766T$	$-4351 + 3.7656T$
$\Delta G_{Fe}^{bcc\to cph}$	$-4280 + 1.224T +$ $7.472E\text{-}3T^2 + 5.124E\text{-}6T^3$	$4280 + 1.224T -$ $7.472E\text{-}3T^2 + 5.1254E\text{-}6T^3$
$\Delta G_{Ti}^{bcc\to fcc}$	$1004 - 3.766T$	$-1004 + 3.766T$
$\Delta G_{Fe}^{bcc\to fcc}$	$5245 - 9.441T +$ $5.295E\text{-}3T^2 + 9.222E\text{-}6T^3$	$5235 - 9.4T +$ $5.295E\text{-}3T^2 - 9.221E\text{-}7T^3$

below the accepted value of 1536°C (correctly predicted by Kaufman's parameters). Other errors were later discovered in the values of Murray's lattice stability parameters, but these will be discussed in a future section. Unfortunately, most of the lattice stability parameters of Murray (with a bcc solid reference state) were initially assumed to be correct, and were used in the preliminary model used for F*A*C*T generation of the phase diagram. However, as mentioned earlier, Kivilahti and Tarasova presented lattice stability parameters for the Ti (bcc ---→ liquid) transformation based on different solid and liquid heat capacities that provided a more accurate Ti-rich liquidus and solidus,

$$\Delta G_{Ti}^{bcc-liq.} = 2348 + 43.097T + 1.55E\text{-}4T^2 - 5.874T\ln T - 2.396E\text{-}21T^7$$

so these parameters were used in favor of those of Murray and Kaufman. The parameters for the Fe (bcc ---→ liquid) transformation proposed by Gustafson [5].

$$\Delta G_{Fe}^{bcc\rightarrow liq.} = 12040 - 6.558T - 3.675E\text{-}21T^7$$

were used in Kivilahti and Tarasova's development of the above equation, so they were also used in favor of those of Murray and Kaufman. When these equations were used, the Ti-rich solidus/liquidus followed the recent experimental data much more closely.

The free energies of fusion for the compounds TiFe and $TiFe_2$ as presented by Murray and Kaufman can be found in Table 2. To remain consistent with the bcc reference state, the parameters of Kaufman were used for TiFe, while those of Murray were used for $TiFe_2$.

The interaction parameters used by Kaufman (see Table 3) were also used in the present model. Note that because all solutions are regular, excess entropy is zero for all solutions, so that the heat of mixing can be used to represent the excess integral free energy of the phases.

TABLE 2 FREE ENERGY OF FUSION FOR COMPOUNDS

	Murray (1981)	Kaufman (1979)
TiFe	-22525 + 8.675T -13800 - 4.6T (L.T.)	-2-292 + 0.188T
$TiFe_2$	-32150 + 70T	-6874 + 3.53T (hcp)

TABLE 3 SOLUTION INTERACTION PARAMETERS (Kaufman, 1979)

Phase	ΔH_{mix}	S^E
Liquid	$X_{Fe}X_{Ti}$ $(-62760X_{Fe} - 46024X_{Ti})$	0
bcc	$X_{Fe}X_{Ti}$ $(46024X_{Fe} - 23012X_{Ti})$	0
fcc	$X_{Fe}X_{Ti}$ $(-33472X_{Fe} - 10460X_{Ti})$	0
hcp	0	0

These selected parameters led to a topographically correct phase diagram, as seen in Figure 4. However, it is apparent that the $\beta/(\beta+\mathrm{TiFe})$ eutectoid temperature and composition are inaccurate. In addition, the γ-Fe (fcc) phase between 911 and 1392°C is absent. This was originally attributed to the very small width of this phase, such that it did not appear on the diagram. Expansion of the Fe-rich side of the phase diagram, however, showed this not to be true. The γ-phase did not appear at all.

3.3 Use of GIBBSPLOT Curves

In order to resolve the causes of the mentioned inaccuracies in the phase diagram, the free energy curve plotting package GIBBSPLOT was used to generate free energy curves at various temperatures. These plots not only provided confirmation of phase compositions at the various temperatures, but also provided invaluable information for the solution of such problems as those discussed above. The free energy curves of phases at 650°C are shown

Temperature 650 C
P = 1 atm

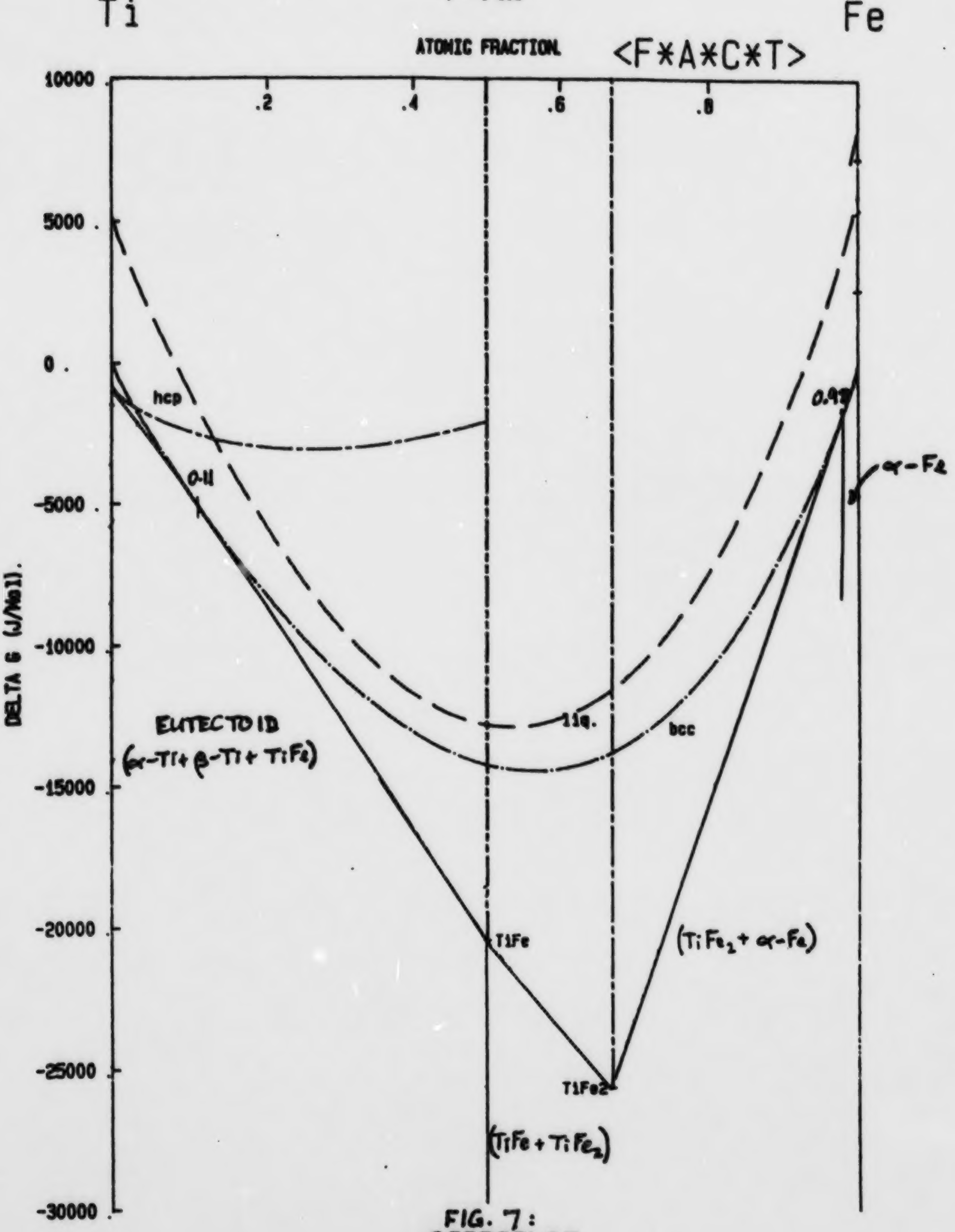

FIG. 7:
GIBBSPLOT
Temperature 650 C

File : C:\GIBBS\Ti-Fe

in the Gibbsplot of Figure 7. This plot clearly shows that for the preliminary model, the Ti-rich eutectoid forms at 650°C with a composition of about 11 at % Fe. It also reveals that if the free energy of formation of TiFe at 650°C was slightly less negative, only a (β/β+TiFe) mixture (of higher at.% Fe) would have existed (the condition predicted by Kaufman and Murray). It should be noted, however that the eutectoid temperature predicted by Kaufman (see Figure 6) is about 640°C. It is reasonable, then, that a higher eutectoid temperature is predicted (using the free energy function of TiFe of Kaufman) by the present model, and it suggests that perhaps Murray's parameters for the heat of fusion of TiFe should be used in preference to those of Kaufman.

The free energy curves of phases at 880°C are shown in the Gibbsplot of Figure 8. This plot shows that at 880°C, α-Ti (hcp) transforms to β-Ti (bcc) as predicted by previous experimental work and by the modelling of Kaufman and Murray. All phases and solutions are present in compositions that are consistent with previous investigations.

The free energy curves of phases at 1085°C are shown in the Gibbsplot of Figure 9. This plot shows that the eutectic forms very close to 1085°C, the eutectic temperature as predicted by previously conducted experiments and the modelling of Kaufman and of Murray. However, the γ-Fe phase should be present at this temperature. The free energy curve for this phase is not present on the plot, and further investigation revealed that the free energy of formation of α-Fe at 1085°C, using the parameters of Murray, was calculated as 25,284 J/mol. Evaluation of these parameters revealed another error in their listing. The free energy of formation of the Fe FCC phase was incorrectly presented in Murray's paper, while Kaufman's paper reported the correct form of the equation (see Table 1).

In addition, it was subsequently recognized that Murray's equation for the free energy of formation of the Ti fcc phase had reversed signs, and

Temperature 880 C
P = 1 atm

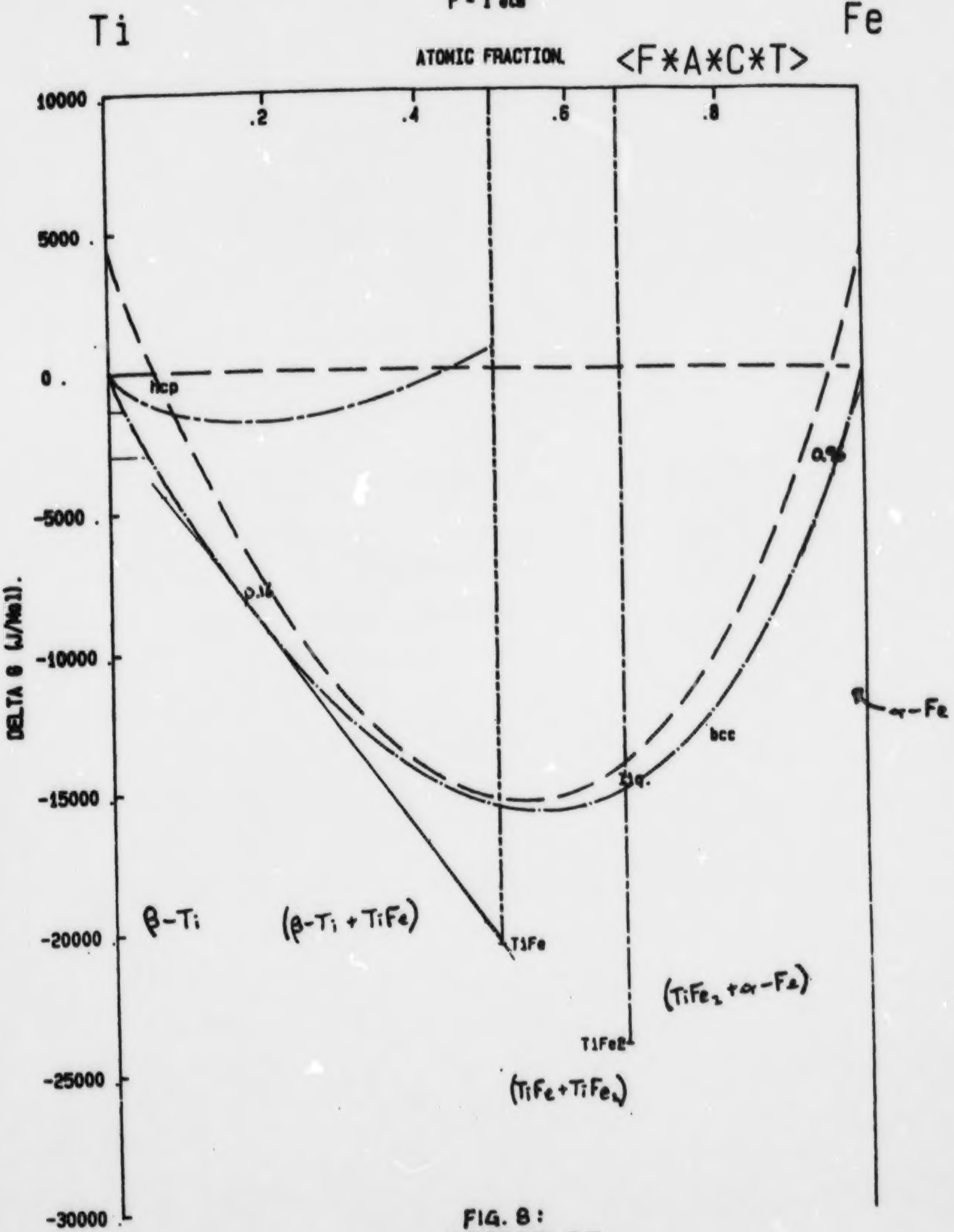

FIG. 8:
GIBBSPLOT
Temperature 880 C

File : c:\gibbs\ti-fe

Temperature 1085 C
P = 1 atm

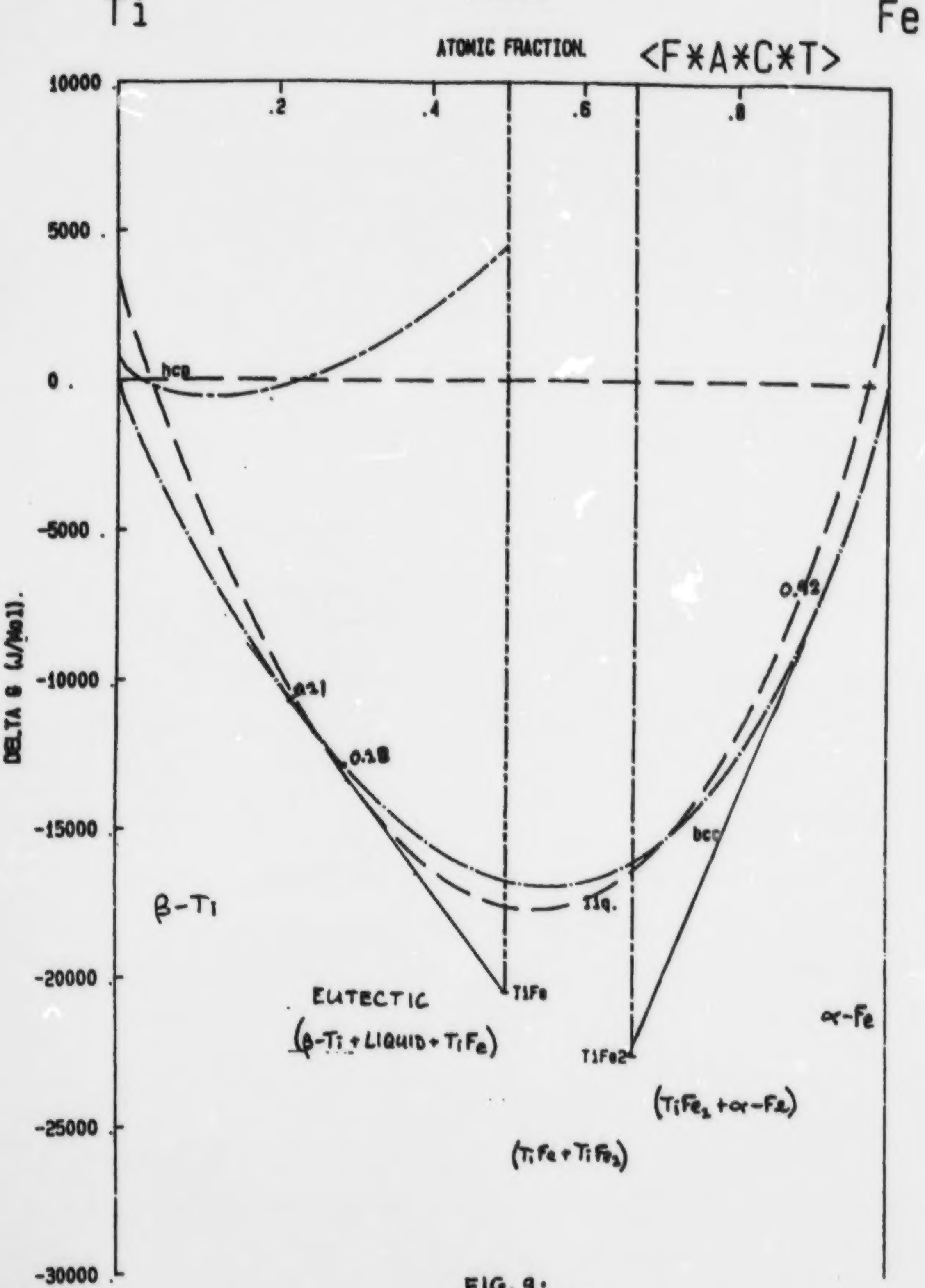

FIG. 9:
GIBBSPLOT
Temperature 1085 C

File : c:\gibbs\ti-fe

pure Ti of 1670°C.

The use of Gibbsplots was thus extremely useful in revealing the source of errors in preliminary modelling. It is expected that corrections made to the model will provide a much more accurate representation of the phase diagram such that is more consistent with previously reported data.

It was indicated by Murray [1] that the equations for the free energy of formation of TiFe (see Table 2) do not reproduce the β-Ti/TiFe boundaries at low temperatures because the predicted eutectoid temperature is too high. This is consistent with the diagram calculated by Kaufman and also with the current analysis, as discussed earlier with reference to the Gibbsplot at 650°C (Figure 7). The TiFe free energy function designated "L.T." ("low temprature) in Table 1, however, correctly predicts the peritectoid and eutectoid temperatures. With proper consideration, this function can be adapted to the current model to not only correctly predict the peritectoid temperature, but also to correctly predict the eutectoid temperature and composition. To correctly predict the peritectoid temperature (1317°C), the free energy of the liquid phase at this temperature and composition must first be evaluated. From the free energy function for liquid Ti and liquid Fe, it can be calculated that at 1317°C, $\Delta G_{Ti}^{bcc\rightarrow liq.} = 2355$ andd $\Delta G_{Fe}^{bcc\rightarrow liq.} = 1518$ J/mol. This seems reasonable with reference to Figure 10. At an equimolar compositon, then,

$$\Delta G_{Fe-Ti}^{bcc\rightarrow liq.} = 0.5\ (2355) + 0.5\ (1518) = 1936.8 \text{ J/mol}$$

The ideal free energy of mixing can be evaluated using equation 4:

$$\Delta G_{ideal}^{L} = X_A RT\ln X_A + X_B RT\ln X_B = -9{,}163 \text{ J/mol}$$

The excess free energy of mixing at this temperature and composition multiplication by -1 would provide the correct equation of Kaufman. It is expected that use of Kaufman's representation of the free energy of formation of Fe and Ti, which predicts $\Delta G_{Fe}^{bcc\rightarrow fcc}$ to be -75 J/mol, will result in the formation of the fcc γ-phase at this temperature.

The free energy curves of phases at 1320°C are shown in the Gibbsplot of Figure 10. This plot shows that any of nine phases can form at this temperature, depending of course on the concentrations of Ti and Fe. The Ti-rich solidus forms at a composition of 10 at.% Fe, while the liquidus forms at 18 at.% Fe. It can be seen that the compound TiFe will melt at a temperature slightly greater than 1320°C, which is somewhat higher than previous reports, again suggesting that Murray's parameters for the free energy of formation of this compound may be preferred to those of Kaufman. At 1320°C, the Fe-rich liquidus forms at a composition of 87 at.%, while the solidus forms at 91 at.% Fe. This Gibbsplot also reveals somewhat strange behaviour of the Ti-rich hcp phase. From the shape of the free energy curve, it is obvious that at 1320°C the free energy of formation of pure Fe hcp must be extremely high. From the related equation of Murray used in the present model (see Table 1), a value for $\Delta G_{Fe}^{bcc\rightarrow hcp}$ of 45,905 J/mol is obtained at 1320°C for the free energy of formation of Fe (hcp). When the correct equation of Kaufman (see Table 1) is used, this value is 7,988 J/mol. Thus, the hcp phase was modelled somewhat incorrectly in the present evaluation, and use of the correct parameters for this phase in a further analysis will affect the temperature and composition of the eutectoid formed between this phase, β-Ti, and the compound TiFe.

The free energy curves of phases at 1700°C are shown in the Gibbsplot of Figure 11. At this temperature, only the liquid phase exists, as shown clearly in the phase diagram of Figure 4 and as predicted by thermodynamic considerations. Pure liquid Ti is only slightly more stable than pure solid Ti (bcc) at 1700°C. This is consistent with the predicted melting point of

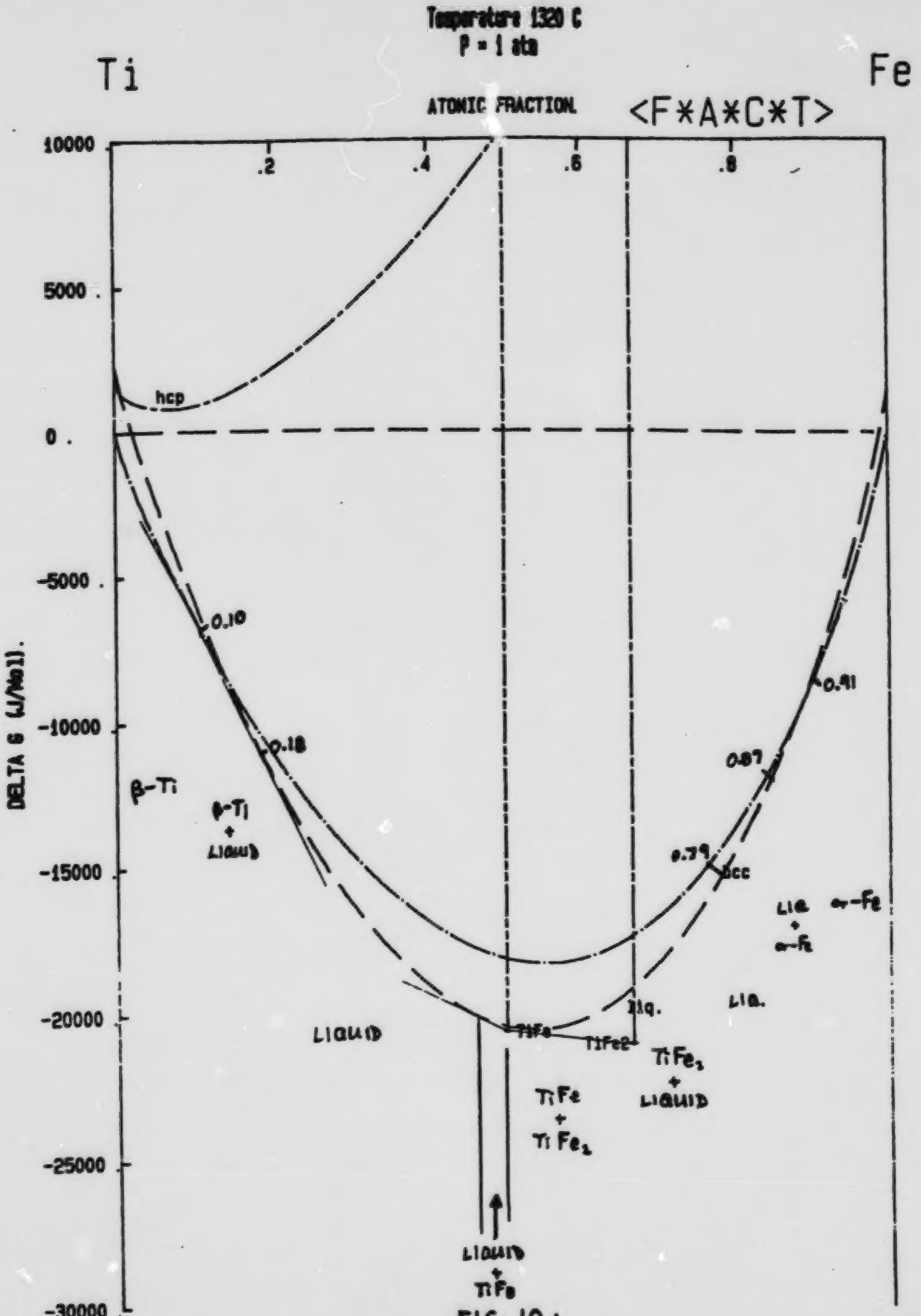

FIG. 10 : *GIBBSPLOT*
Temperature 1320 C

File : c:\gibbs\ti-fe

can be evaluated using the interaction parameters listed in Table 3 for the liquid phase:

$$G^{E}_{L} = X_{Fe}X_{Ti}\,(-62760\,X_{Fe} - 46024\,X_{Ti}) = -13{,}598 \text{ J/mol}$$

The total integral excess energy of the liquid phase is the sum of $\Delta G^{bcc\rightarrow liq.}_{Fe-Ti}$, ΔG^{L}_{ideal}, and G^{E}_{L} :

$$\Delta G_{mix} = -20{,}825 \text{ J/mol}$$

Thus, for the formation of TiFe at 1317°C,

$$\Delta G_{TiFe} < -20{,}825 \text{ J/mol}$$

The low-temperature function of Murray (see Table 2) can be used with slight modification such that

$$\Delta G_{TiFe} = -13800 - 4.42T$$

which at 1317°C yields a value of $\Delta G_{TiFe} = -20{,}828$.

As discussed earlier, a slightly less negative free energy of formation of TiFe at 650°C would lower the eutectoid temperature and increase the at.% Fe at the β-Ti/(β+TiFe) boundary. With the current free energy function of Kaufman, $\Delta G_{TiFe} = -20{,}118$ J/mol at 650°C. If, however, the proposed free energy function is used, a free energy of formation ΔG_{TiFe} at 650°C of -17,800 J/mol is predicted. Therefore, the use of the proposed free energy function would correctly predict the peritectoid temperature, lower the eutectoid temperature, and increase the at.% Fe at the β-Ti/(β-Ti+TiFe) boundary as required to increase consistency with previous experimental data

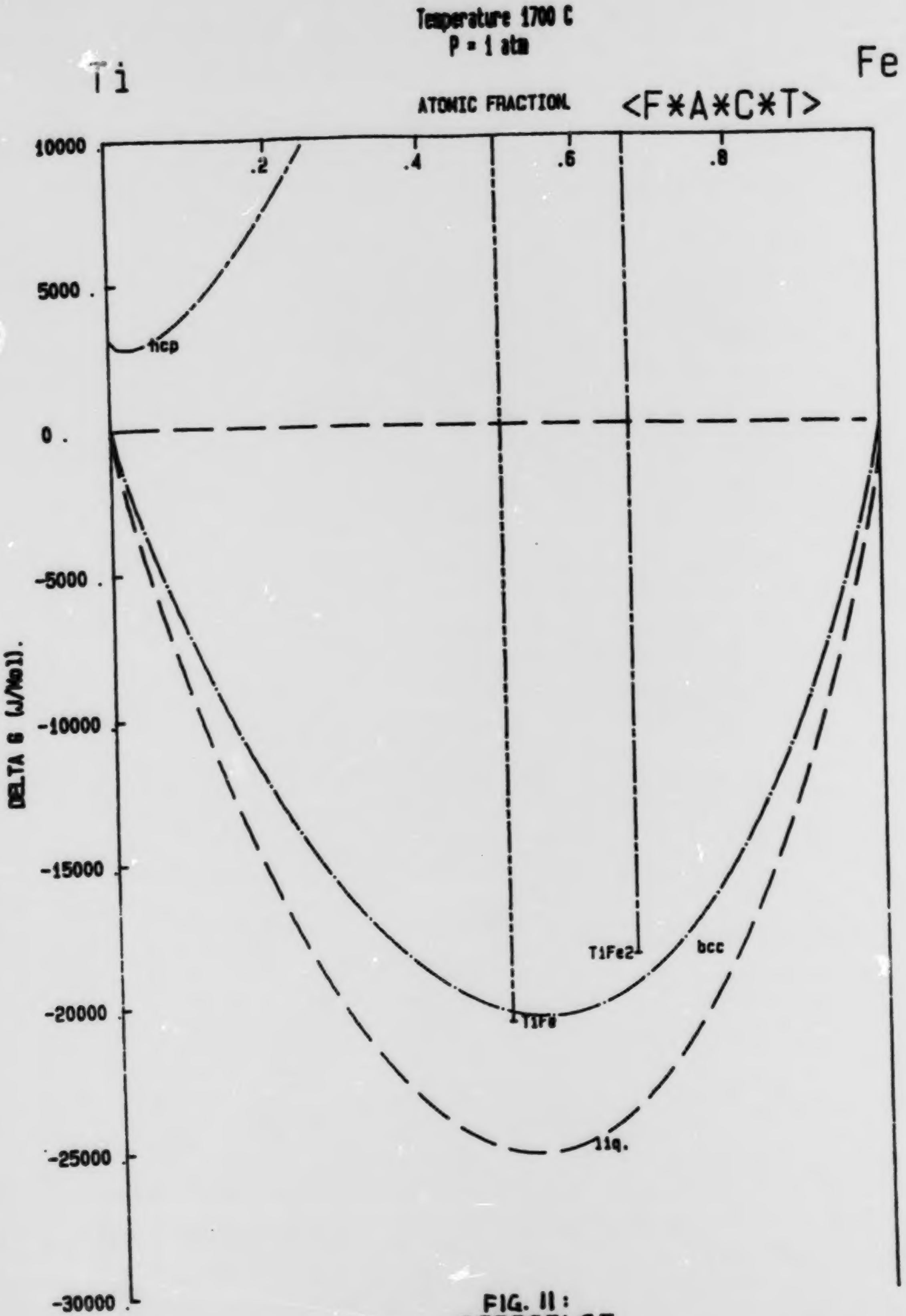

FIG. 11 :
GIBBSPLOT
Temperature 1700 C

File : c:\gibbs\Ti-Fe

and theoretical considerations.

4. CONCLUSIONS

The Ti-Fe binary system can be modelled by the F*A*C*T system with knowledge of the phase transformation temperature, related heats of formation, heat capacities of the phases, and interaction parameters (heats of mixing). Calculations for this system are simplified since all solutions are regular (excess entropies are negligible). Calculations can be further simplified if well-established free energy functions of intermediate compounds are available. Caution must be exercised when using previously reported data, however, since erroneously presented data can make modelling very difficult.

The Ti-rich solidus and liquidus in the present phase diagram could be modelled more accurately than previously, since recently reported data on the liquid phase, made more reliable through careful use of pure substances and controlled experimental methods, was available for incorporation into the model. This has helped to make the Ti-rich portion of the phase diagram more reliable and accurate.

The free energy curve plotting package GIBBSPLOT is extremely useful in confirming temperatures and compositions of the eutectoid, eutectic, peritectoid, etc., and also in detecting problems associated with the system parameters.

5. FURTHER INVESTIGATIONS

From the present preliminary investigations on computer modelling of the Ti-Fe binary system, it is possible to immediately formulate plans for further investigations:

1) Completion of an accurate, consistent Ti-Fe binary system model.

2) Re-calculation of the system model using

i) lattice stability parameters calculated from well-established phase transformation temperatures and heats of fusion and heat capacities of the various phases (F*A*C*T program FITBIN)

ii) free energies of formation of intermediate compounds as calculated using a previously established phase diagram and the F*A*C*T system FITBIN,

iii) excess entropies of mixing for solutions for which phase boundaries are inconsistent with previously reported data (using the previously established phase diagram and the F*A*C*T program FITBIN).

3) Modelling of the binary systems Fe-Si and Ti-Si, followed by modelling of the ternary system Fe-Si-Ti using the F*A*C*T program TERNFIG.

6. REFERENCES

1. Murray, J., Bulletin of Alloy Phase Diagrams, 2(3), 320-324, 1981.
2. Duwez, P., and Taylor, J.L., Trans. Am. Inst. Min. Met. Eng., 188, 1173-1176, 1950.
3. Dew, H.D., Met. Trans. A, 11A, 1219-1225, 1980.
4. Kivilahti, J.K., and Tarasova, O.B., Met. Trans. A, 18A, 1679-1680, 1987.
5. Gustafson, P., Scand. J. Met., 14, 259, 1985.
6. Kaufman, L., CALPHAD, 3 (3), 175-203, 1979.

COMPUTER CALCULATION OF THE Ti-Si PHASE DIAGRAM USING THE F*A*C*T FACILITY

ABSTRACT

The goal of this work is to develop thermodynamic functions which will adequately represent the known titanium - silicon system. This can then be used to describe the separate phases of the system precisely and information such as the activities of Ti and Si in the melt at any temperature could be evaluated.

The F*A*C*T system not only performs the repetitive thermodynamic calculations but it can also fit the data, this is done using a program called Fitbin. The Fitbin program is actually a Phase Diagram/Thermodynamics Optimisation of the Binary System A-B. By introducing known free energies, compositions and temperatures, Fitbin is able to model the particular phase. The Fitbin model is then loaded into the Potcomp program. The Potcomp program is used for Potential-Composition Phase Diagram Calculations. The Potcomp program will then represent graphically the Fitbin information. This enables the operator to assess the adequacy of each Fitbin model and to adjust the necessary input to shape the model until it accurately represents the particular system being studied.

It is also interesting to note that very little work has been done towards the development of ternary phase diagrams, and even less on modeling these diagrams. By modeling three binary phase diagrams and using another F*A*C*T program called Ternfig, it is possible to model ternary systems which would never be modeled by hand. This gives researchers information where none was available before.

RESULTS

The following is a summary of the mathematical models developed for the seven phases of the titanium - silicon system modeled.

The modeling equation of the liquid phase:

$$G^E = X_{Ti} X_{Si} (-26031 * 10^1) + X_{Ti} X_{Si}^2 (16409 * 10^1)$$

The modeling equation of the compound:

i) Ti_5Si_3

$$G^E = -92048 - 13.8407T$$

ii) TiSi

$$G^E = -83780.4 - 13.3888T$$

iii) $TiSi_2$

$$G^E = -71128 - 15.0624T$$

The modeling equation of the Beta phase:

$$G^E = X_{Ti} X_{Si} (-34281 * 10^2) + X_{Ti} X_{Si}^2 (-24172 * 10^2)$$

The modeling equation of the Alpha phase:

$$G^E = X_{Ti} X_{Si} (a + b/2\, X_{Si} + c/3\, X_{Si}^2 + \ldots + f/6\, X_{Si}^5)$$

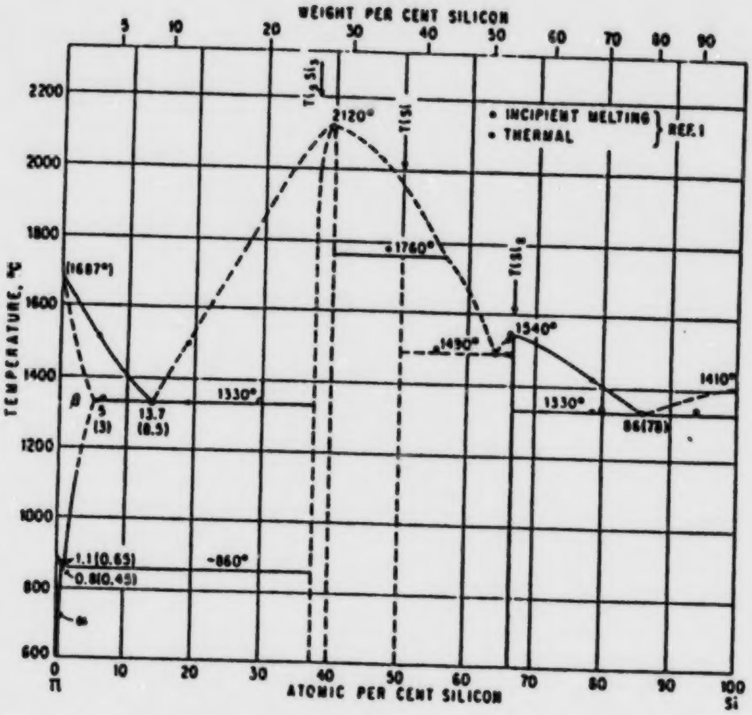

Figure 1: Phase Diagram for the Ti-Si System.

Si-Ti

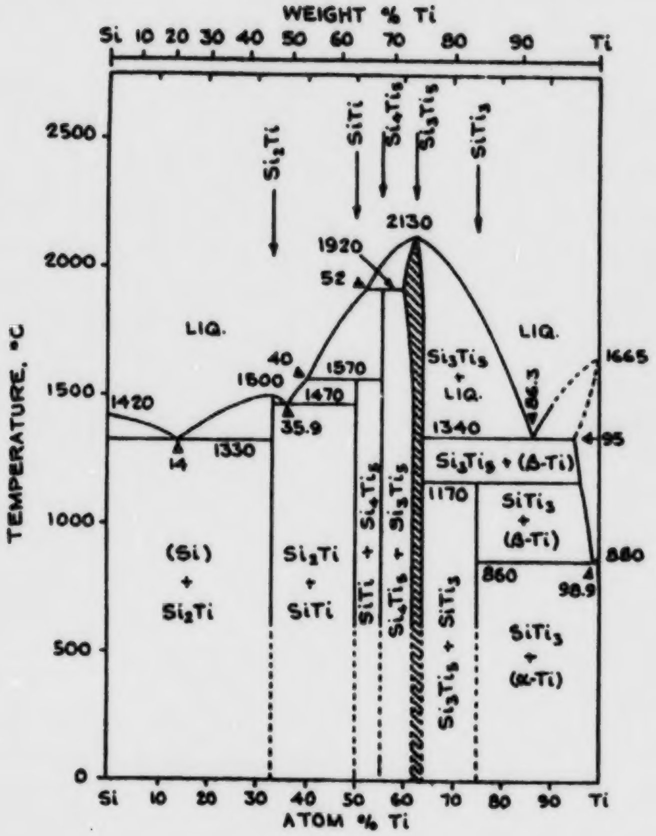

Diagram from ref. 1, with two corrections (Si_3Ti_5 is incorrectly labelled Si_4Ti_5 on diagram, but correct in text; and elimination of extension of the line compound $SiTi_3$ upward to 1340°C, clearly a drawing error). Crystal structures and lattice parameters of the intermediate phases are given.

(1) Svechnikov, V.N.; Kocherzhinskii, Yu.A.; Yupko, L.M.; Kulik, O.G.; and Shiskin, E.A.
"Constitution Diagram of the System Titanium-Silicon."
DOKL. AKAD. NAUK SSSR; 193, No. 2 (1970); pp 393-396

Figure 2: More Recent Phase Diagram for the Ti-Si System.

where $a = -11413.8$

$b = -84.7812$

$c = -0.524213 * 10^{-2}$

$d = 0$

$e = 0$

$f = 13.40553$

DISCUSSION OF MODEL

To model the Ti-Si system, first the free energy of fusion was retrieved from the F*A*C*T data bank for each of the compounds. The fusion temperature was estimated for each compound based on the phase diagram, see Figure 1, as givenin Hanson's Phase Diagram book. More recent research has indicated the presence of another compound on the phase diagram, namely Ti_5Si_4. This newer phase diagram is shown in Figure 2.

Using the free energies retrieved from F*A*C*T, the known composition of these compounds, and the F*A*C*T program Fitbin, a mathematical description of the free energy behaviour of each phase was developed. The compound models were also developed using the free energy of mixing and the ideal free energy to give the excess free energy equations. The beta phase modeling was done by fixing the model at the eutectic point at 13.7 atomic % silicon and the melting point of pure titanium. The alpha phase was more complicated to model. It required that again the free energy from the eutectic point be utilized but also the equation:

$$RT\ln (aTi)L - RT\ln (aTi)S = - (\hat{Gf})Ti$$

Finally as a verification of the free energy model, Gibbs free energy plots were produced from 300 to 2200 °C at 100 °C intervals. These plots showed the complexity of the free energy minimization required of the F*A*C*T program potcomp to produce the binary phase diagram of the Ti-Si

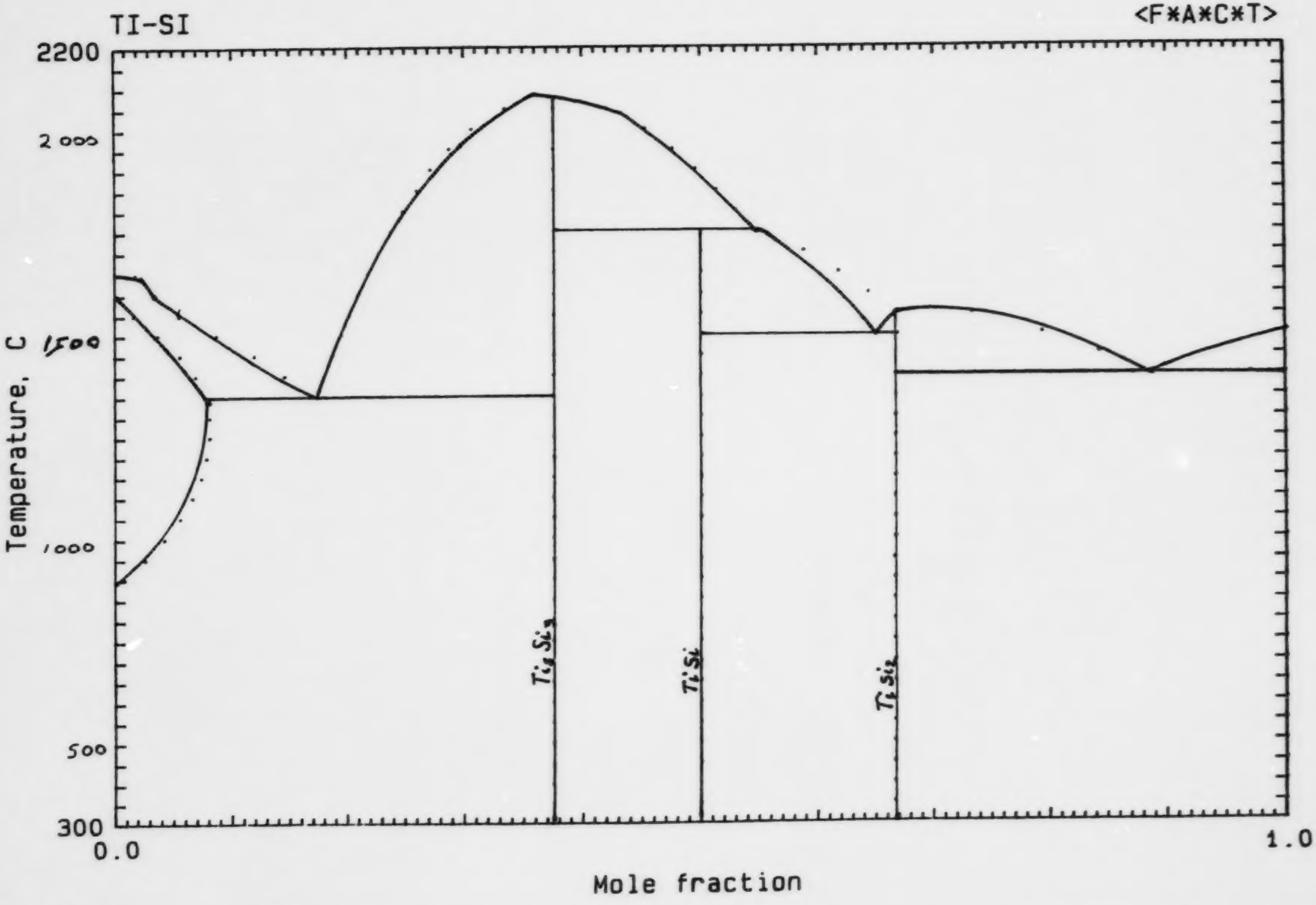

Figure 3: Ti-Si Phase Diagram Calculated Using the F*A*C*T System.

system. The phase diagram model developed adheres closely to the original Hanson diagram used and is quite sufficient for a first fit model. To improve the overall fit of the model, the initial liquid phase modeling would need to be reworked to provide a better solidus curve profile. This would also help in improving the modeling of the alpha region which is not accurate on the plot of the system model, see Figure 3.

CONCLUSIONS

The titanium - silicon system was modeled using the F*A*C*T system and the concepts involved in modeling such a system have been investigated.

METALLOTHERMIC REDUCTION

INTRODUCTION

Metal Silicide Systems

The existence of metal silicides has been recognized for over a century. In particular, titanium silicides were produced in 1895, when H. Moissan [1] and L. Levy [2] both produced the silicide. In the case of Moissan the composition of his product was unknown, while Levy is known to have produced $TiSi_2$. In 1908, P. Askenasy and C. Ponnaz [4] reported that they had produced Ti_2Si_3. However, they were unable to confirm the homogeneity of their product. The major problem faced by these early resarchers was their inability to analyze their products accurately. It has only been since the development of modern phase-analytical methods, notably thermal analysis, metallography and x-ray diffraction, that scientists have been able to ensure that the reaction products were actually composed of a pure and singular phase. The ability to analyze the product accurately was an important step towards determining the most suitable method to produce intermetallics in binary systems. The product of a binary system reaction is determined by a large number of variables. Usually the primary factor is the equilibrium state of the system being studied. Other variables of interest are composition, temperature range, and pressure. In alloy chemistry, the vapor pressures of the elements are usually small enough to be ignored. It can then be stated that in a binary system the temperature and composition are the only two important variables which can be used to describe the methods of preparation of the metal silicides.

Although there seems to be only a few methods of preparation for metal

Li_4Si Li_2Si										
NaSi	Mg_2Si									
KSi	Ca_2Si CaSi $CaSi_2$	Sc_5Si_3	Ti_3Si Ti_5Si_3 TiSi $TiSi_2$	V_3Si V_5Si_3 VSi_2	Cr_3Si Cr_5Si_3 CrSi $CrSi_2$	Mn_3Si Mn_5Si_3 MnSi $MnSi_{1.7}$	Fe_3Si Fe_5Si_3 FeSi $FeSi_2$*	Co_2Si CoSi $CoSi_2$	Ni_3Si Ni_5Si_2 Ni_2Si* Ni_3Si_2 NiSi $NiSi_2$	α(CuSi) β(CuSi) γ-Cu_5Si $Cu_{31}Si_8$ $Cu_{15}Si_4$
RbSi	Sr_2Si SrSi $SrSi_2$	Y_5Si_3 YSi YSi_2*	Zr_3Si Zr_2Si Zr_3Si_2 Zr_6Si_5 ZrSi $ZrSi_2$	Nb_3Si Nb_5Si_3* $NbSi_2$	Mo_3Si Mo_5Si_3 $MoSi_2$		Ru_2Si RuSi* Ru_2Si_3	Rh_2Si Rh_5Si_3 $Rh_{20}Si_{13}$ Rh_3Si_2 RhSi	Pd_3Si Pd_2Si PdSi	
CsSi	BaSi $BaSi_2$*	$LaSi_2$	Hf_2Si Hf_3Si_2 HfSi $HfSi_2$	Ta_3Si Ta_2Si Ta_5Si_3* $TaSi_2$	W_5Si_3 WSi_2	Re_5Si_3 ReSi $ReSi_2$	OsSi Os_2Si_3	Ir_3Si Ir_2Si Ir_3Si_2 IrSi $IrSi_3$	Pt_3Si* Pt_2Si* Pt_6Si_5 PtSi	

$LaSi_2$	CeSi $CeSi_2$	$PrSi_2$*	$NdSi_2$*		$SmSi_2$*	$EuSi_2$	Gd_5Si_3 $GdSi_2$*	Tb_5Si_3 $TbSi_2$	Dy_5Si_3 $DySi_2$*	Ho_5Si_3 $HoSi_2$	Er_5Si_3	Tm_5Si_3	Yb_5Si_3	Lu_5Si_3

	Th_3Si_2 ThSi Th_3Si_5 $ThSi_2$*		U_3Si U_3Si_2 USi* U_3Si_5 USi_2*	$NpSi_2$	Pu_5Si_3 PuSi Pu_3Si_5 $PuSi_2$

SILICIDES

* There is more than one phase with or near this composition.

Table I: Summary of Silicide Systems which have been Characterized

silicides, the number of different metal silicides which have been produced is abundant. Silicides exist in combination with the alkali and alkaline earth metals, group IVa to VIa metals, manganese, iron, nickel, the platinum metals, the rare earth metals, and the actinides. Although the existence of these metal silicides is no longer questioned, they are not all well understood. Conflicting data on the crystal structure, formation temperature, and the specific composition of individual systems are still being reported. However, some systems are fairly well understood due to extensive research. Table I [5] summarizes the silicide systems which have been well characterized.

There has been particular interest in the transition metal silicidces for several decades due to their corrosion resistance, refractory properties, and hardness. In the past decade a new field of research has developed since these materials can be used as gate electrodes and conductors in very-large-scale integration (VLSI) devices. This new interest has led to an improved understanding of the stable phases in several transition metal silicides and related systems. It may also give insight into the factors affecting the strengths of chemical bonds in solids. It is thus important to establish reliable methods of preparation for the transition metal silicides in order to continue to enlarge an already extensive database.

1.2 Preparation of Titanium Silicides

Nearly all the methods which are used for the preparation of carbides, nitrides, and borides can be applied to the production of metal silicides. Silicon like carbon and boron, will react with metals only at relatively high temperatures to produce metal silicides. Often these reactions are hampered by slow reaction kinetics. The reaction kinetics for metal silicide production can be improved by using mixtures of the reactants in finely divided form. The current methods of production for metal silicides are:

i) Synthesis by fusion or sintering;

ii) Reduction of the metal oxides with silicon;

iii) Reaction of the metal oxides with SiO_2 and C;

iv) Reduction of the oxides with Al or Mg;

v) Reaction of oxides in a molten alloy;

vi) Reaction of metal with silicon halide or of a metal halide with silicon;

vii) Fused-salt electrolysis.

The purity, structure, and cost of the metal silicide desired will be the deciding factors in selecting the production method. To ensure a pure and homogeneous product several precautions should be taken: (1) the reactants should be pure, (2) the preparation must be performed without risk of contamination from the crucible or the furnace atmosphere, (3) the subsequent heat treatment of the sample must be performed carefully to ensure that equilibrium conditions are obtained in the final product.

The introduction of impurities into the final products is often very difficult to avoid. Some of these impurities have a negligible influence on the equilibrium state of the system being studied. However, even a trace amount of a particular impurity can have disastrous effects on the mechanical properties of the product. In the silicide systems, impurity atoms such as carbon, nitrogen, or oxygen can promote the formation of metal-rich ternary phases which can easily be mistaken for binary phases. Impurities are usually introduced into the final product by the refractory container and/or the processing atmosphere. It is possible to produce pure silicides by sintering fine powders of metal and silicon. However, care

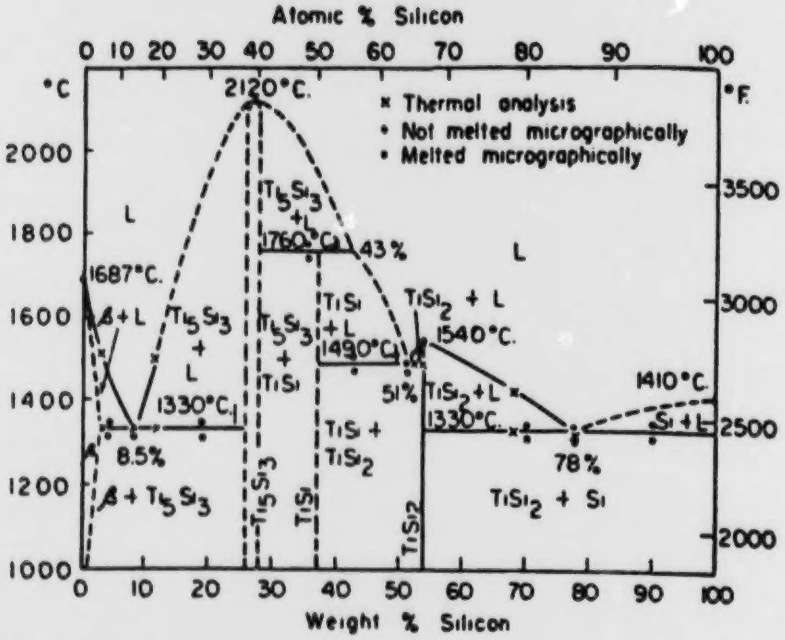

Figure 1: The Phase Diagram for the Ti-Si System

must be taken to avoid contaminating the final product if further grinding or sintering is required. The silicide product of fused salt electrolysis is in the form of a dendritic powder which is difficult to handle. Silicides can be formed at elevated temperatures in a plasma furnace. Different metals and metal oxides have been reacted with silicon or silica in a plasma furnace [6]. The most important discovery of this work was that when metal oxides were used as starting materials silicon was lost by evaporation. It was concluded that the production of many metal silicides was possible using the plasma furnace. The silicide products were well crystallized and were of a high purity.

The group IVa to VIa metal silicides are now fairly well characterized. More specifically, the titanium silicides are now fairly well established. Titanium silicide has been produced at low temepratures by reacting silica with pure titanium metal [7]. Also in the same work, titanium silicide was produced by reacting pure silicon metal with pure titanium metal. The titanium metal was in the form of a thin film, which resulted in an interfacial silicide. The metal thin film was reacted on silica and pure silicon substrates. The silica substrate required a temperature 200 degrees celsius higher than the reaction temperature required for the silicon substrate. The silicides produced from both these ractions were found to be of differing compositions. In Japan, in the mid-seventies, a group at Hitachi [8] produced Ti_5Si_3, TiSi, and $TiSi_2$. These silicides were all produced at temperatures less than 700 degrees celsius.

As of 1952, three binary phases were identified for the Ti-Si system: (1) TiSi, (2) $TiSi_2$, and (3) Ti_5Si_3. Figure 1 shows the phase diagram of the Ti-Si system, as reported by M. Hanson, H.D. Kessler, and D.J. McPherson, [9]. Titanium disilicide, $TiSi_2$, has a slightly deformed orthorhombic crystal lattice, while Ti_5Si_3 has an hexagonal lattice structure. The heat of formation of TiSi is approximately 40 Kcal/mol. The melting point for TiSi is 1900°C while the melting point for titanium disilicide is 1500°C. The hardness of both silicides and discilicides can be approximated. Silicides in general have a Vickers micro-hardness value which ranges from 800 to 1500 kg/mm^2. These hardness values are well above the hardness of nickel and are about equivalent to those obtained in a carbon-rich martensitic steel. Although the silicides exhibit great hardness they are nonetheless very brittle. However, due to their excellent corrosion resistance and good mechanical properties, the silicides have been used in some space-flight and turbine technologies. Their high thermal-shock resistance compared to oxide ceramics is largely due to their higher thermal conductivity. Another important application for the silicides is as oxidation resistant coatings for refractory metals. A limiting factor in their use is due to pin hole and/or pest corrosion which reduces their reliability.

In this research titanium silicide was produced by metallothermic reduction of silica and rutile using a plasma arc furnace according to the following reactions:

$$TiO_2 + SiO_2 + 4\ Mg - TiSi + 4\ MgO$$

$$TiO_2 + SiO_2 + 4Ca - TiSi + 4\ CaO$$

$$\frac{3}{2}\ TiO_2 + \frac{3}{2}\ SiO_2 + 4Al - \frac{3}{2}\ TiSi + 2\ Al_2O_3$$

The major advantages of this process are the low cost of reactants and also the silicide can be produced as fine spherical particles.

REFERENCES

(1) Moissan, H., Compt. rend., 120, 290 (1895).

(2) Levy, L., Compt. rend., 121, 1148, (1895).

(3) Honigschmid, O., Compt. rend., 143, 224, (1906).

(4) P. Askenasy and C. Ponnaz, Z. Electrochem. 14, 810, (1980).

(5) Schwarkopf, P., and Kieffer, R., Refractory Hard Metals, Borides, Carbides, Nitrides, The Macmillan Company, New York, 319, (1953).

(6) De Vynck, Y.A., Utilisation de Fours a Plasma dans le Domaine de la Ceramique Special. Formation de Silicures, Silicates Industriels, 4, 109, (1974).

(7) Krauetle, H., M.A. Nicolet, J:.W. Mayer, Phys. Status Solidi A, 20(1), K33, (1973).

(8) Kato, H., Y. Nakamura, Thin Solid Films, 34(1), 135-138, (1976).

(9) Hansen, M., H:.D. Kessler, and D.J. McPherson, Trans. ASM, 44, 518, (1952).

EXPERIMENTAL

A schematic diagram of the plasma arc furnace is shown in Figure 2. The furnace was operated in the single phase mode at a power level of 24 Kw (115V, 210A). The steel furnace shell was lined with magnesia (98% MgO). The graphite electrodes were 20mm in diameter. The electrodes were supported by aluminum water-cooled holders.

Rutile powder (TiO_2) was supplied by Canadian Titanium Pigments Limited. Reagent grade silica (BDH) and reagent grade magnesium (Fisher) were employed. The magnesium was in the size range of 40 to 80 mesh. The standard mixture was as follows:

6 moles of magnesium, calcium or aluminum
1 mole of titania
6 moles of silica

The powdered reactants were weighed, mixed and then tumbled in a ball mill. A small amount of water was added to the powder which was then briquetted in a hardened steel die at about 5000 psi. The briquette weighed about six grams and had a height of about 3/8 of an inch and a diameter of 1-1/2 inches. In some cases alumina or copper was incorporated into the briquettes. In addition, the briquette was placed on a bed of alumina in the graphite crucible. The crucible dimensions are shown in Figure 3. The variables investigated included the following:

(1) energy input (Kwh),
(2) TiO_2 to SiO_2 ratio,
(3) magnesium addition, and
(4) alumina addition.

Experiments were performed in which magnesium and prefused mixtures of titania and silica were passed through an argon-magnesium vapour plasma. These tests were performed to demonstrate the possibility of the in-flight continuous production of titanium silicide by plasma techniques. In addition, magnesium vapour was passed through a prefused mixture of titania and silica in a two stage reactor in an argon atmosphere.

The metal and slag products were analysed for titanium, silicon, calcium, aluminum and magnesium. Also, the various phases were examined by optical and scanning electron microscopy. X-ray analyses was performed on a number of the reaction products. The thermodynamics of the system were studied using F*A*C*T.

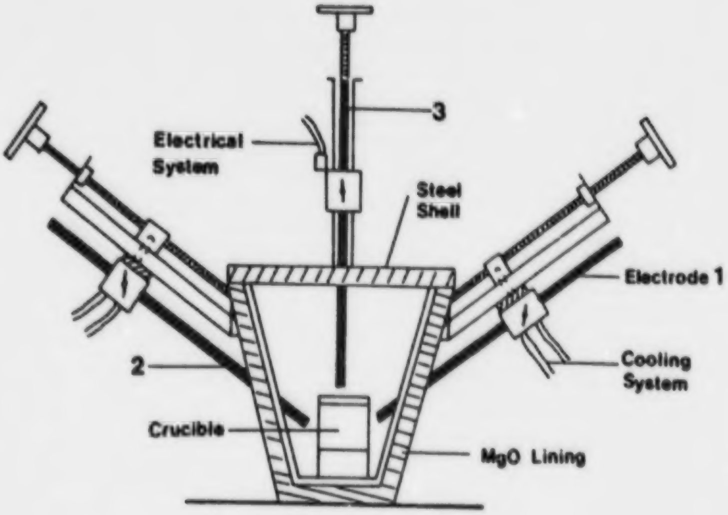
3
Electrical System
Steel Shell
Electrode 1
Cooling System
2
Crucible
MgO Lining

Figure 2: Schematic Diagram of the Plasma Arc Furnace.

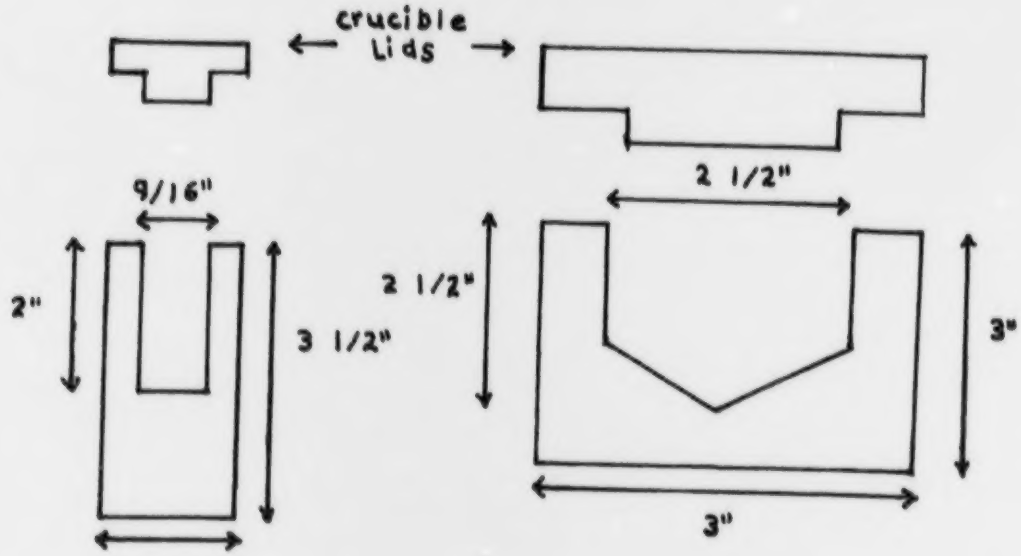
crucible
Lids
9/16"
2"
3 1/2"
2 1/2"
2 1/2"
3"
3"

Figure 3 : Schematic Diagram of the Two Graphite Crucible Assemblies Used.

RESULTS AND DISCUSSION FOR ALUMINOTHERMIC REDUCTION

The F*A*C*T analyses using the EQUILIB program for aluminothermic reduction is summarized in Figures 1 to 4. The overall reaction is as follows:

$$TiO_2 + SiO_2 + 2\,\tfrac{2}{3}Al - TiSi + \tfrac{4}{3}Al_2O_3$$

Figure 1 which shows the effect of aluminum additions demonstrates that 2.67 moles of aluminum are required to achieve conversion. As the titania to silica ratio increases then the amount of Ti_5Si_3 increases in the product while the amount of TiSi decreases - Figure 2. At low ratios, increased amounts of silicon are produced. The effect of temperature is complex - Figure 3. Below 1200°C the reaction products are Ti_5Si_3, SiO_2, Ti_2O_3 and (Al_2O_3) (SiO_2). Between 1200 and 1600°C the products are TiSi, Ti_5Si_3, $3(Al_2O_3.2SiO_2)$ and SiO_2. Above 1600°C TiO forms and above about 2000°C SiO is produced. Although there are indications in the literature that sulphur has beneficial effects on the separation of metal and slag the F*A*C*T analysis indicates that titanium and aluminum sulfides can form. These sulfides would contaminate the final product.

This part of the research involved the production of titanium silicide in a graphite crucible in a plasma furnace by aluminothermic reduction. A series of melting experiments were performed under the experimental conditions to determine the carbon pick-up from the crucible. These results are summarized in Figure 5, for mixtures of titanium and silicon powders. The carbon pick-up was relatively small and in general was less than half-a-percent.

The results of the aluminothermic reduction experiments are shown in Figures 6 and 7. These tests show that the silicon content decreases with increasing plasma energy input and that the stoichiometric addition of aluminum according to the following equation:

$$SiO_2 + TiO_2 + 8/3Al - TiSi + 4/3Al203$$

results in high aluminum contents in the final alloy. Lower aluminum contents, of about two mass percent can be achieved by reducing the aluminum addition below the stoichiometric value.

Both titanium silicide and titanium-iron silicides have been produced. The effect of the titania to silica ratio and iron additions on the analyses of the product are shown in Figures 8 and 9 respectively. It can be seen that even a small iron addition results in a large increase in the iron content of the product. The titanium to silicon ratio of the product can be controlled quite readily by changing the titania to silica ratio of the feed. The aluminum content of the metal varied within the range of about 2 to 8 mass percent.

The morphology of the reaction product is shown in Figure 10. It has been found that even with relatively large energy inputs and iron contents the product is disseminated in the slag. There are some indications in the literature that the slag can be leached so as to give a fine titanium-silicide product which can be sintered. Sulphur is said to improve the leachability. Thus, some sulphur additions were made in the feed and the metal analyses from these tests is reported in Figure 11. Again, even a small sulphur addition results in a large increase in the sulphur content of the metal and also silicon losses increase, presumably due to the formation of volatile silicon sulphide.

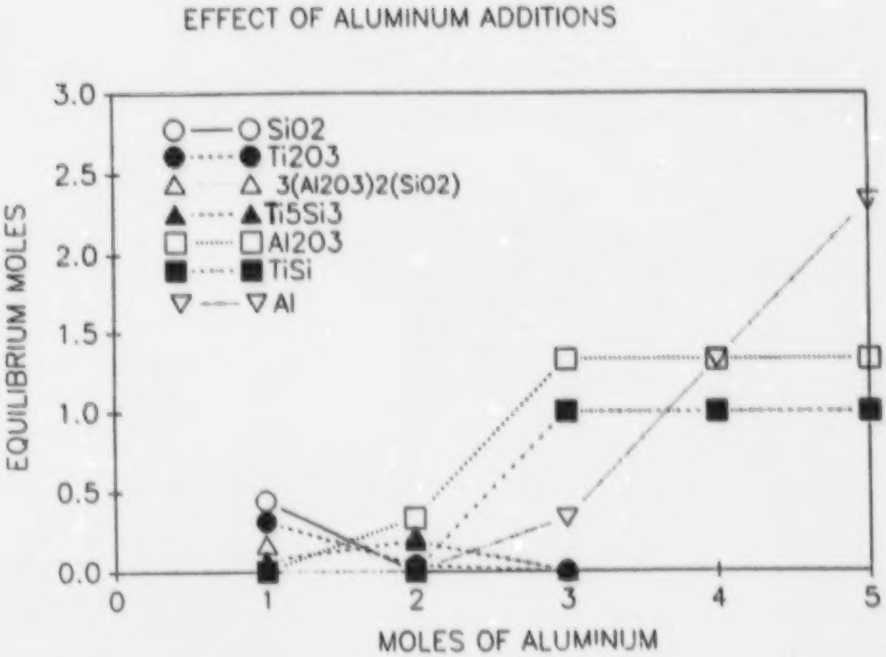

Figure 1: The Effect of Aluminum Additions on the Product Composition as Calculated by F*A*C*T.

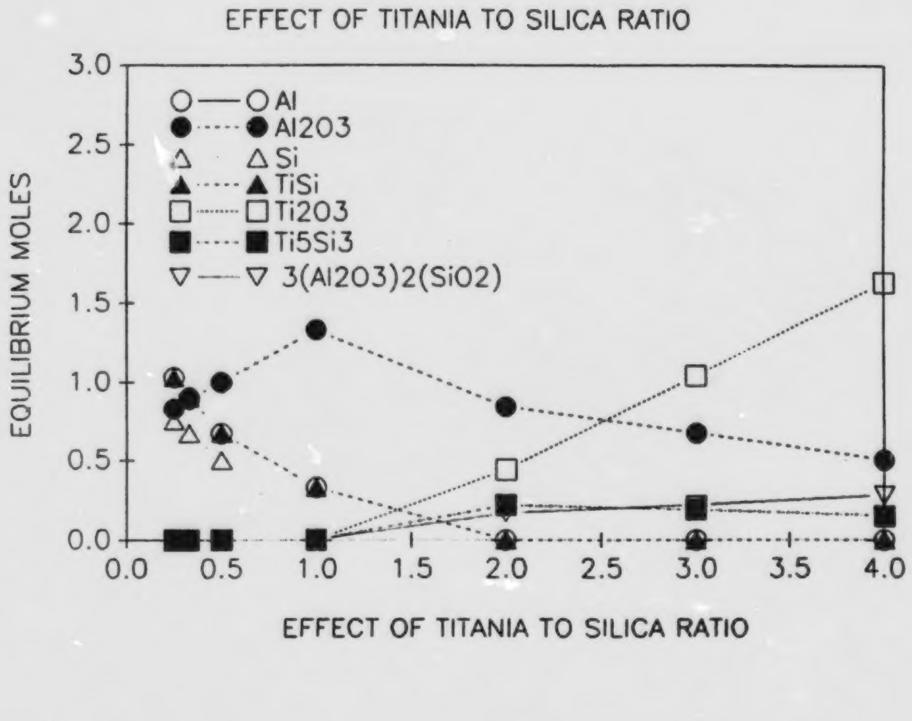

Figure 2: The Effect of Titania to Silica Ratio on the Product Composition as Calculated by F*A*C*T.

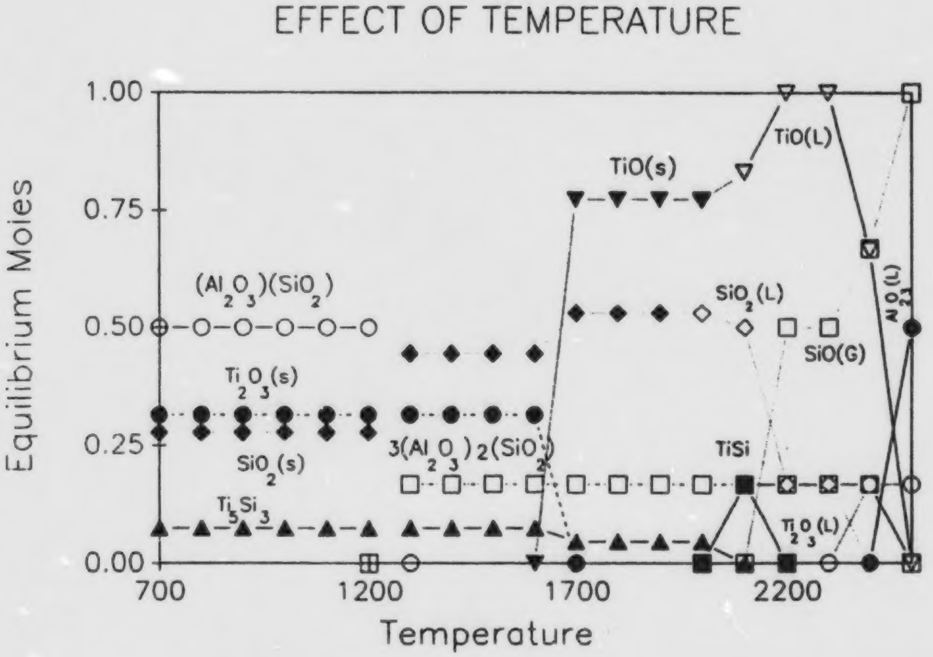

Figure 3: The Effect of Temperature on the Product Composition as Calculated by F*A*C*T.

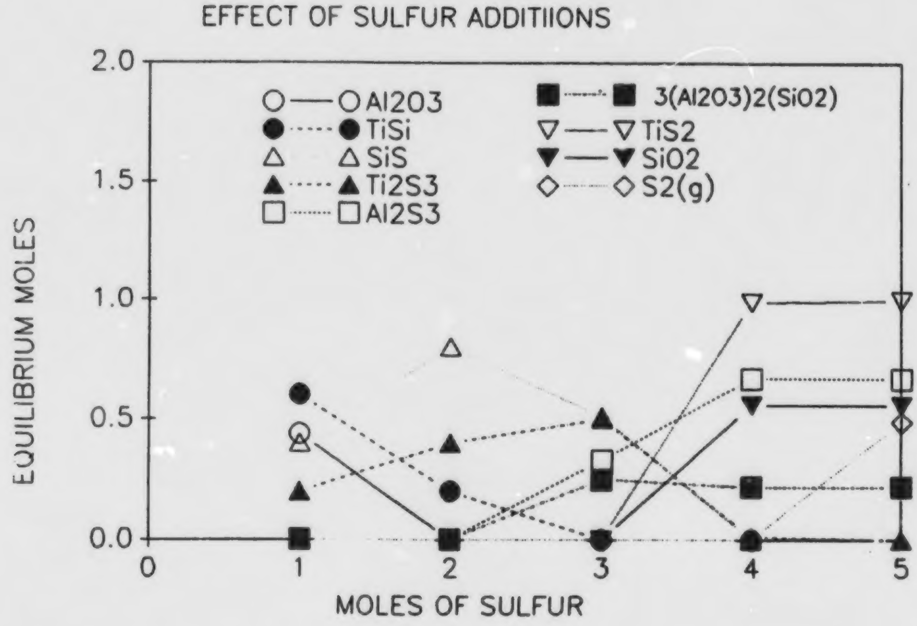

Figure 4: The Effect of Sulfur Additions on the Product Composition as Determined by F*A*C*T.

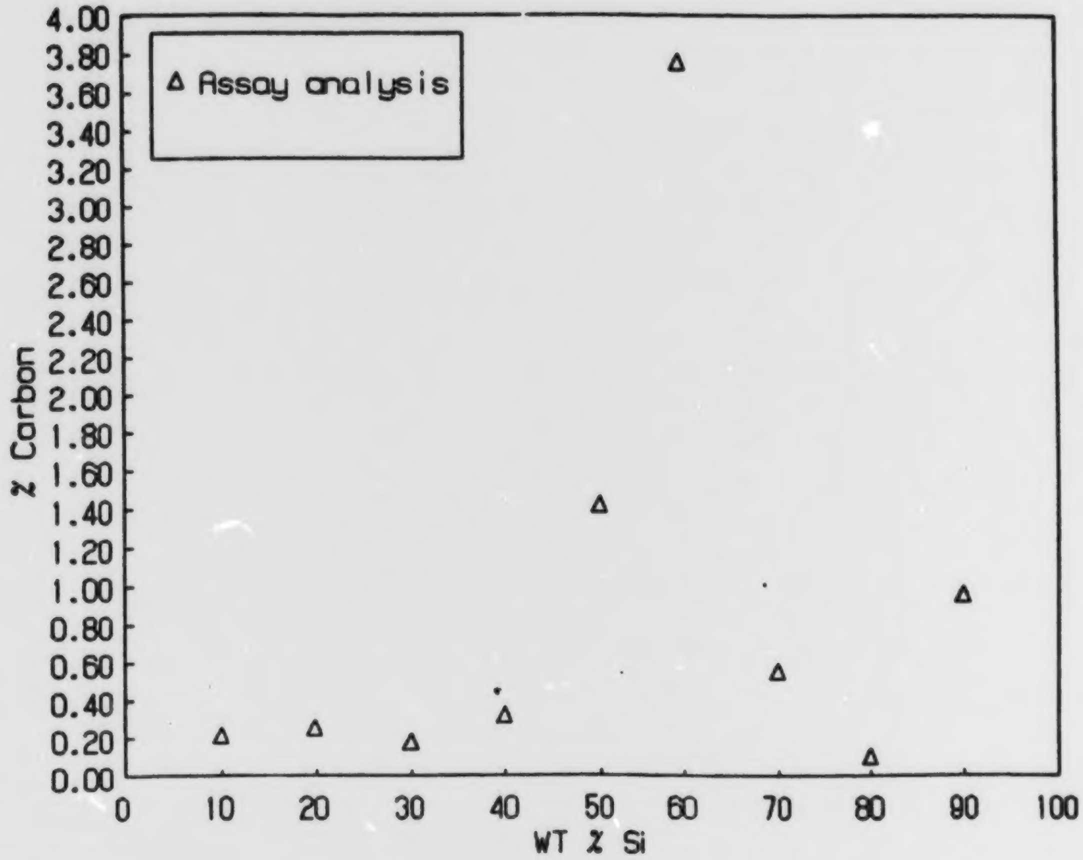

Figure 5: The Effect of Melt Composition on Carbon Pick-up.

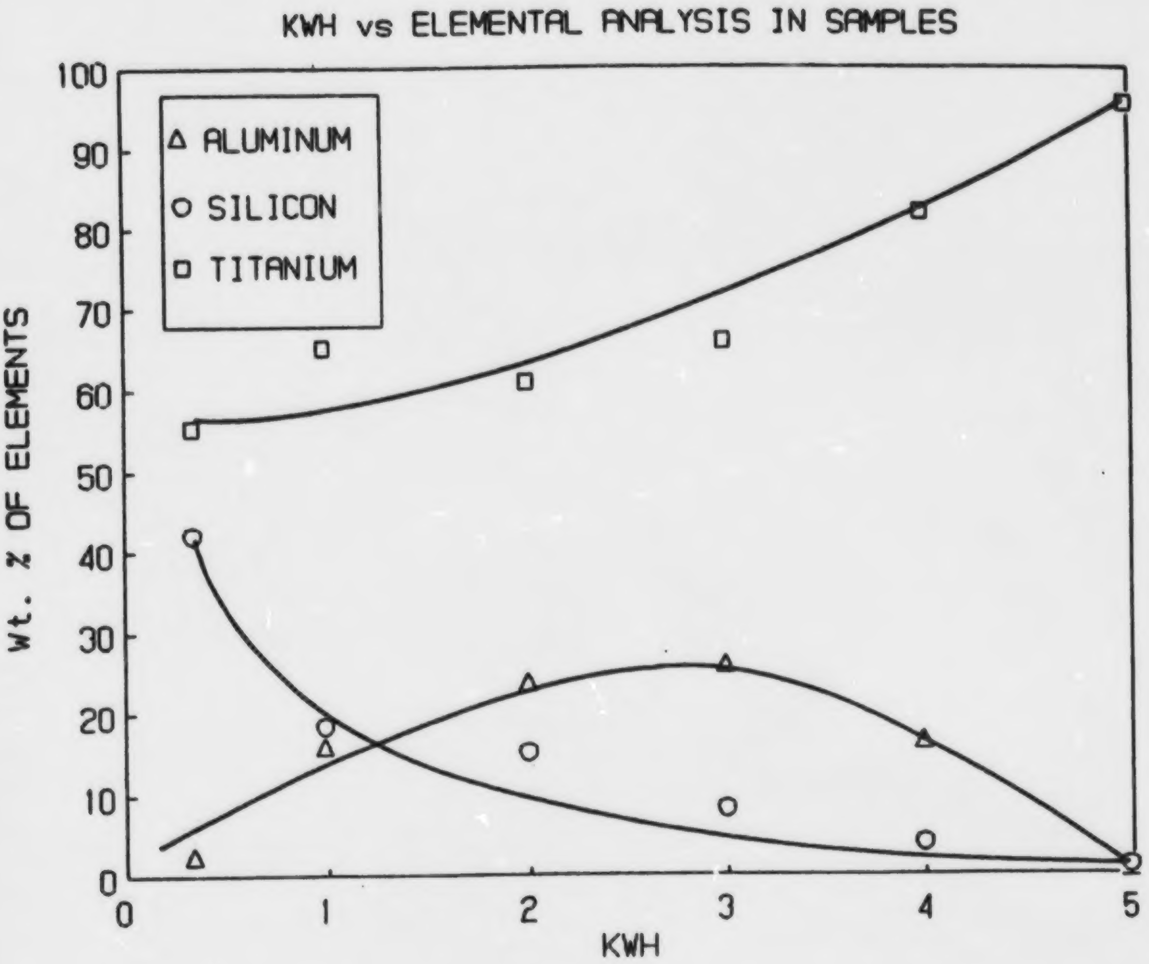

Figure 6: The Effect of Energy Consumption on the Aluminum, Silicon, and Titanium Contents of the Metal Product.

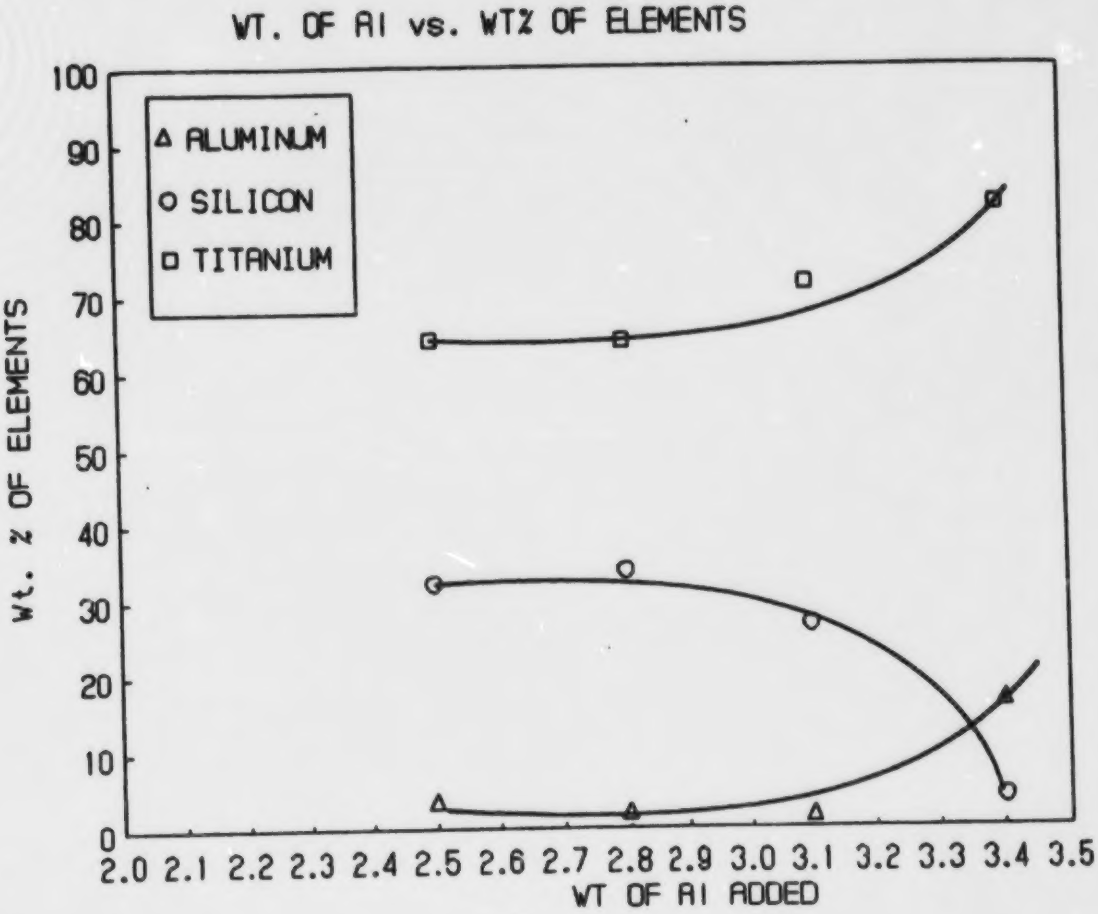

Figure 7 : The Effect of Aluminum Addition on the Titanium, Silicon, and Aluminum Contents of the Metal Product.

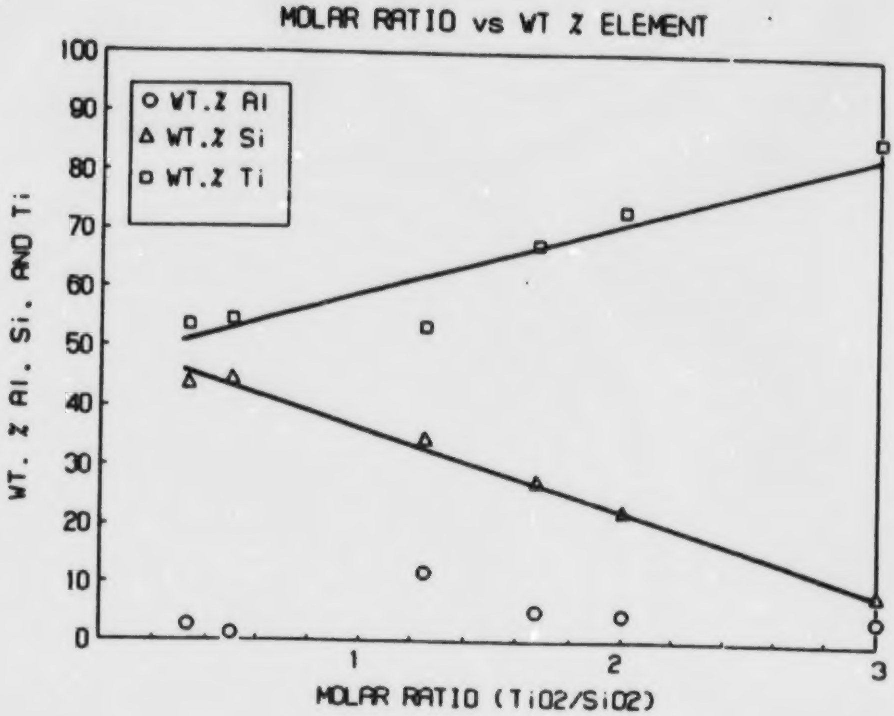

Figure 8 : The Effect of the Titania to Silica Ratio on the Analyses of the Metal Product.

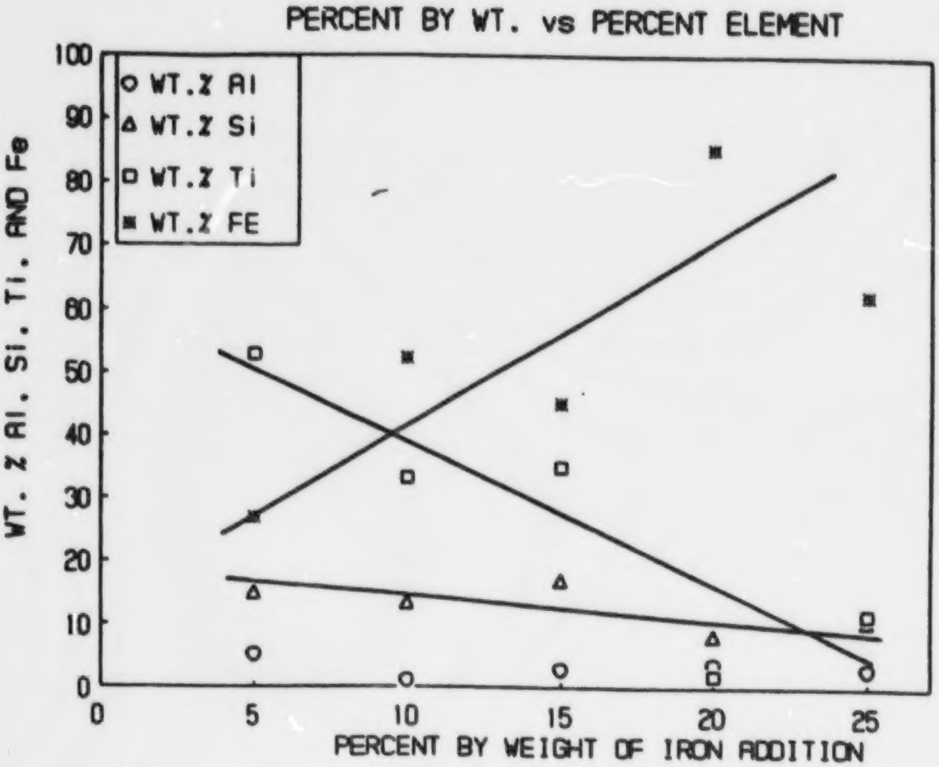

Figure 9: The Effect of Iron Additions on the Analyses of the Metal Product.

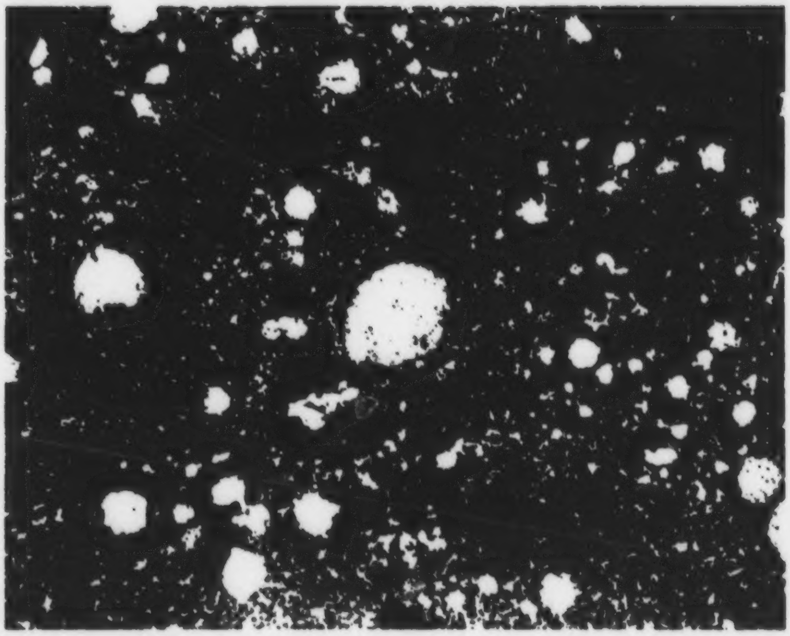

600X
Figure 10. Morphology of the Reaction Product.

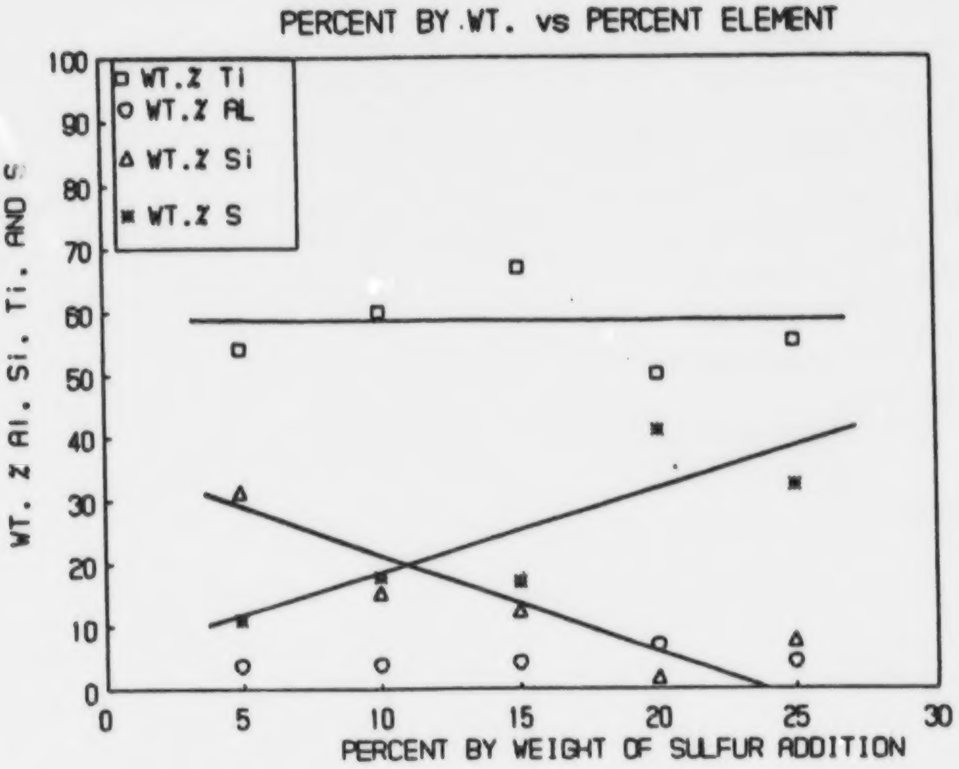

Figure 11 : The Effect of Sulphur Additions on the Analyses of the Metal Product.

RESULTS AND DISCUSSION FOR MAGNESIOTHERMIC REDUCTION

The results of the F*A*C*T analysis using the EQUILIB program are shown in Figures 1 to 4. Figure 1 demonstrates that in the temperature range of about 1000 to 2000°C the reaction products are titanium silicide (TiSi), silicon, magnesium silicates and in the presence of alumina, magnesium aluminates. At temperatures over 2000°C the reaction product becomes complex. Silicon monoxide gas, magnesium vapour, titanium monoxide, and magnesium titanates can form.

The effect of magnesium additions, which is shown in Figure 2 can be conveniently divided into three regions as follows:

(1) below five moles of Mg,

(2) between five and seven moles of Mg, and

(3) above seven moles of Mg.

Below five moles there is insufficient magnesium to reduce all of the silica and thus the amount of titanium silicide produced is less than one mole. Above five moles, the major reaction products are titanium silicide, silicon, magnesium silicates and magnesium aluminates. Above seven moles, free magnesium oxide occurs, the amount of silicon increases and eventually aluminum is produced.

Similarly, the effect of the titania to silica ratio can be divided into two regions - Figure 3. Below a ratio of 0.5, TiSi and silicon are produced. Above 0.5, the amount of Ti_2O_3 increases rapidly and thus TiSi is replaced by Ti_5Si_3. At high titania to silica ratios only a small amount of titanium silicide is produced. The addition of alumina which was added as a flux, promotes the formation of magnesium aluminates and alumino-silicates at the expense of the magnesium silicates - Figure 4. At alumina additions of over 12 moles, free alumina is present and the magnesium silicates have disappeared.

Figure 5 shows the morphology of the reaction product from the experiments performed with briquettes. It can be seen that the silicide is in particulate form. X-ray analysis of the reaction products indicated the presence of titanium silicides, silica, titania, and magnesium silicates, - Figure 6.

The effect of energy consumption on the composition of the titanium silicide is shown in Figure 7. At low energy consumptions the silicon content was high and the titanium concentration was low. On the other hand, at high energy levels the silicon level decreased. As shown in Figures 8 and 9 magnesium and alumina additions did not have an effect on the titanium to silicon ratio of the product. In general, the magnesium content of the titanium silicide was approximately 0.1 mass percent, while the aluminum content was about one mass percent when alumina was added. The titanium to silicon ratio of the product could be changed by varying the titania to silica ratio of the feed - Figure 10. At high ratios very little metal was produced.

The reaction product when copper was added to the briquette is shown in Figure 11. Titanium silicide crystals were found in the copper matrix.

The results of magnesiothermic in-flight reduction of prefused titania-silica mixtures are summarized in Figure 12. It can be seen that titanium silicide has formed as discrete droplets in spheroidized titania-silica particles. Since the slag phase contains magnesium oxide this confirms that in-flight reduction is possible. Metallic product was observed to form at the surface of the particles which indicates that the reducing agent is magnesium vapour. This process has considerable potential as a continuous technique for the production of silicides by magnesiothermic reduction.

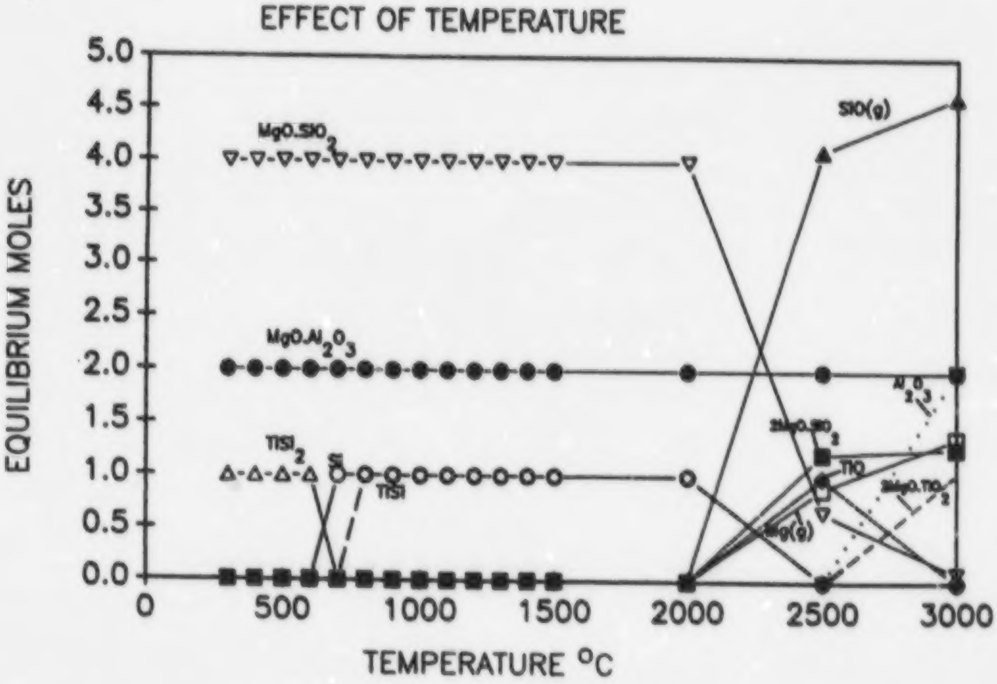

Figure 1: The Effect of Temperature on the Product Composition as Calculated by F*A*C*T.

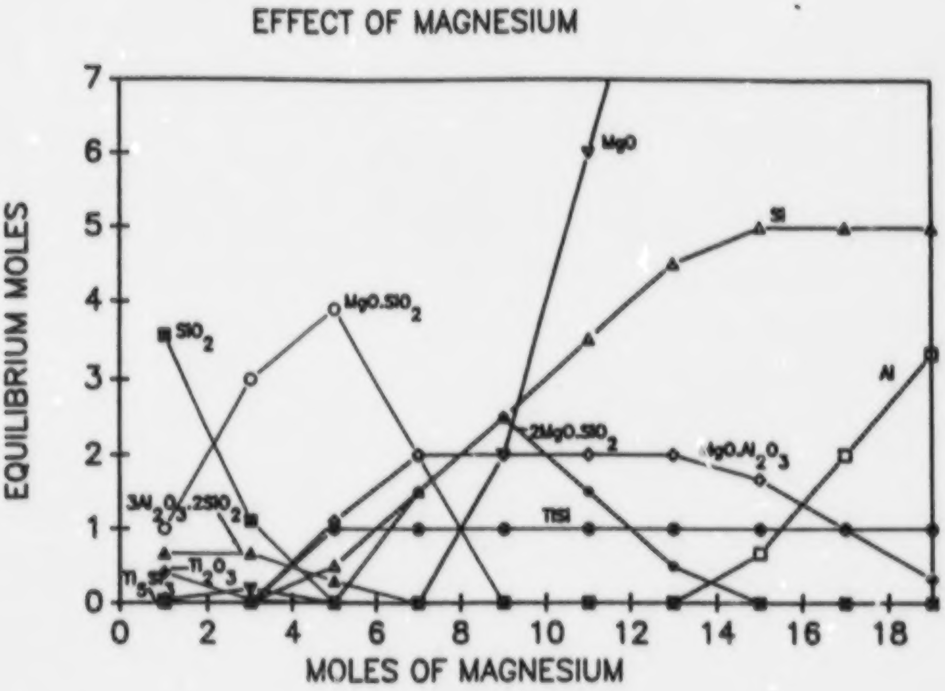

Figure 2: The Effect of Magnesium Additions on the Product Composition as Calculated by F*A*C*T

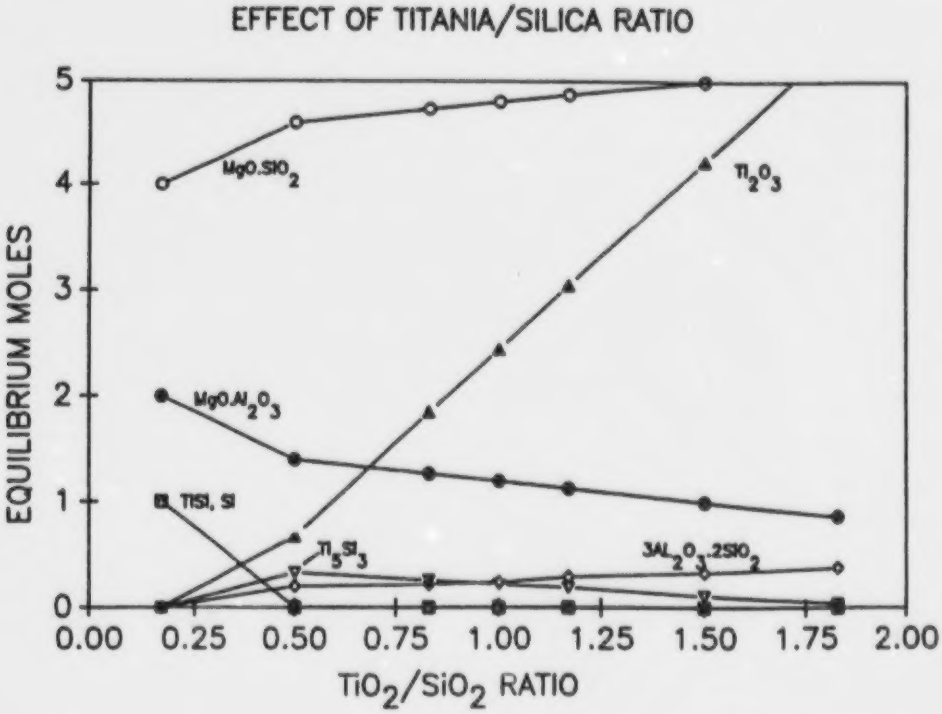

Figure 3: The Effect of Titania to Silica Ratio on the Product Composition as Calculated by F*A*C*T.

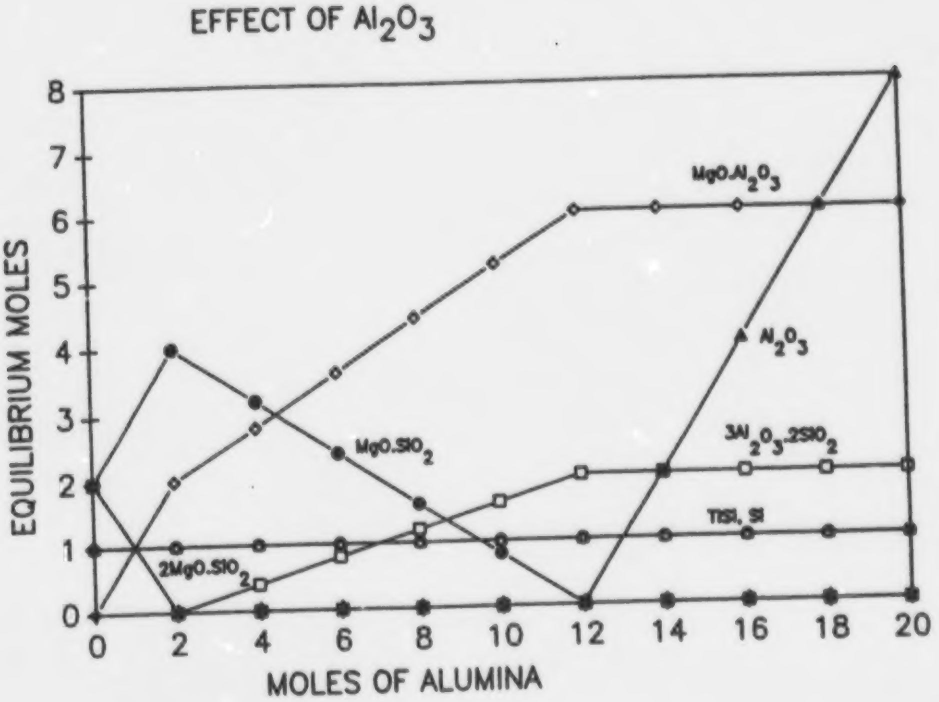

Figure 4: The Effect of Alumina Additions on the Product Composition as Calculated by F*A*C*T.

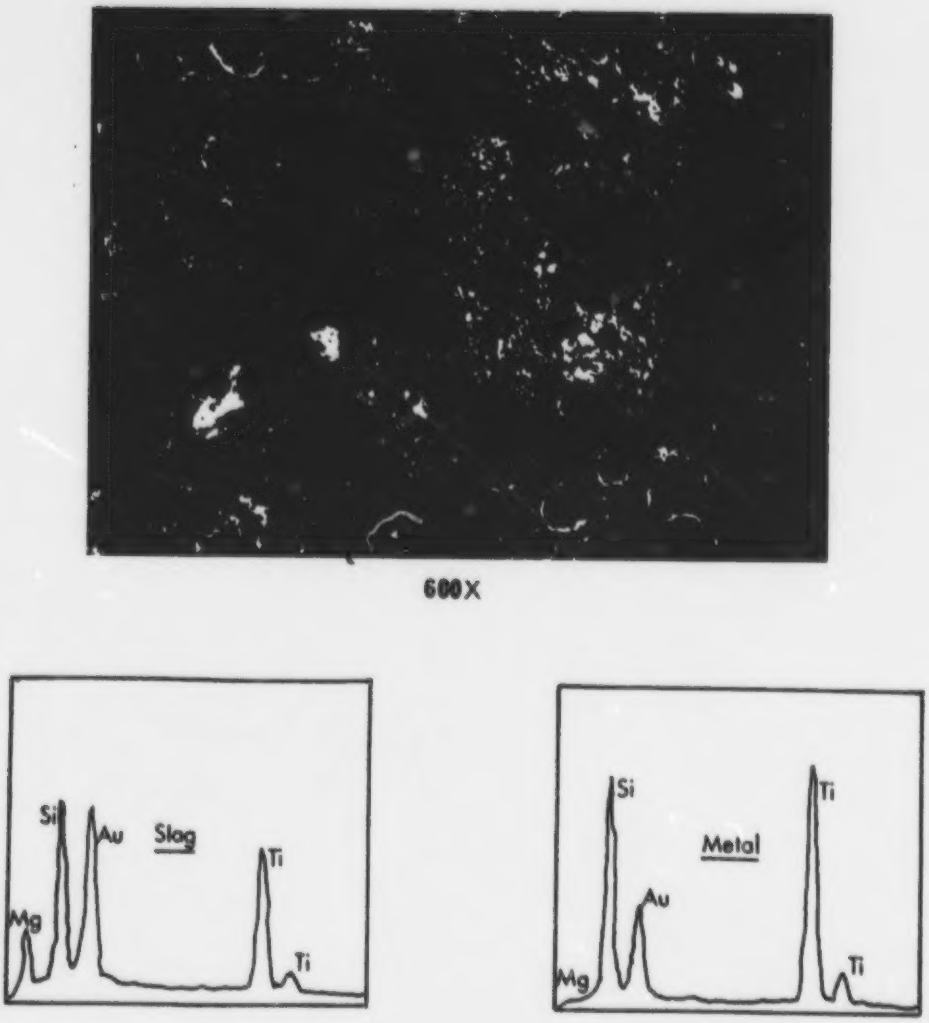
600X
Mg
Si
Au
Slag
Ti
Ti
Si
Ti
Metal
Au
Ti
Mg

Figure 5: The Morphology of the Reaction Products Produced by Magnesiothermic Reduction.

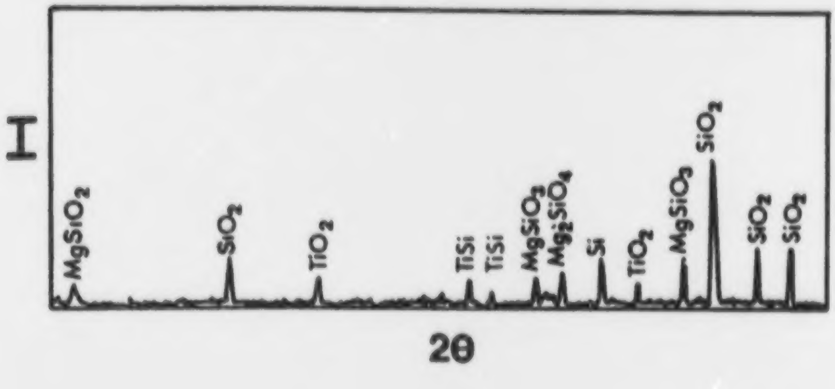

Figure 6: X-Ray Analysis of the Reaction Products.

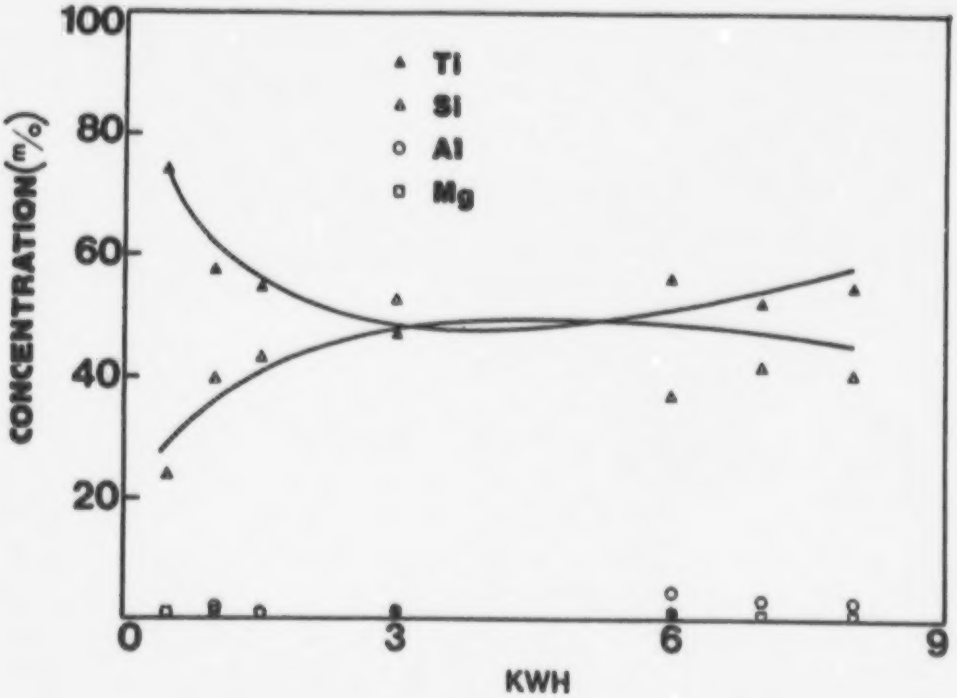

Figure 7: The Effect of Energy Consumption on the Product Composition.

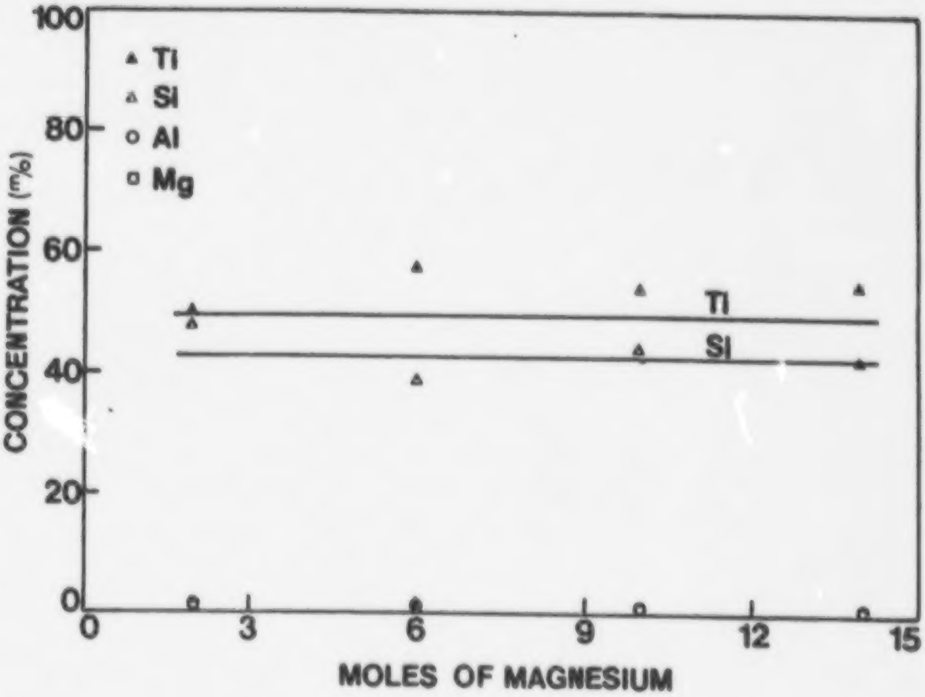

Figure 8: The Effect of Magnesium Additions on the Product Composition.

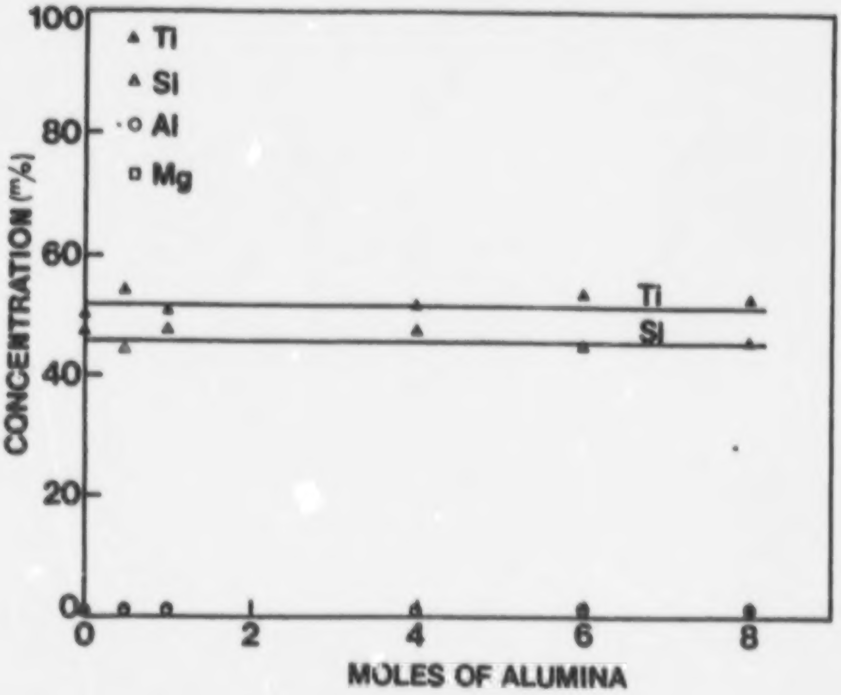

Figure 9: The Effect of Alumina Additions on the Product Composition.

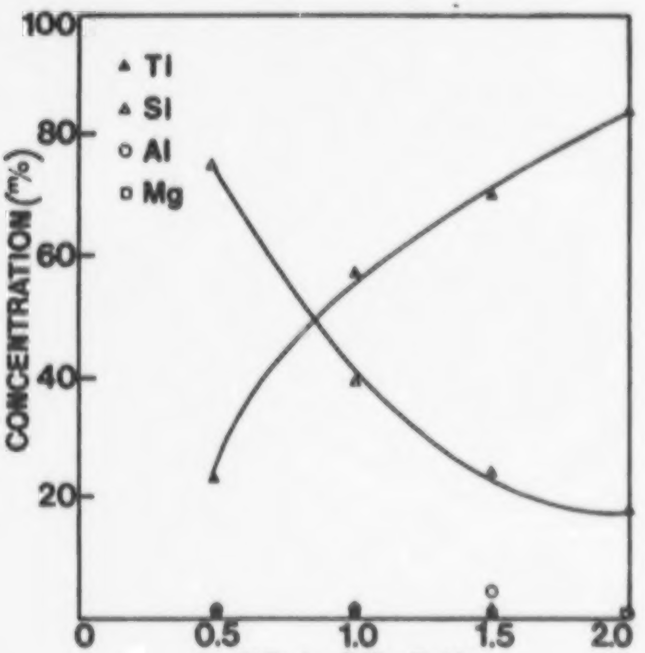

Figure 10: The Effect of Titania to Silica Ratio on the Product Composition.

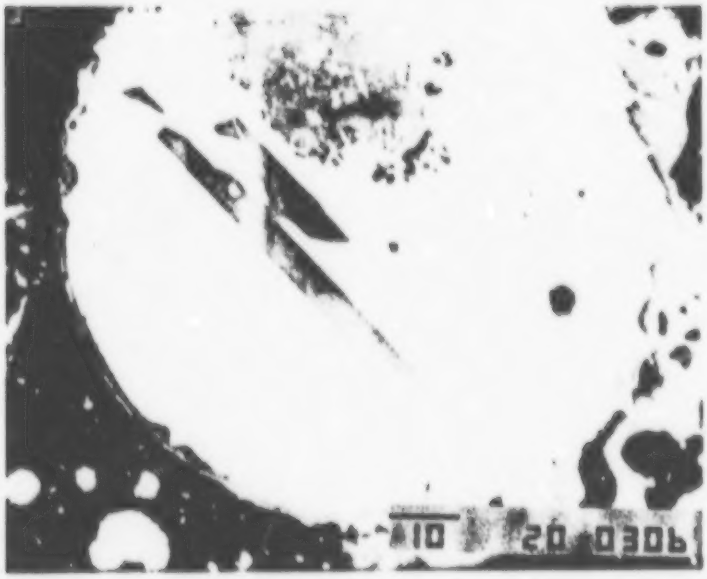

Figure 11: Titanium Silicide Crystals in a Copper Matrix.

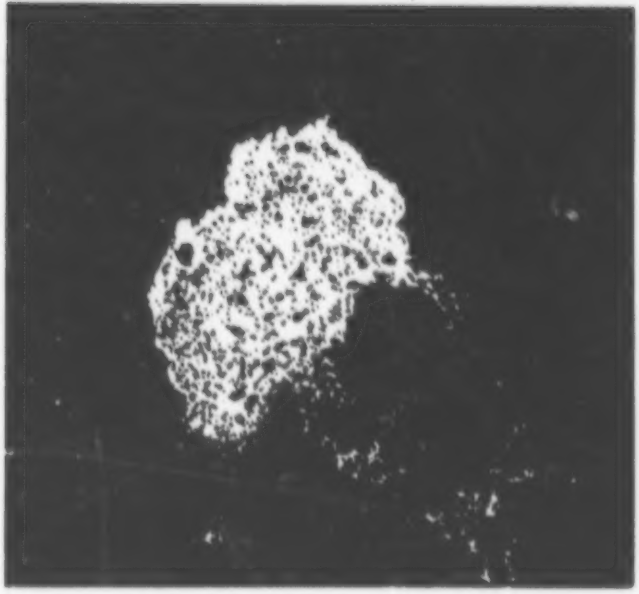

Figure 12: Morphology of the Reaction Products from the In-Flight Magnesiothermic Reduction.

RESULTS AND DISCUSSION FOR CALCIOTHERMIC REDUCTION

Preliminary work was done using the F*A*C*T system on the mainframe computer. Using this program, the thermodynamics of the system were predicted and this gave some direction in which to follow when choosing the starting variables. The results are summarized in Figures 1 to 4. For example, from the F*A*C*T it was determined that the intermetallic metal TiSi would only form at high ratios of titania to silica. Also, the temperature range in which titanium silicide would form was found. Knowing the temperature range for the reaction, the number of kilowatt-hours required to obtain these temperatures, could be calculated. Figure 5 represents a plot which converts kilowatt-hours (energy) into temperature. The theoretical analysis of the system is a very important step which should be performed prior to any experimental analysis.

The effect of energy consumption on the metal product composition is shown in Figure 6. Because the objective is to form the intermetallic alloy TiSi, the energy input which would produce a 1:1 molar ratio of titanium to silicon, was sought. From this graph we can clearly see that the optimum energy input to achieve this is 3 KWH. Above this critical value it can be seen that the ratio of titanium to silicon increases quickly and deviates from the required ratio.

The effect of the calcium additions on the metal product composition is shown in Figure 7. This graph illustrates that a relatively constant composition of the metal product results. At the six mole point it can be seen that the 1:1 ratio is almost achieved. This graph represents the composition of the metal product. It may therefore appear that the amount of calcium introduced into the system is not of great importance. By varying the amount of calcium added into the system, it was found that although the metal product composition remained fairly constant, the amount of metal product had varied. When the calcium content became to high, calcium silicides formed and thereby reduced the amount of titanium silicide produced. It was found that between 3-6 moles the greatest amount of TiSi would be formed.

Figure 8 shows the effect of the titania to silica ratio on the metal product composition. By visual inspection it can be seen that the desired 1:1 ratio of titanium to silicon occurs at .16. This indicates that the intermetallic metal TiSi will only form if the reactant powders are mixed at a 6:1, silica:titania molar ratio. Above this critical ratio, the composition of the metal product indicates a product other than TiSi is present.

The effect of the alumina additions on the metal product composition are shown in Figure 9. The alumina was added to the reactants as a fluxing agent and to promote the formation of TiSi. It appears from this graph that only small amounts of alumina are required to accomplish this. As the amount of alumina is increased the composition of the metal product appears to deviate from the ideal composition 1:1, Ti:Si. It can also be seen from this graph that the amount of aluminum in the final metal product is quite low.

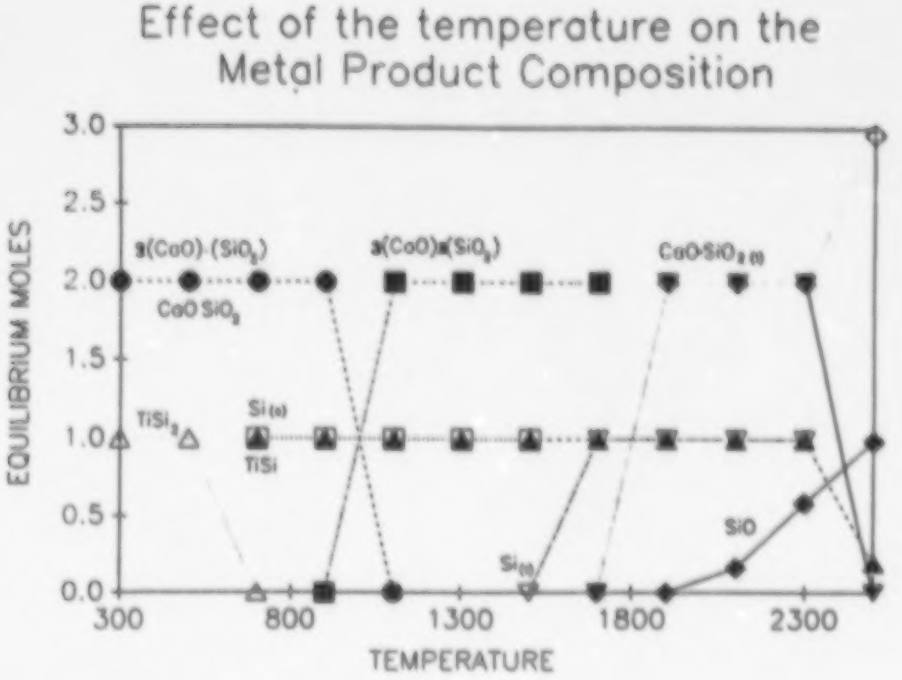

Figure 1: The Effect of Temperature on the Product Composition as Calculated by F*A*C*T.

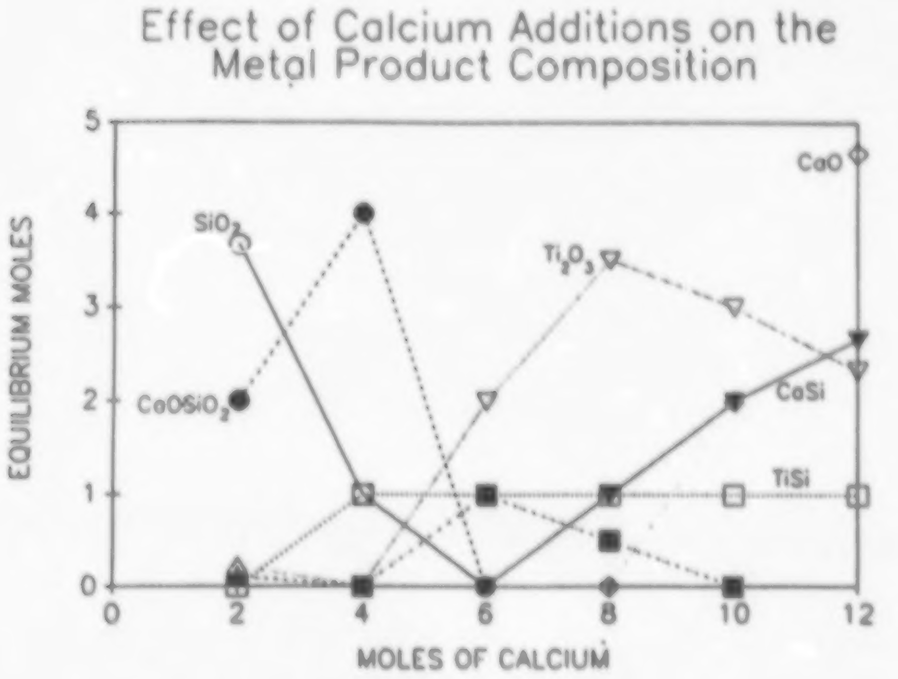

Figure 2: The Effect of Calcium Additions on the Product Composition as Calculated by F*A*C*T.

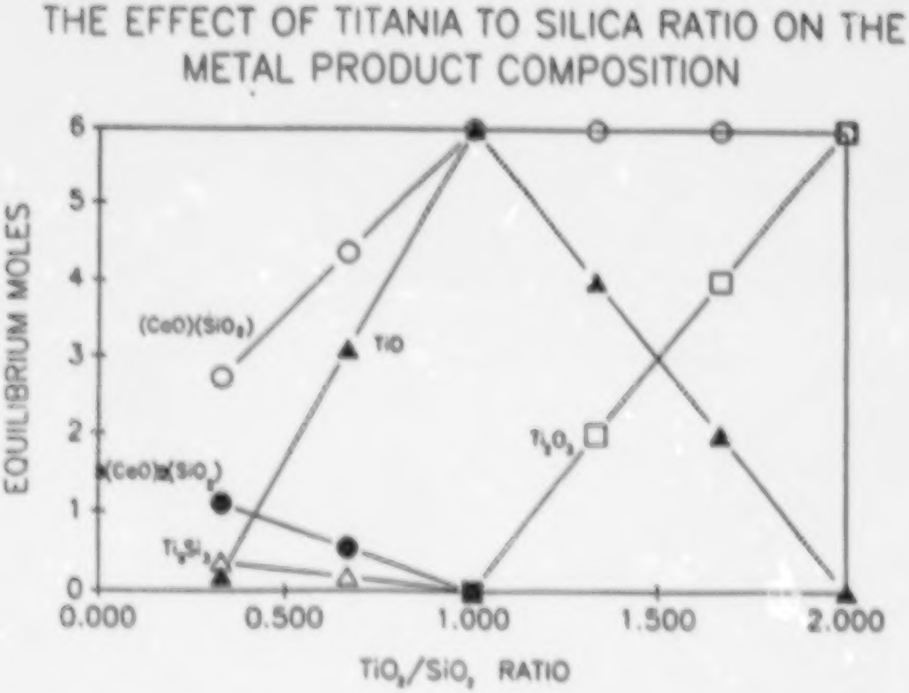

Figure 3: The Effect of Titania to Silica Ratio on the Product Composition as Calculated by F*A*C*T.

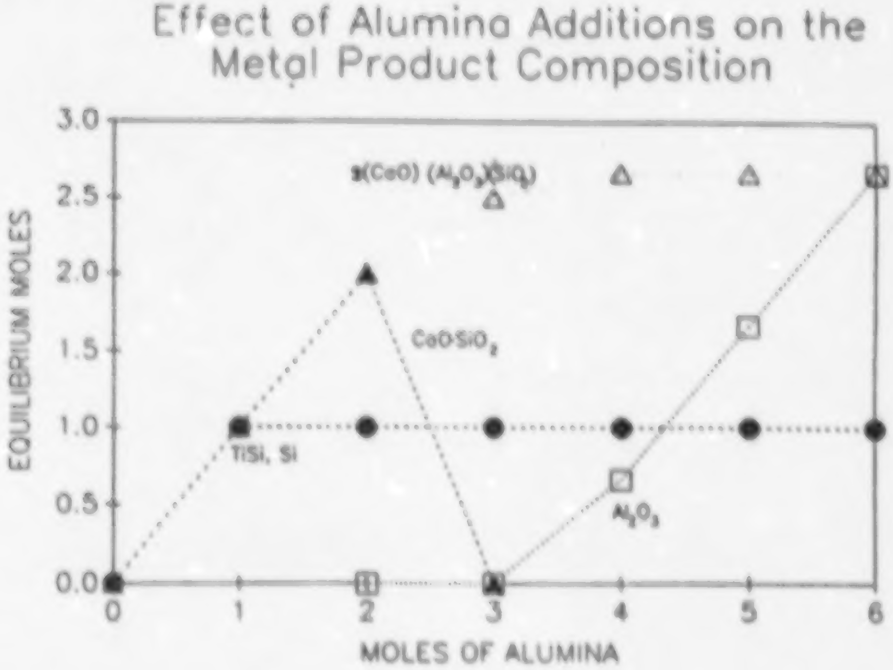

Figure 4: The Effect of Alumina Additions on the Product Composition as Calculated by F*A*C*T.

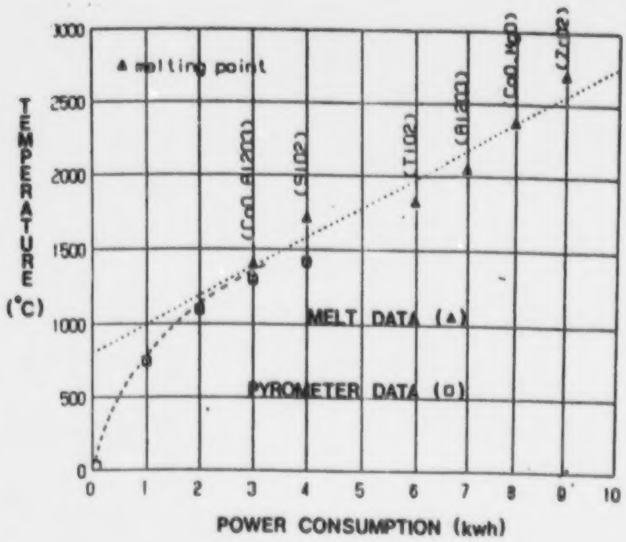

Figure 5: The Effect of Energy Consumption on the Crucible Temperature.

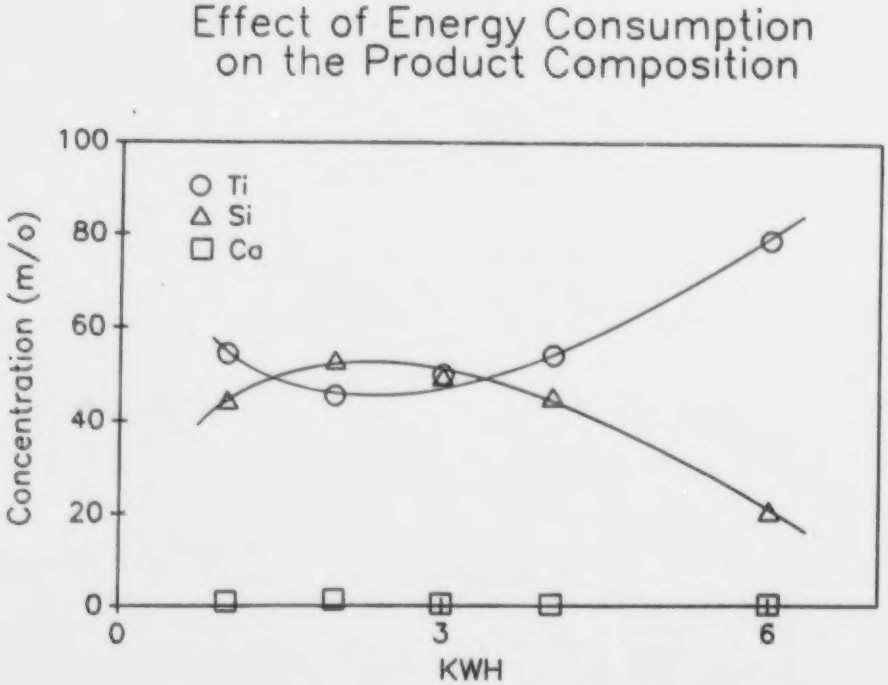

Figure 6: The Effect of Energy Consumption on the Product Composition.

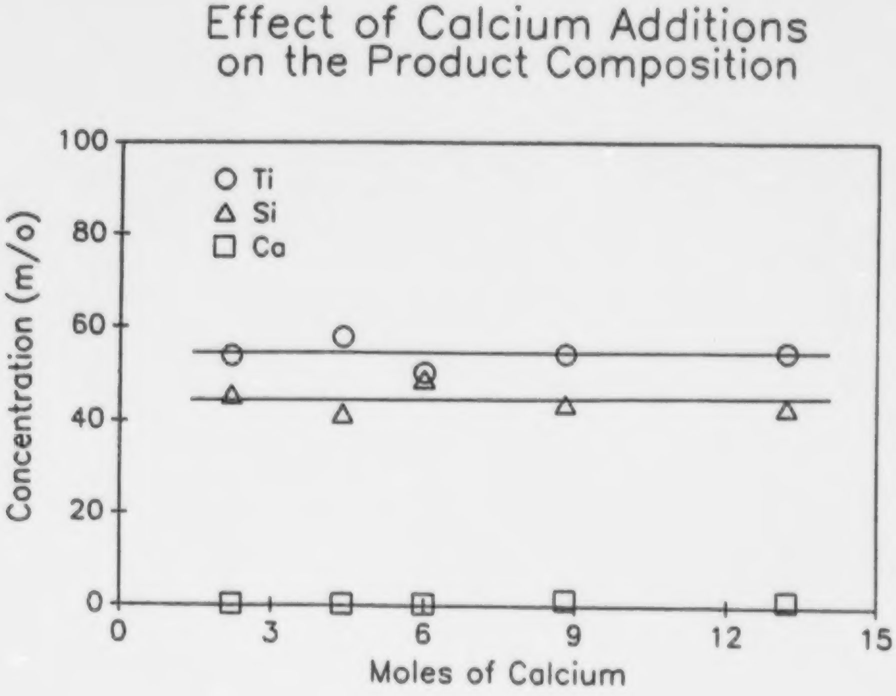

Figure 7: The Effect of Calcium Additions on the Product Composition.

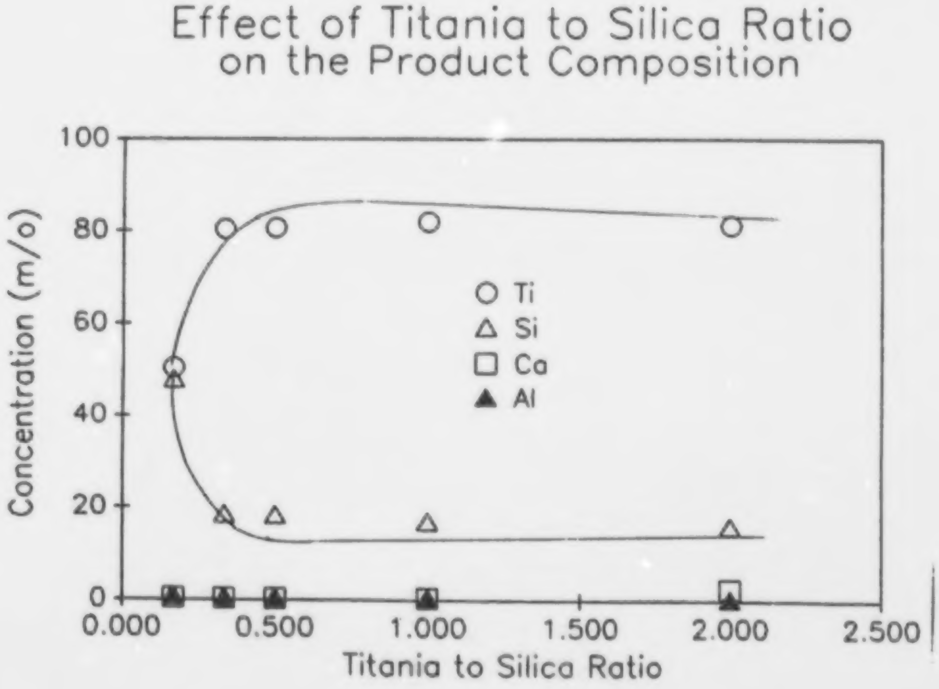

Figure 8: The Effect of Titania to Silica Ratio on the Product Composition.

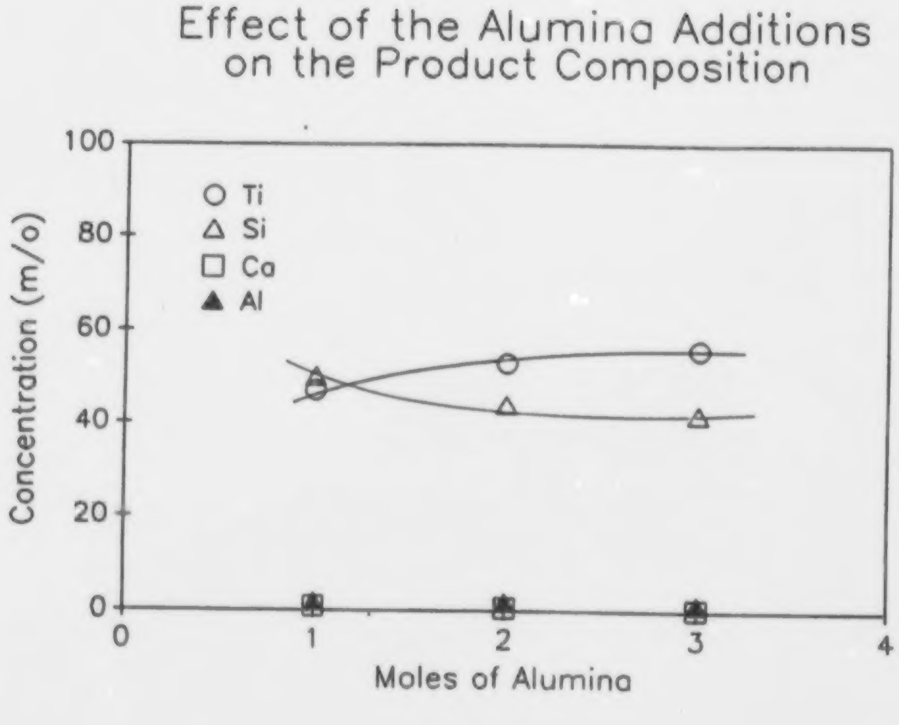

Figure 9: The Effect of Alumina Additions on the Product Composition.

RECOVERY OF TITANIUM SILICIDES FROM A COPPER MELT

In these tests titanium silicide was grown by precipitation from a copper melt. The titanium silicide was then recovered by selectively leaching the copper. The starting mixture consisted of 0.98g of -200 mesh reagent grade titanium, 1.16g of -150 + 325 mesh reagent grade silicon and 2.01g of -65 + 100 mesh electrolytically purified copper. The powders were mixed and placed into a fireclay combustion boat in a resistance tube furnace at 1200°C in an argon atmosphere. To ensure homogenization the sample was held in the furnace at temperature for about six hours. Then, the melt was allowed to furnace cool. About twelve runs were performed in order to provide enough samples for the subsequent leaching experiments. The solidified samples, which were relatively brittle were crushed and ground in a mortar and pestle. Then, the particulates were screened into various size fractions in preparation for the leaching tests. The variables studied in the leaching were as follows:

(1) leaching acid concentration

(2) particle size

(3) stirring, and

(4) temperature.

The conditions employed in the experiments are summarized in Table I.

SAMPLE NUMBER	MESH SIZE	ACID CONC. (molar)	TEMPERATURE (^{o}C)	STIRRED	INITIAL SAMPLE WEIGHT (g)	FINAL SAMPLE WEIGHT (g)
1	-35+65	1	25	NO	2.004	1.124
2	-35+65	2	25	NO	2.005	0.929
3	-35+65	4	25	NO	2.001	0.966
4	-20+35	2	25	NO	2.110	1.013
5	-35+65	4*	25	NO	1.960	0.924
6	-35+65	2	59	NO	2.026	0.997
7	-20+35	2	25	YES	2.109	0.959
8	-65+100	2	25	NO	2.207	1.022
9	-100+150	2	25	NO	1.890	0.844
10	-150	2	25	NO	2.225	0.980
11	-150	1	25	NO	2.273	0.884

* leach solution was used for one hour and then was replaced by a fresh 4 molar leach solution for the rest of the leach test.

TABLE I: Leaching Schedule

For each leaching experiment 500 ml of nitric acid solution, of the desired concentration (1,2 or 4 molar) were prepared from stock nitric acid (Anachemica reagent, assay 69.0 - 71.0% nitric acid). The leach solution was then placed into a 500 ml beaker at the appropriate temperature. An accurately weighed sample of the copper containing titanium silicide was added to the solution and the experiment was started. At the appropriate time intervals 5ml samples were pipetted from the solution and stored for analysis. The samples were analysed for copper by atomic absorption (A.A.). After the leaching experiment was completed the residue was filtered, washed, dried and weighed. These samples were analysed by x-ray diffraction, energy dispersive x-ray spectroscopy, scanning electron microscopy and optical microscopy.

RESULTS AND DISCUSSION

In hydrometallurgical systems, it is well known that the leaching process occurs in three steps:

(a) the diffusion of reactants through a solid product or aqueous boundary layer to the reaction interface,

(b) the chemical or surface reaction, and

(c) the diffusion of soluble products away from the reaction interface.

For the case of diffusion control it has been shown that:

$$1 - \frac{2}{3}\alpha - (1-\alpha)^{2/3} = \frac{2VDC_Bt}{r_o}$$

Where r_o is the initial radius of the particle (assuming spherical).

t is the time.

C_B is the bulk concentration of the aqueous reagent.

D is the diffusion coefficient of the solid species which is dissolving

V is the volume of the reactant dissolved during the leaching process.

From equation (1) it can be seen that if diffusion is the rate determining step then a plot of $1 - \frac{2\alpha}{3} (1-\alpha)^{2/3}$ versus time will yield a straight line of slope S.

Where $S = \frac{2VDC_B}{r_o}$

On the other hand, if the surface reaction is rate-limiting then it can be shown that

$$[1-(1-\alpha)^{1/3}] = \frac{Vk'C_Bt}{r_o}$$

Where k' is a rate constant. In this case, a plot of $[1-(1-\alpha)^{1/3}]$ versus time will yield a straight line with slope S' where $S' = \frac{Vk'C_B}{r_o}$.

The effect of nitric acid concentration on the rate of dissolution of copper is shown in Figures 1 and 2. An increase in concentration resulted in an increase in the rate of dissolution. This can be attributed to the steeper concentration gradient of reactants around the particle.

Figure 3 demonstrates that the rate of dissolution increases with decreasing particle size. At extended times and fine particle sizes there is no significant increase in dissolution rate with decreasing particle size.

Stirring had no significant effect on the dissolution rate - Figure 4. Also the addition of fresh leach solution during one of the experiments had an insignificant effect on the reaction rate Figure 5. These results would indicate that, under the present experimental conditions, the reaction is surface controlled rather than diffusion controlled. Linear regression testing of the surface reaction model and the diffusion models confirmed that the copper dissolution was controlled by the surface reaction Figures 6 to 16. However, for very fine particle sizes and for extended leaching times diffusion will play a role.

Temperature had a dramatic effect on the rate of reaction. As shown in Figure 17 it was possible to achieve almost total removal of the copper at a leach temperature of $59^{\circ}C$ in 100 minutes as compared to about 800 minutes for the sample leached at room temperature.

Scanning electron microscope analysis of the products is shown in Figure 18. In general, the Ti to Si ratio of the products varied between 1 to 1 and 2 to 1 with some small traces of copper. The titanium silicide products had a high degree of porosity. This structure would support the kinetic models proposed in the leaching experiments. At the later stages of the leaching process diffusion would become more important as there is no longer any free copper available and the copper must diffuse out of the titanium silicide particle. X-ray analyses of the leached products showed that the major constituents were $TiSi_2$, $TiSi$ and $Cu_{0.1}Si_{1.9}Ti$.

Effect of Nitric Acid Concentration

Figure 1

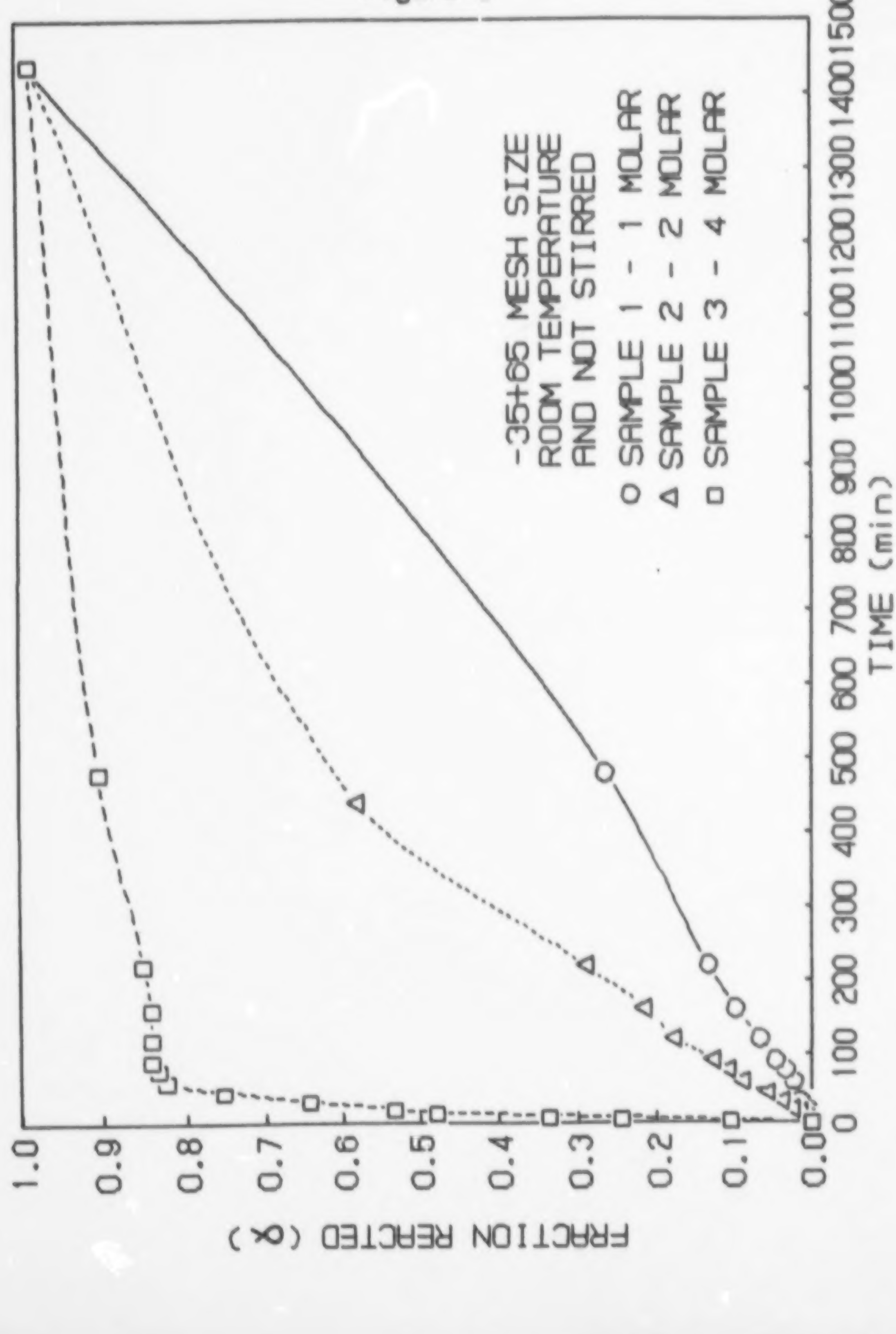

Effect of Nitric Acid Concentration

Figure 2

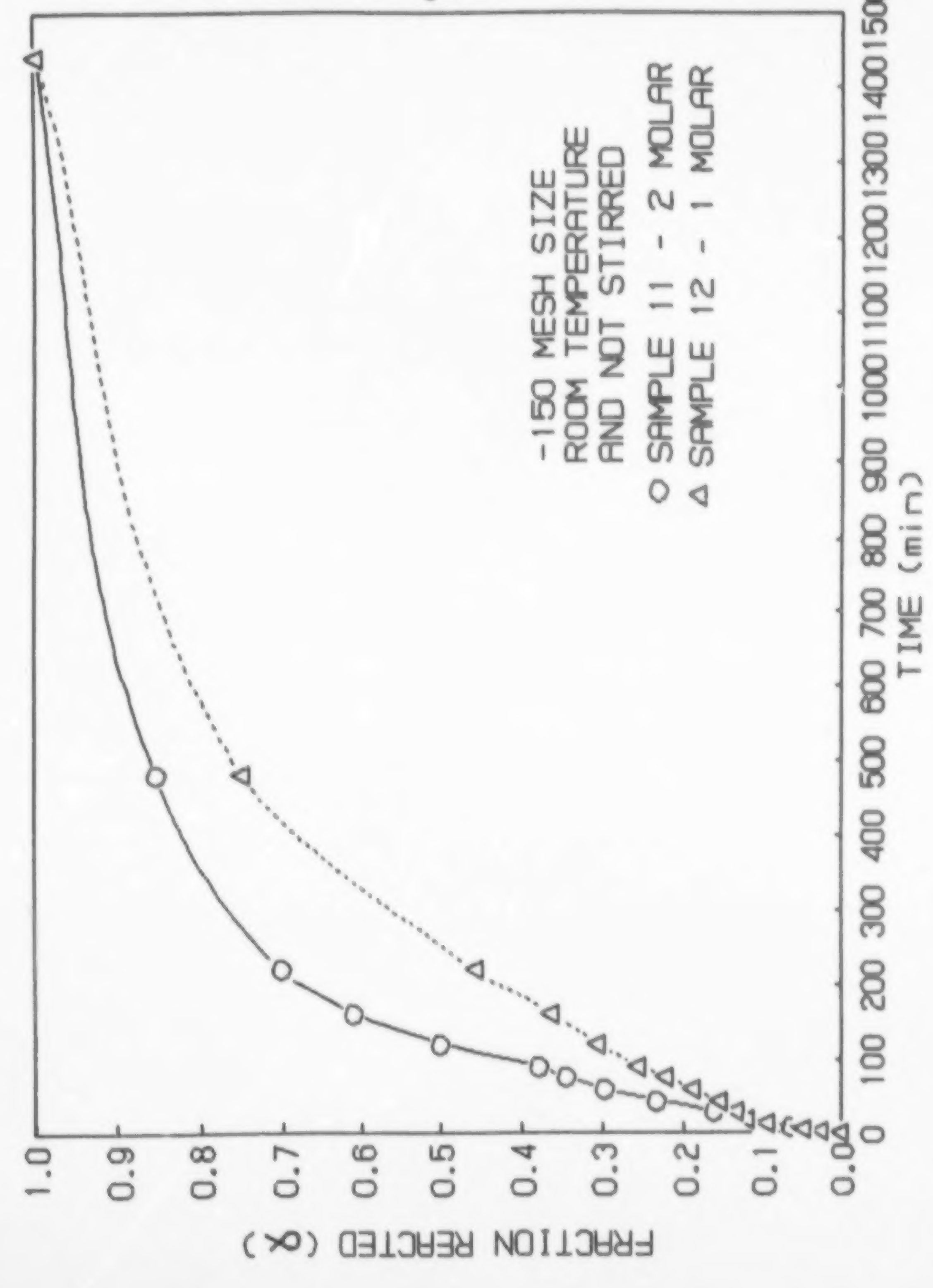

Effect of Particle Size

Figure 3

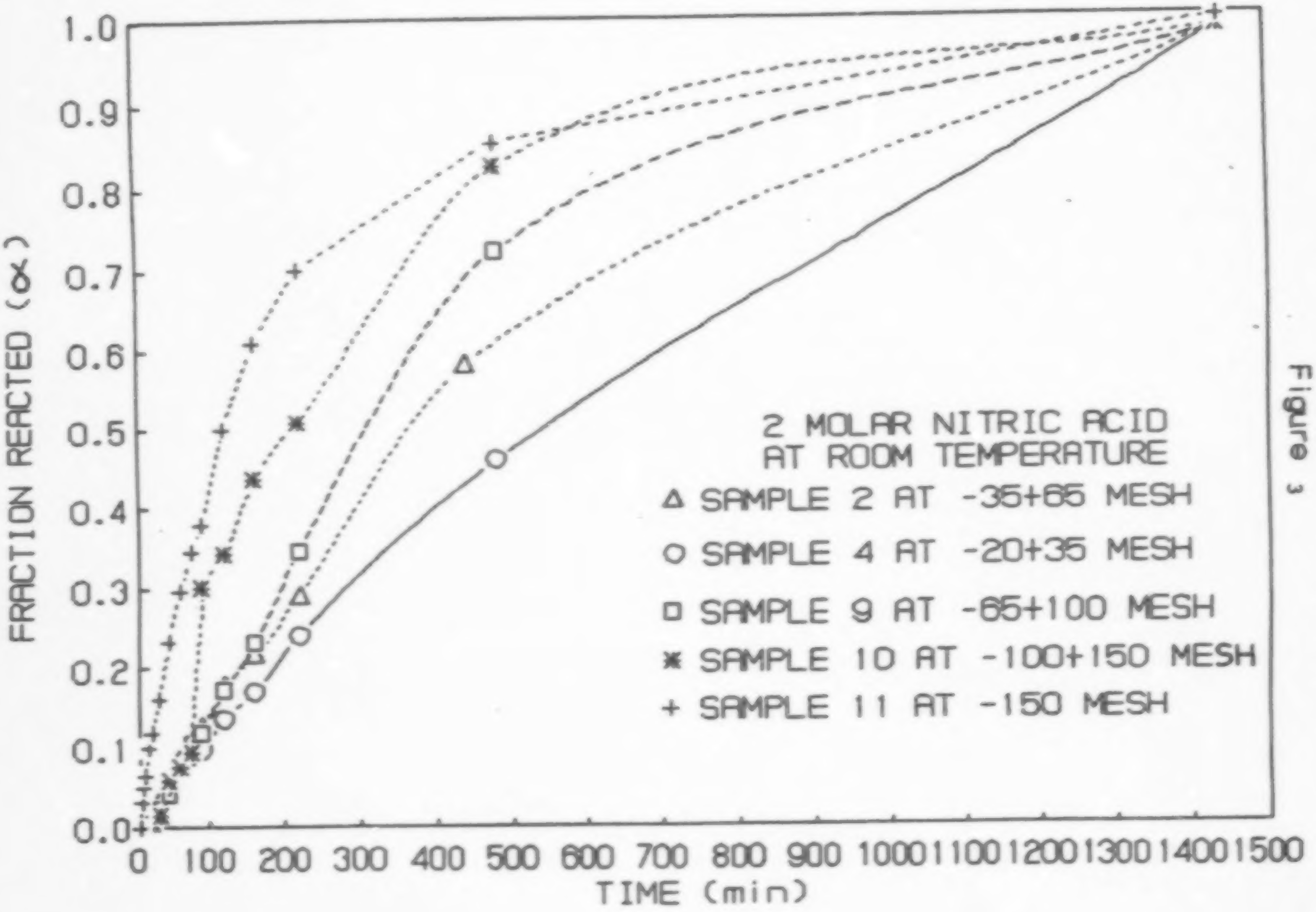

Effect of Stirring

Figure 4

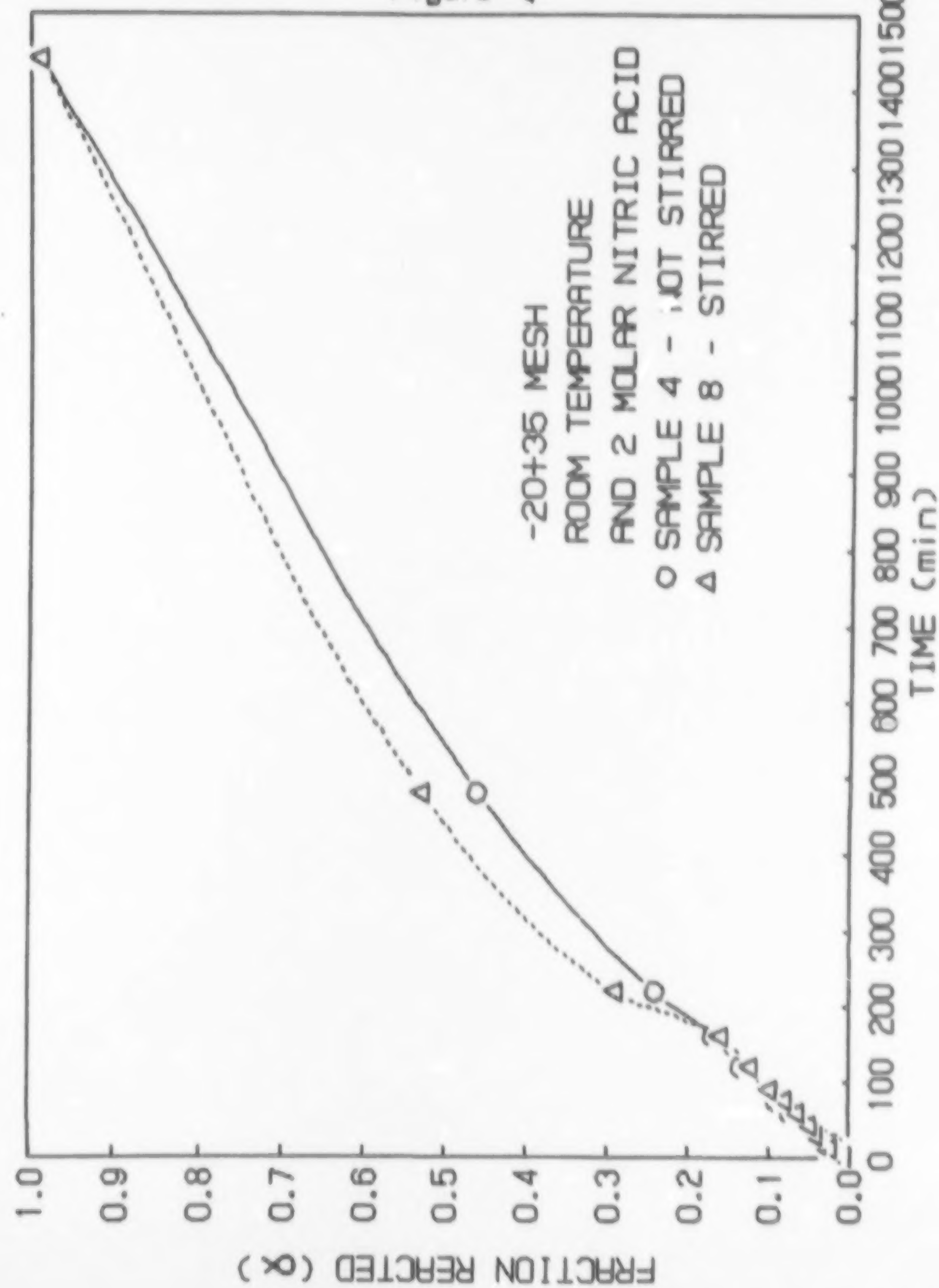

Effect of Renewing Nitric Acid Solution After One Hour

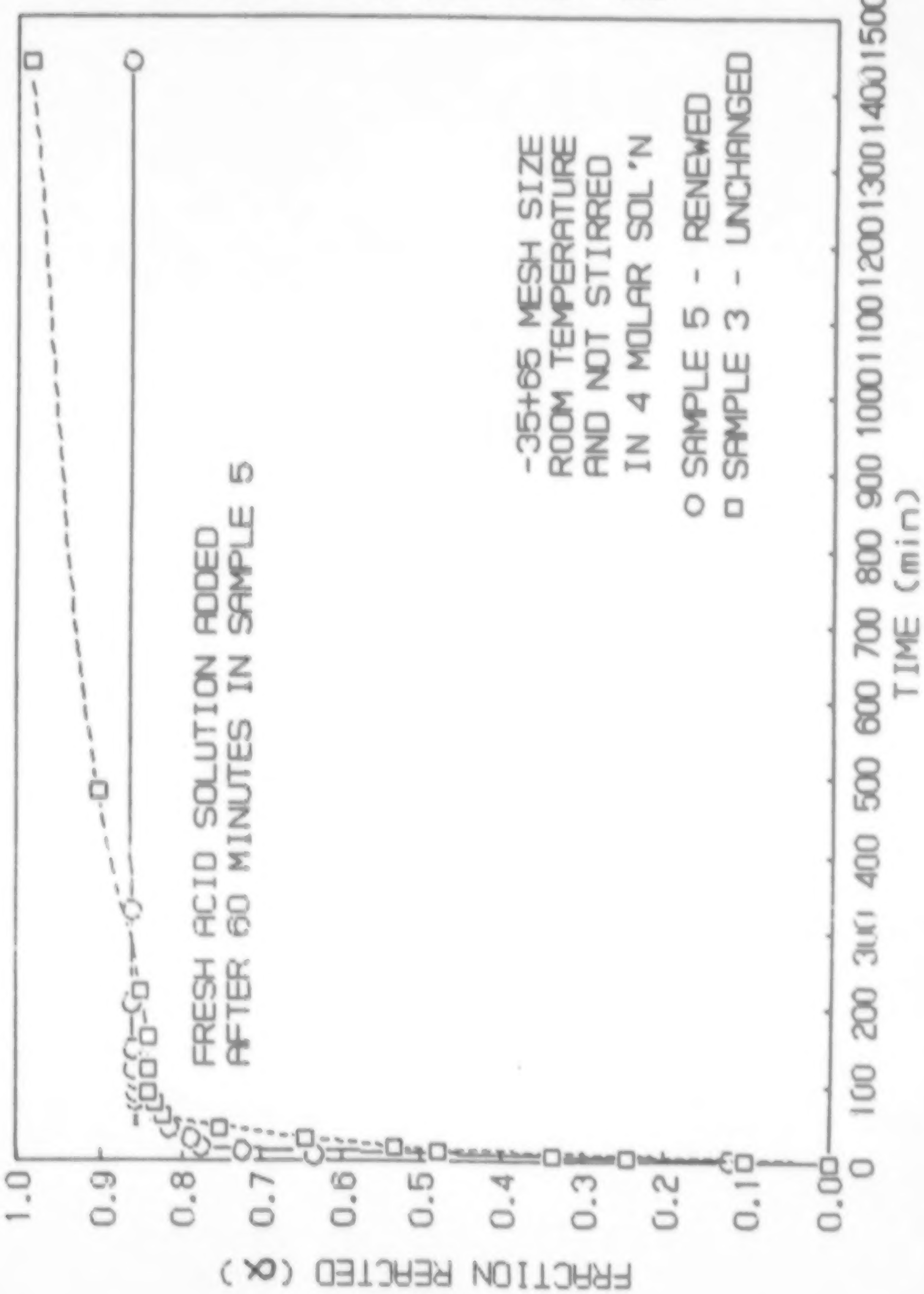

Figure 5

Linear Regression Testing of the Surface and Diffusion Reaction Models

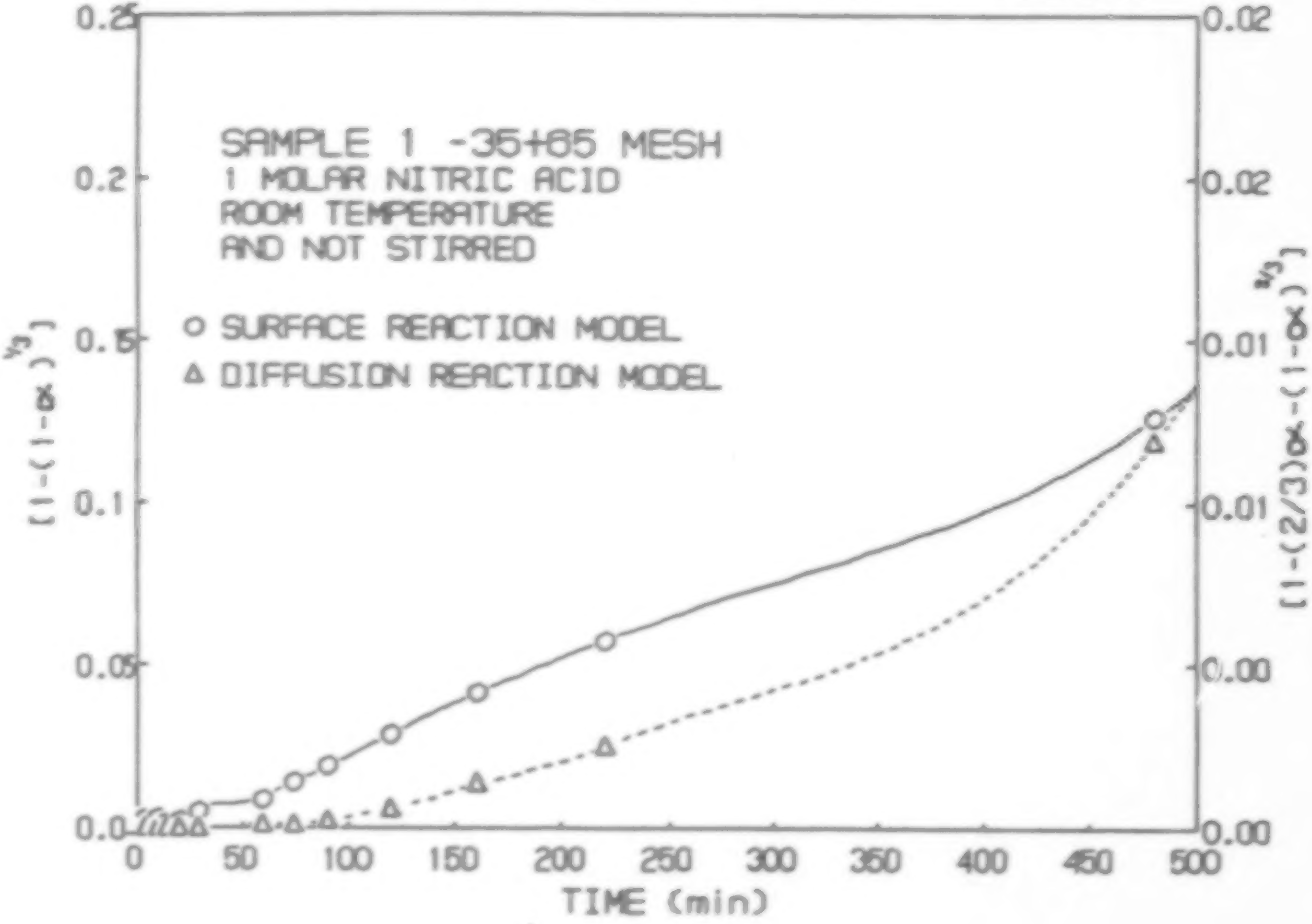

Figure 6

Linear Regression Testing of the Surface and Diffusion Reaction Models

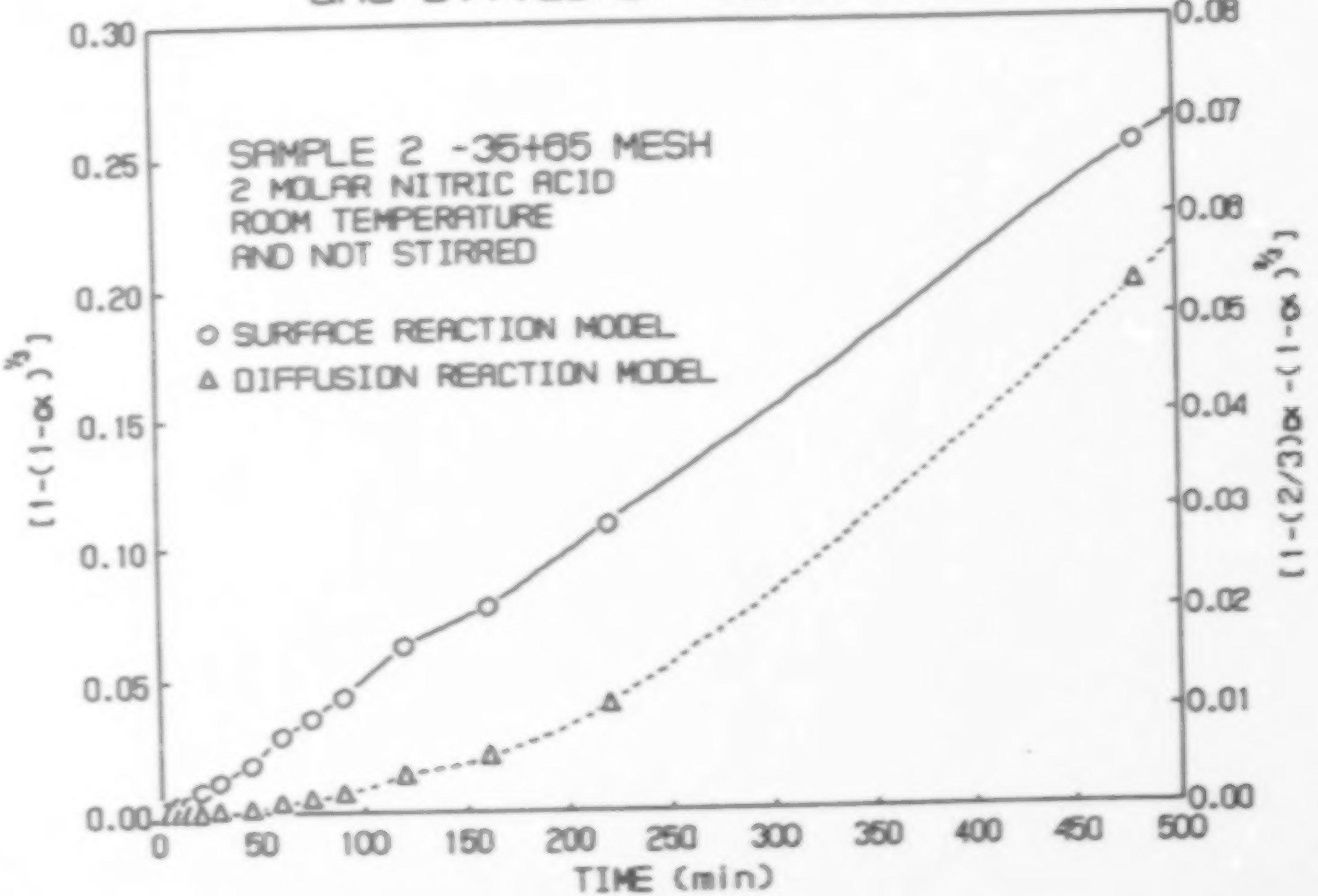

Figure 7

Linear Regression Testing of the Surface and Diffusion Reaction Models

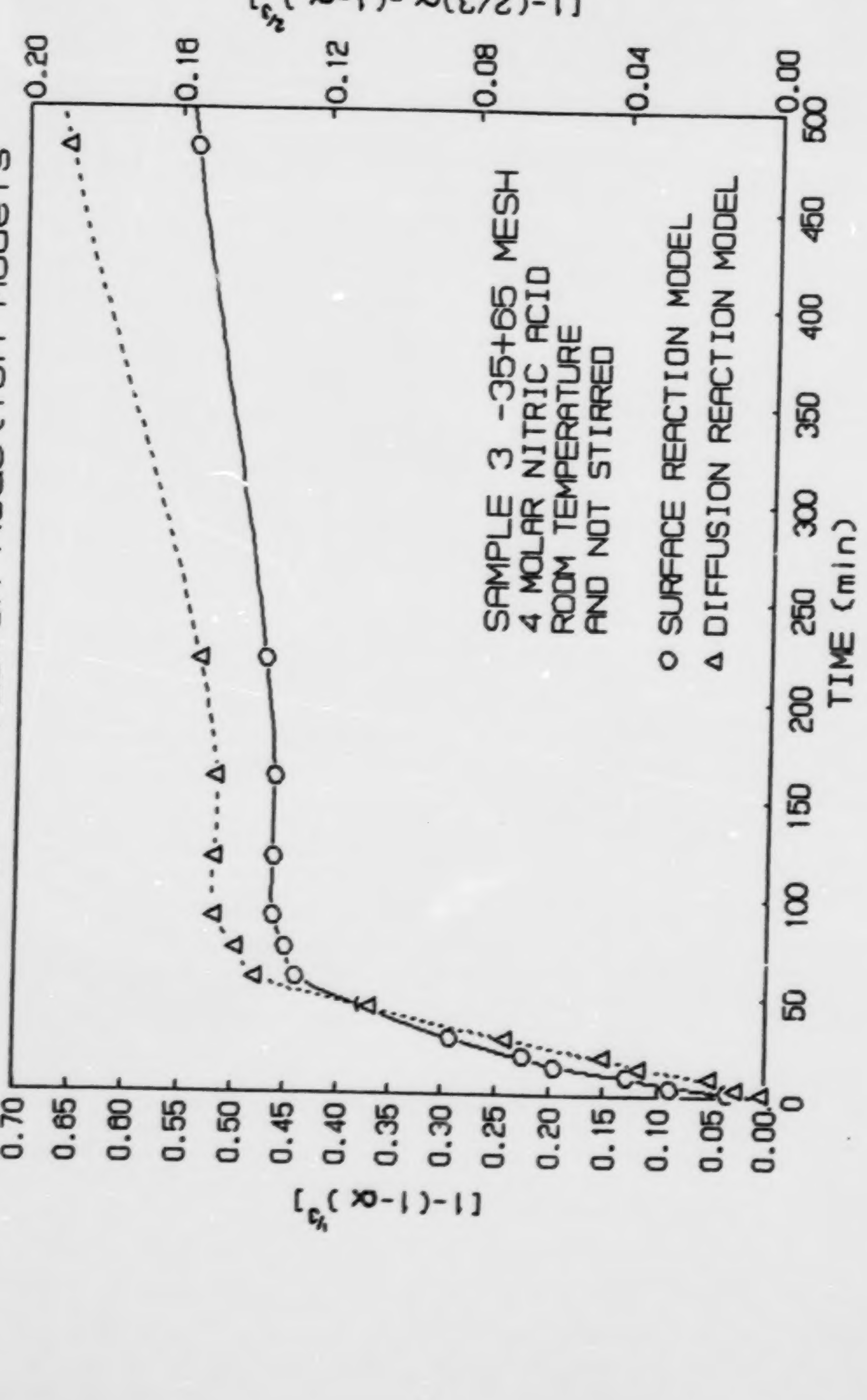

Figure 8

Linear Regression Testing of the Surface and Diffusion Reaction Models

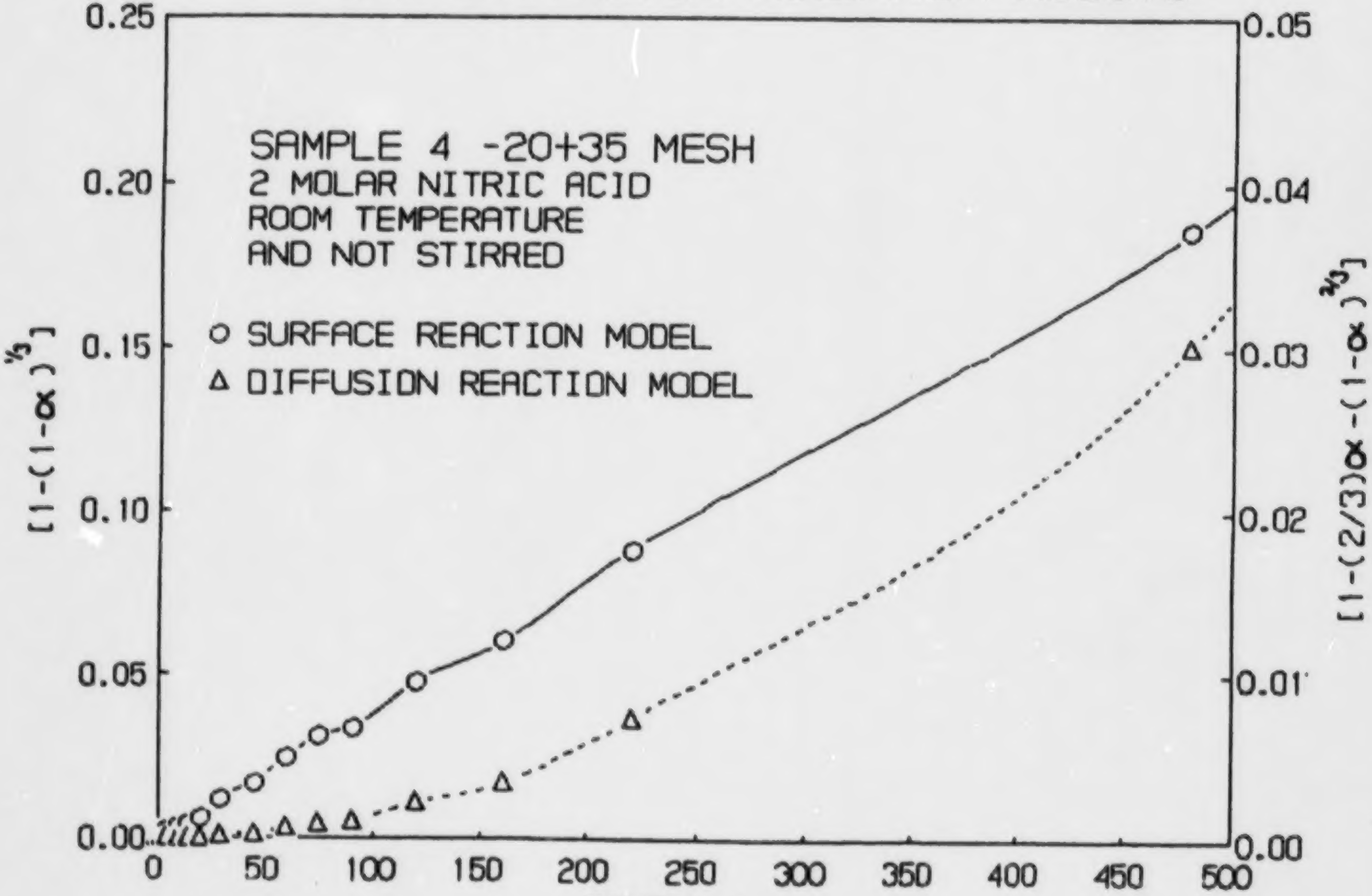

Figure 9

Linear Regression Testing of the Surface and Diffusion Reaction Models

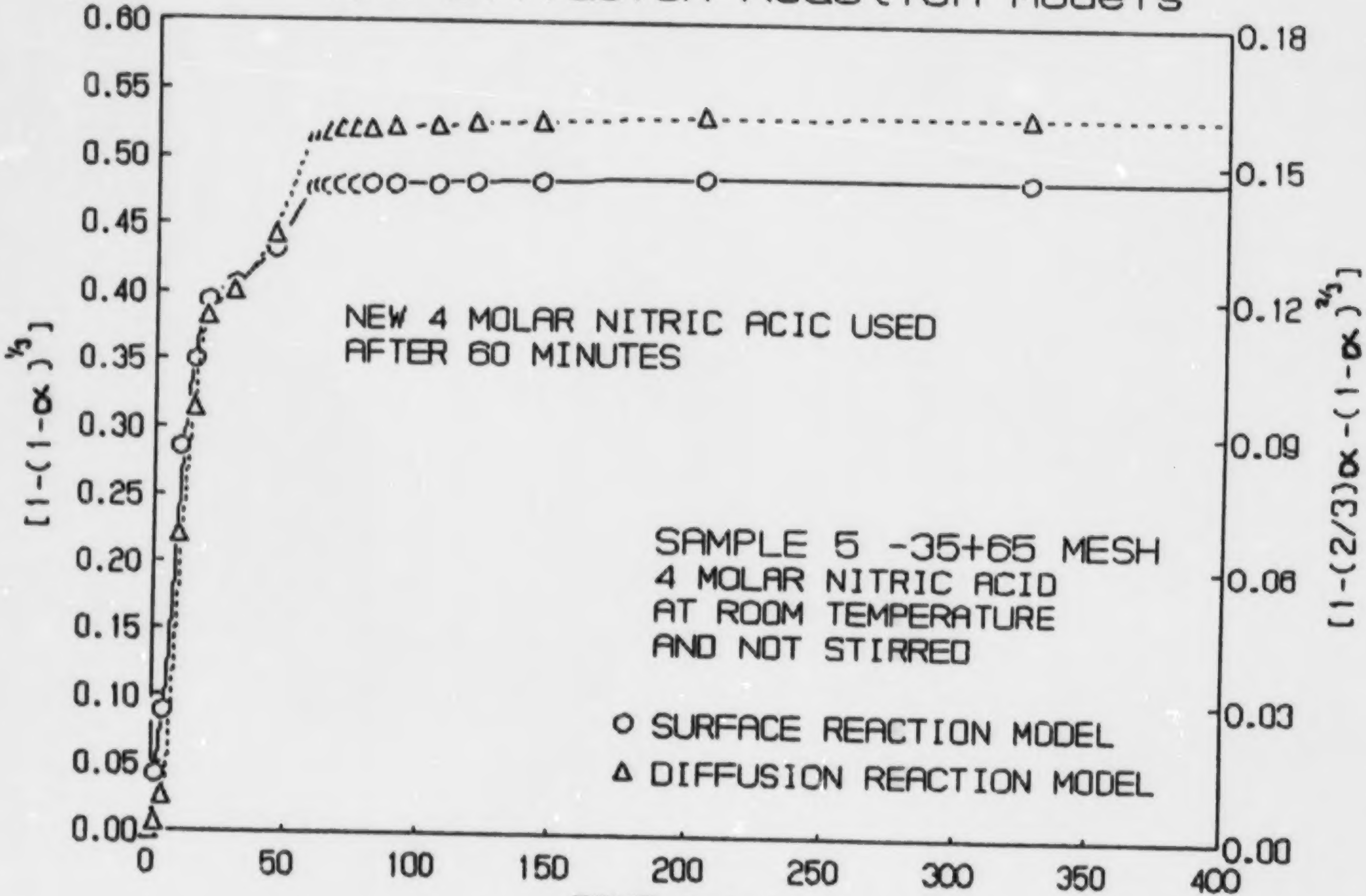

Figure 10

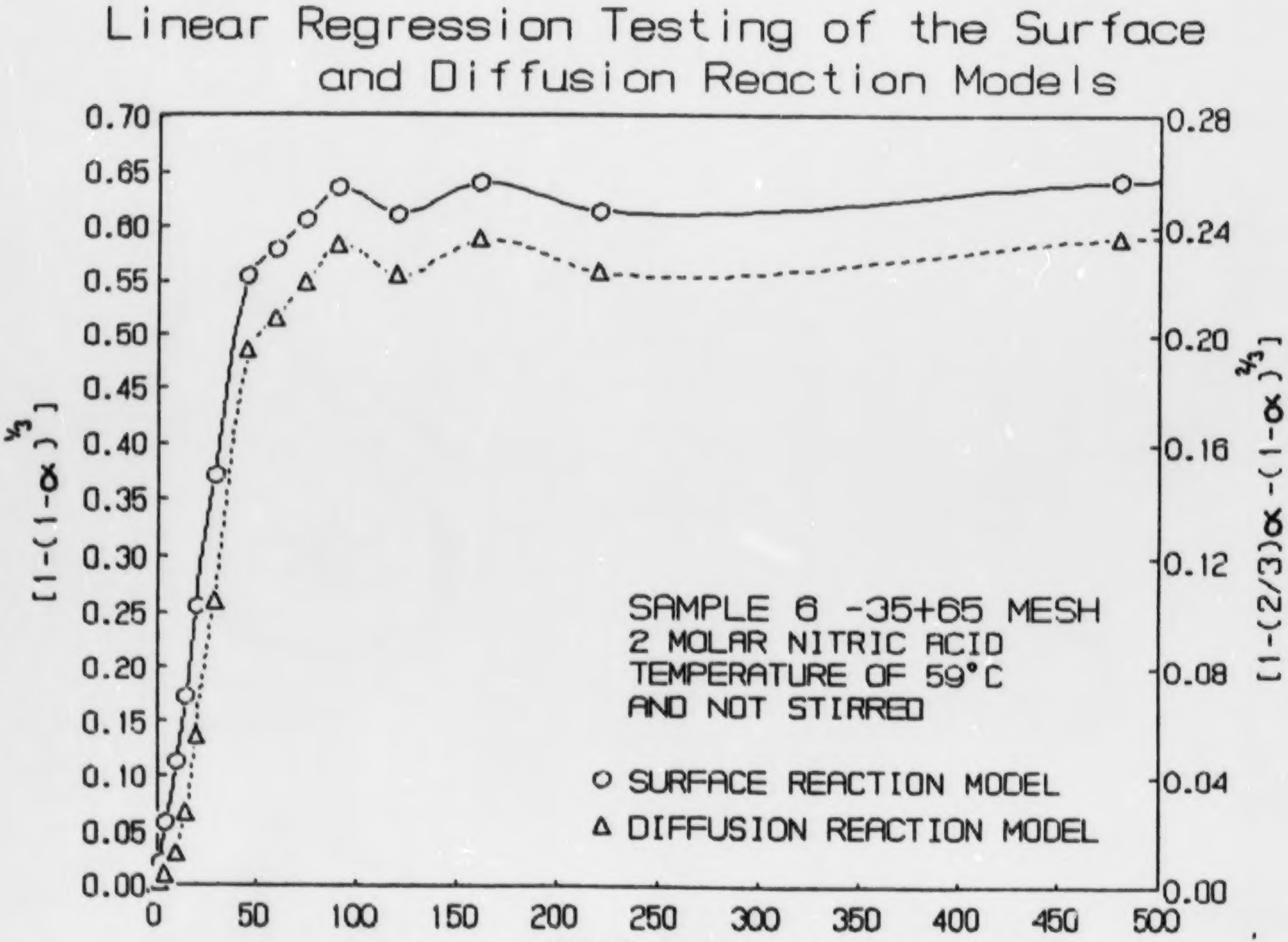
Linear Regression Testing of the Surface and Diffusion Reaction Models
0.70
0.65
0.60
0.55
0.50
0.45
0.40
0.35
0.30
0.25
0.20
0.15
0.10
0.05
0.00
$[1-(1-\alpha)^{1/3}]$
0.28
0.24
0.20
0.16
0.12
0.08
0.04
0.00
$[1-(2/3)\alpha-(1-\alpha)^{2/3}]$
0
50
100
150
200
250
300
350
400
450
500
TIME (min)
SAMPLE 6 -35+65 MESH
2 MOLAR NITRIC ACID
TEMPERATURE OF 59°C
AND NOT STIRRED
○ SURFACE REACTION MODEL
△ DIFFUSION REACTION MODEL

Figure 11

Linear Regression Testing of the Surface and Diffusion Reaction Models

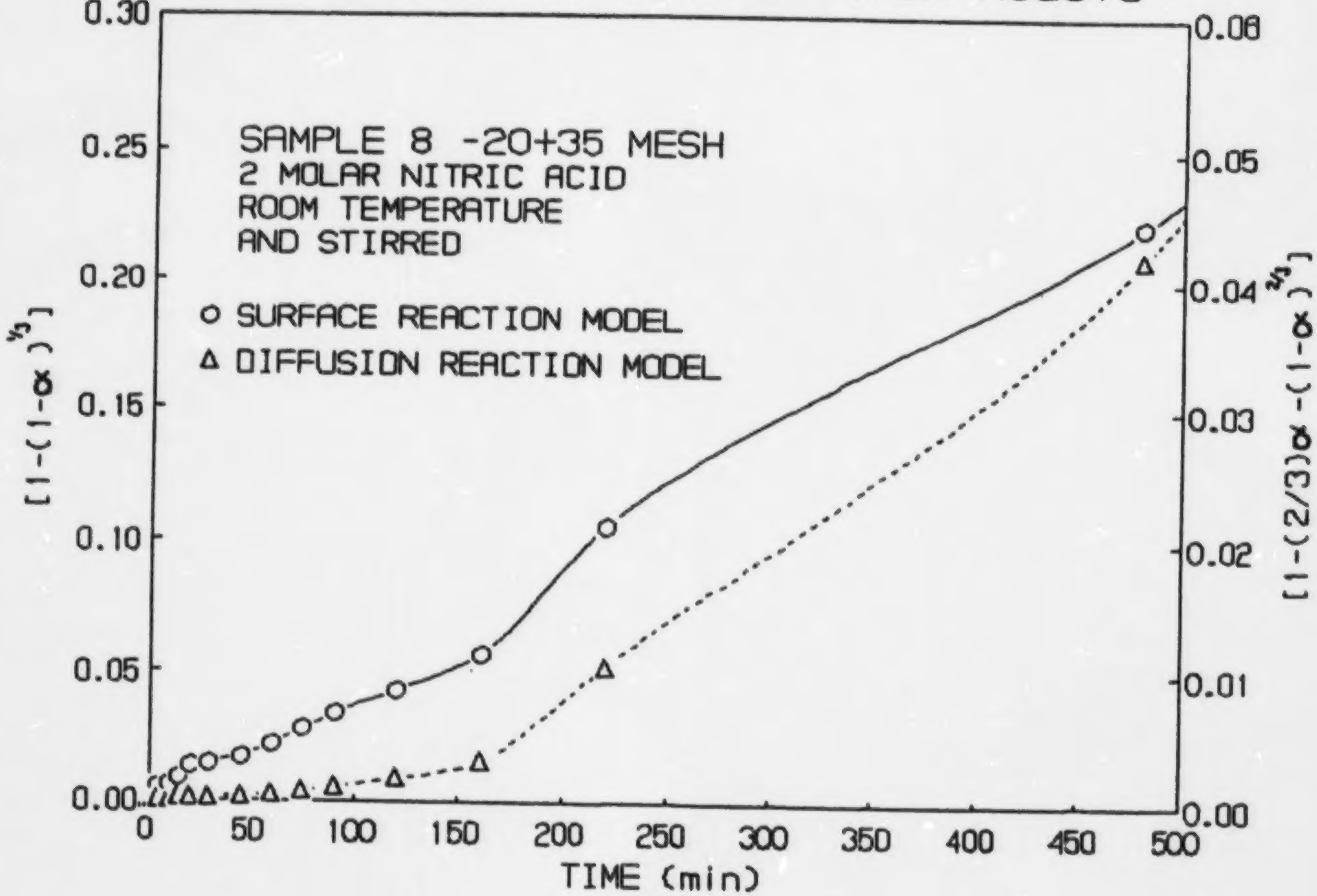

Figure 12

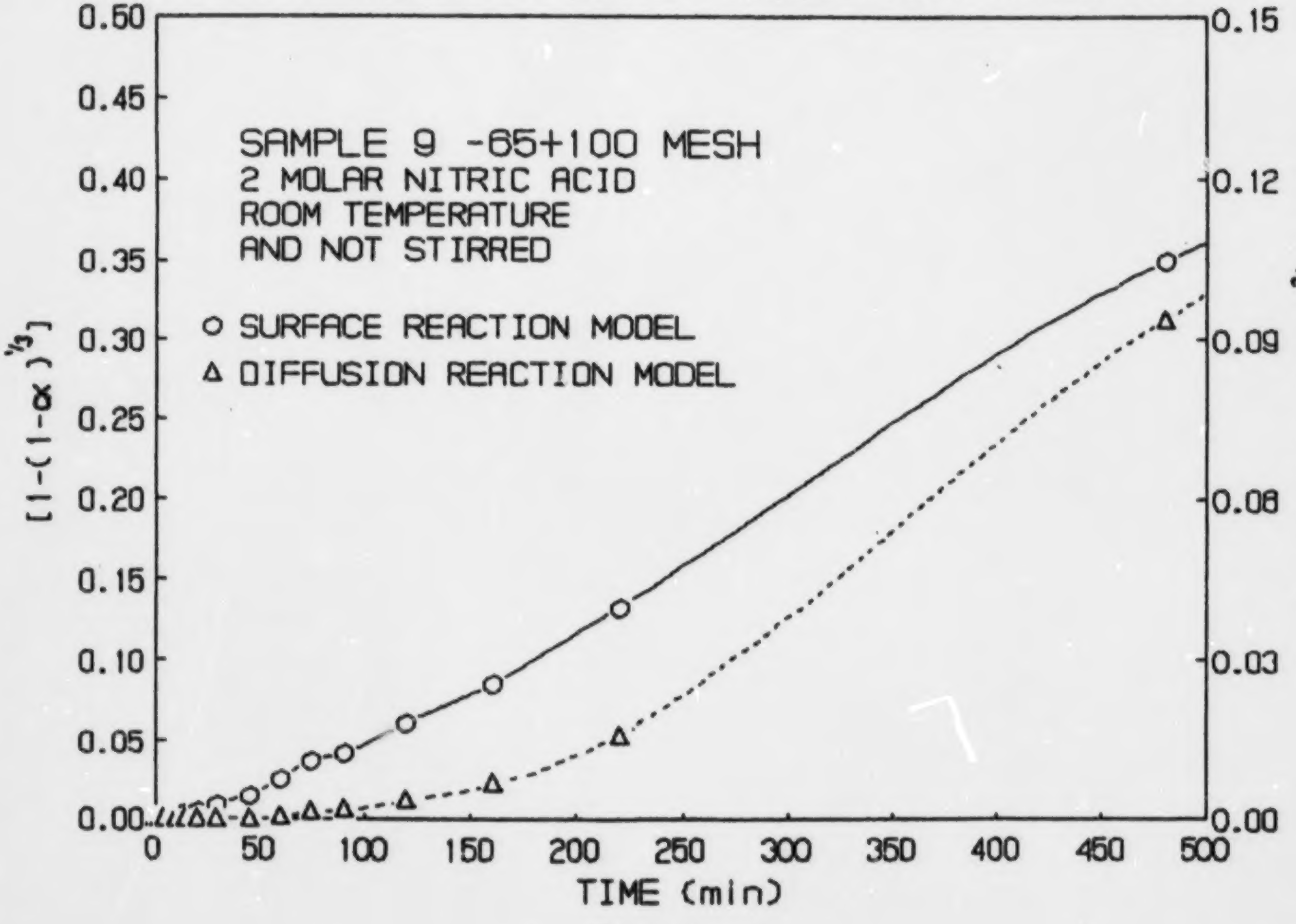

Linear Regression Testing of the Surface and Diffusion Reaction Models

Figure 13

Linear Regression Testing of the Surface and Diffusion Reaction Models

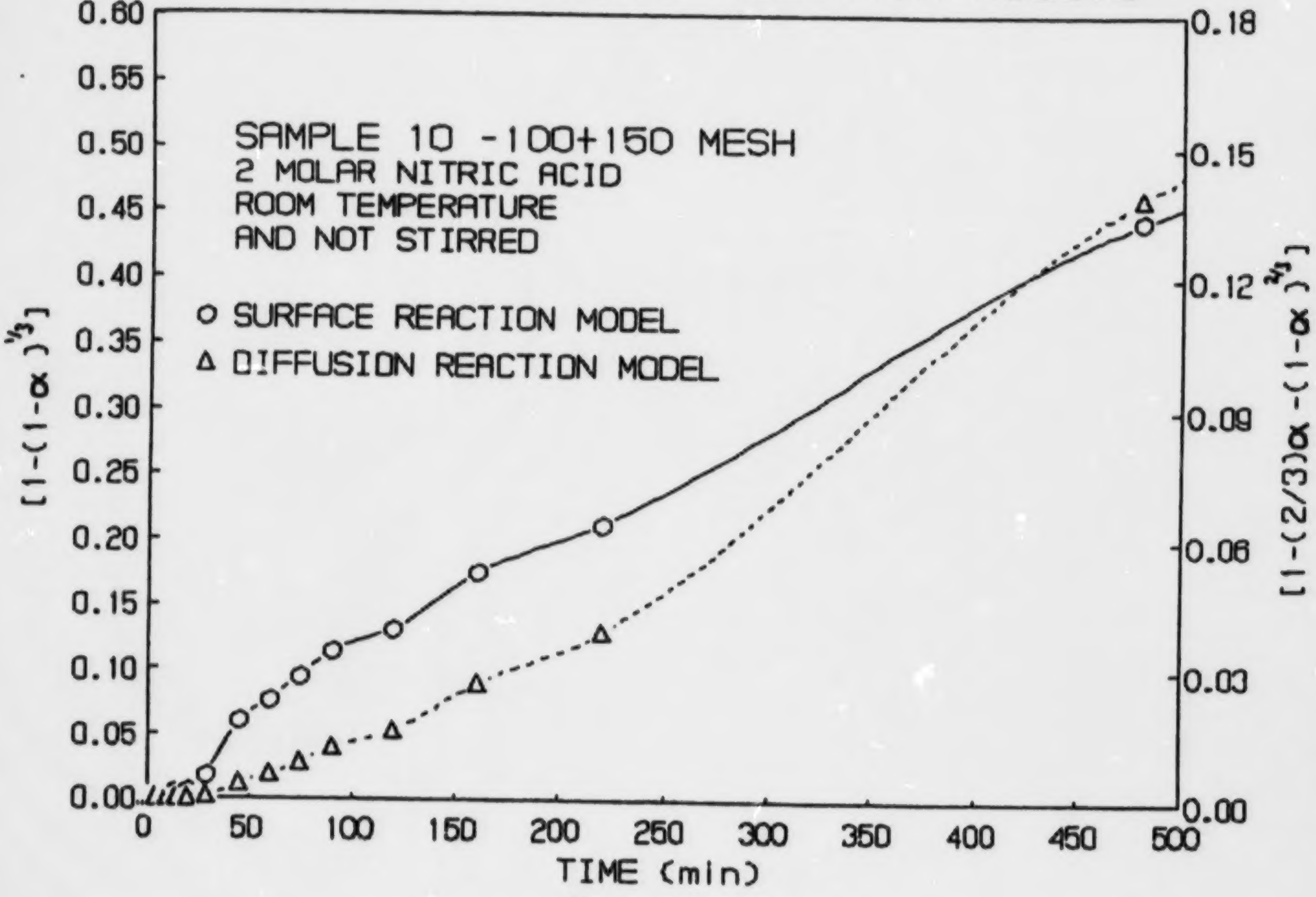

Figure 14

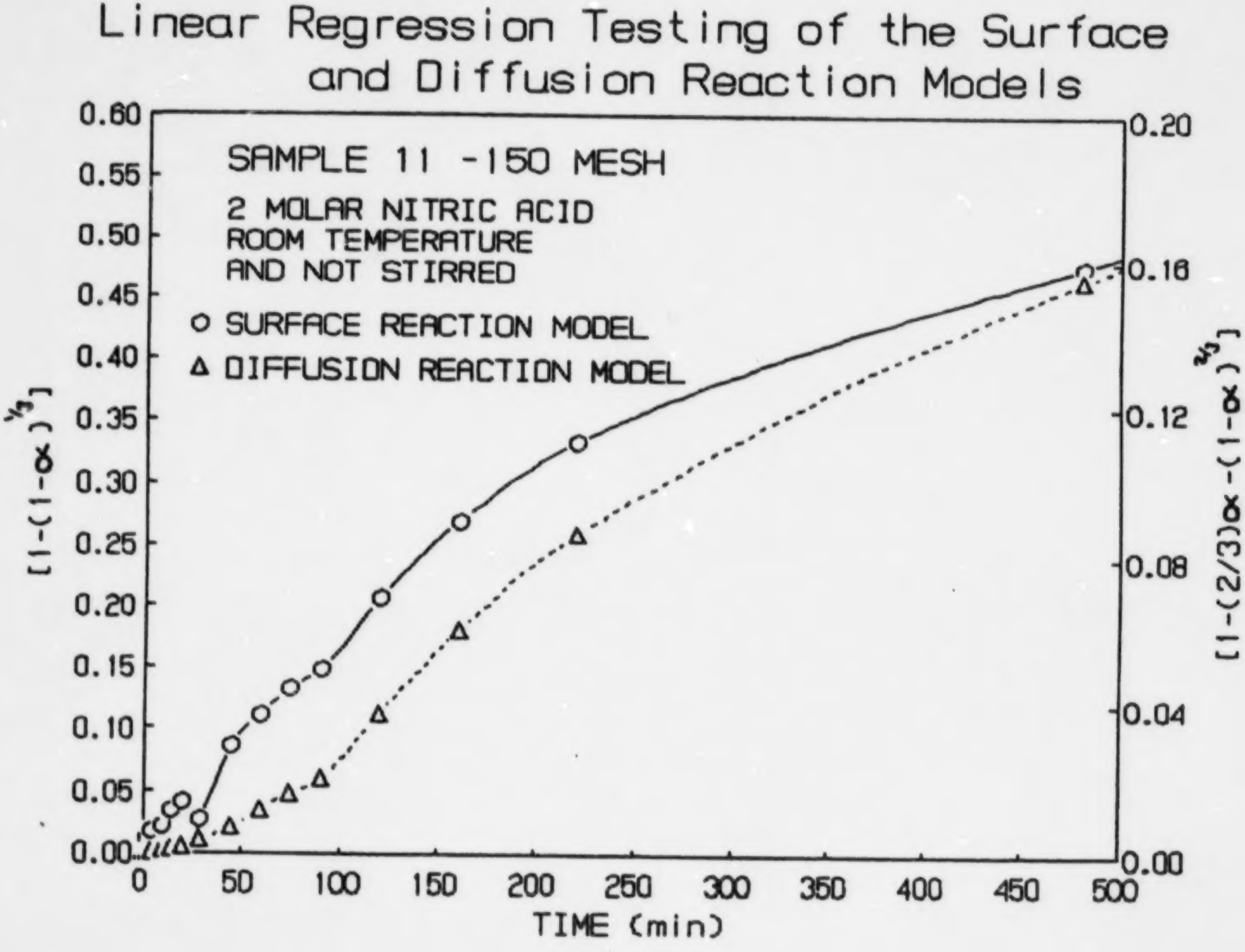
Linear Regression Testing of the Surface and Diffusion Reaction Models
SAMPLE 11 -150 MESH
2 MOLAR NITRIC ACID
ROOM TEMPERATURE
AND NOT STIRRED
○ SURFACE REACTION MODEL
△ DIFFUSION REACTION MODEL
$[1-(1-\alpha)^{1/3}]$
0.00
0.05
0.10
0.15
0.20
0.25
0.30
0.35
0.40
0.45
0.50
0.55
0.60
$[1-(2/3)\alpha-(1-\alpha)^{2/3}]$
0.00
0.04
0.08
0.12
0.16
0.20
0
50
100
150
200
250
300
350
400
450
500
TIME (min)

Figure 15

Linear Regression Testing of the Surface and Diffusion Reaction Models

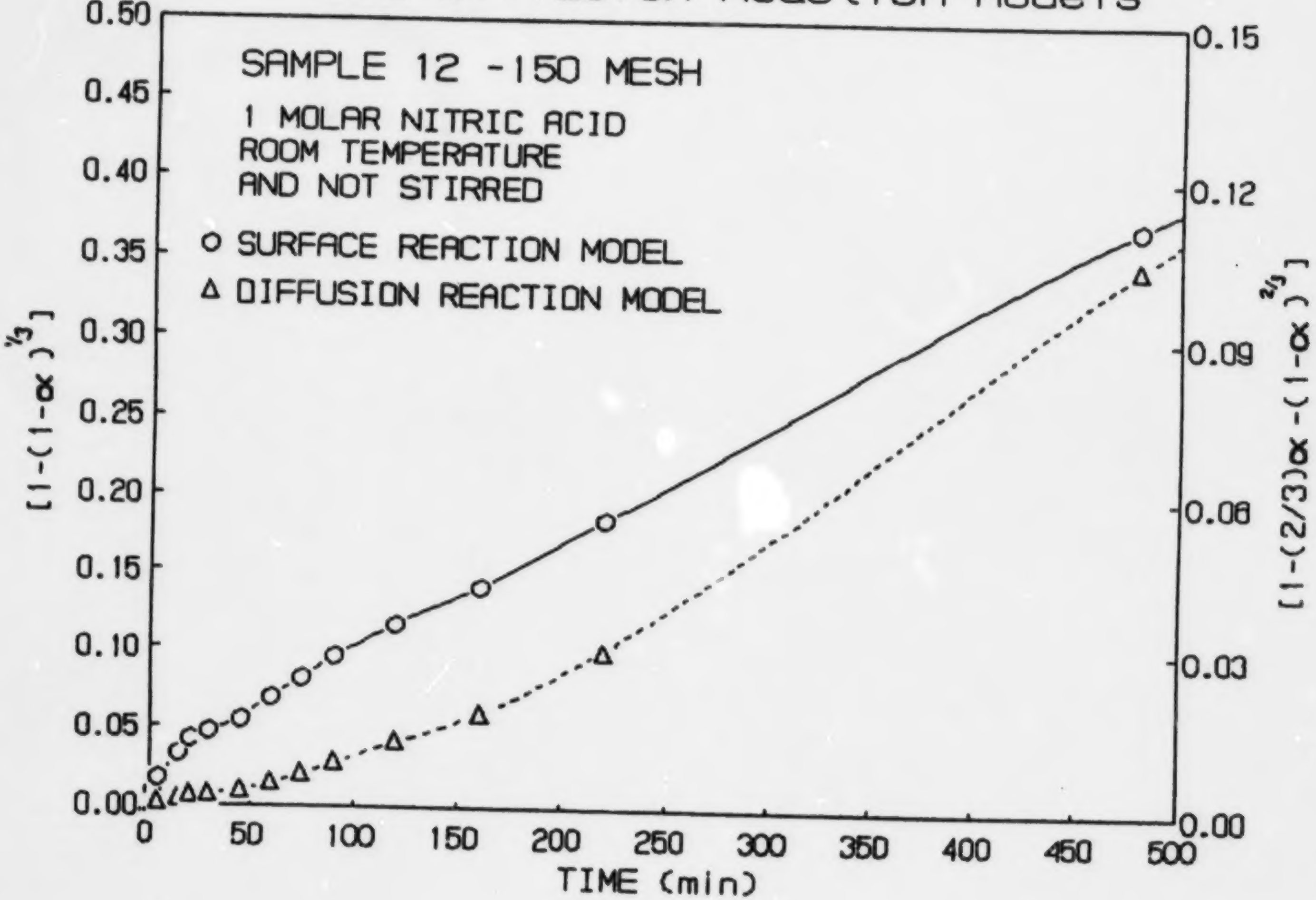

Figure 16

Effect of Temperature on Reaction Rate

Figure 17

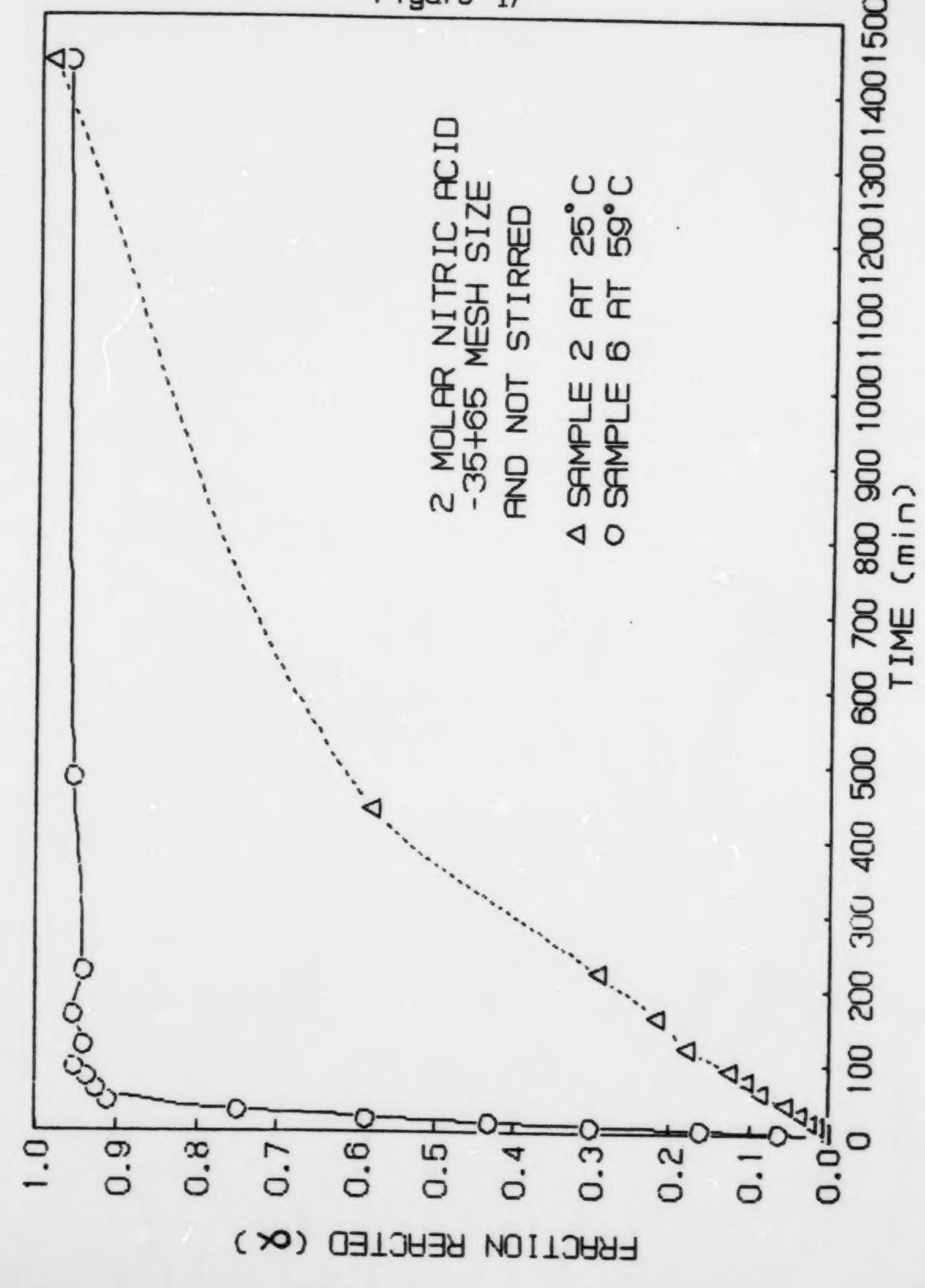

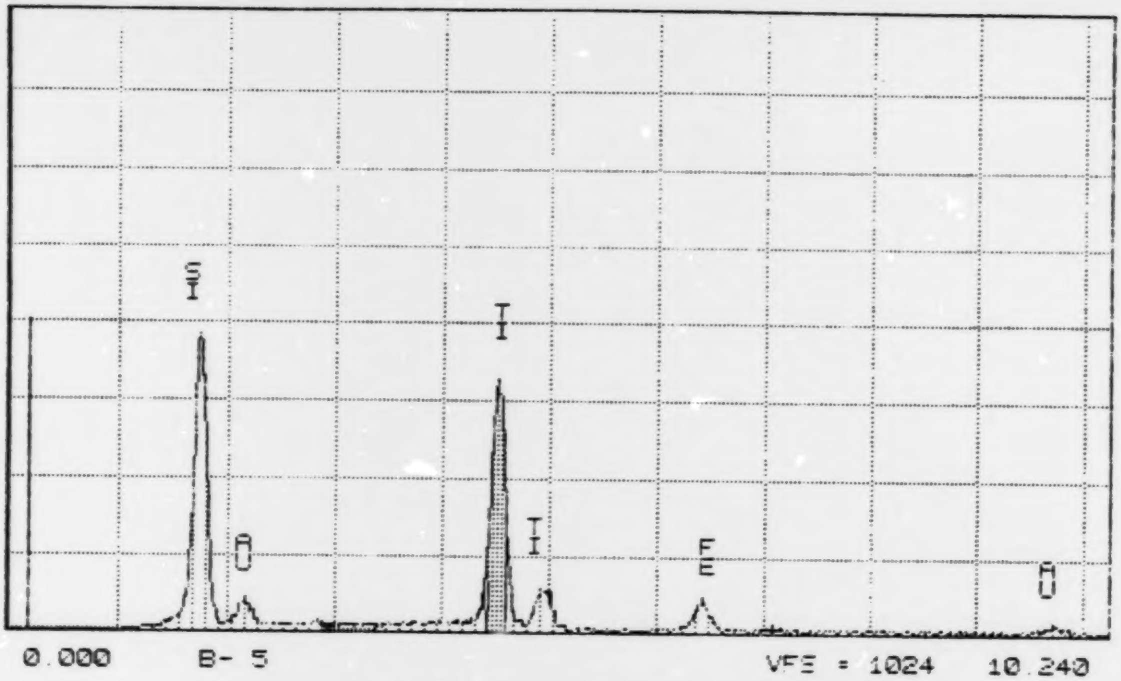

```
              SEMI-QUANTITATIVE ANALYSIS:

----      K      [Z]     [A]     [F]    [ZAF]   ATOM.%   WT.%
CU-K  0.004   1.092   1.041   1.000   1.137    0.25    0.43
SI-K  0.355   0.937   1.381   0.996   1.290   52.70   39.35
TI-K  0.640   1.050   1.043   0.999   1.096   47.05   60.22
```

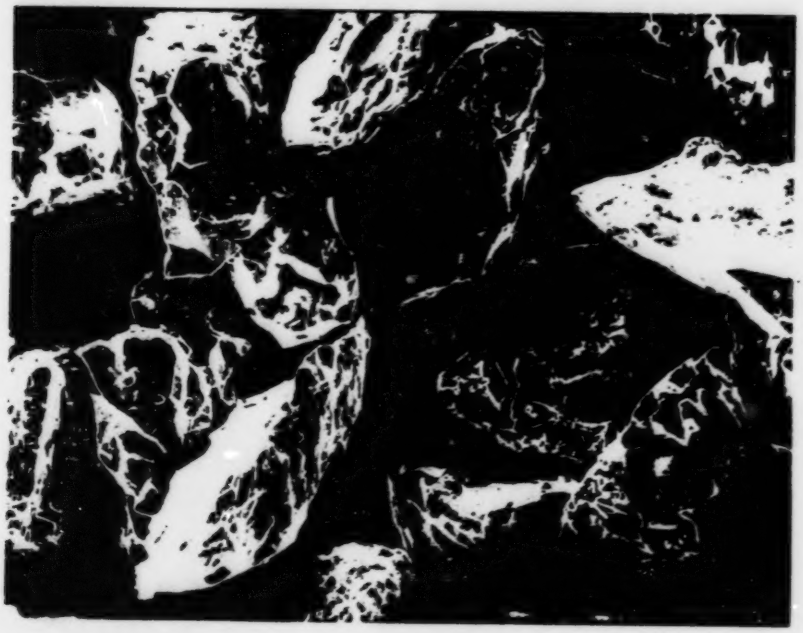

Figure 18: SEM Micrograph of the Product.

CARBOTHERMIC PRODUCTION OF TITANIUM SILICIDE

A number of tests were performed with mixtures of silica, titania and carbon which were pressed into briquettes and smelted in the plasma furnace in a graphite crucible. It was found that under slow heating conditions the silica was converted to silicon monoxide gas and the titania was converted to titanium carbide according to the following reactions

$$SiO_{2(s\ or\ l)} + C_{(s)} = SiO_{(g)} + CO_{(g)}$$

$$TiO_{2(s\ or\ l)} + 3C_{(2)} = TiC_{(s)} + 2CO_{(g)}$$

Thus, as shown in Figure 1 titanium carbide crystals were produced. The silicon monoxide gas back reacted with carbon as it was exiting the system. Thus, silicon carbide crystals grew on the walls of the graphite crucible as shown in Figure 2.

In order to increase the rate of heating during the carbothermic reduction process all further tests were performed in machined boron nitride crucibles. Also, the titania and silicon mixture was prefused before briquetting. Typical results of these tests are shown in Figure 3. In this case stoichiometric TiSi could be produced from a mixture of TiO_2 and SiO_2 with a molar ratio of 1:1. The rapid heating and the intimate mixing of titania and silica minimized both the loss of silicon monoxide and the amount of titanium carbide produced. The carbon content of the product was about 0.2%. Similar results were obtained for varying TiO_2 to SiO_2 ratios. Also the effect of carbon addition was studied.

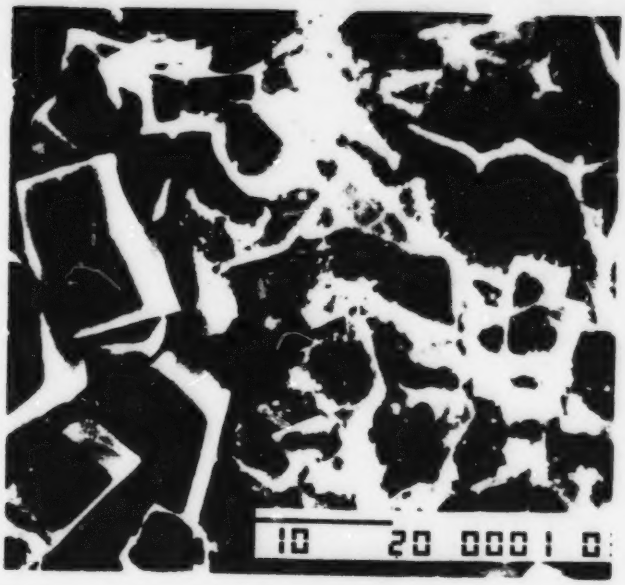

Figure 1: Titanium Carbide Crystals.

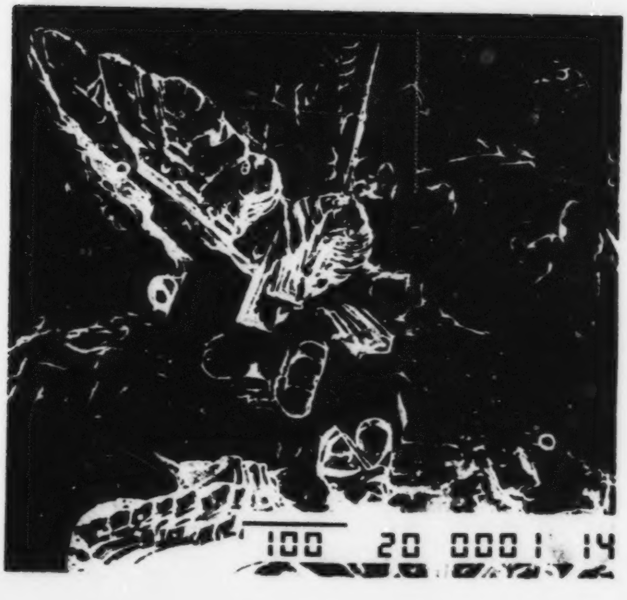
100
20 0001 14

Figure 2: Silicon Carbide Crystals.

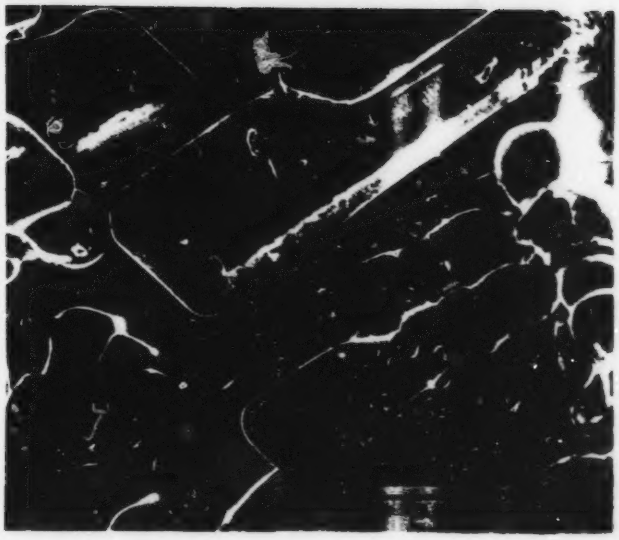

Figure 3: Titanium Silicide Crystals Produced by Carbothermic Reduction.

COMPARISON OF REDUCING AGENTS (C, Al, Mg and Ca)

Four reducing agents were employed in the present work: C, Al, Mg and Ca. Although carbon is a relatively cheap reagent it is difficult to avoid the formation of titanium carbide. Once titanium carbide is formed then further reactions proceed very slowly. However, by prefusing the titania-silica mixture and by adding carbon at about 10% excess of the stoichiometric a titanium silicide product could be obtained.

With regards to the three metallic reducing agents tested, aluminum was superior. Calcium and magnesium have relatively high vapour pressures in comparison to aluminum at the operating temperature and thus magnesium and calcium additions of 100% or more in excess of the stoichiometric are required. Also, the calcium and magnesium silicates which from have high melting points and thus the slag is viscous and agglomeration of the fine titanium silicide droplets is more difficult. The aluminum silicates have lower viscosities and thus agglomeration is promoted and larger size droplets can be obtained which would be easier to separate. When aluminum is employed the metal contains about one percent aluminum while for magnesium and calcium there is virtually no contamination by the reducing agent.

OXIDATION STUDIES

INTRODUCTION

Because of their excellent oxidation resistance and ability to withstand very high temperatures, metal silicides have potential use as a conductor in microelectronics or as a coating or bulk refractory material. Extensive research has thus been made to investigate the oxidation behaviour of refractory silicides such as those of molybdenum, columbium, tantalum, and titanium.

Several studies have been made on the oxidation behaviour of titanium silicide (1-9). Various mechanisms have been proposed to describe this behaviour, all of which are based on a qualitative analysis of the oxidized silicide. Conflict in models arises from the complexity of behaviour encountered over a temperature range, as considerations must be made for the thermodynamic, kinetic, physical, and transport properties of the system. It is, however, agreed that, in general, the resistance to oxidation is due to the formation of a protective film of oxides on the surface of the silicide that is effective in reducing further oxidation of the substrate material.

One proposed method of producing titanium silicide ($TiSi_2$) is by the reduction of ilmenite ($FeO.TiO_2$) in the presence of silica (SiO_2) and a reducing agent, such as carbon or aluminum. However, the effect of an inherent iron impurity in the silicide on its resistance to oxidation at high temperatures must be known before this method of production can be considered feasible. The present study was undertaken in order to determine the effect of iron, copper, and aluminum impurities on the oxidation resistance of titanium silicide.

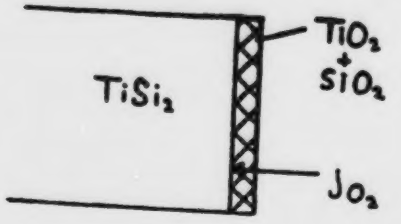
TiSi$_2$
TiO$_2$ + SiO$_2$
J$_{O_2}$

Figure 1: oxidation in the initial phase

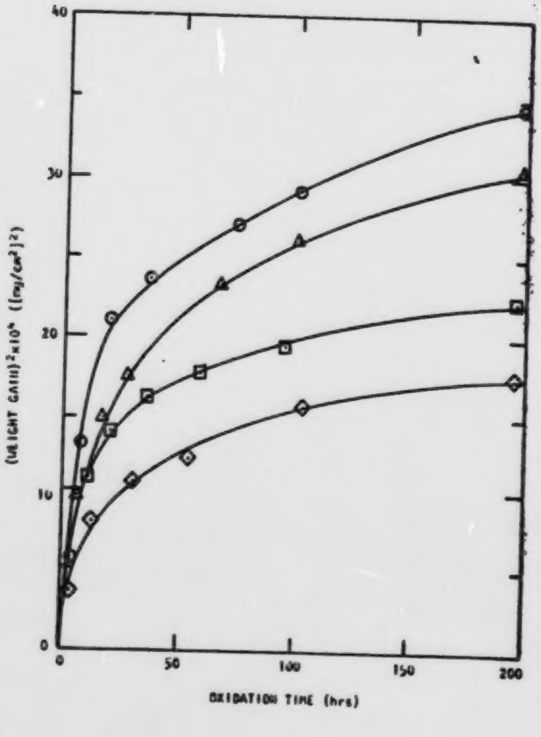

Fig. 2: Rate data for TiSi$_2$ oxidized at 600°C (1)

THEORETICAL CONSIDERATIONS FOR THE OXIDATION OF $TiSi_2$

The time and temperature dependence of the oxidation of bulk $TiSi_2$ has been studied by Schwettman et al (1) in order to provide data and a mechanism for oxidation. The proposed typical oxidation reaction.

$$TiSi_2 + O_2 - Ti_xO_y + SiO_2 + Ti_5Si_3 \qquad (1)$$

was shown to be significant only above 300°C, with the amount of produced Ti_5Si_3 too small to positively identify.

The controlling mechanism of oxidation in the range of 300°C to 700°C is a combination of the oxidation reaction (r1) at the solid-gas interface and diffusion of oxygen through the oxide film. In the initial phase of oxidation, diffusion through micropores in the forming oxide film is rapid, and thus reaction at the surface is rate-controlling, as depicted in Fig. 1.

Because the free energy of formation of titanium oxides is very close to that of silica selective oxidation of titanium or silicon is unlikely to occur. Instead, an amorphous titania-silica glass will form on the surface of the silicide. As oxidation proceeds and this oxide film grows in thickness, the micropores become blocked and diffusion of oxygen through the film becomes rate-controlling. Since diffusion through a silica film at low temperatures is slow (1), the rate of oxidation gradually decreases with time, as shown in Figure 2.

It has been found that, at temperatures below 600°C, some silicides exhibit an increase rather than a decrease in oxidation rate. Molybdenum disilicide, although highly oxidation-resistant at temperatures above 600°C (2), oxidizes quite rapidly at temperatures under 600°C (3). This "pest corrosion" is due to the presence of molybdenum oxide, MoO_3, which is

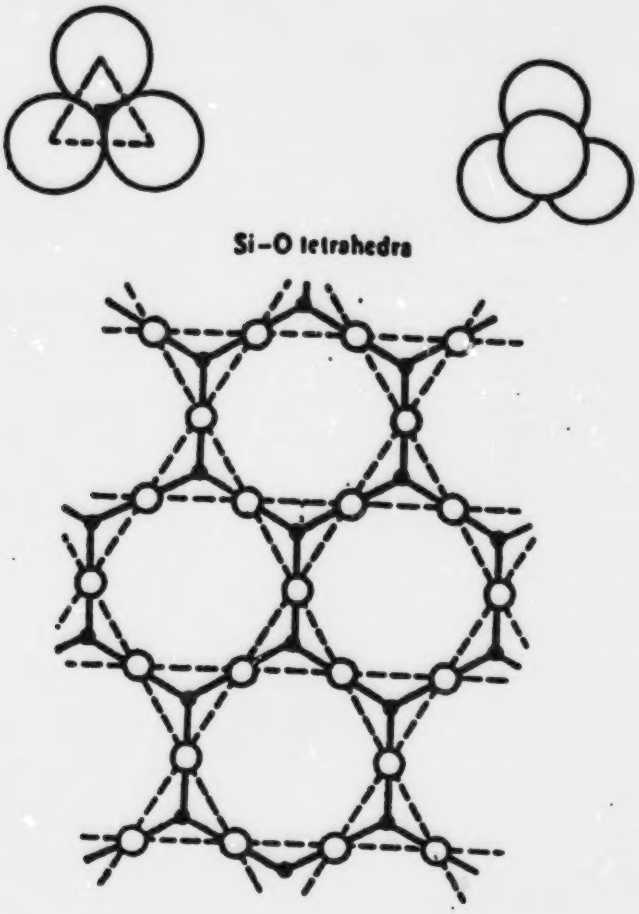
Si–O tetrahedra

Fig. 3: Schematic of the silica tetrahedral network

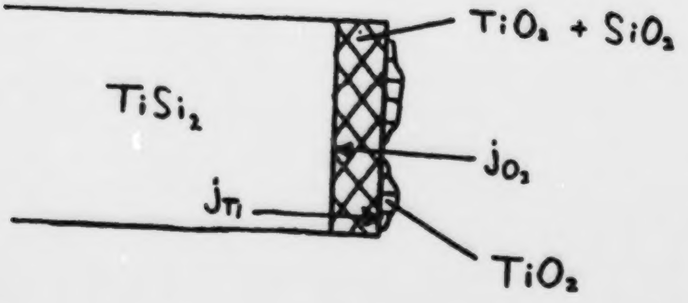
TiO₂ + SiO₂
TiSi₂
j_O₂
j_Ti
TiO₂

Figure 4: continued oxidation of bulk $TiSi_2$

incompatible with SiO_2 and, upon formation, causes severe volume expansion in any surface crack it may form in. The subsequent collection of oxides causes crack propagation, which promotes deterioration of the silicide. Above 600°C, MoO_3 becomes volatile, allowing for the formation of a film of pure SiO_2 that tends to bridge across any surface cracks in the silicide, forming a very protective film. However, pest corrosion has not been observed during the oxidation of titanium silicide at any temperature. Since TiO_2 is compatible with SiO_2 a bridge-like film forms over the surface cracks, which eliminates pesting at low temperatures. Schwettman et al (1) have suggested that this is partly due to the ability of titanium to assume fourfold coordination and replace silicon in the growing silica film without disrupting the tetrahedral network (see Fig. 3).

At temperatures of 1000°C and above, the initial stage of oxidation is unchanged (i.e. reaction at the surface is rate-controlling). However, as the oxide film continues to grow in thickness, counter-diffusion of Ti to the gas-oxide interface occurs as the solubility limit of titanium in silica is surpassed. Crystalline clumps of TiO_2 are formed at that interface (1) As before, a virtually impenetrable layer of amorphous SiO_2 forms, slowing further diffusion and slowing the oxidation rate. This phenomenon is represented in Fig. 4.

However, as diffusion increases with temperature, it can be expected that the amount of material gained through oxidation will continue to grow as temperature increases. Schwettman et al (1) observed this phenomenom, with parabolic kinetics demonstrated at temperatures of 1000°C and above as shown in Fig. 5.

It is the purpose of this study to investigate the effect of additions of iron on the oxidation resistance of titanium silicide. Previous work has investigated the nature of the mechanisms of oxidation of silicides, as

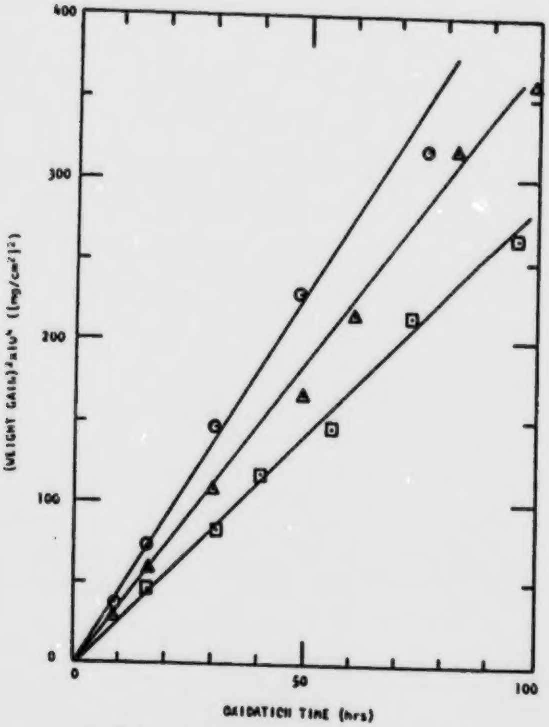

Fig. 5 Rate data for $TiSi_2$ oxidized at 1000°C (1)

described earlier, but little has been accomplished toward determining the effect of a modifying agent on the resistance of a silicide to oxidation.

Lavendel et al (6) investigated the effect of a modifying agent on the oxidation of $TaSi_2$-coated tantalum and found that the addition of aluminum was effective in moderately increasing the oxidation resistance. This was due to the greater stability of aluminum oxide over the substrate base metal oxide, Ta_2O_5, such that selective oxidation occurred Also, the oxidized aluminum increased the thermodynamic stability of the protective film with respect to the base metal oxide, Ta_2O_5.

If a modifying agent whose oxide had a greater thermodynamic stability than TiO_2 was introduced to bulk $TiSi_2$, selective oxidation would favor the oxidation of the modifying agent over that of titanium, and the oxidation of the titanium silicide may be effectively reduced. However, according to thermodynamic data, the free energy of formation of iron oxide is less negative than that for the titanium oxides. Therefore, it is unlikely that the oxidation resistance will be improved by the formation of iron oxide due to selective oxidation.

EXPERIMENTAL

Iron powder (J.T. Baker Chemical Co., 97.9%) was added to $TiSi_2$ (Alfa Products, 95%) in concentrations varying from 0 wt.% to 10 wt.% and mixed in a rolling mill. Binder (H_2O) was added and 1 1/4 in. diameter wafers were pressed in a hardened steel die at 6,000 psi. Sample thickness was typically 3/4 in. The binder was removed by heating samples for several hours at 100°C.

Wafers were placed on an alumina dish in a graphite crucible containing zirconium chips used as an oxygen getter during sintering. Sintering of the wafers was carried out in an argon atmosphere at 1400°C for 15 minutes. An extremely thin layer of oxide that formed on the faces of the wafers during sintering was removed by grinding successively on carbide paper of 240, 320, 400, and 600 grit coarseness.

Oxidation of the wafers was carried out in a high-temperature furnace with a PID controller at 1300°C for 24 hours. Additional runs were also made at temperatures of 900°C, 1050°C, and 1200°C for 24 hours using samples containing 0 wt.% Fe and 5 wt.% Fe in order to investigate the effect of temperature on oxidation rate. The oxidizing atmosphere for all oxidations was air ($P_{O_2} \cong 0.21$ atm.). Samples were placed on alumina dishes in the middle of the furnace.

Oxidation data were obtained by measuring the gain of mass of the sample on a Mettler AE50 analytical balance. In addition some samples were oxidized and their weight gain was monitored continuously with a transducer. Samples were coated with gold using a Varian VE-10 vacuum evaporator in preparation for qualitative analysis, by scanning electron microscopy SEM and energy dispersive spectroscopy (EDS). A JEOL JSM-T300 was used for the SEM work. EDS was performed with a Tracor Northern X-ray tube (TN5550-10) in conjunction with a Tracor Northern X-ray analyzer (TN5500) and Flextran software package.

RESULTS AND DISCUSSION

Oxidation studies were performed on two silicides of titanium: Ti_5Si_3 and $TiSi_2$. These results are summarized in Figures 6 to 10. A number of general comments can be made. At high temperatures the briquettes lost weight due to the evaporation of silica as silicon monoxide. At low temperatures the effect of the additions was not significant. However, at higher temperatures iron and copper were detrimental and their addition resulted in increased rate of either weight loss or weight gain. There are two reasons for this effect. Firstly, the addition can modify the oxide and increase the rate of diffusion of reactants through the oxide. Secondly, metallic additions to the titanium silicide can result in the formation of ternary phases which have increased rates of oxidation. Some examples of the oxide formed are shown in Figure 29. At high temperatures silica whiskers were observed to grow on the surface of the samples - Figure 30.

REFERENCES

1. Schwettmann, F.N., R.A. Graff, and M. Kolodney, J. of Electrochem. Soc., 1973 (Dec. 1971).
2. Wirkus, C.D., and D.R. Wilder, J. Am. Ceram. Soc., 49(4), 173 (1966).
3. Berkowitz-Mattuck, Joan B., Paul E. Blackburn, and Edward J. Felten, Trans. Met. Soc. AIME, 233, 1093 (1965).
4. Valyi, G., Lu Zhaokang, A. Steffen, M. Maier, and P. Balk, Thin Solid Films, 116(4), 383 (1984).
5. Yang, Wei Yi, Hiroaki Iwakuro, Hideichi Yagi, Tsukasa Kuroda, and Shogo Nakamura, Jap. J. of App. Phys., 23(12), 1560 (1984).
6. Lavendel, H.W., and A. Grant Elliot, Trans. Met. SoC. AIME, 239, 143 (1967).
7. d'Heurle, F., E.A. Irene, and C.Y. Ting, Appl. Phys. Lett., 42(4), 361 (1983).
8. Stone, H.E.N., J. of Mat. Sci. Lett., 2, 609 (1980).
9. Chen, J.-R., M.-P. Houng, S.-K. Hsiung, and Y.-C. Liu, Appl. Phys. Lett., 37(9), 824 (1980).
10. Levin, Ernest M., C.R. Robbins, and H.F. McMurdie, Phase Diagrams for Ceramists, The American Ceramic Society, Columbus, Ohio. 1974.
11. Hansen, Dr. Max, Constitution of Binary Alloys, McGraw-Hill Book Company, Inc., New York, 1958.

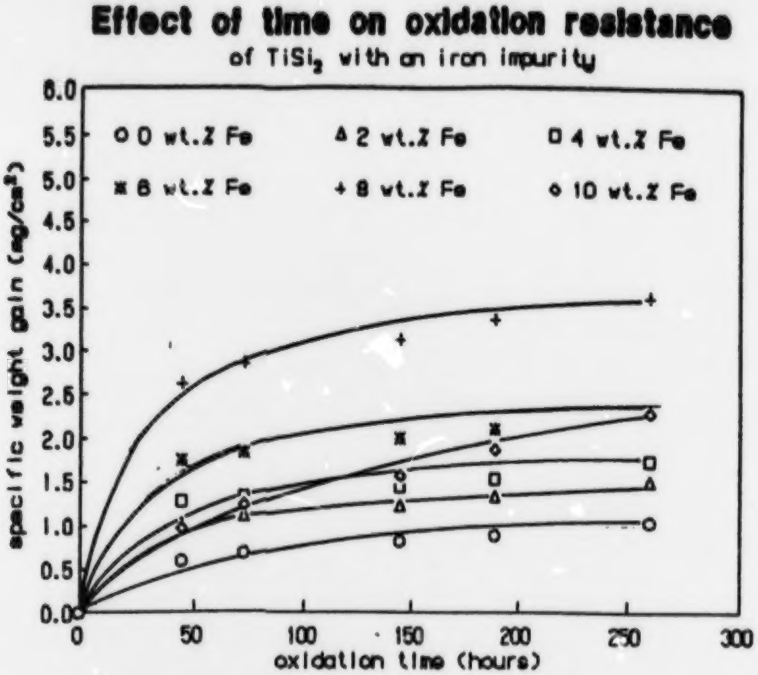

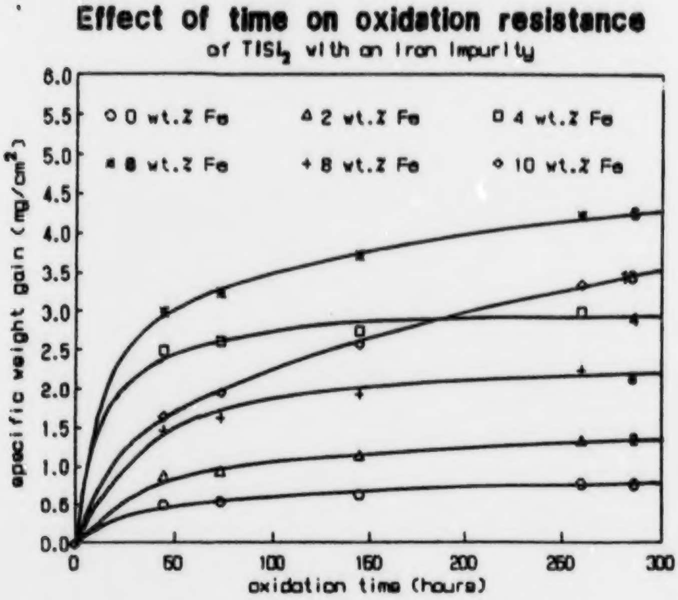

Figure 6: Effect of Time on the Weight Gain of TiSi$_2$ at 1200°C.

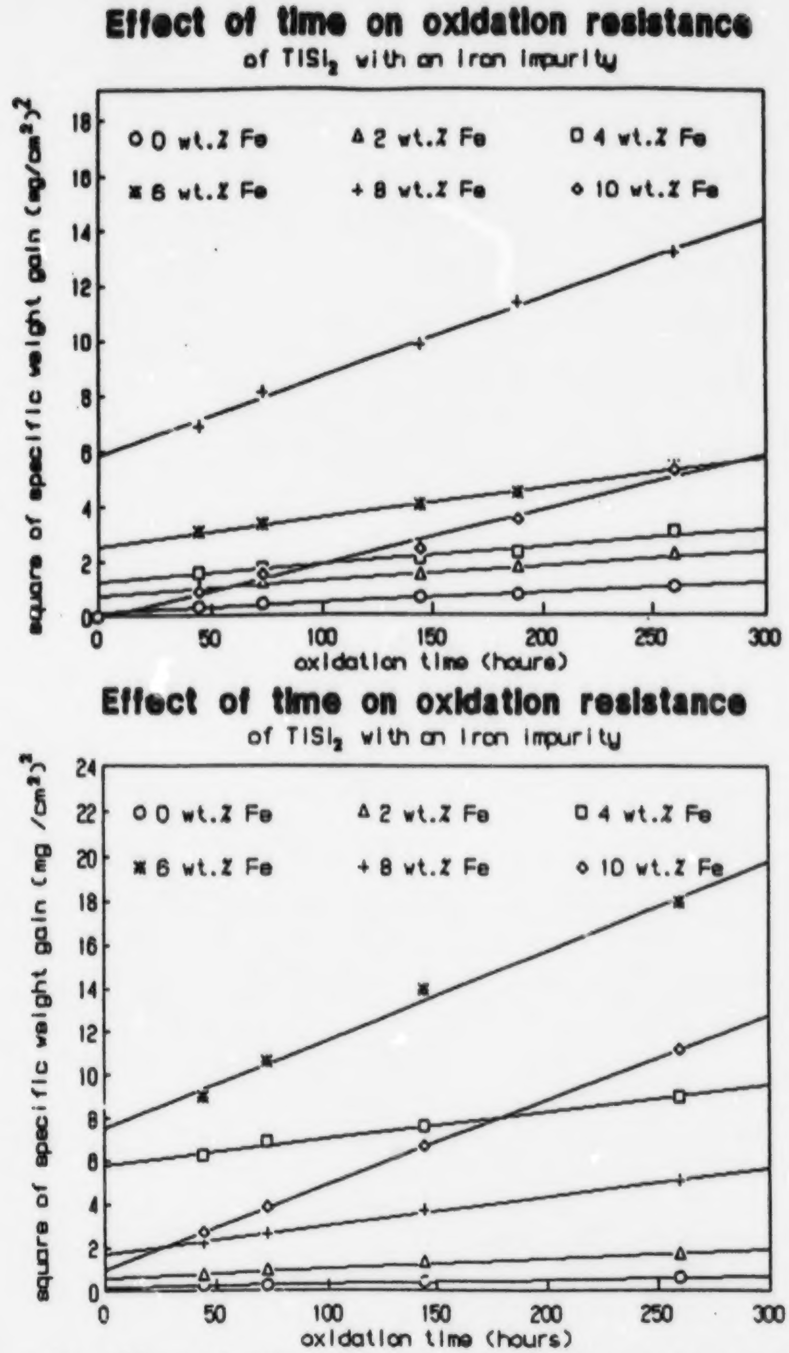

Effect of time on oxidation resistance of $TiSi_2$ with an iron impurity

Effect of time on oxidation resistance of $TiSi_2$ with an iron impurity

Figure 7: Effect of Time on the Square of the Specific Weight Gain of $TiSi_2$ at 1200°C.

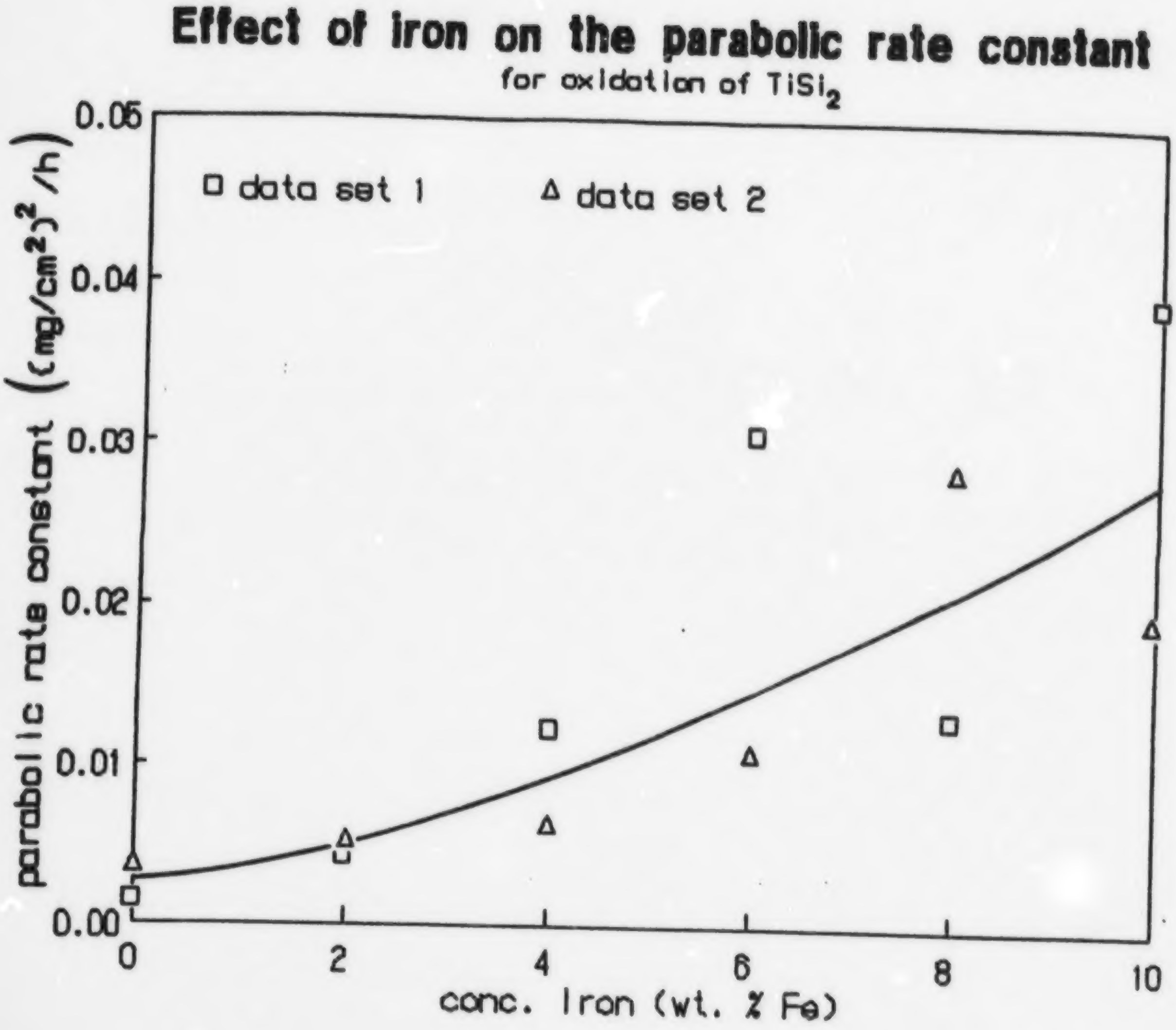

Figure 8: Effect of Iron Concentrations on the Parabolic Rate Constant at 1200°C for $TiSi_2$.

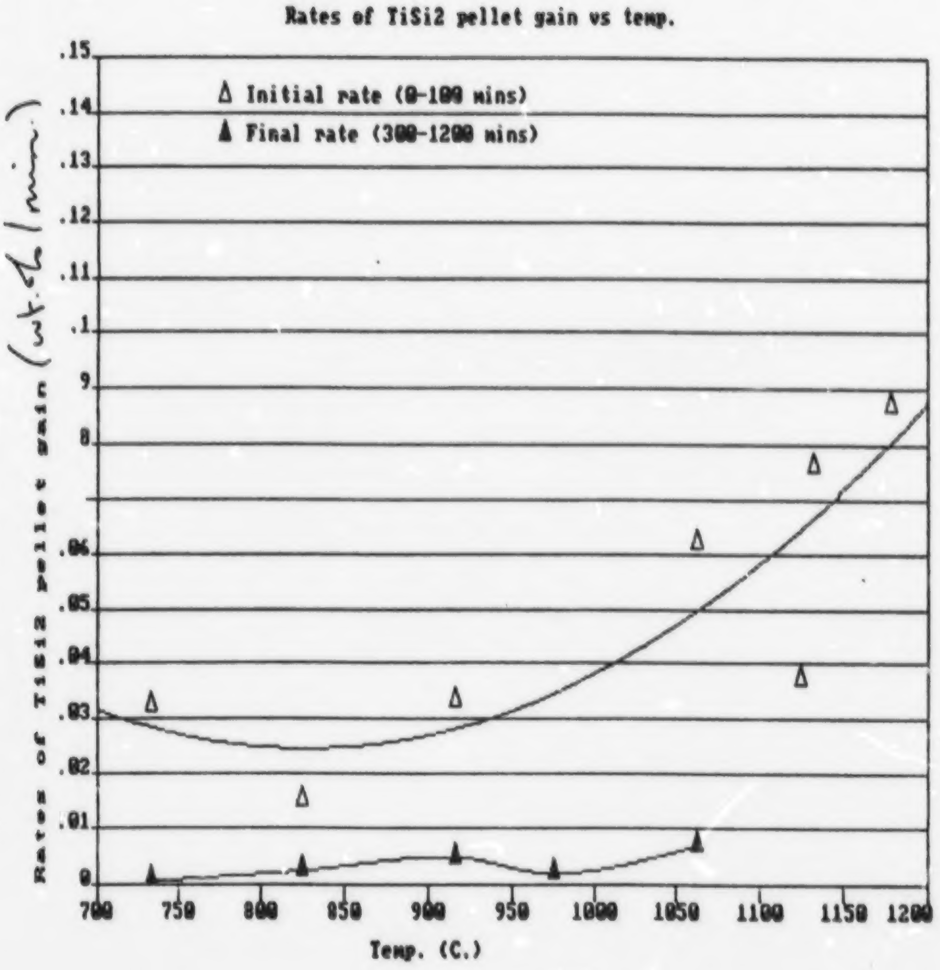

Figure 9: Effect of Temperature on the Rate of Weight Gain for $TiSi_2$ Briquettes.

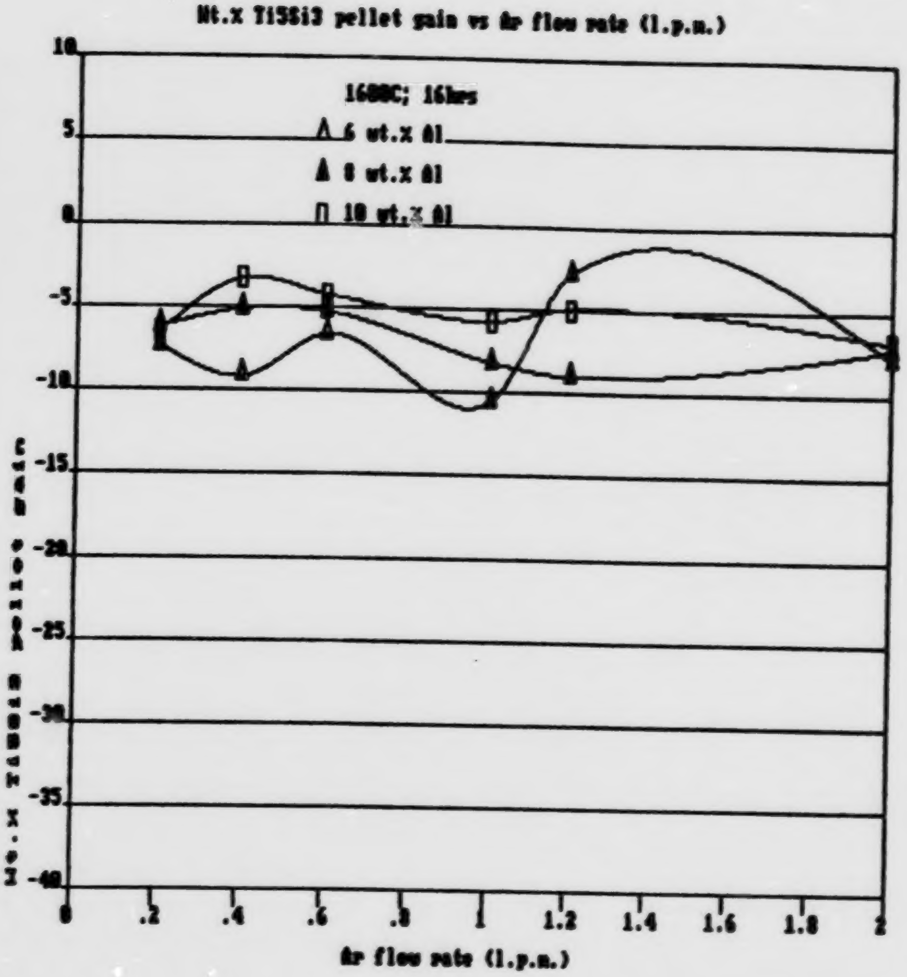

Figure 10: Effect of Argon Flowrate on the Oxidation of Ti_5Si_3.

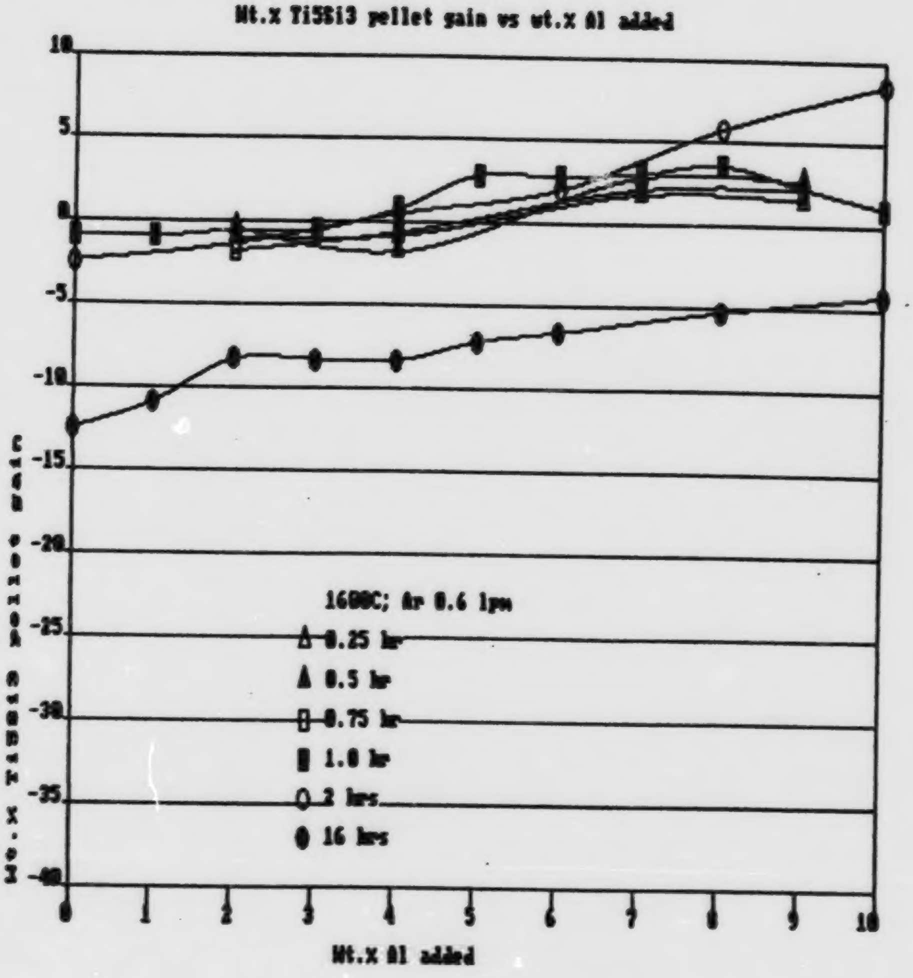

Figure 11: Effect of Aluminum Additions on the Oxidation of Ti_5Si_3.

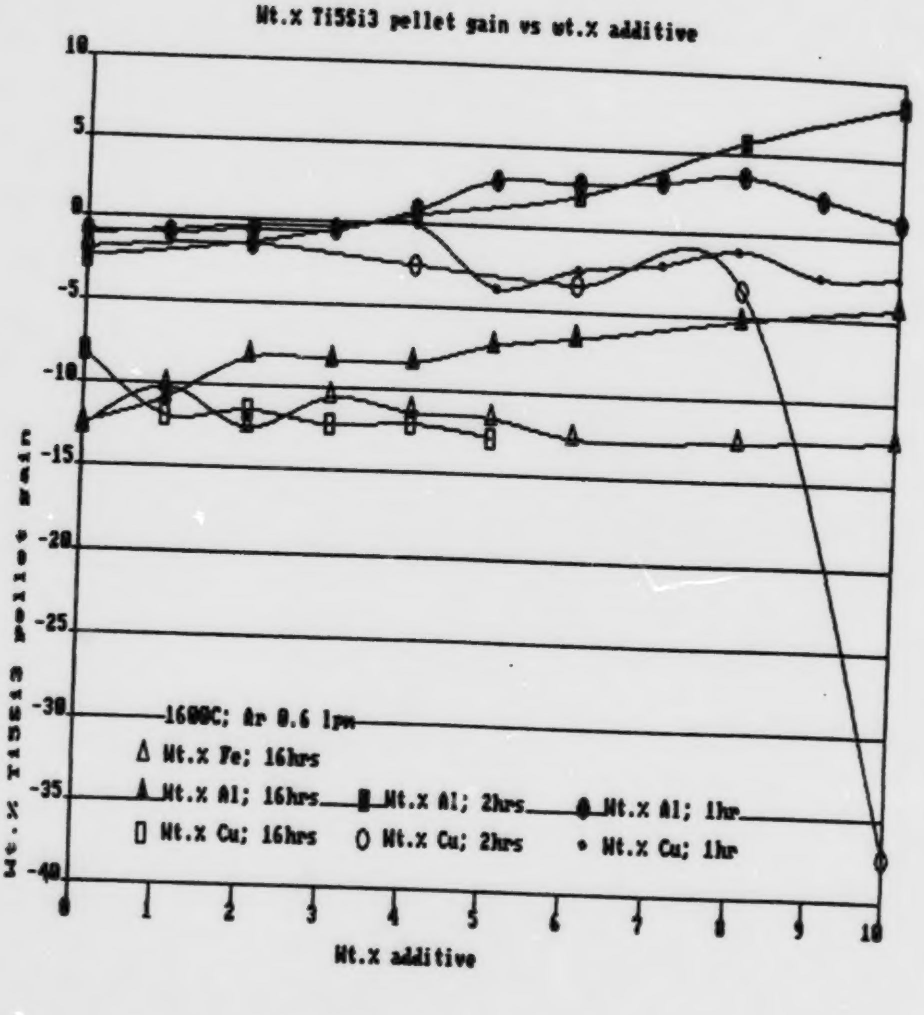

Figure 12: Effect of Al and Cu Additions on the Oxidation of Ti_5Si_3 at Various Times.

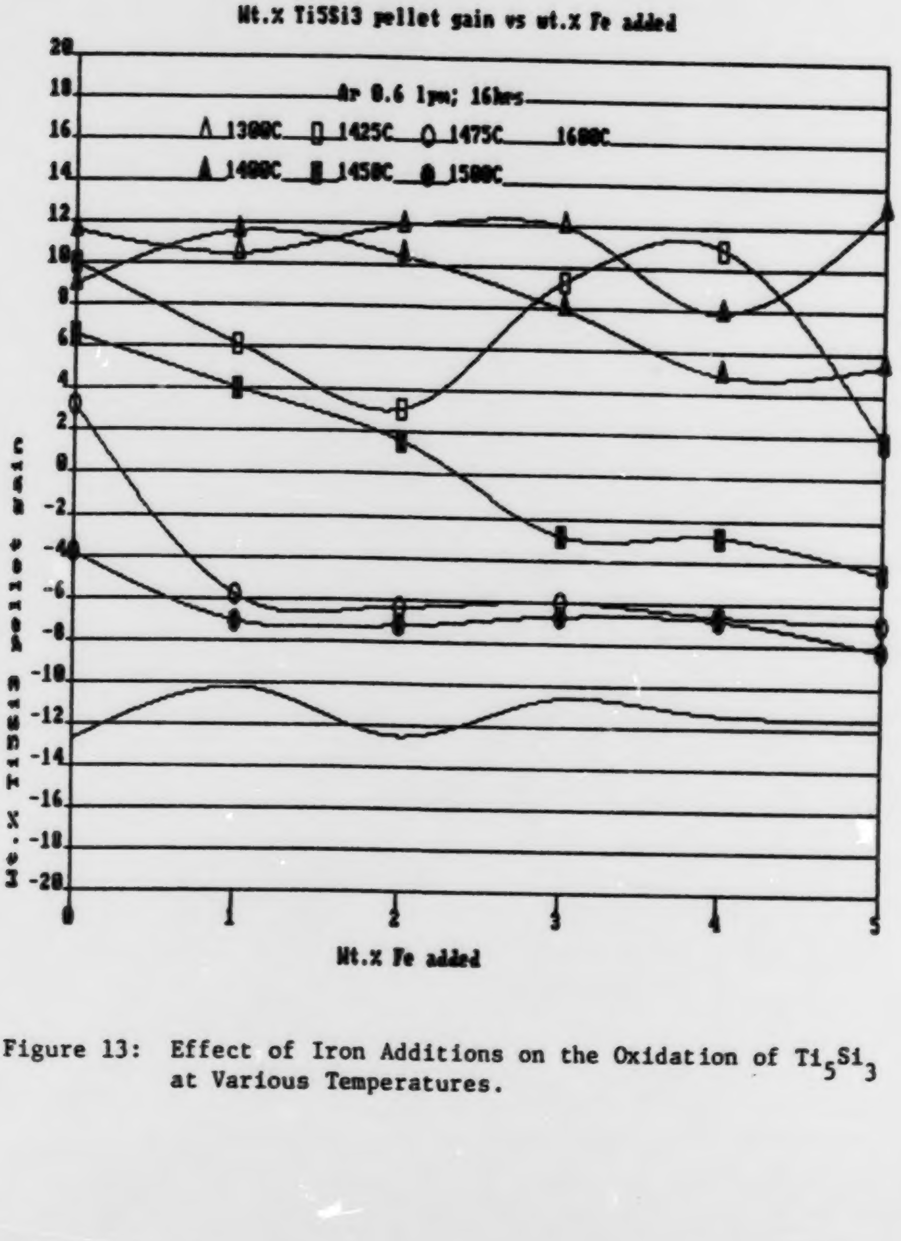

Figure 13: Effect of Iron Additions on the Oxidation of Ti_5Si_3 at Various Temperatures.

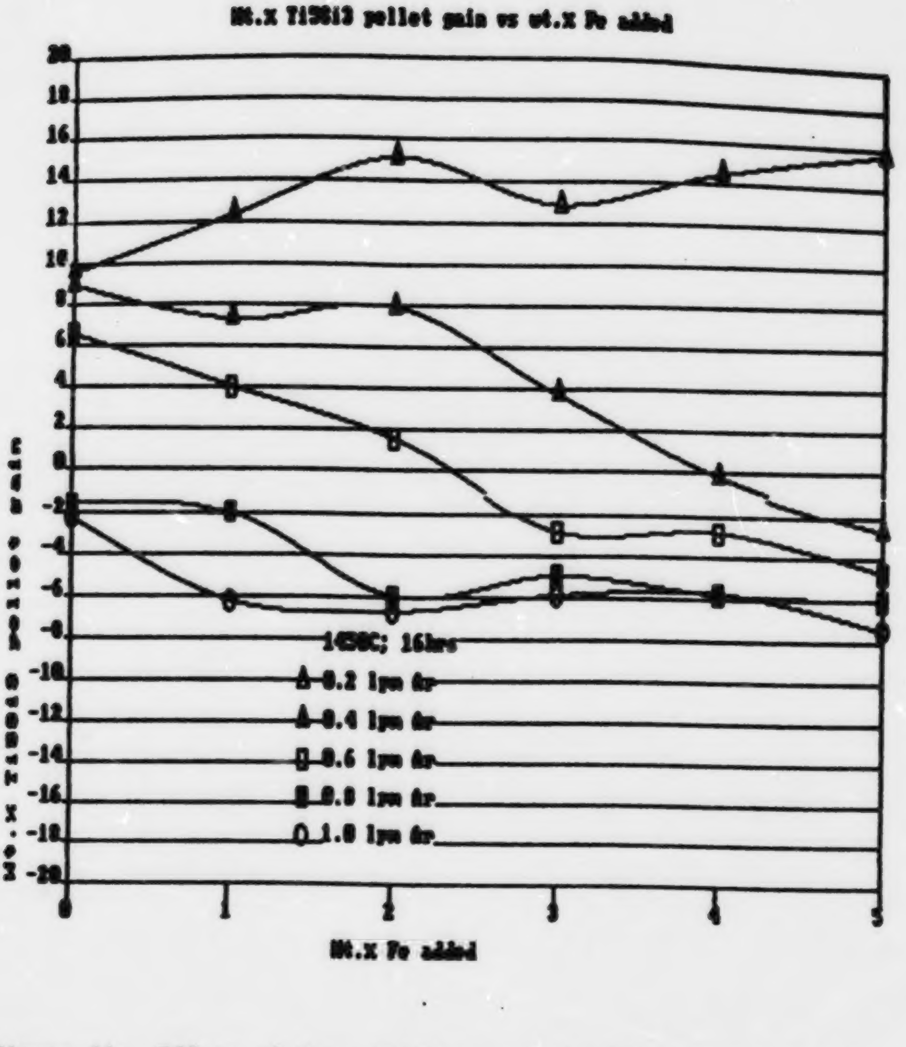

Figure 14: Effect of Iron Additions on the Oxidation of Ti_5Si_3 at Various Argon Flowrates at 1450° C.

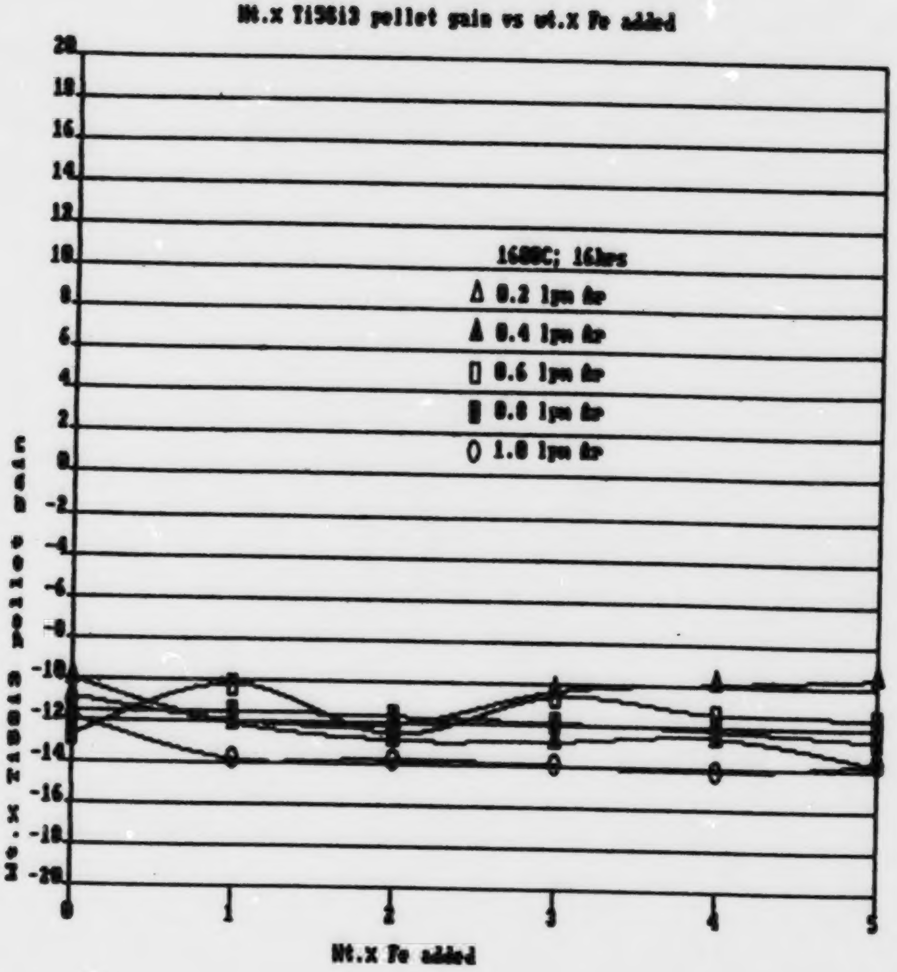

Figure 15: Effect of Iron Additions on the Oxidation of Ti_5Si_3 at Various Argon Flowrates at 1600°C.

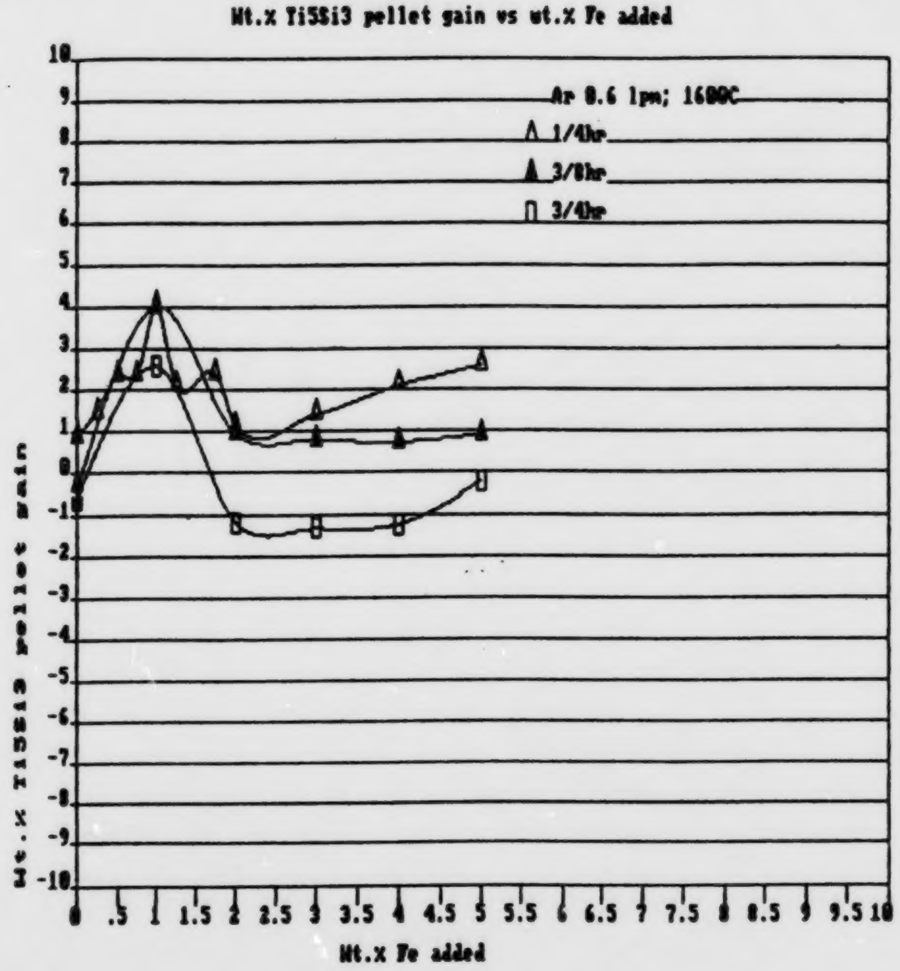

Figure 16: Effect of Iron Additions on the Oxidation of Ti_5Si_3 at Various Times at 1600°C.

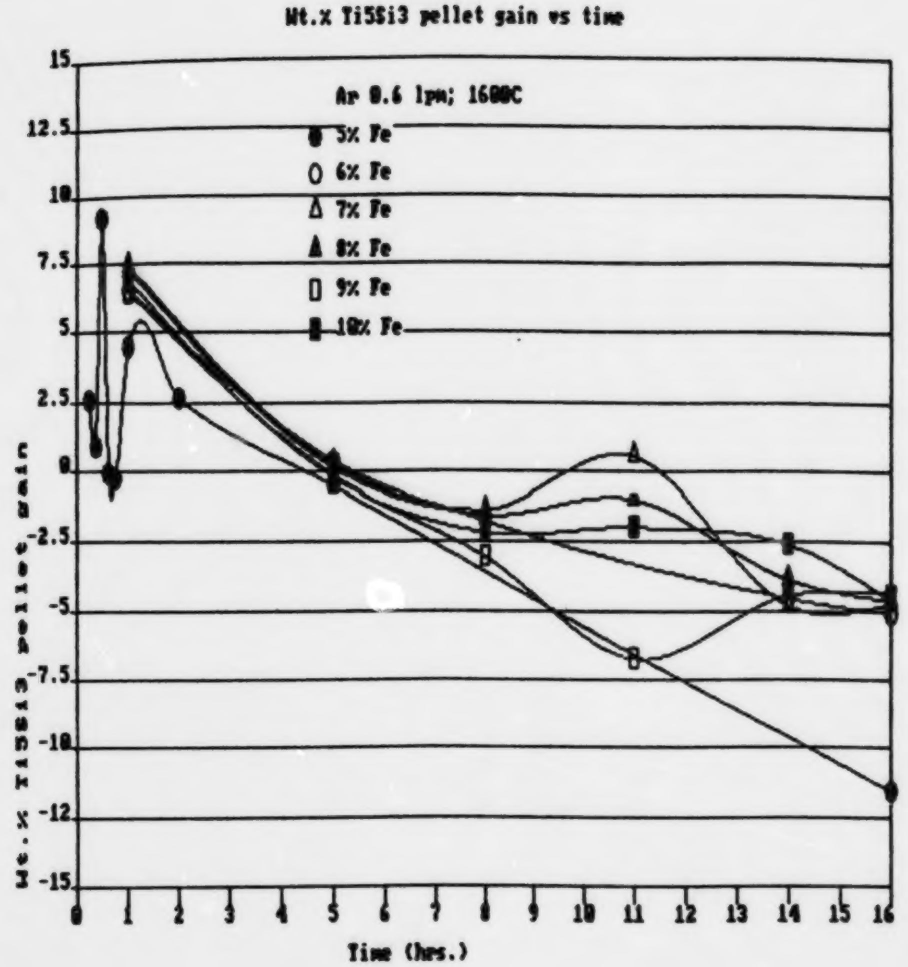

Figure 17: The Effect of Iron Additions on the Oxidation of Ti_5Si_3 at 1600°C.

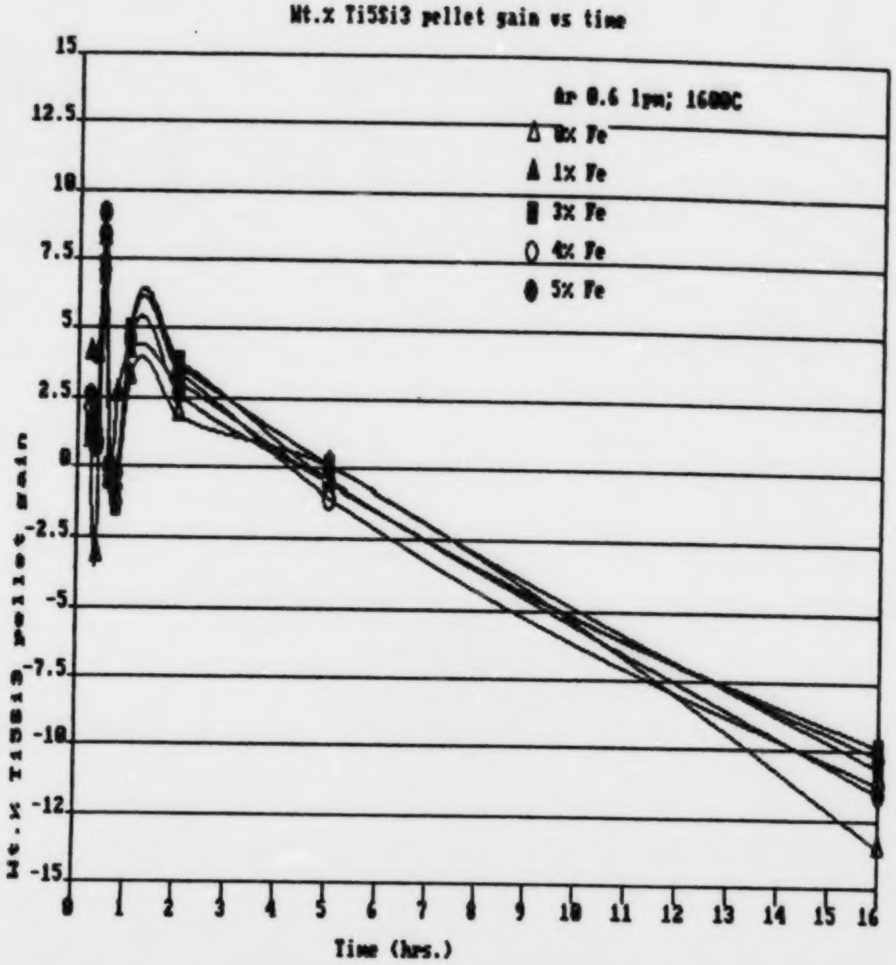

Figure 18: The Effect of Iron Additions in the Oxidation of Ti_5Si_3 at 1600°C.

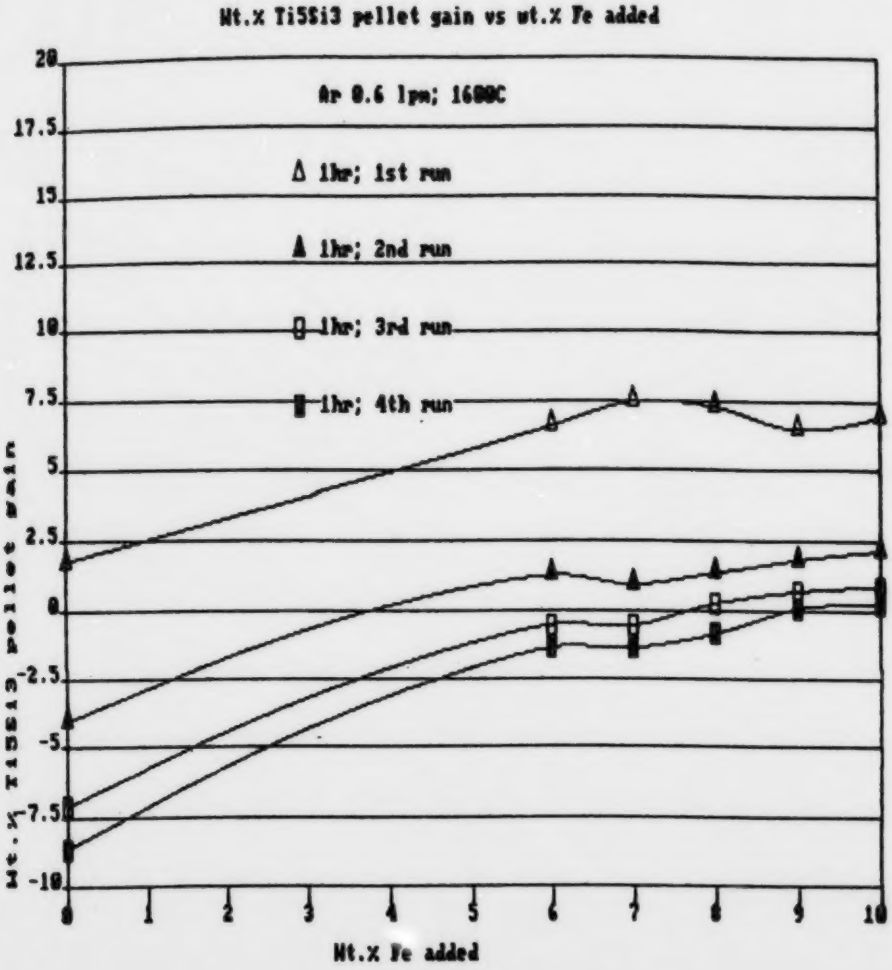

Figure 19: The Effect of Thermal Cycling on the Oxidation of Ti_5Si_3 at 1600°C.

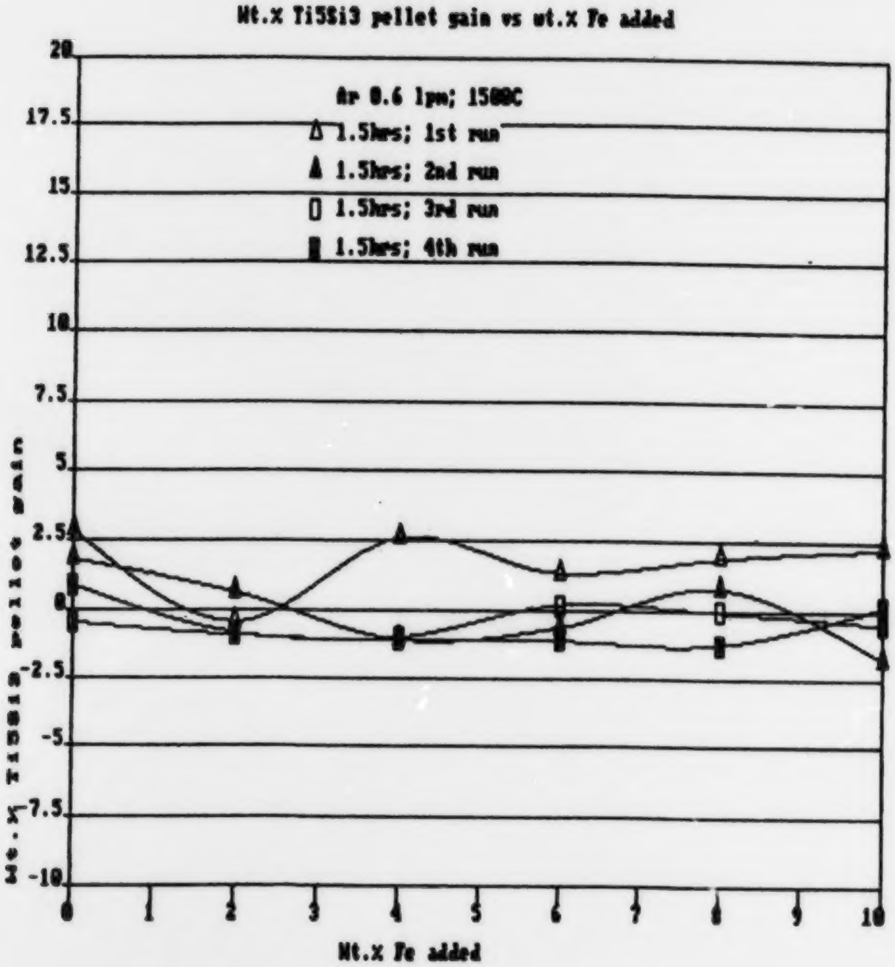

Figure 20: The Effect of Thermal Cycling on the Oxidation of Ti_5Si_3 at 1500°C.

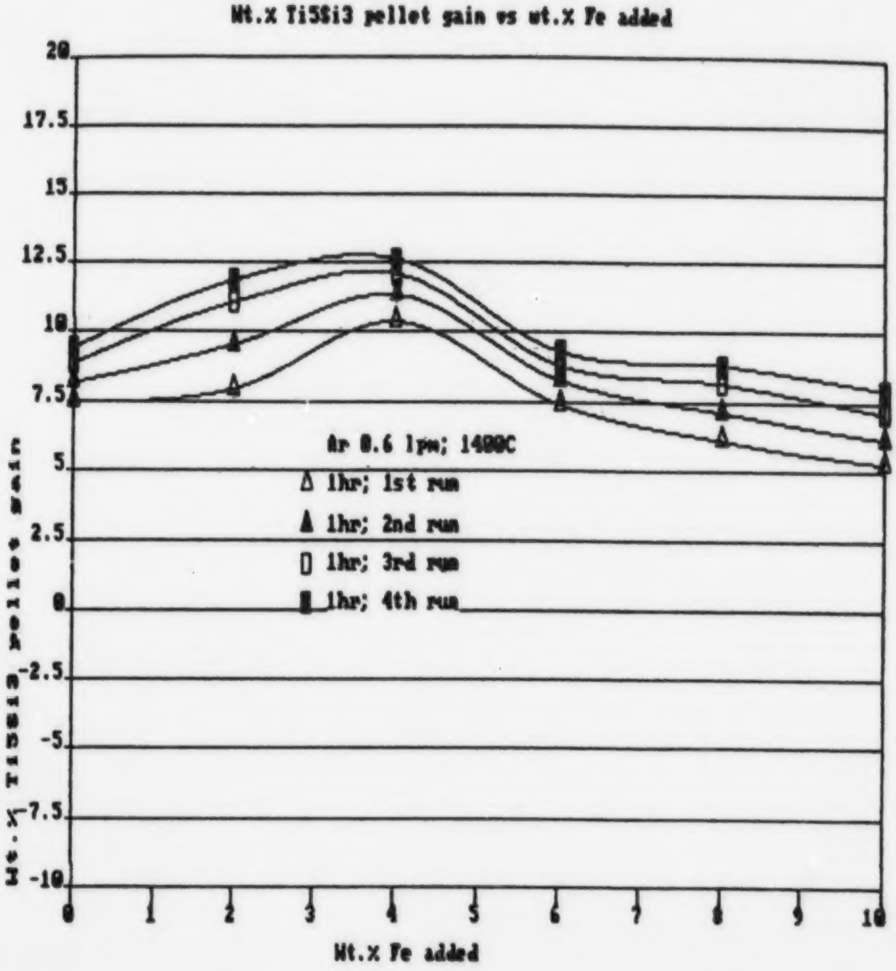

Figure 21: The Effect of Thermal Cycling on the Oxidation of Ti_5Si_3 at 1400°C.

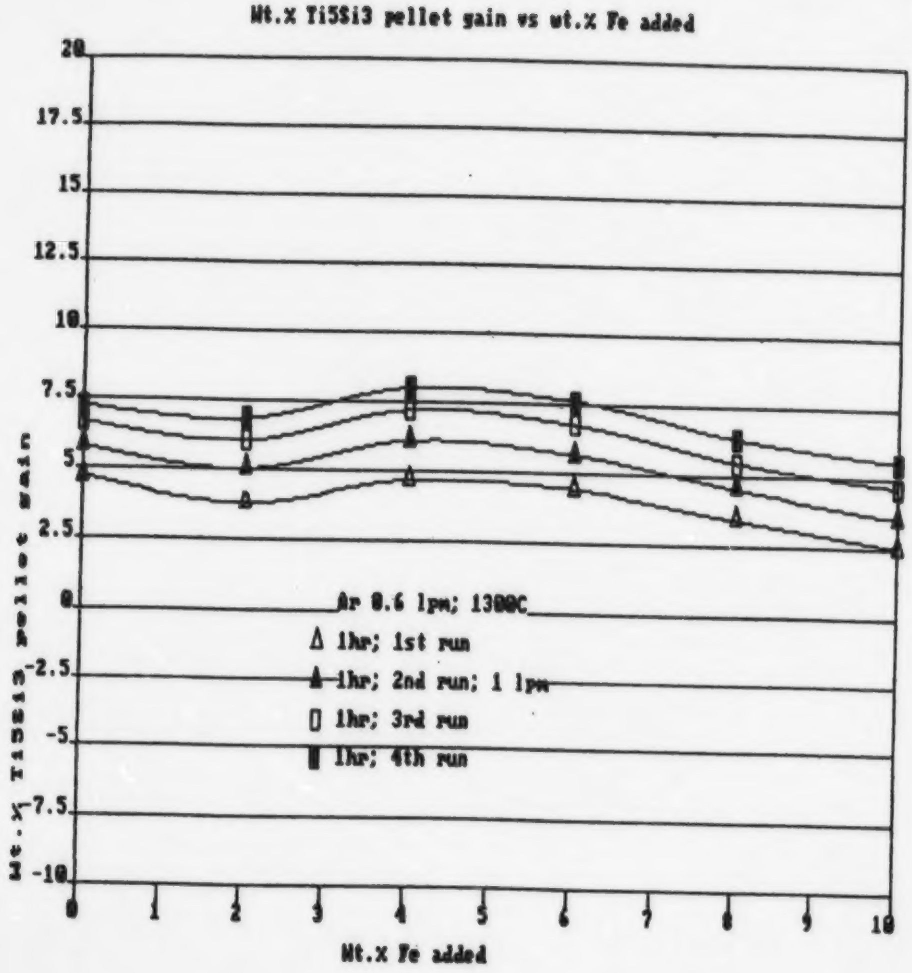

Figure 22: The Effect of Thermal Cycling on the Oxidation of Ti_5Si_3 at 1300°C.

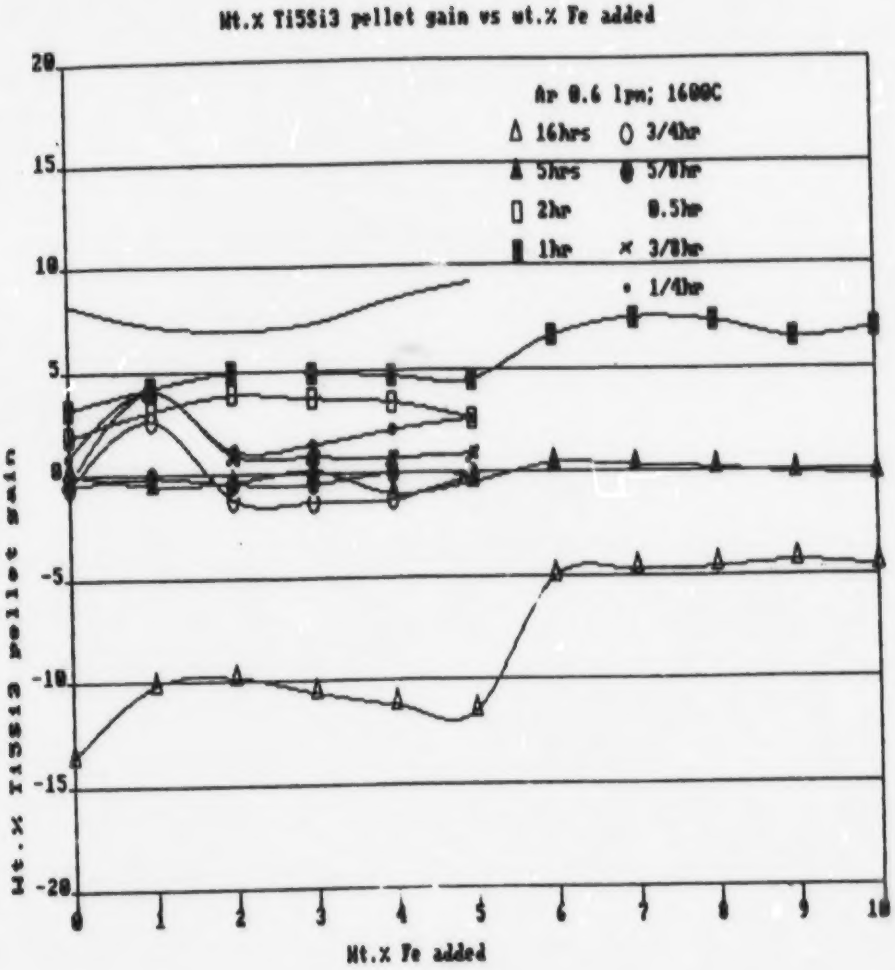

Figure 23: The Effect of Iron Additions on the Oxidation of Ti_5Si_3 at 1600°C at Various Times.

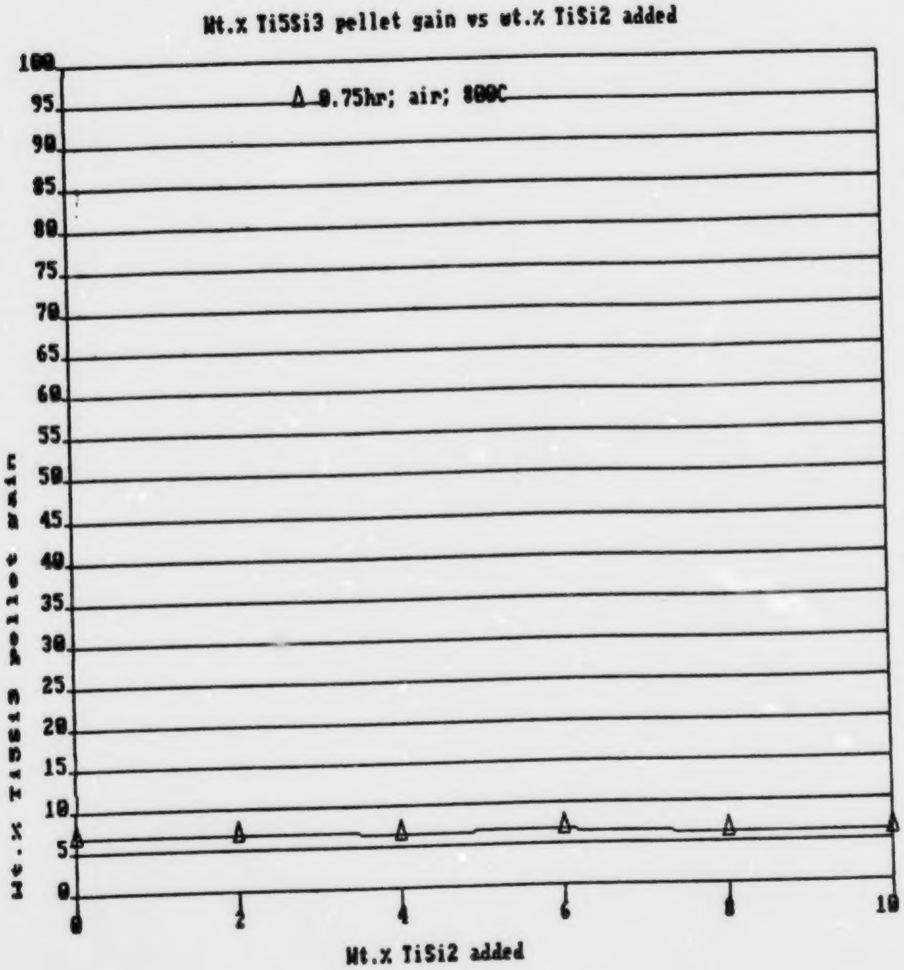

Figure 24: The Effect of $TiSi_2$ Additions on the Oxidation of Ti_5Si_3 at 800°C.

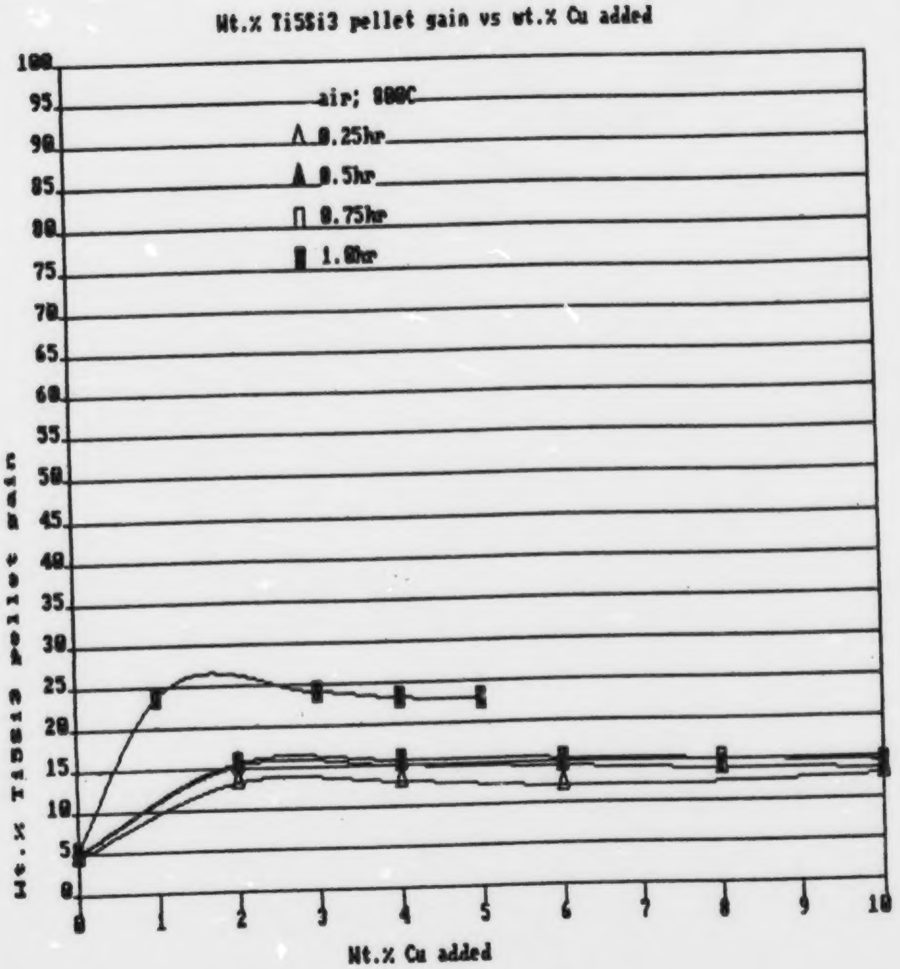

Figure 25 : The Effect of Copper Additions on the Oxidation of Ti_5Si_3 at 800°C.

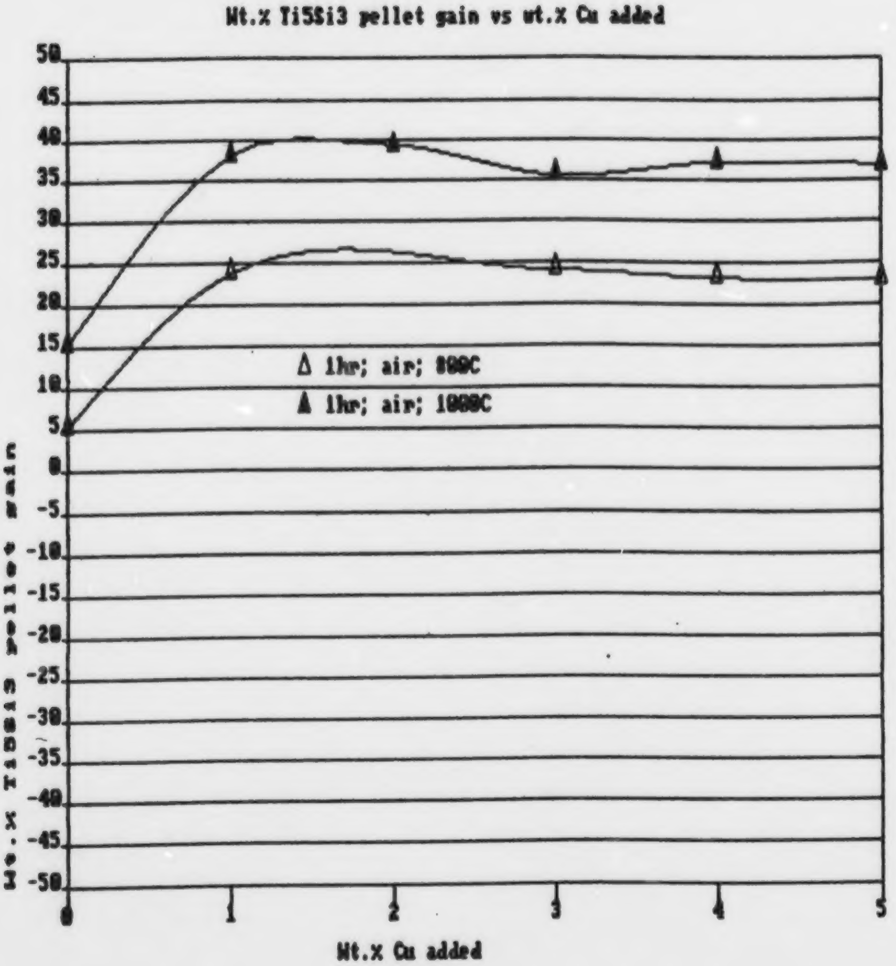

Figure 26 : The Effect of Copper Additions on the Oxidation of Ti_5Si_3 at 800°C and 1000°C.

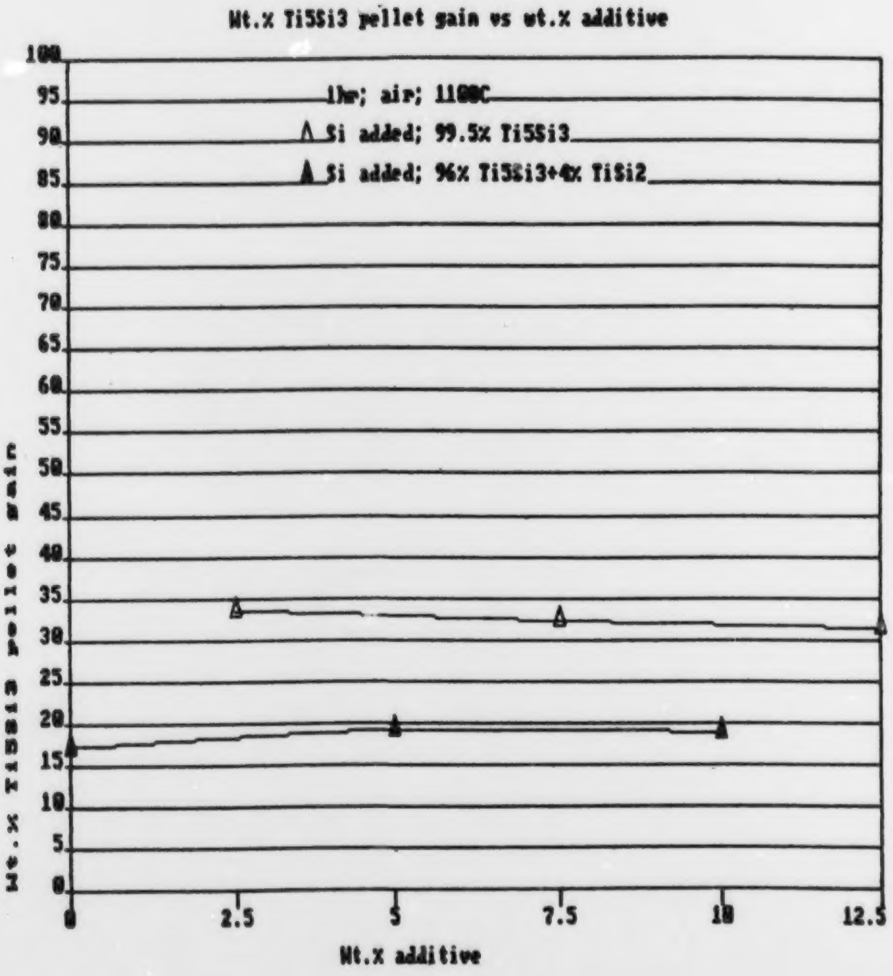

Figure 27: The Effect of Powder Types on the Oxidation of Ti_5Si_3 at 1100°C.

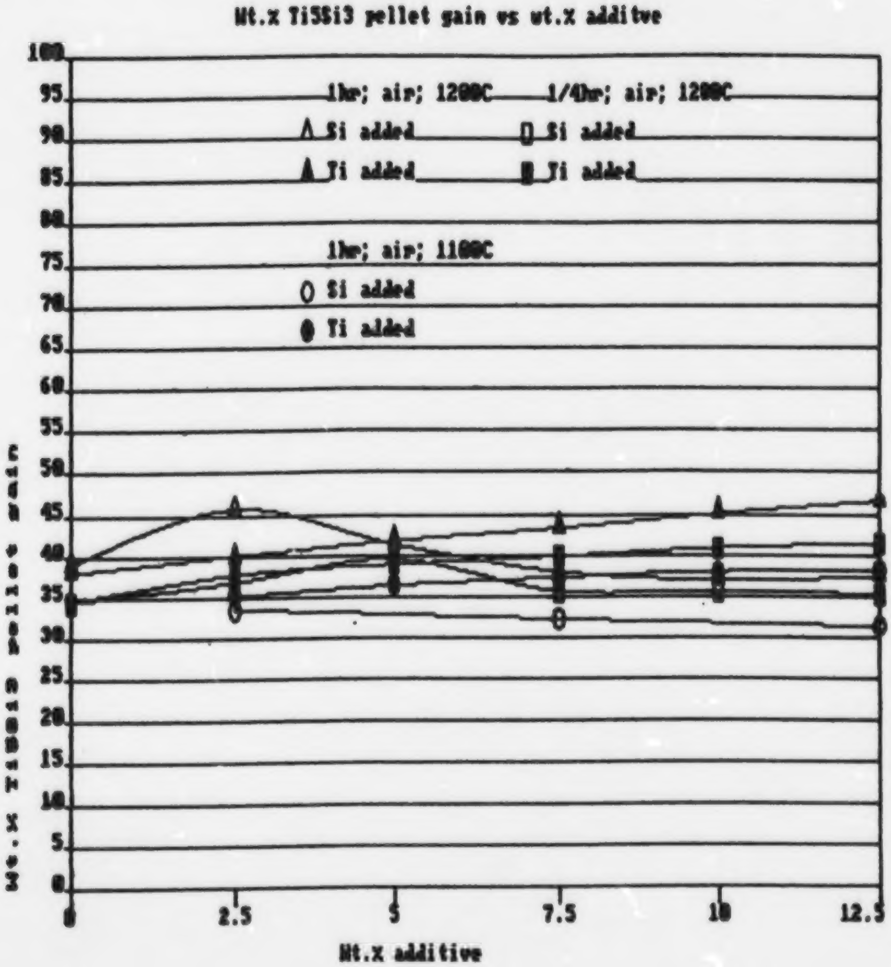

Figure 28 : The Effect of Silicon and Titanium Additions on the Oxidation of Ti_5Si_3 at 1200°C.

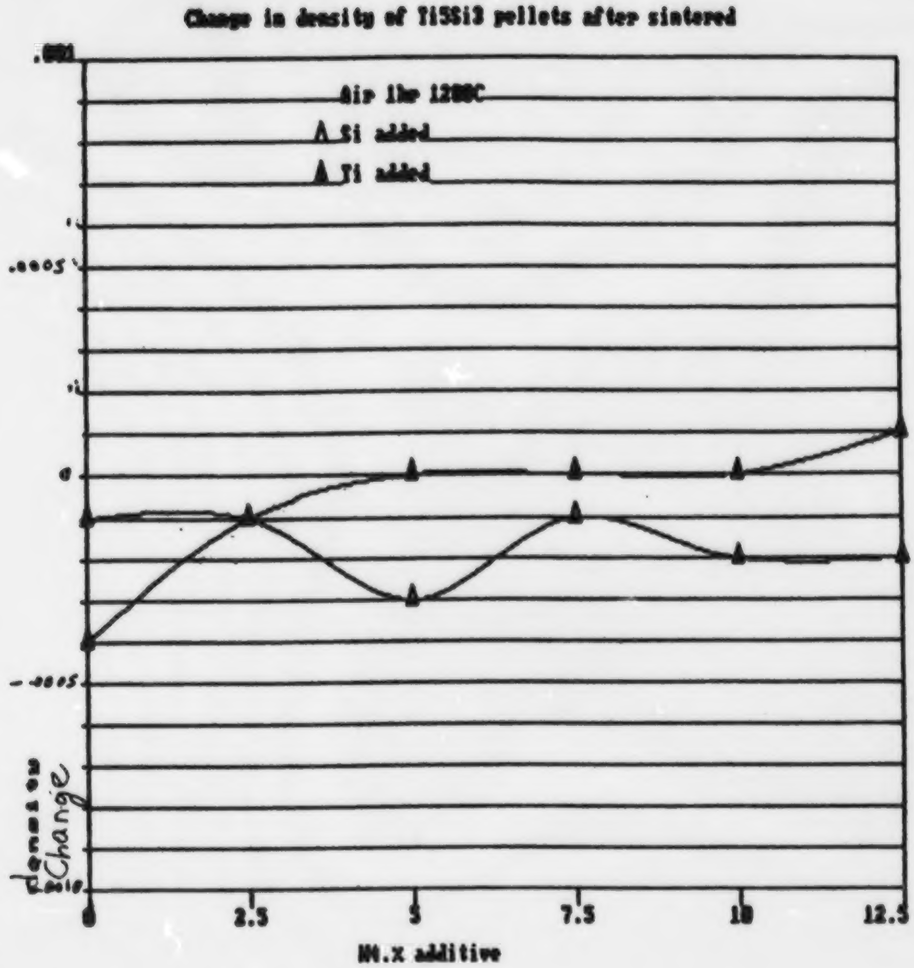

Figure 29: The Effect of Silicon and Titanium Additions on the Density of Ti_5Si_3 in Air at 1200°C.

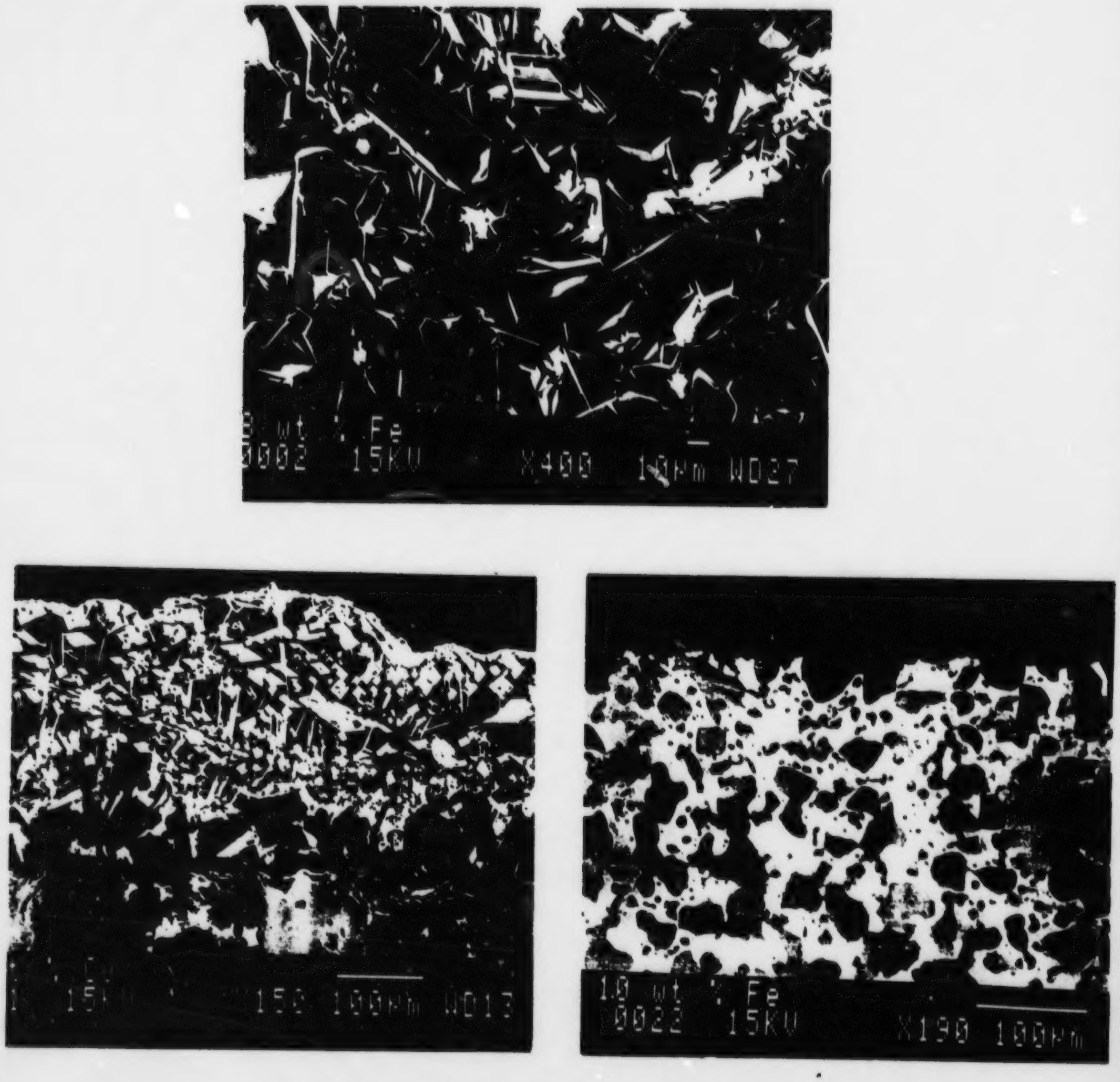
8 wt % Fe
0002 15KV X400 10µm WD27
15K 150 100µm WD13
10 wt % Fe
0022 15KV X190 100µm

Figure 30: Oxide Growth on Titanium Silicide.

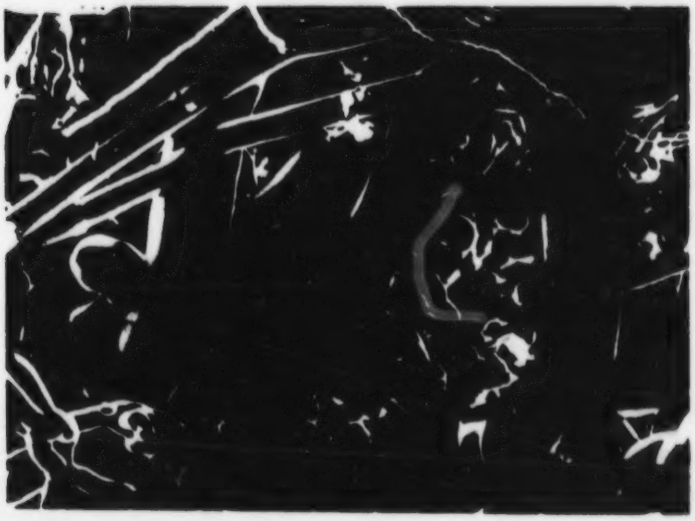

Figure 31: Silica Whiskers Observed on the Surface of Oxidized Titanium Silicide at High Temperature.

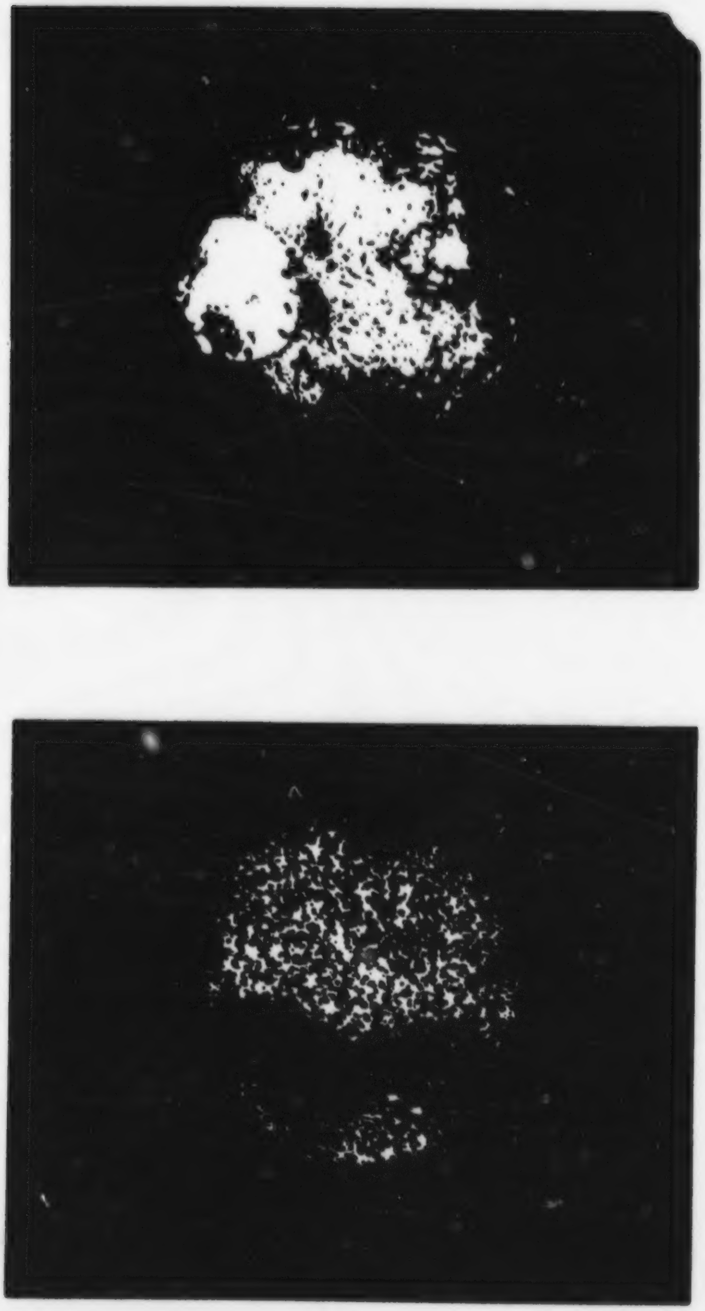

Figure 1: Optical Micrographs of Plasma Treated Titanium Silicide.

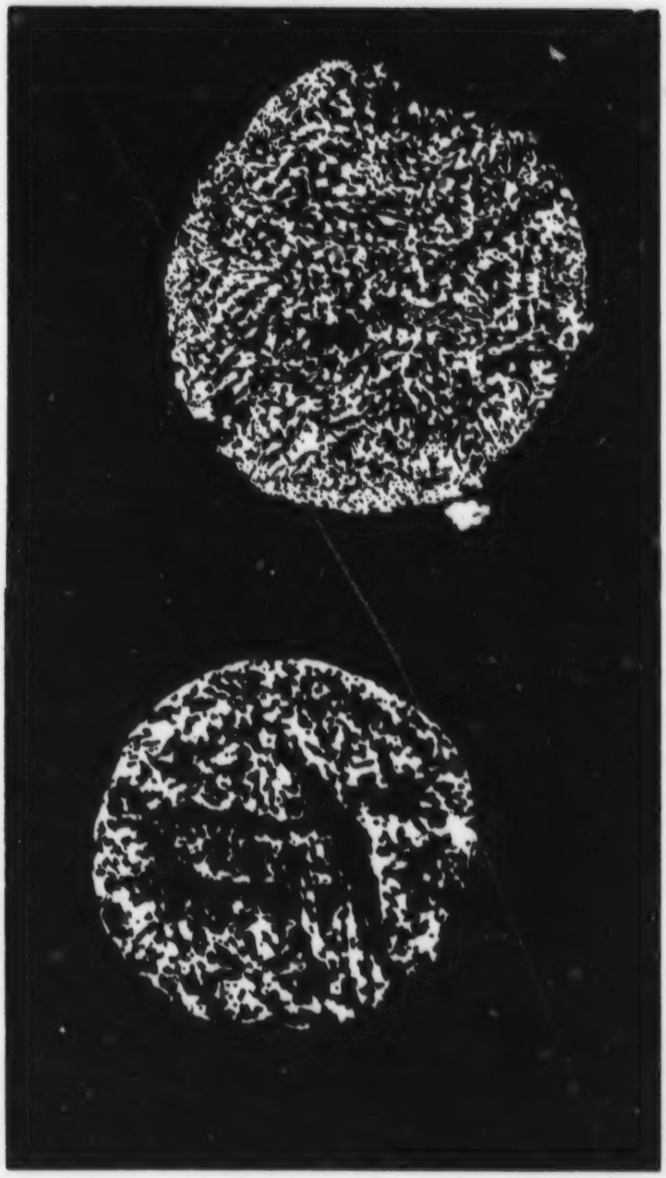

600X

Figure 2: Optical Micrograph of Plasma Treated Titanium Silicide.

RAPID MELTING AND SOLIDIFICATION OF TITANIUM SILICIDES

A series of experiments were performed in which prefused mixtures of titanium silicides of varying composition were passed through the plasma. These plasma processed particles showed unusual and fine microstructures. Some examples of the microstructures obtained are shown in Figures 1 and 2.

RESEARCH SUMMARY

This research has demonstrated that it is possible to produce titanium silicides by reduction with carbon, aluminum, magnesium, and calcium. When carbon is employed the product contains some carbon. With magnesium and calcium there is virtually no contamination by the reductant. For aluminum the titanium silicide contains about one percent of aluminum impurity. Aluminum is considered to be the best reducing agent as its vapour pressure is low at the operating temperature and also a molten slag phase is readily obtained. The silicide is produced in particulate form in the slag and further research is required to study methods of extraction. Electrostatic separation is a process which could be employed to recover the silicide if the silicide can be obtained in particulate form then it could be employed to produce coatings. Also, it is possible to dissolve the silicide in a copper bath while performing reduction and then during cooling, titanium silicide crystals precipitate from the melt. These crystals can then be extracted from the melting by leaching.

Oxidation tests were performed on both Ti_5Si_3 and $TiSi_2$ containing impurities. In general, the oxidation resistance of the pure silicides was excellent. However, impurity additions increased the oxidation rate. The addition of copper resulted in catastrophic oxidation due to the formation of liquid oxide phases. Iron additions had only a slight effect on the oxidation rate particularly at low iron levels. On the other hand, with aluminum there was a more pronounced increase in the rate of oxidation.

In summary, this work has demonstrated the technical feasibility of producing titanium silicide in particulate form by metallothermic reduction. This material could be employed to produce oxidation resistance coatings.

CONCLUSIONS

(1) Phase diagrams were determined for the Fe-Ti and Ti-Si systems using the F*A*C*T system. Work is being completed on the ternary Fe-Ti-Si system.

(2) F*A*C*T analysis using the EQUILIB program was performed for the metallic reducing agents. The optimum conditions were determined for the effects of temperature, amount of reducing agent, and titania to silica ratio.

(3) Titanium silicides can be produced by aluminothermic, calciothermic, and magnesiothermic reduction. Aluminum is the preferred reductant due to its relatively low vapour pressure and the reaction product (Al_2O_3) has a lower melting point than either CaO or MgO. The titanium silicide was obtained as small particulates. The reactions were as follows:

$$TiO_2 + SiO_2 + 2\ 2/3\ Al - TiS + 4/3\ Al_2O_3$$

$$TiO_2 + 6SiO_2 + 6Mg - TiSi + Si + 2(MgO.SiO_2) + 2(2MgO.SiO_2)$$

$$TiO_2 + 6SiO_2 + 6Ca - TiSi + Si + 2(CaO.SiO_2) + 2(2CaO.SiO_2)$$

(4) In-flight magnesiothermic reduction of titania-silica mixtures was demonstrated on a laboratory-scale.

(5) Titanium silicide crystals can be grown from a copper melt either during the reduction of titania and silica or by adding titanium and silicon in powder form to the melt. The titanium silicide crystals can then be recovered from the copper melt by leaching to give titanium silicide crystals containing less than 0.5 mass percent copper.

(6) In the carbothermic reduction process bulk titanium silicide was produced. There was considerable loss of the silicon in the form of $SiO_{(g)}$ during the reduction process. The silicon monoxide gas reacted with graphite crucible to produce silicon carbide crystals

(7) The excellent oxidation resistance of pure $TiSi_2$ at high temperatures can be attributed to the formation of a uniform, protective silica-titania glass that tends to minimize the effect of initial surface defects. Parabolic rate constants are typically $2.4\times10^{-3} (^{mg}/_{cm^2})^2/h$ at 1200°C and $4\times10^{-3} (^{mg}/_{cm^2})^2/h$ at 1300°C.

(8) Titanium disilicide containing up to 10 wt.% iron can be sintered at 1420°C for 20 minutes to provide samples with maximum surface porosity of 10%. Such samples show a slight decrease in oxidation resistance, with parabolic rate constants increasing with iron content to a value of about $3\times10^{-2} (^{mg}/_{cm^2})^2/h$ for a sample containing 10 wt.% Fe oxidized at 1200°C. Iron additions have the identical effect on oxidation resistance at 1300°C, with all samples experiencing an increase in the

parabolic rate constant of about 2×10^{-3} $(\mathrm{mg/cm^2})^2/\mathrm{h}$ over corresponding samples oxidized at 1200°C. The decrease in oxidation resistance with the addition of iron is attributed to the presence of a phase low in silicon content which cannot provide sufficient silica upon oxidation to provide a protective film. This results in more rapid localized oxidation, eventually leading to the separation of the $TiSi_2$ grains.

(9) Titanium disilicide containing up to 10 wt.% aluminum can be sintered at a maximum temperature of 1300°C for 4 hours to provide samples with maximum surface porosity of 16%. Such samples show a dramatic decrease in oxidation resistance, with parabolic rate constants increasing with aluminum content to a value of about $8 \times 10^{-1} (\mathrm{mg/cm^2})^2/\mathrm{h}$ for a sample containing 10 wt% Al oxidized at 1200°C. The decrease in oxidation resistance is again attributed in part to the presence of a phase of low Si:Me atomic ratio. In addition, the aluminum oxide is believed to act as a network modifier in the silica glass, reducing its protective properties considerably. This results in the complete preferential oxidation of the phase high in Al and low in Si that separates grains of $TiSi_2$. This intergranular oxidation leads to a drastic reduction in the strength of the material.

(10) Titanium disilicide containing up to 10 wt% copper can be sintered at a maximum temperature of 1350°C for 60 minutes to provide samples with maximum surface porosity of 8%. Such samples show no useful resistance to oxidation at temperatures as low as 1000°C due to the formation of a liquid oxidation product upon localized oxidation of one phase very high in copper content but very low in silicon content.

PERSONNEL

Personnel involved in the project

Graduate Students: - D. Mallette
- C. Lelievre

Technicians: - D. Smith
- M. Niedbala

Post-Doctorate:

Research Associate - Dr. M. Ghoreshy

APPENDIX

PUBLICATIONS RESULTING FROM THIS WORK

Ferrous and Non-Ferrous Alloy Processes

CIM, 1990

Magnesiothermic production of titanium silicide in a plasma furnace

C. Lelievre, H. Baas, C.A. Pickles
Department of Metallurgical Engineering, Queen's University,
Kingston, Ontario, Canada, K7L 3N6

J.M. Toguri
Department of Metallurgy and Materials Science, University of Toronto,
Toronto, Ontario, Canada, M5S 1A4

ABSTRACT

Titanium silicide has excellent oxidation resistance and is employed as a protective coating. Magnesiothermic production of titanium silicide was studied in a plasma furnace according to the following reaction:

$$TiO_2 + 6SiO_2 + 6Mg - TiSi + Si + 2(MgO.SiO_2) + 2(2MgO.SiO_2)$$

The effects of the TiO_2 to SiO_2 ratio, energy consumption, and alumina and magnesium additions on the product are discussed. Also the reaction was performed in the presence of copper, in which case titanium silicide crystals grew from the copper melt during solidification. The copper could then be removed by leaching. In addition, in-flight plasma magnesiothermic reduction of prefused titania-silica mixtures was investigated.

KEYWORDS: Titanium Silicide, Plasma Smelting.

INTRODUCTION

Metal Silicide Systems

The existence of metal silicides has been recognized for over a century. In particular, titanium silicides were produced in 1895, when H. Moissan [1] and L. Levy [2] both produced the silicide. In the case of Moissan the composition of his product was unknown, while Levy is known to have produced $TiSi_2$. Eleven years later, O. Honigschmid [3], using the aluminothermic method, produced $TiSi_2$. In 1908, P. Askenasy and C. Ponnaz [4] reported that they had produced Ti_2Si_3. However, they were unable to confirm the homogeneity of their product. The major problem faced by these early workers was their inability to analyze their products accurately. It has only been since the development of modern phase-analytical methods, notably thermal analysis, metallography and x-ray diffraction, that scientists have been able to ensure that the reaction products were actually composed of a pure and singular phase. The ability to analyze the product accurately was an important step towards determining the most suitable method to produce intermetallics in binary systems. The product of a binary system reaction is determined by a large number of variables. Usually the primary factor is the equilibrium state of the system being studied. Other variables of interest are composition, temperature, and pressure. In alloy chemistry, the vapor pressures of the elements are usually small enough to be ignored.

Although there seems to be only a few methods of preparation for metal silicides, the number of different metal silicides which have been produced is abundant. Silicides exist in combination with the alkali and alkaline earth metals, group IVa to VIa metals, manganese, iron, nickel, the platinum metals, the rare earth metals, and the actinides. Although the existence of these metal silicides is no longer questioned, they are not all well understood. Conflicting data on the crystal structure, formation temperature, and the specific composition of individual systems are still being reported. However, some systems are fairly well understood due to extensive research. Table I summarizes the silicide systems which have been well characterized.

Li_4Si Li_2Si										
$NaSi$	Mg_2Si									
KSi	Ca_2Si $CaSi$ $CaSi_2$	Sc_5Si_3	Ti_3Si Ti_5Si_3 $TiSi$ $TiSi_2$	V_3Si V_5Si_3 VSi_2	Cr_3Si Cr_5Si_3 $CrSi$ $CrSi_2$	Mn_3Si Mn_5Si_3 $MnSi$ $MnSi_{1.7}$	Fe_3Si Fe_5Si_3 $FeSi$ $FeSi_2$*	Co_2Si $CoSi$ $CoSi_2$	Ni_3Si Ni_5Si_2 Ni_2Si Ni_3Si_2 $NiSi$ $NiSi_2$	$\alpha(CuSi)$ $\beta(CuSi)$ γ-Cu_5Si $Cu_{33}Si_7$ $Cu_{15}Si_4$
$RbSi$	Sr_2Si $SrSi$ $SrSi_2$	Y_5Si_3 YSi YSi_2*	Zr_3Si Zr_2Si Zr_5Si_3 Zr_4Si_3 $ZrSi$ $ZrSi_2$	Nb_3Si Nb_5Si_3* $NbSi_2$	Mo_3Si Mo_5Si_3 $MoSi_2$		Ru_2Si $RuSi$* Ru_2Si_3	Rh_3Si Rh_5Si_3 $Rh_{20}Si_{13}$ Rh_4Si_5 $RhSi$	Pd_3Si Pd_2Si $PdSi$	
$CsSi$	$BaSi$ $BaSi_2$*	$LaSi_2$	Hf_2Si Hf_5Si_3 $HfSi$ $HfSi_2$	Ta_3Si Ta_2Si Ta_5Si_3* $TaSi_2$	W_5Si_3 WSi_2	Re_5Si_3 $ReSi$ $ReSi_2$	$OsSi$ Os_2Si_3	Ir_3Si Ir_2Si Ir_3Si_2 $IrSi$ $IrSi_3$	Pt_3Si* Pt_2Si* Pt_6Si_5 $PtSi$	

$LaSi_2$	$CeSi$ $CeSi_2$	$PrSi_2$*	$NdSi_2$*		$SmSi_2$*	$EuSi_2$	Gd_5Si_3 $GdSi_2^{\delta}$	Tb_5Si_3 $TbSi_2$	Dy_5Si_3 $DySi_2^{\delta}$	Ho_5Si_3 $HoSi_2$	Er_5Si_3	Tm_5Si_3	Yb_5Si_3	Lu_5Si_3

	Th_3Si_2 $ThSi$ Th_3Si_5 $ThSi_2^{\delta}$		U_3Si U_3Si_2 USi* U_3Si_5 USi_2^{δ}	$NpSi_2$	Pu_5Si_3 $PuSi$ Pu_3Si_5 $PuSi_2$

* There is more than one phase with or near this composition.

TABLE I: Summary of the Silicide Systems which have been Characterized from Borides, Silicides, and Phosphides by B. Aronsson, T. Lundstrom and S. Rundqvist, Methuen, p. 17 (1964).

There has been particular interest in the transition metal silicides for several decades due to their corrosion resistance, refractory properties, and hardness. In the past decade, a new field of research has developed since these materials can be used as gate electrodes and conductors in very-large-scale integration (VLSI) devices. This new interest has led to an improved understanding of the stable phases in several transition metal silicides and related systems. These studies may also give insight into the factors affecting the strengths of chemical bonds in solids. It is thus important to establish reliable methods of preparation for the transition metal silicides in order to continue to enlarge an already extensive database.

Preparation of Titanium Silicides

Nearly all the methods which are used for the preparation of carbides, nitrides, and borides can be applied to the production of metal silicides. Silicon like carbon and boron, will react with metals only at relatively high temperatures to produce metal silicides. Often these reactions are hampered by slow reaction kinetics. The reaction kinetics for metal silicide production can be improved by using mixtures of the reactants in finely divided form. The current methods of production of metal silicides are [5]:

i) Synthesis by fusion or sintering;
ii) Reduction of the metal oxides with silicon;
iii) Reaction of the metal oxides with SiO_2 and C;
iv) Reduction of the oxides with Al or Mg;
v) Reaction of oxides in a molten alloy;
vi) Reaction of metal with silicon halide or of a metal halide with silicon;
vii) Fused-salt electrolysis.

The purity, structure, and cost of the metal silicide desired will be the deciding factors in selecting the production method. To ensure a pure and homogeneous product several precautions should be taken: (1) the reactants should be pure, (2) the preparation must be performed without risk of contamination from the crucible or the furnace atmosphere, and (3) the subsequent heat treatment of the sample must be performed carefully to ensure that equilibrium conditions are obtained in the final product.

The introduction of impurities into the final product is often very difficult to avoid. Some of these impurities have a negligible influence on the equilibrium state of the system being studied. However, even a trace amount of a particular impurity can have a disastrous effect on the mechanical properties of the silicide. In the silicide systems, impurity atoms such as carbon, nitrogen, or oxygen can promote the formation of metal-rich ternary phases which can easily be mistaken for binary phases. Impurities are usually introduced into the final product by the refractory container and/or the processing atmosphere. It is possible to produce pure silicides by sintering fine powders of metal and silicon. However care must be taken to avoid contaminating the final product if further grinding or sintering is required. The silicide product of fused salt electrolysis is in the form of a dendritic powder which is difficult to handle.

Silicides can be formed at elevated temperatures in a plasma furnace. Different metals and metal oxides have been reacted with silicon or silica in a plasma furnace [6]. The most significant aspect of this work was that when metal oxides were used some silicon was lost by evaporation. The silicide products were well crystallized and were of a high purity. It was concluded that the production of many metal silicides was possible using the plasma furnace.

The group IVa to VIa metal silicides are now fairly well characterized. More specifically, the titanium silicides have now been established. Titanium silicide has been produced at low temperatures by reacting silica with pure titanium metal [7]. Also in the same work, titanium silicide was produced by reacting pure silicon metal with pure titanium metal. The titanium metal was in the form of a thin film, which resulted in an interfacial silicide. The metal thin film was reacted on silica and pure silicon substrates. The silica substrate required a temperature 200 degrees celsius higher than the reaction temperature required for the silicon substrate. The silicides produced from both these reactions were found to be of differing compositions. In Japan, in the mid-seventies, a group at Hitachi [8] produced Ti_5Si_3, TiSi, and $TiSi_2$. These silicides were all produced at temperatures below 700 degrees celsius.

As of 1952, three binary phases were identified in the Ti-Si system: (1) TiSi, (2) $TiSi_2$, and (3) Ti_5Si_3. Figure 1 shows the phase diagram of the Ti-Si system, as reported by M. Hanson, H.D. Kessler, and D.J. McPherson [9]. Titanium disilicide, $TiSi_2$, has a slightly deformed

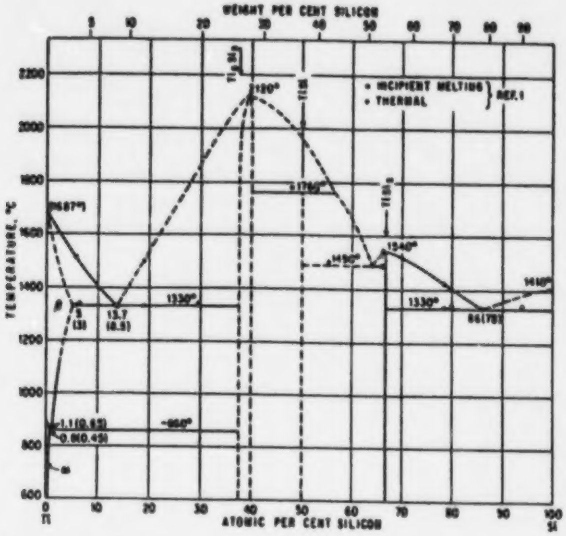

Figure 1: Phase Diagram of the Ti-Si System (9)

orthorhombic crystal lattice, while Ti_5Si_3 has an hexagonal lattice structure. The heat of formation of TiSi is approximately 40 kcal/mol and the heat of formation for $TiSi_2$ is about 44 kcal/mol. The melting point of TiSi is 1900°C while the melting point of titanium disilicide is 1500°C. In general, silicides have a Vickers micro-hardness value which ranges from 800 to 1500 kg/mm^2. These hardness values are well above the hardness of nickel and are about equivalent to those obtained in carbon-rich martensitic steels. Although the silicides exhibit great hardness they are nonetheless very brittle. However, due to their excellent corrosion resistance and good mechanical properties, the silicides have been used in some space-flight and turbine technologies. Their high thermal-shock resistance compared to oxide ceramics is largely due to their higher thermal conductivity. Another important application for the silicides is as oxidation resistant coatings for refractory metals. A limiting factor in their use is pin-hole and/or pest corrosion which reduces their reliability.

In this research titanium silicide was produced by magnesiothermic reduction of silica and rutile using a plasma arc furnace according to the following reaction:

$$TiO_2 + 6SiO_2 + 6\ Mg - TiSi + Si + 2(MgO.SiO_2) + 2(2MgO.SiO_2) \quad ...(1)$$

The effects of energy consumption, magnesium and alumina additions and the titania to silica ratio of the feed were studied. The major advantages of this process are the low cost of reactants and also the silicide can be produced as fine spherical particles.

EXPERIMENTAL

A schematic diagram of the plasma arc furnace is shown in Figure 2. The furnace was operated in the single phase mode at a power level of 24 Kw

---

(115V, 2
The gra
supporte
Rut

Limited.
were emp
standard

The powd
A small
in a har
grams a
inches.
briquett
the grap
variable

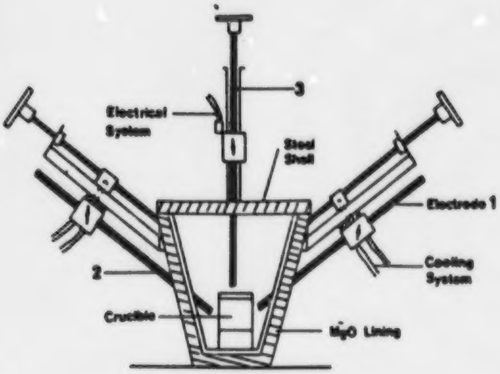

Figure 2: Schematic Diagram of the Plasma Arc Furnace.

(115V, 210A). The steel furnace shell was lined with magnesia (98% MgO). The graphite electrodes were 20mm in diameter. The electrodes were supported by aluminum water-cooled holders.

Rutile powder (TiO_2) was supplied by Canadian Titanium Pigments Limited. Reagent grade silica (BDH) and reagent grade magnesium (Fisher) were employed. The magnesium was in the size range of 40 to 80 mesh. The standard mixture was as follows:

6 moles of magnesium
1 mole of titania
6 moles of silica

The powdered reactants were weighed, mixed and then tumbled in a ball mill. A small amount of water was added to the powder which was then briquetted in a hardened steel die at about 5000 psi. The briquette weighed about six grams and had a height of about 3/8 of an inch and a diameter of 1-1/2 inches. In some cases alumina or copper was incorporated into the briquettes. In addition, the briquette was placed on a bed of alumina in the graphite crucible. The crucible dimensions are shown in Figure 3. The variables investigated included the following:

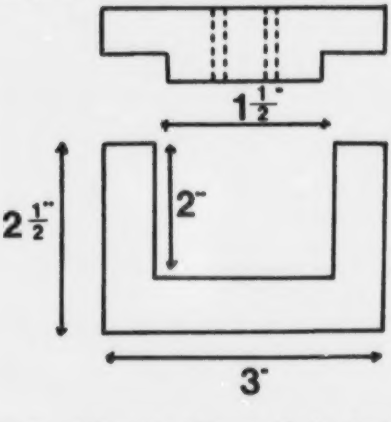

Figure 3: Schematic Diagram of the Crucible Assembly.

(1) energy input (Kwh),
(2) TiO_2 to SiO_2 ratio,
(3) magnesium addition, and
(4) alumina addition.

Experiments were performed in which magnesium and prefused mixtures of titania and silica were passed through an argon-magnesium vapour plasma. These tests were performed to demonstrate the possibility of the in-flight continuous production of titanium silicide by plasma techniques. In addition, magnesium vapour was passed through a prefused mixture of titania and silica in a two stage reactor in an argon atmosphere.

The metal and slag products were analysed for titanium, silicon, aluminum and magnesium. Also, the various phases were examined by optical and scanning electron microscopy. X-ray analyses was performed on a number of the reaction products. The thermodynamics of the system were studied using F*A*C*T.

RESULTS AND DISCUSSION

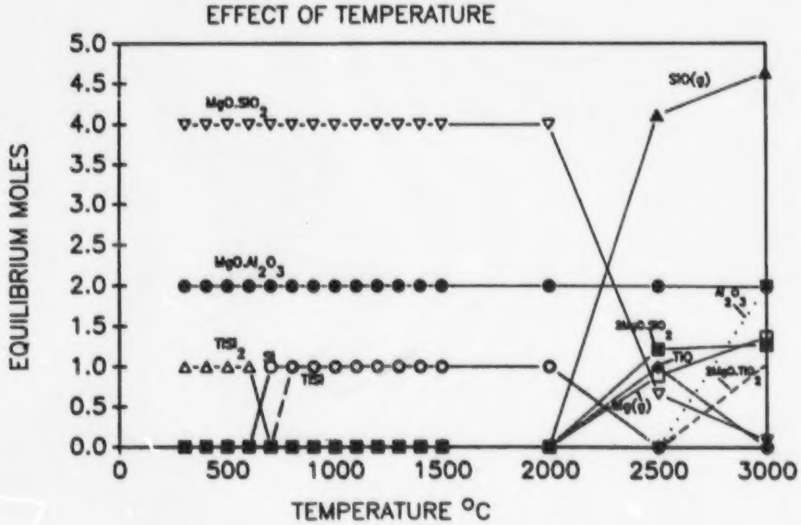

Figure 4: The Effect of Temperature on the Product Composition as Calculated by F*A*C*T.

The results of the F*A*C*T analysis using the EQUILIB program are shown in Figures 4 to 7. Figure 4 demonstrates that in the temperature range of about 1000 to 2000°C the reaction products are titanium silicide (TiSi), silicon, magnesium silicates and in the presence of alumina, magnesium aluminates. At temperatures over 2000°C the reaction product becomes complex. Silicon monoxide gas, magnesium vapour, titanium monoxide, and magnesium titanates can form.

The effect of magnesium additions, which is shown in Figure 5, can be conveniently divided into three regions as follows:

(1) below five moles of Mg,
(2) between five and seven moles of Mg, and
(3) above seven moles of Mg.

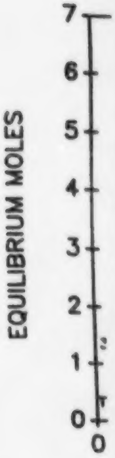

Figure 5:

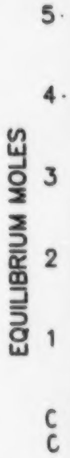

Figure 6

Below f
silica
mole.
silicon,
free ma

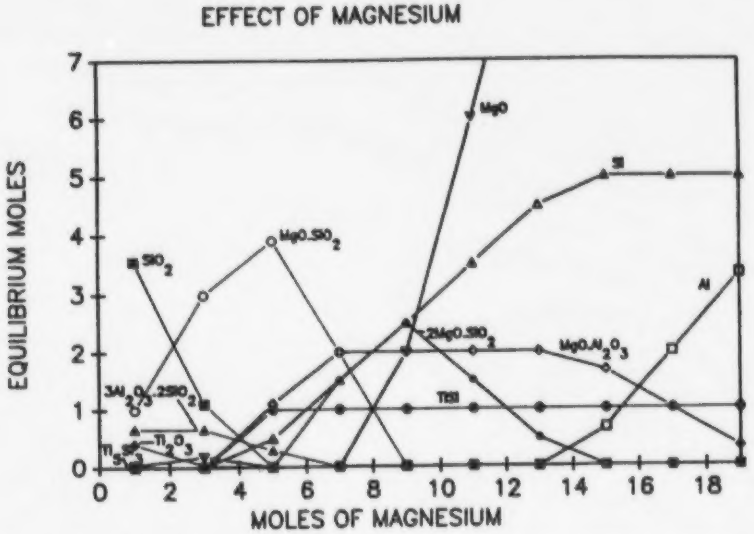

Figure 5: The Effect of Magnesium Additions on the Product Composition as Calculated by F*A*C*T.

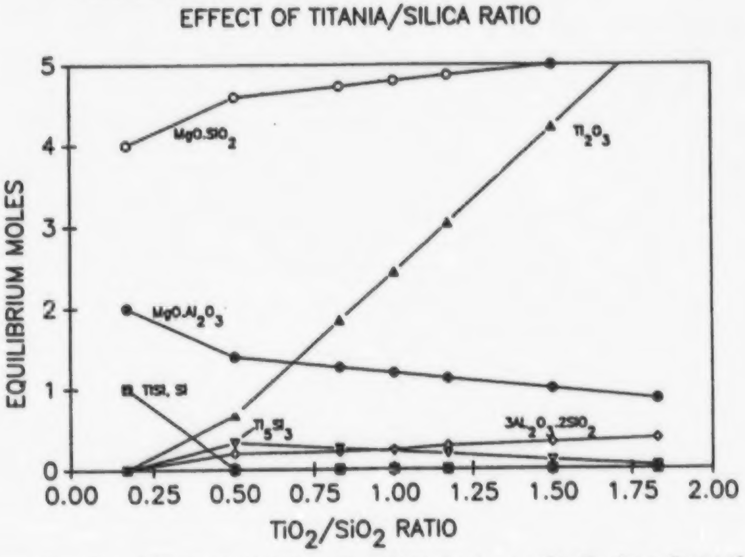

Figure 6: The Effect of Titania to Silica Ratio on the Product Composition as Calculated by F*A*C*T.

Below five moles there is insufficient magnesium to reduce all of the silica and thus the amount of titanium silicide produced is less than one mole. Above five moles, the major reaction products are titanium silicide, silicon, magnesium silicates and magnesium aluminates. Above seven moles, free magnesium oxide occurs, the amount of silicon increases and eventually

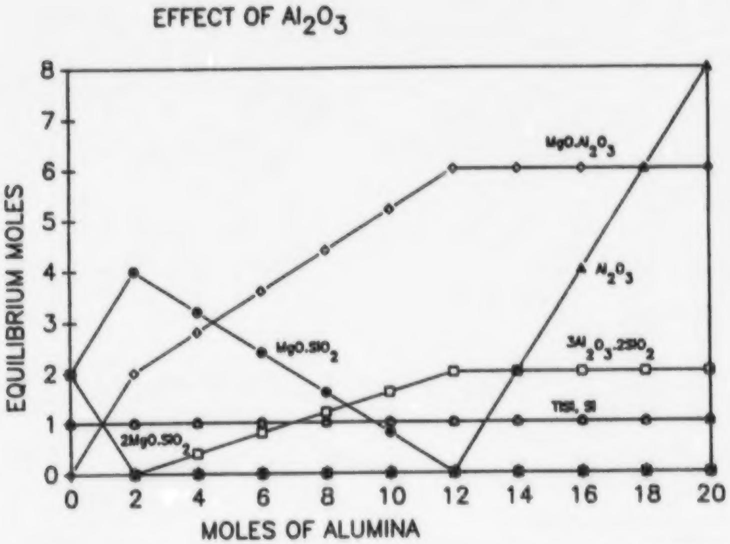

Figure 7: The Effect of Alumina Additions on the Product Composition as Calculated by F*A*C*T.

aluminum is produced.

Similarly, the effect of the titania to silica ratio can be divided into two regions - Figure 6. Below a ratio of 0.5, TiSi and silicon are produced. Above 0.5, the amount of Ti_2O_3 increases rapidly and thus TiSi is replaced by Ti_5Si_3. At high titania to silica ratios only a small amount of titanium silicide is produced. The addition of alumina which was added as a flux, promotes the formation of magnesium aluminates and alumino-silicates at the expense of the magnesium silicates - Figure 7. At alumina additions of ove- 12 moles, free alumina is present and the magnesium silicates have disappeared.

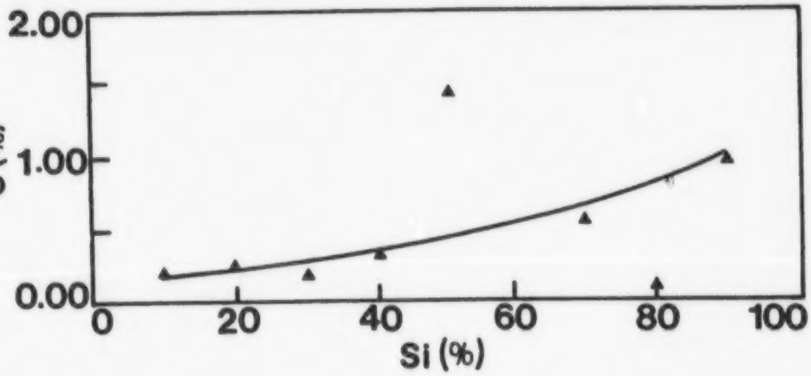

Figure 8: The Effect of Silicon on the Carbon Content of Fused Mixtures of Titanium Silicide.

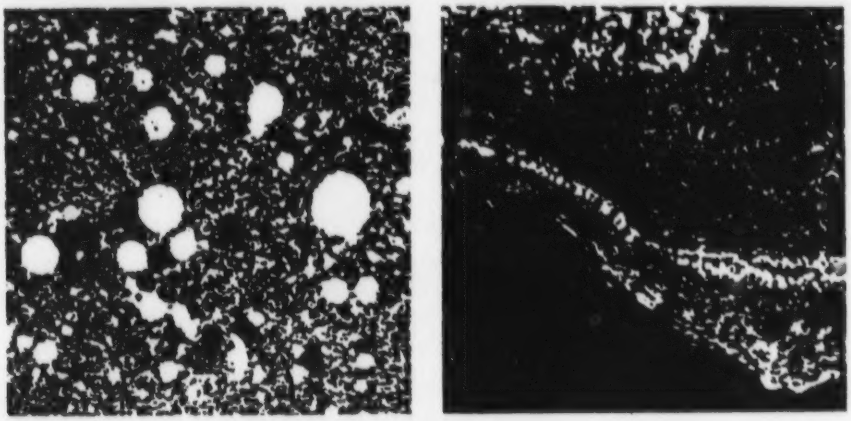

600X 1800X

Figure 9: The Morphology of the Reaction Products Produced by Magnesiothermic Reduction.

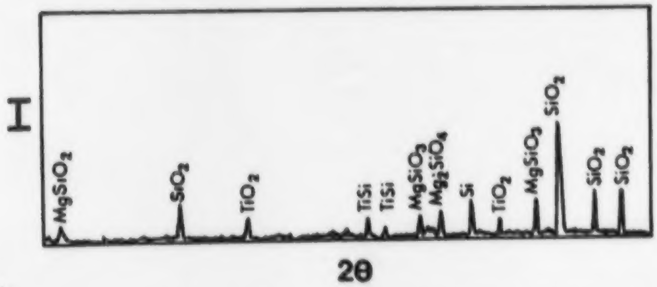

Figure 10: X-Ray Analysis of the Reaction Products.

Since the experiments were performed in a graphite crucible the maximum possible carbon content of the product was determined by melting a mixture of titanium and silicon. The carbon content of the fused product was determined as a function of the silicon content. In general, the carbon content, below sixty percent silicon, was less than one percent - Figure 8.

Figure 9 shows the morphology of the reaction product from the experiments performed with briquettes. It can be seen that the silicide is in particulate form. X-ray analysis of the reaction products indicated the presence of titanium silicides, silica, titania, and magnesium silicates, - Figure 10.

The effect of energy consumption on the composition of the titanium silicide is shown in Figure 11. At low energy consumptions the silicon content was high and the titanium concentration was low. On the other hand, at high energy levels the silicon level decreased. As shown in Figures 12 and 13, magnesium and alumina additions did not have an effect on the titanium to silicon ratio of the product. In general, the magnesium content of the titanium silicide was approximately 0.1 mass percent, while the aluminum content was about one mass percent when alumina was added.

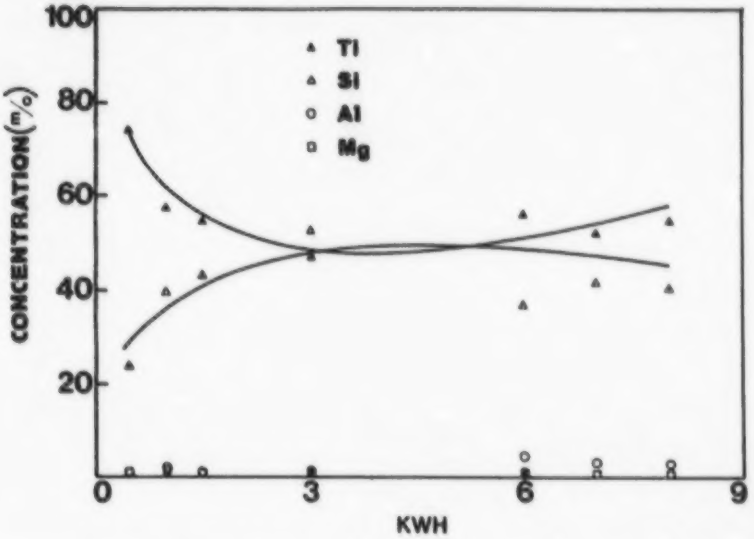

Figure 11: The Effect of Energy Consumption on the Product Composition.

The titanium to silicon ratio of the product could be changed by varying the titania to silica ratio of the feed - Figure 14. At high ratios very little metal was produced.

The reaction product when copper was added to the briquette is shown in Figure 15. Titanium silicide crystals were found in the copper matrix. In a separate study, titanium silicide crystals were grown in a copper melt by adding titanium and silicon to a copper bath (10). The solidified melt

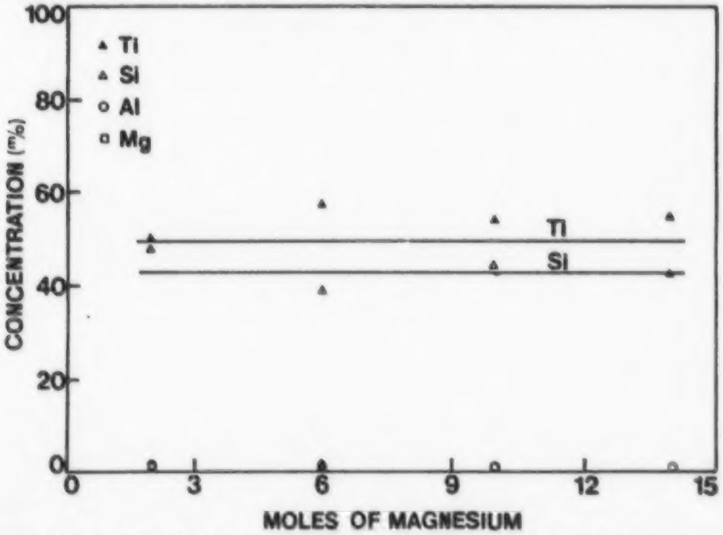

Figure 12: The Effcctof Magnesium Additions on the Product Composition.

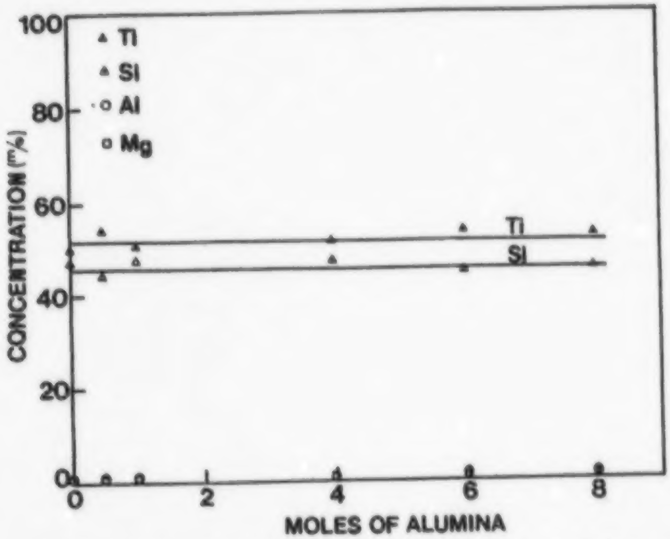

Figure 13: The Effect of Alumina Additions on the Product Composition.

was crushed and leached in nitric acid. The leaching results for different particle sizes are summarized in Figure 16. In general, leaching times of about 1500 minutes were necessary to achieve copper contents of less than 0.5 mass percent. X-ray analyses of the leach residue demonstrated that the major constituents were $TiSi_2$, TiSi and a small amount of $Cu_{0.1}Si_{1.9}Ti$.

The results of magnesiothermic in-flight reduction of prefused titania-silica mixtures are summarized in Figure 17. It can be seen that

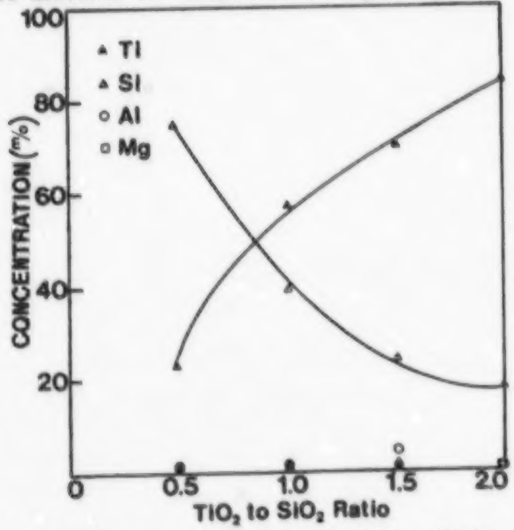

Figure 14: The Effect of Titania to Silica Ratio on the Product Composition.

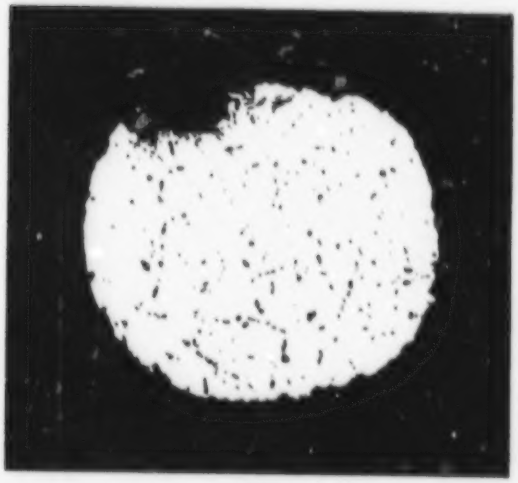

Figure 15: Titanium Silicide Crystals in a Copper Matrix.

titanium silicide has formed as discrete droplets in spheroidized titania-silica particles. Since the slag phase contains magnesium oxide this confirms that in-flight reduction is possible. Metallic product was observed to form at the surface of the particles which indicates that the reducing agent is magnesium vapour. This process has considerable

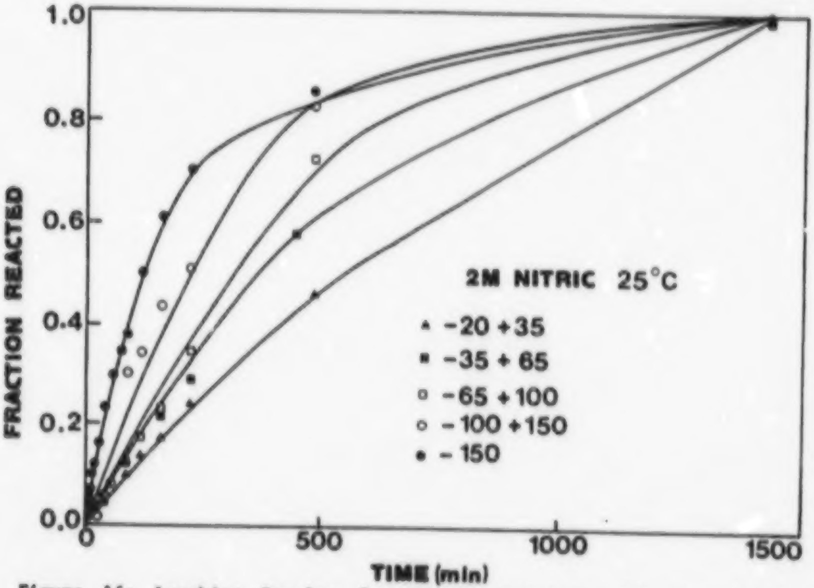

Figure 16: Leaching Results for Copper Containing Titanium Silicide Crystals at Various Size Fractions.

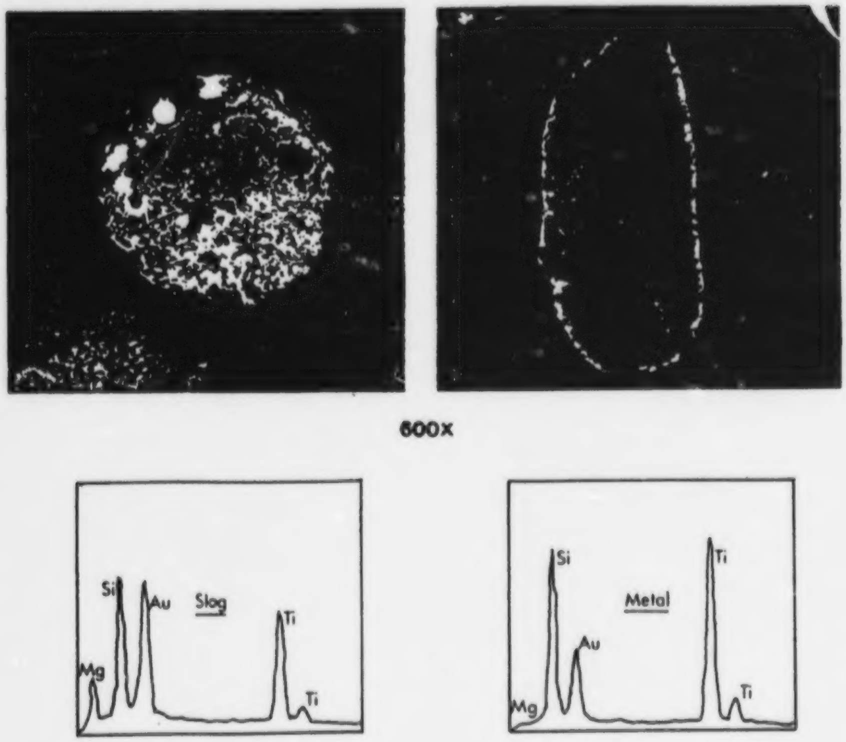

Figure 17: Morphology of the Reaction Products from the In-Flight Magnesiothermic Reduction of Prefused Mixtres of Titania and Silica.

potential as a continuous technique for the production of silicides by magnesiothermic reduction.

CONCLUSIONS

(1) Titanium silicide was produced in particulate form by magnesiothermic reduction of titania and silica. The general reaction is as follows:

$$TiO_2 + 6SiO_2 + 6Mg = TiSi + Si + 2(MgO.SiO_2) + 2(2MgO.SiO_2)$$

The magnesium content of the product was about 0.1 mass percent. In the presence of alumina the silicide contained about 1 mass percent aluminum.

(2) Titanium silicide was recovered in a copper melt which could be subsequently leached to give titanium silicide crystals containing less than 0.5 mass percent copper.

(3) In-flight plasma magnesiothermic reduction of titania-silica mixtures is technically feasible.

ACKNOWLEDGEMENTS

This work was funded by the Department of Energy, Mines and Resources (Canada) through DSS Contract No. 555S.23440-7-9161.

REFERENCES

(1) Moissan, H., Compt. rend., 120, 290, (1895).
(2) Levy, L., Compt. rend., 121, 1148, (1895).
(3) Honigschmid, O., Compt. rend., 143, 224, (1906).
(4) P. Askenasy and C. Ponnaz, Z. Electrochem. 14, 810, (1908).
(5) Schwarkopf, P., and Kieffer, R., Refractory Hard Metals, Borides, Carbides, Nitrides, The Macmillan Company, New York, 319, (1953).
(6) De Vynck, Y.A., Utilisation de Fours a Plasma dans le Domaine de la Ceramíque Special. Formation de Silicures, Silicates Industriels. 4, 109, (1974).
(7) Krauetle, H., M.A. Nicolet, J.W. Mayer, Phys. Status Solidi A, 20(1), K33, (1973).
(8) Kato, H., Y. Nakamura, Thin Solid Films, 34(1), 135-138, (1976).
(9) Hansen, M., H.D. Kessler, and D.J. McPherson, Trans. ASM, 44, 518, (1952).
(10) Baas, H., C.A. Pickles, and J.M. Toguri, "Recovery of Titanium Silicide Crystals from a Copper Melt", to be published.

High Temperature Oxidation and
Sulphidation Processes CIM, 1990

High-temperature oxidation studies of titanium disilicide

D. Mallette and C.A. Pickles
Department of Metallurgical Engineering, Queen's University,
Kingston, Ontario, Canada, K7L 3N6

Abstract

The effect of impurities on the oxidation resistance of $TiSi_2$ was studied. Iron additions caused a slight increase in the oxidation rate, while samples containing aluminum or copper showed no useful resistance to oxidation. The oxidized samples were examined by optical and SE microscopy, EDS, and thin film diffractometry.

Introduction

Because of their excellent oxidation resistance and ability to withstand very high temperatures, metal silicides have potential use as a conductor in microelectronics or as a coating or bulk refractory material. Extensive research has been made to investigate the oxidation behaviour of refractory silicides such as those of molybdenum, columbium, tantalum, and titanium. However, very little is known about the oxidation of such silicides with metallic impurities.

Several studies have been made on the oxidation behaviour of pure titanium silicide (1-9). Various mechanisms have been proposed to describe this behaviour, all of which are based on a qualitative analysis of the oxidized silicide. Conflict in models arises from the complexity of behaviour encountered over a temperature range, as considerations must be made for the thermodynamic, kinetic, physical, and transport properties of the system. It is, however, agreed in general that the resistance to oxidation is due to the formation of a protective film of oxides on the surface of the silicide that is effective in reducing further oxidation of the substrate material.

One proposed method of producing titanium disilicide ($TiSi_2$) is by the reduction of ilmenite ($FeO \cdot TiO_2$) in the presence of silica (SiO_2) and a reducing agent such as carbon, aluminum, magnesium, or calcium. Titanium silicide can also be precipitated from a copper melt (10). However, the effect of an inherent impurity in the silicide on its resistance to oxidation at high temperatures must be known before this method of production can be considered feasible. The present study was undertaken in order to determine the effect of iron, copper, and aluminum impurities on the oxidation resistance of titanium disilicide.

The time and temperature dependence of the oxidation of bulk $TiSi_2$ has been studied by Schwettman et al (1) in order to provide data and a mechanism for oxidation. The proposed typical oxidation reaction,

$$TiSi_2 + O_2 \longrightarrow Ti_xO_y + SiO_2 + Ti_5Si_3 \qquad (R1)$$

was shown to be significant only above 300°C, with the amount of Ti_5Si_3 too small to be positively identified.

The controlling mechanism of oxidation in the range 300°C to 700°C is a combination of the oxidation reaction (R1) at the solid-gas interface and diffusion of oxygen through the oxide film. In the initial phase of oxidation, diffusion through micropores in the forming oxide film is rapid, and thus reaction at the surface is rate-controlling, as depicted in Figure 1.

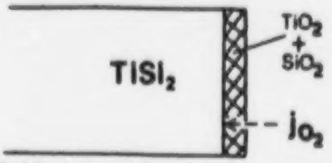

FIG. 1. Oxidation of TiSi$_2$ in the Initial Phase

Because the free energy of formation of titanium oxides is very close to that of silica, selective oxidation of titanium or silicon is unlikely to occur. Instead, an amorphous titania-silica glass will form on the surface of the silicide. As oxidation proceeds and this oxide film grows in thickness, the micropores become blocked and diffusion of oxygen through the film becomes rate-controlling. Since diffusion through a silica film at low temperatures is slow, the rate of oxidation gradually decreases with time, as shown in Figure 2 (1).

It has been found that, at temperatures below 600°C, somesilicides exhibit an increase rather than a decrease in oxidation rate. Molybdenum disilicide, although highly oxidation-resistant at temperatures above 600°C (2), oxidizes quite rapidly at temperatures under 600°C (3). This "pest corrosion" is due to the presence of molybdenum oxide, MoO_3, which is incompatible with SiO_2 and, upon formation, causes severe volume expansion in any surface crack in which it may form. The subsequent collection of oxides causes crack propogation, which promotes deterioration of the silicide. Above 600°C, MoO_3 becomes volatile, allowing for the formation of a film of pure SiO_2 that tends to bridge across any surface cracks in the silicide, forming a very protective film. However, pest corrosion has not been observed during the oxidation of titanium silicide at any temperature. Since TiO_2 is not volatile in the range of temperatures of interest, and initial surface cracks are inevitable, it must be that the TiO_2 is compatible enough with the SiO_2 to form the observed bridge-like film over the surface cracks, thus eliminating pesting at low temperatures. Schwettman et al (1) have suggested that this is partly due to the ability

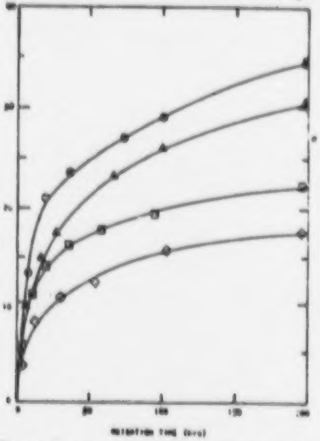

FIG. 2. Rate Data for TiSi$_2$ Oxidized at 600°C

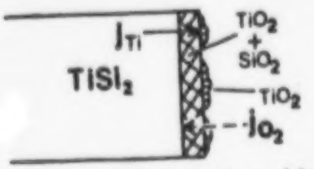

FIG. 3. Continued Oxidation of $TiSi_2$ at high temperatures

of titanium to assume fourfold coordination and replace silicon in the growing silica film without disrupting the tetrahedral network.

At temperatures of 1000°C and above, the initial stage of oxidation is unchanged (i.e. reaction at the surface is rate-controlling). However, as the oxide film continues to grow in thickness, counter-diffusion of Ti to the gas-oxide interface occurs as the solubility limit of titanium in silica is surpassed. Crystalline clumps of TiO_2 are formed at that interface (1). As before, a virtually inpenetrable layer of amorphous SiO_2 forms, slowing further diffusion and hence the oxidation rate. This phenomenon is represented schematically in Figure 3.

However, as diffusion increases with temperature, it can be expected that the amount of material gained through oxidation will continue to grow as temperature increases. Schwettman et al (1) observed parabolic kinetics at temperatures of 1000°C and above, as shown in Figure 4 (1).

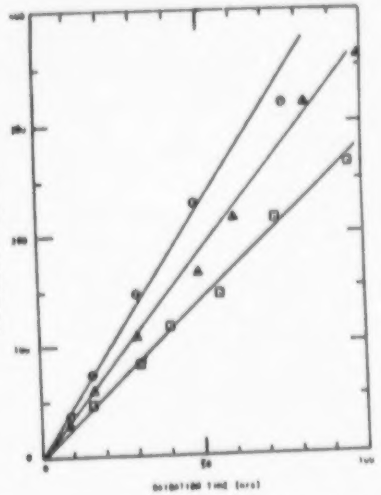

FIG. 4. Rate Data for $TiSi_2$ Oxidized at 1000°C

Experimental

Iron powder (J.T. Baker Chemical Co., 97.9%), aluminum powder (BDH Chemicals, 99.9%), and copper powder (BDH Chemicals, 99.9%) were used as the added impurities to $TiSi_2$ (Alfa Products, 95%). These elements were added separately in concentrations varying from 0 wt.% to 10 wt.% and mixed in a rolling mill. Binder (H_2O) was added and 1.25 in. diameter wafers were pressed in a hardened steel die at 4-6 tsi. Sample thickness was typically

0.5 in. The binder was removed by heating samples for several hours at 100°C.

Wafers were placed on an alumina dish in a graphite crucible containing zirconium chips as an oxygen getter during sintering, carried out in an argon atmosphere. The extremely thin layer of oxide which formed on the faces of the wafers during sintering was removed by grinding successively on carbide paper of 120, 240, 320, 400, and 600 grit coarseness. Final preparation of the wafers involved polishing with 5 μm diamond paste.

Oxidation of the wafers was carried out in a high-temperature furnace with a PID controller. The oxidizing atmosphere for all oxidations was air (p_{O_2} = 0.21 atm.). Samples were placed on a porous alumina brick in the middle of the furnace.

Oxidation data were obtained by measuring the gain of mass of the samples on a Mettler AE50 analytical balance. Some samples were analyzed by thin film diffractometry using a high-intensity x-ray diffractometer to determine the nature of the oxide product. Oxidized samples were gold-coated using a Varian VE-10 vacuum evaporator in preparation for qualitative analysis by scanning electron microscopy (SEM) and energy dispersive spectroscopy (EDS). A JEOL JSM-840 was used for the SEM work. EDS was performed with a Tracor Northern X-ray tube (TN5550-10) in conjunction with a Tracor Northern X-ray analyzer (TN5500) and Flextran software package.

Results and Discussion

Sintering of Powder Compacts

The theoretical density of $TiSi_2$ as determined by x-ray diffraction is 4.13 g/cm^3 (11). Powder compacts containing pure $TiSi_2$ could be densified to 93-97 % of the theoretical value by heating at 1420°C for 20 minutes. The surface of a polished and lightly etched sintered sample is shown in the optical micrograph of Figure 5. It can be seen that pores are for the most part concentrated at the triple points of the grains. A second phase occurring in small amounts, again mostly along grain boundaries, is most likely free silicon. Average grain size is approximately 20 μm.

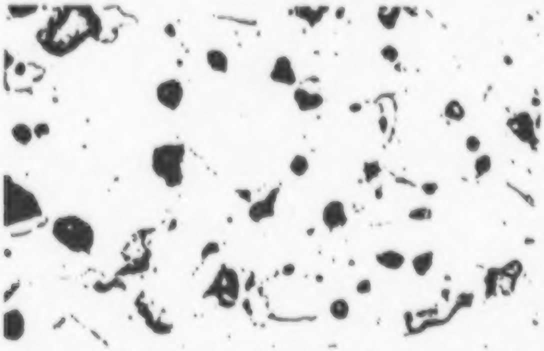

FIG. 5. Optical Micrograph of Surface of Sintered $TiSi_2$ (500x)

Powder compacts of $TiSi_2$ containing varying amounts of iron could be densified at 1420°C for 20 minutes to provide samples containing surface porosity of at most 10 percent. There was little variation in porosity among samples with different levels of iron as an impurity. However, the pores that formed in samples containing iron were several times larger than those found in a sample of pure $TiSi_2$, as shown in the optical micrograph of Figure 6. It is apparent that at least one other phase forms and diffuses along the grain boundaries, separating grains of pure $TiSi_2$, and that the majority of pores are formed in this second phase. When this sample was investigated under SEM, it was found that there were in fact three phases formed (see Figure 7). The chemical analysis of these phases as determined by EDS can be found in Table 1. It is at present unknown whether all phases exist at high temperatures. Average size of $TiSi_2$ grains in a sample containing 10 wt.% Fe is about 40 μm.

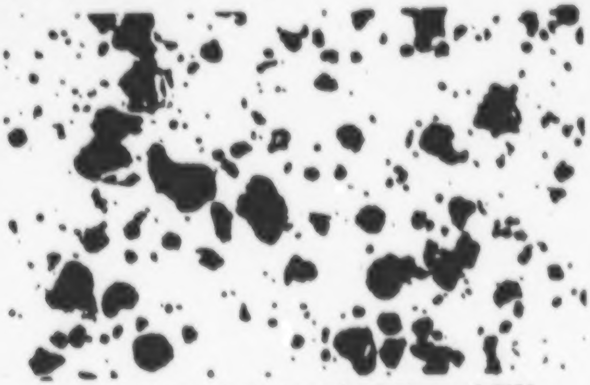

FIG. 6. Optical Micrograph of Sintered $TiSi_2$ with 10 wt.% Fe (100x)

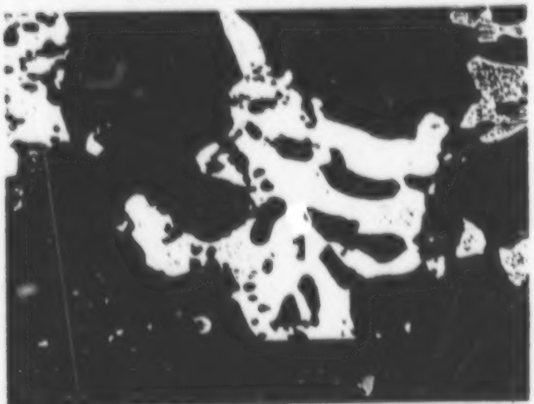

FIG. 7. Backscattered Image of Sintered $TiSi_2$ with 10 wt.% Fe

Due to the low melting point of aluminum, sintering of powder compacts of $TiSi_2$ containing aluminum could not be achieved above 1300°C without deformation of the samples. Longer sintering times of up to 4 hours were required to obtain a densified product. These samples showed a slight increase in porosity with the addition of Al, up to a maximum of about 16 percent. As was observed in the case of iron, pores in these samples were larger than in pure samples. It is again apparent, as seen in the scanning

TABLE 1
Chemical analysis of phases present
in sample of Figure 7

Phase no.	EDS analysis	standard deviation
1	28.29 at.% Ti	3.27
	41.27 at.% Si	2.71
	30.44 at.% Fe	0.99
2	42.75 at.% Ti	2.96
	50.94 at.% Si	1.84
	6.31 at.% Fe	0.52
3	38.57 at.% Ti	5.07
	61.30 at.% Si	4.94
	0.13 at.% Fe	0.11

electron micrograph of Figure 8, that a separate phase forms and diffuses along the grain boundaries to eventually separate the grains of $TiSi_2$, and that most pores are formed in this second phase. Although it could be determined that this phase was high in aluminum content (see Table 2), it was not possible to get a consistent analysis by EDS. It was observed, however, that this phase was much softer than that containing little or no aluminum, resulting in an uneven surface due to accelerated wear of the phase during polishing. Average size of $TiSi_2$ grains in a sample containing 10 wt.% Al is about 40 µm.

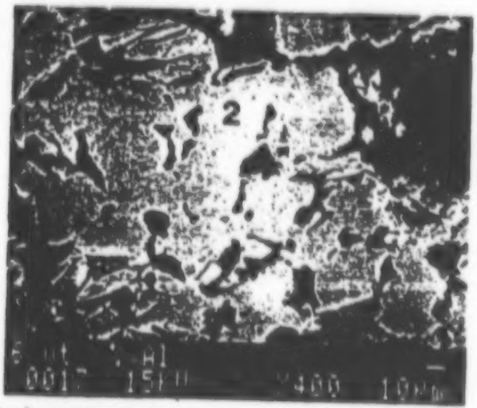

FIG. 8. Backscattered Image of Sintered $TiSi_2$ with 6 wt.% Al

TABLE 2
Chemical analysis of phases present
in sample of Figure 8

Phase no.	EDS analysis	standard deviation
1	20.12 at.% Ti	10.22
	40.25 at.% Si	11.78
	39.63 at.% Al	11.54
2	45.84 at.% Ti	2.75
	52.82 at.% Si	1.98
	1.34 at.% Al	0.63

Powder compacts of $TiSi_2$ containing varying amounts of copper could be densified at 1350°C for 60 minutes to provide samples with no deformation and surface porosity of at most 8 percent. Pores in these samples were again larger than in pure samples, as seen in the scanning electron micrograph of Figure 9. Some samples high in copper content contained a few larger, spherical pores. The bright phase of the micrograph of Figure 9 has formed and diffused along grain boundaries of $TiSi_2$ and contains most of the pores, suggesting that this phase may have been in a liquid state at the sintering temperature. The chemical analysis of these phases as determined by EDS can be found in Table 3. It is apparent that the bright phase is composed almost entirely of copper, with some dissolved silicon. The presence of dissolved silicon in the phase suggests that some $TiSi_2$ dissociates during sintering to a lower silicide and free silicon. This is supported by the chemical analysis of the dark phase, which indicates less silicon than that which would correspond stoichiometrically to pure $TiSi_2$. Average size of $TiSi_2$ grains in a sample containing 10 wt.% Cu is approximately 50 µm.

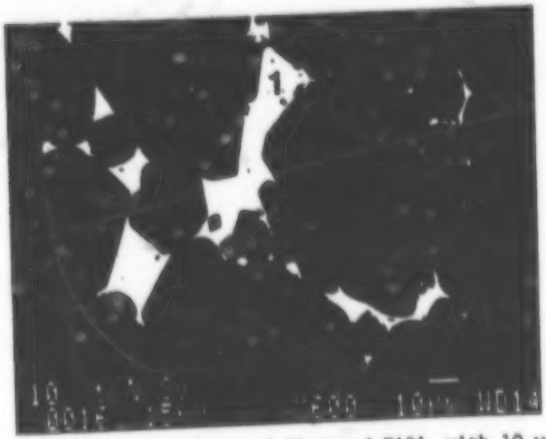

FIG. 9. Backscattered Image of Sintered $TiSi_2$ with 10 wt.% Cu

TABLE 3
Chemical analysis of phases present
in sample of Figure 9

Phase no.	EDS analysis	standard deviation
1	0.99 at.% Ti	0.83
	17.09 at.% Si	3.19
	81.92 at.% Cu	3.46
2	45.37 at.% Ti	2.59
	54.63 at.% Si	2.11
	0.12 at.% Cu	0.38

Oxidation of Pure $TiSi_2$

A scanning electron micrograph of the surface of a wafer of pure $TiSi_2$ oxidized for 260 hours at 1200°C is shown in Figure 10. It can be seen that a thin but uniform protective oxide layer forms on the surface of the

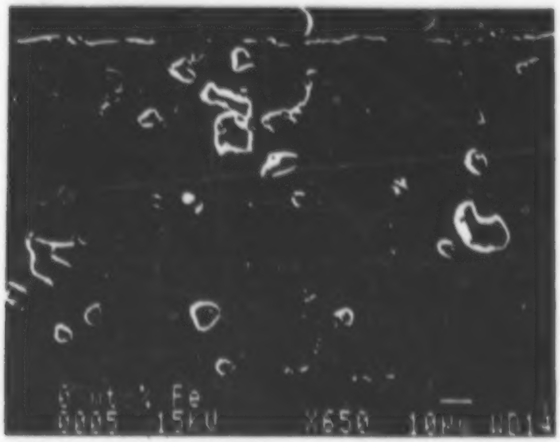

FIG. 10. SEM Micrograph of $TiSi_2$ Oxidized for 260 h at 1200°C

sample. EDS analysis of this film indicated that this oxide contains up to 95 at.% silicon, most likely in the form of silica, with a small amount of titanium in the form of titania or elemental Ti. If a stoichiometric reaction occured during oxidation, the oxide should contain twice as many Si atoms as Ti atoms. The phase diagram for the SiO_2-TiO_2 system (12) indicates a solid solubility of about 10 wt.% TiO_2 in SiO_2 between the temperatures of 300 and 1500°C. It is possible that at oxidation temperatures, the oxide film contains the solid solubility limit of TiO_2 in SiO_2, with the remaining titanium having reacted to form a lower silicide:

$$6\ TiSi_2 + 10\ O_2 \longrightarrow TiO_2 + 9\ SiO_2 + Ti_5Si_3 \qquad (R2)$$

$$2\ TiSi_2 + 4\ O_2 \longrightarrow TiO_2 + 3\ SiO_2 + TiSi \qquad (R3)$$

It is also possible that some Ti atoms counter-diffuse through the oxide to the gas-oxide interface as the solubility limit in silica is surpassed. This is supported by the presence of crystals on the surface of the sample, analyzed by EDS to contain about 98 at.% Ti, undoubtebly in the form of titania. The presence of crystalline titania on the surface of these samples was also confirmed by x-ray diffraction. While the kinetics of the oxidation of pure $TiSi_2$ will be discussed in the next section, it is very important to mention here one very important feature of these oxidized samples. As seen in Figure 11, the presence of surface pits does not prohibit the formation of a uniform glassy phase. Thus, initial weight gains of a porous sample may be high due to a relatively high surface area in comparison to a pore-free sample. These pits may initially act as a nucleation site resulting in rapid localized diffusion. However, once the oxide film grows to a point where the rate becomes diffusion controlled, the effect of these surface pits will be minimized.

Oxidation of $TiSi_2$ with an Iron Impurity

Typical weight gain data for the oxidation at 1200°C of pure $TiSi_2$ and with varying iron additions are shown in Figures 12 and 13. When the square of weight gain is plotted against time, straight lines are obtained, as shown in Figures 14 and 15. Some general comments can be made at this point. While some samples may have experienced very large weight gains in

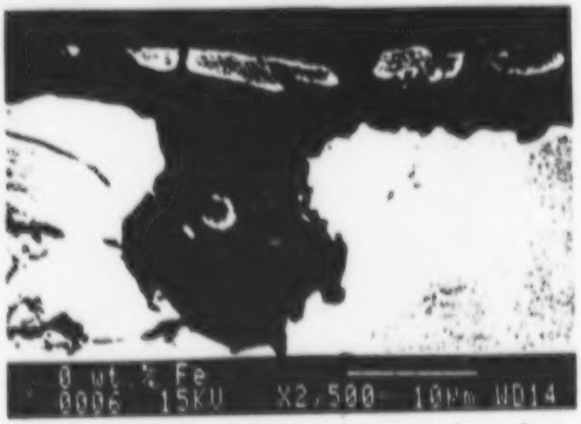

FIG. 11. Formation of Protective Oxide Layer Over Surface Pit of $TiSi_2$ Oxidized at 1200°C

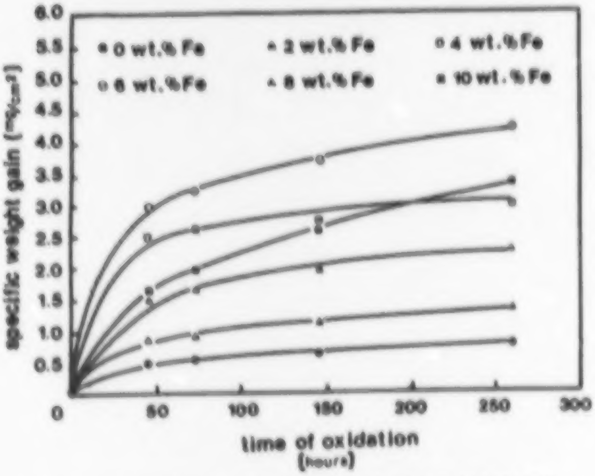

FIG. 12. Effect of Time on Oxidation Resistance of $TiSi_2$ with an Iron Impurity (1200°C)

the first 50 hours, subsequent gains are often relatively low, such that parabolic rate constants (the slope of the lines in Figures 14 and 15) have a low value compared to some samples experiencing lower initial weight gains. This suggests that, like samples of pure $TiSi_2$, surface porosity can lead to high initial rates of oxidation, but this does not hinder the formation of a uniform barrier of silica that minimizes the effect of initial surface defects and leads to slower rates of oxidation. This is the point at which the rate in these localized areas changes from surface-controlled to diffusion-controlled. To determine the final rate at which samples can be expected to oxidize, parabolic rate constants were determined by least squares regression, and the effect of iron additions on the rate constant at 1200°C is shown in Figure 16.

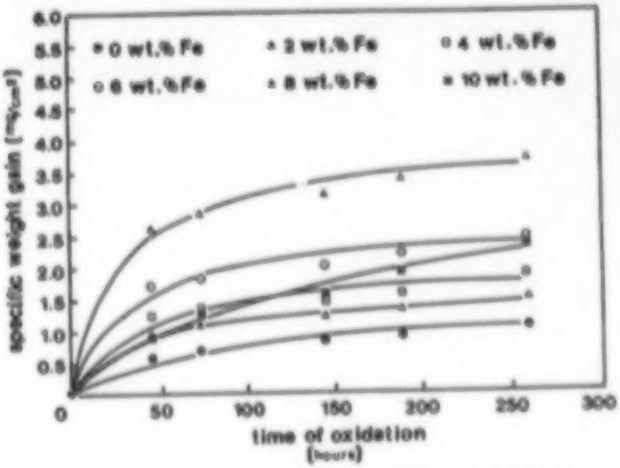

FIG. 13. Effect of Time on Oxidation Resistance of $TiSi_2$ with an Iron Impurity (1200°C)

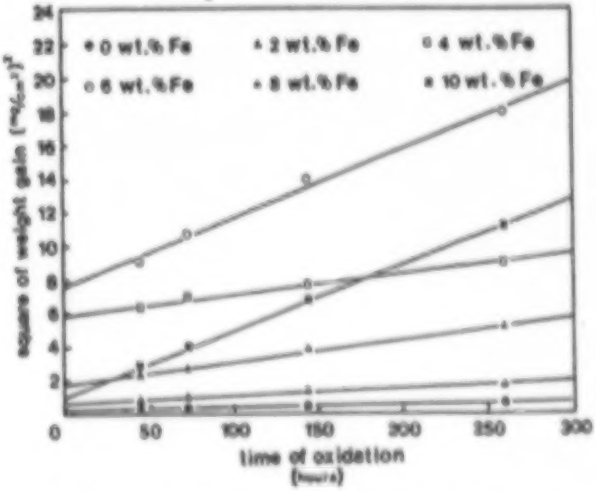

FIG. 14. Effect of Time on Square of Weight Gain Using Data of Fig. 12

Weight gain data for oxidation at 1300°C, shown in Figure 17, was very similar to that obtained at 1200°C except that parabolic rate constants, again determined from the plot of the square of weight gain versus time (see Figure 18), were slightly higher at 1300°C. This can be attributed to the higher rates of oxygen diffusion through the silica layer that can be expected at higher temperatures. The effect of iron additions on the rate constant at 1300°C is shown in Figure 19.

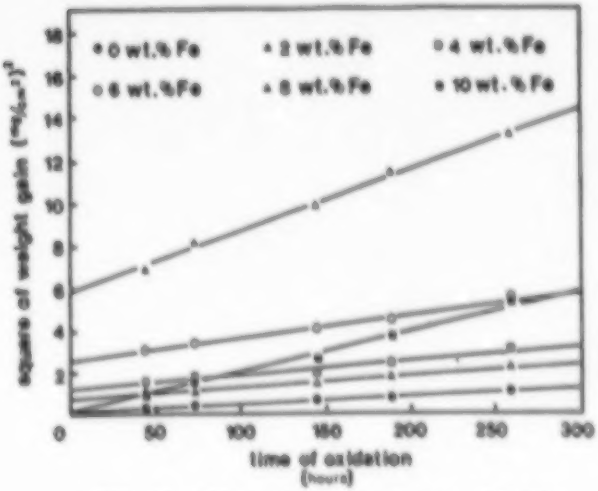

FIG. 15. Effect of Time on Square of Weight Gain Using Data of Fig. 13

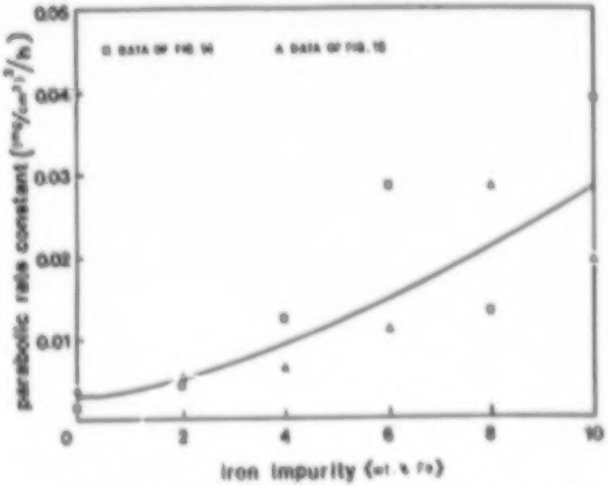

FIG. 16. Effect of Iron Additions on Parabolic Rate Constant (1200°C)

A scanning electron micrograph of a cross-section of a wafer of $TiSi_2$ containing 10 wt.% Fe oxidized for 260 hours at 1200°C is shown in Figure 20. It can immediately be seen that the oxide layer formed is similar to that formed on a sample of pure $TiSi_2$ except in its uniformity. It is apparent that localized oxidation occurs at a higher rate, such that the oxide penetrates the sample surface more in some areas than others. The boxed area of Figure 20 is shown magnified several times in Figure 21.

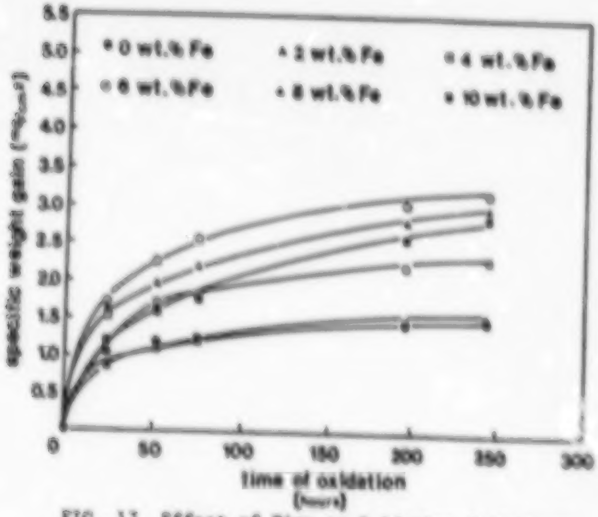

FIG. 17. Effect of Time on Oxidation Resistance of $TiSi_2$ with an Iron Impurity (1300°C)

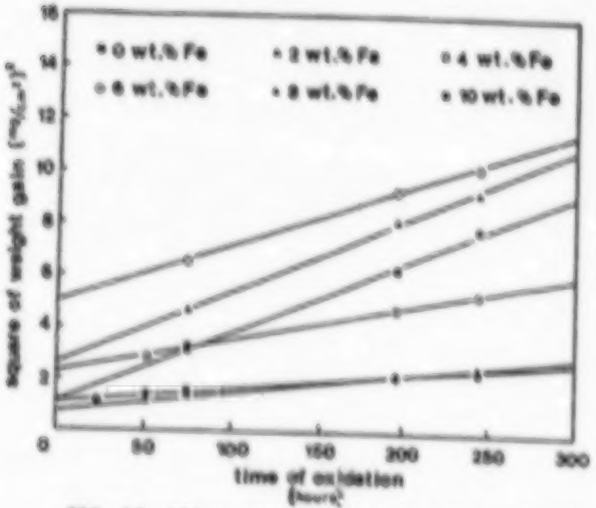

FIG. 18. Effect of Time on Square of Weight Gain Using Data of Fig. 17

Preferrential oxidation of the lighter phase can be explained in terms of its chemical composition as tabulated earlier. Searcy (13) recognized that in order to have a consistent, protective silica coating, it is necessary that metal silicides have a silicon-to-metal atomic ratio of 3:2 or higher. In the preferrentially oxidized phase here, the silicon-to-metal ratio is only 2:3. If this phase cannot in fact provide sufficient silica upon oxidation to form a protective layer, it might be expected that more

---

titanium oxid
oxides, than
concentrated
formed in the
98-100% Ti ato
of such oxidi
crystals with
crystals can

Further
chemical analy
containing lig

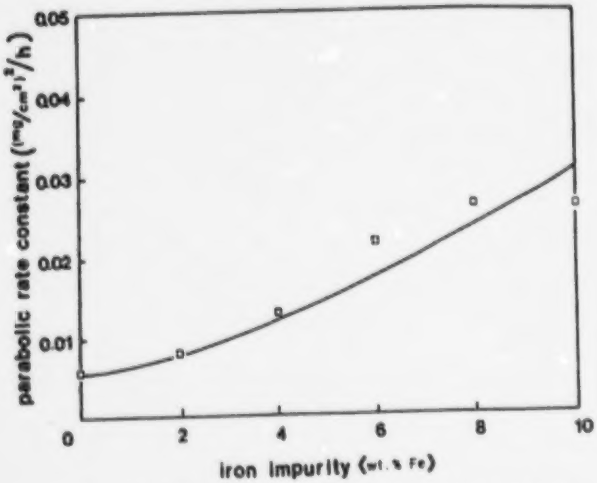

FIG. 19. Effect of Iron Additions on Parabolic Rate Constant (1300°C)

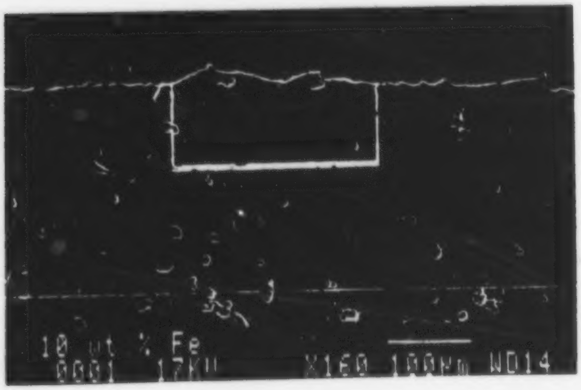

FIG. 20. SEM Micrograph of $TiSi_2$ with 10 wt.% Fe Oxidized for 260 hours at 1200°C

titanium oxides might be produced, since they are more stable than iron oxides, than in a sample containing no iron. The large pieces of material concentrated on the surface of the oxide layer, immediately above the pits formed in the phase deficient in silicon, have been found by EDS to contain 98-100% Ti atoms, most likely in the form of titania crystals. The surface of such oxidized samples visibly contain an increasing amount of titania crystals with increasing iron content. An SEM micrograph of such surface crystals can be found in Figure 22.

Further evidence of this phenomenon was found through an investigative chemical analysis of the bulk oxide. The oxide formed above the dark phase containing high amounts of Si was found to contain only 6 at.% Ti atoms, the

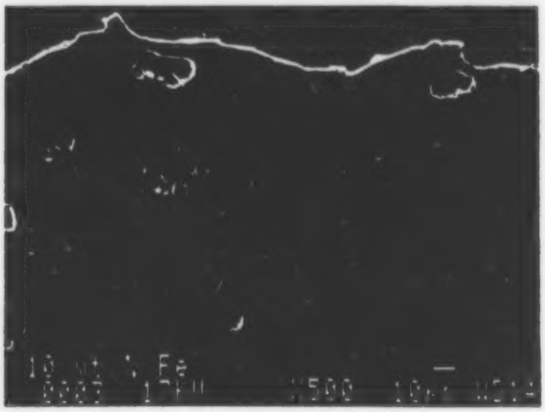

FIG. 21. SEM Micrograph Showing Magnification of Boxed Area of Figure 20

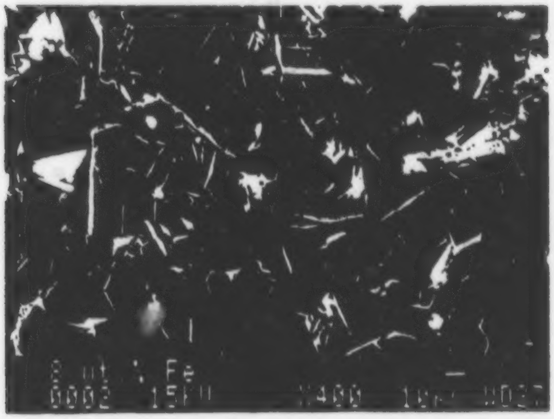

FIG. 22. SEM Micrograph of Surface Crystals Grown on Surface of Oxidized $TiSi_2$ Containing 8 wt.% Fe

remainder being Si atoms. However, the oxide formed above the phase low in Si and high in Fe and Ti atoms was found to contain 22 at.% Ti atoms, the remainder again being Si atoms. Furthermore, the oxide formed within the pits of this same phase contained about 40 at.% Ti and 60 at.% Si atoms. This represents the same atomic ratio of Si:Ti as the bulk phase from which the oxide formed. This oxide phase thus provides little protection to the bulk phase, so that all the Ti atoms are oxidized along with those of Si resulting in rapid localized oxidation.

It can be seen in the micrograph of Figure 23 that the oxide formed upon preferrential attack of this phase also contains a large number of crystals that seem to be migrating toward the surface of the sample. These were found to be very high in titanium. It is possible that these have precipitated as Ti crystals once the saturation limit in silica is

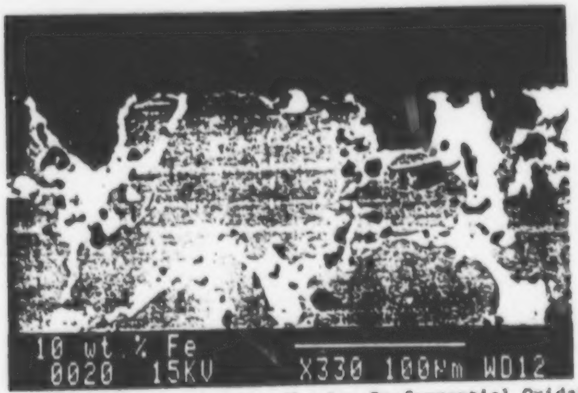

FIG. 23. Backscattered Image Showing Preferrential Oxidation of One Phase in TiSi$_2$ Containing 10 wt.% Fe

surpassed, or that they are crystals of titania that precipitate once the saturation limit of TiO$_2$ in SiO$_2$ is surpassed. A higher rate of oxidation in these localized areas might be expected due to faster oxygen diffusion along the surface of these crystals, as proposed in an earlier paper by Schlichting (14), or by some modification of the protective properties of the silica layer by the high level of impurity.

An x-ray map for iron in an oxidized sample containing 10 wt.% Fe is shown, along with the corresponding micrograph, in Figure 24. The presence of iron in surface crystals indicates that counter-diffusion of iron through the oxide layer must occur during oxidation at high temperatures. Chemical analysis showed an absence of Si atoms and a Ti:Fe atomic ratio of approximately 2:1, indicating that pseudobrookite or crichtonite may form.

After an extended period of oxidation, preferrential attack of the phase low in silicon eventually results in the depletion of Si and Ti, leaving grains high in iron, which could oxidize. This is accompanied by the separation of many TiSi$_2$ grains initially connected by the preferentially oxidized phase. While this indicates a loss of the material's strength, it also aids in holding the oxide layer together so that spalling, the flaking of the oxide resulting in rapid transport of oxygen, does not occur during thermal cycling.

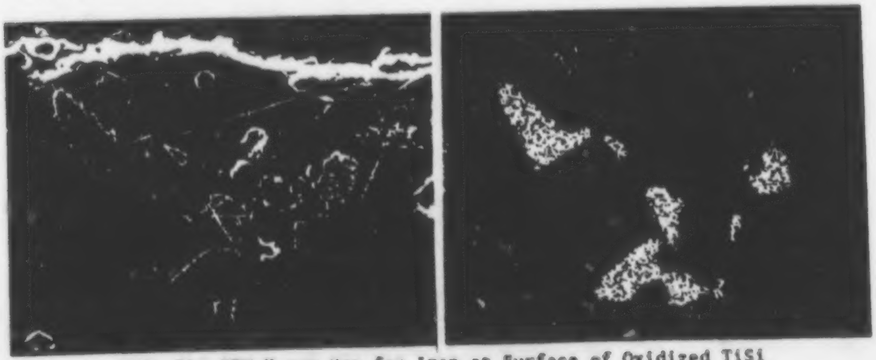

FIG. 24. SEM X-ray Map for Iron at Surface of Oxidized TiSi$_2$ Containing 10 wt.% Fe (850 x)

Oxidation of $TiSi_2$ with an Aluminum Impurity

Typical weight gain data for the oxidation at 1200°C of pure $TiSi_2$ and varying aluminum additions are shown in Figure 25. When the square of weight gain is plotted against time, straight lines are again obtained, as shown in Figure 26. Once more, surface porosity is likely responsible for high initial rates of oxidation in localized areas. Oxidation of samples containing aluminum required approximately twice as long as samples containing iron to exhibit parabolic kinetics.

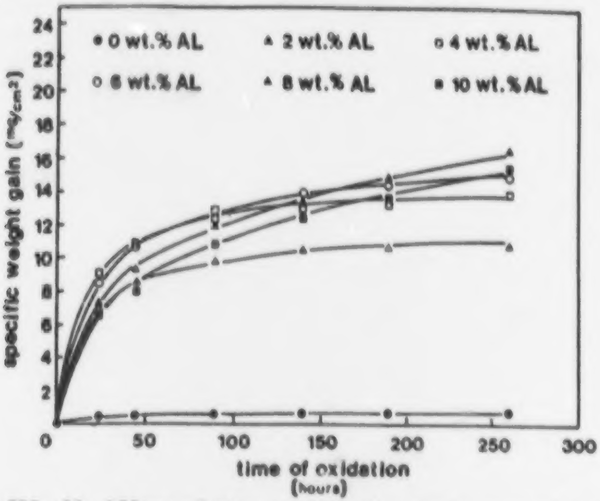

FIG. 25. Effect of Time on Oxidation Resistance of $TiSi_2$ with an Aluminum Impurity (1200°C)

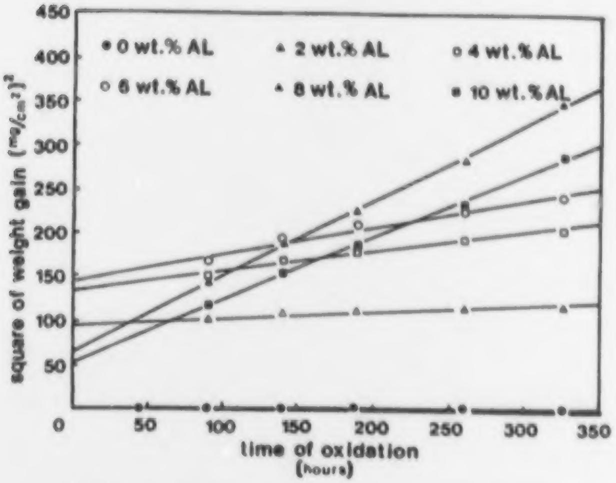

FIG. 26. Effect of Time on Square of Weight Gain Using Data of Fig. 25

Parabolic rate constants are plotted as a function of aluminum content of the samples in Figure 27. It is apparent that even small additions of Al result in a drastic reduction in oxidation resistance. Samples high in aluminum content showed no useful resistance to oxidation at this temperature, and oxidation of such samples resulted in a complete loss of strength after only two hundred hours.

A scanning electron micrograph of a cross-section of a wafer of $TiSi_2$ containing 10 wt.% Al oxidized for over 300 hours at 1200°C is shown in Figure 28. The oxide layer formed on samples containing aluminum was not uniform or thick enough to provide much protection of the substrate. In contrast, the phase high in aluminum appeared to have been almost complete-

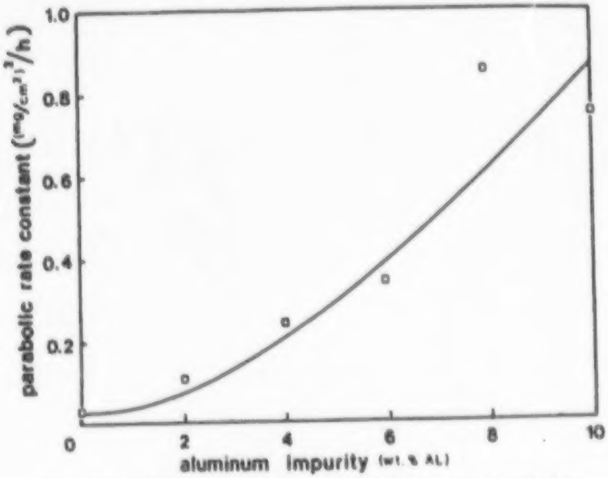

FIG. 27. Effect of Aluminum Additions on Parabolic Rate Constant (1200°C)

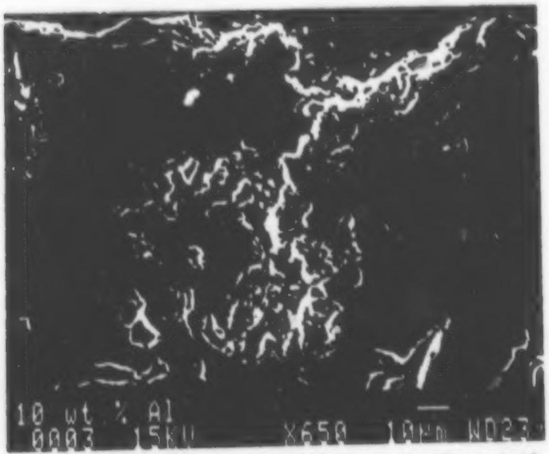

FIG. 28. SEM Micrograph of $TiSi_2$ with 10 wt.% Al Oxidized for 300 hours at 1200°C

ly oxidized preferentially, accounting for the material's drastic reduction in strength. This preferential oxidation can be attributed to two factors. First, the silicon-to-metal atomic ratio is only 2:3 and, as discussed earlier, such a phase cannot provide sufficient silica upon oxidation to form a protective layer. It is even possible that this phase is in a liquid state, which would oxidize faster than the solid, at the oxidation temperature. Second, because aluminum oxide is thermodynamically slightly more stable than silicon or titanium oxides, it could be expected that the aluminum in the phase will oxidize and join any silica-titania glass, possibly forming aluminum silicates that may result in a marked reduction in viscosity. The chemical composition of the oxidized phase was very close to that of the bulk phase deficient in Si, again suggesting that this phase is completely oxidized preferentially to the phase deficient in aluminum. Eventual separation of grains of pure $TiSi_2$ due to intergranular oxidation can be expected.

Oxidation of $TiSi_2$ with a Copper Impurity

The high-temperature oxidation of $TiSi_2$ with a copper addition proceeds without resistance due to the formation of a low-viscosity liquid phase, resulting in extremely high weight gains even after only 24 hours. This has been observed at temperatures as low as 1000°C. At 1200°C, this liquid oxide or copper silicate has a low enough viscosity that it can flow off the sample.

A scanning electron micrograph of a cross-section of a wafer of $TiSi_2$ containing 10 wt.% Cu oxidized for 24 hours at 1200°C can be found in Figure 29. It shows the collection of the oxide in a liquid droplet on the surface of the sample, and the absence of the oxide on the underside from which it was able to flow off during oxidation. A magnified portion of the "droplet" of Figure 29 can be found in the micrograph of Figure 30. It can be seen that there are several different products formed, some of which appear to have precipitated during sample cooling. The dark area directly above the substrate surface was analyzed by EDS to contain about 95 at.% Si, 2 at.% Ti, and 3 at.% Cu. These species are all likely in oxide form. The large grey crystals were analyzed by EDS to contain 99 at.% Ti. It is reasonable to expect that these are crystals of titania.

In addition to these features similar to those observed in pure samples and those containing iron, there are the large white crystals and smaller, whisker-like features assumed to have precipitated during sample cooling. EDS analysis of the large white crystals showed a composition of 98 at.% Cu

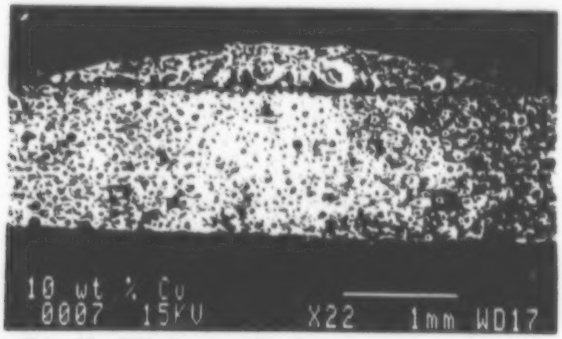

FIG. 29. SEM Micrograph of $TiSi_2$ with 10 wt.% Cu Oxidized for 24 hours at 1200°C

---

and 2 at.
colour, i
grew from

78 at.% Cu
It i
form befo
copper (o
tures. C
glass, fo
silicates

an 8% Cu_2
and above
layer pro

The

attribute
that tenc

rate cons
$\left(mg/cm^2\right)^2$

Tita
1420°C fo
%. Such
parabolic
x 10^{-2}

Iron add
with all

about 2

The decr
to the
sufficie
in more

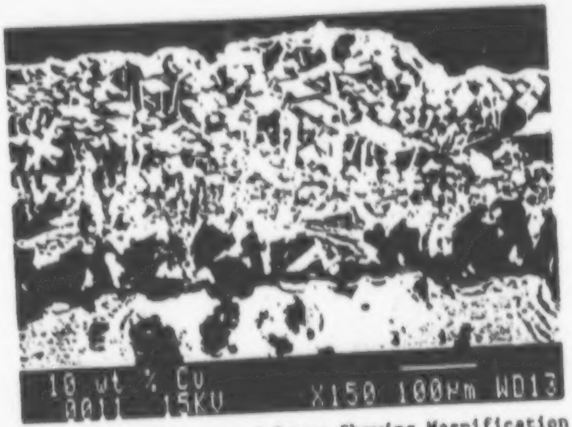

FIG. 30. Backscattered Image Showing Magnification of Oxide Features of Figure 29

and 2 at.% Si. Since the surface of the oxidized sample was black in colour, it can be expected that these crystals are CuO, which presumably grew from those of Cu_2O during cooling. The whisker-like features contain 78 at.% Cu and 22 at.% Ti.

It is apparent that, since copper oxides thermodynamically should not form before silicon or titanium oxides, the bulk phase that is rich in copper (over 80 at.%) cannot be protected from oxidation at high temperatures. Copper is oxidized in localized areas and joins the silica-titania glass, forming a low-viscosity modified silica network or possibly copper silicates of low viscosity. The phase diagram for Cu_2O-SiO_2 (15) indicates an 8% Cu_2O eutectic at 1060°C. In either case, the layer formed at 1000°C and above is not protective in nature, and diffusion of oxygen through the layer proceeds at a very high rate.

Conclusions

The oxidation resistance of pure $TiSi_2$ at high temperatures can be attributed to the formation of a uniform, protective silica-titania glass that tends to minimize the effect of initial surface defects. Parabolic rate constants are typically $2.4 \times 10^{-3} \left(mg/cm^2\right)^2/h$ at 1200°C and $4 \times 10^{-3} \left(mg/cm^2\right)^2/h$ at 1300°C.

Titanium disilicide containing up to 10 wt.% iron can be sintered at 1420°C for 20 minutes to provide samples with maximum surface porosity of 10 %. Such samples show a slight decrease in oxidation resistance, with parabolic rate constants increasing with iron content to a value of about $3 \times 10^{-2} \left(mg/cm^2\right)^2/h$ for a sample containing 10 wt.% Fe oxidized at 1200°C. Iron additions have the identical effect on oxidation resistance at 1300°C, with all samples experiencing an increase in the parabolic rate constant of about $2 \times 10^{-3} \left(mg/cm^2\right)^2/h$ over corresponding samples oxidized at 1200°C. The decrease in oxidation resistance with the addition of iron is attributed to the presence of a phase low in silicon content which cannot provide sufficient silica upon oxidation to provide a protective film. This results in more rapid localized oxidation, eventually leading to the separation of

$TiSi_2$ grains.

Titanium disilicide containing up to 10 wt.% aluminum can be sintered at a maximum temperature of 1300°C for 4 hours to provide samples with maximum surface porosity of 16 %. Such samples show a dramatic decrease in oxidation resistance, with parabolic rate constants increasing with aluminum content to a value of about $8 \times 10^{-1} \left(^{mg}/_{cm^2}\right)^2/h$ for a sample containing 10 wt.% Al oxidized at 1200°C. The decrease in oxidation resistance is again attributed in part to the presence of a phase of low Si:Me atomic ratio. In addition, the aluminum oxide is believed to act as a network modifier in the silica glass, reducing its protective properties considerably. This results in the complete preferrential oxidation of the phase high in Al and low in Si that separates grains of $TiSi_2$. This intergranular oxidation leads to a drastic reduction in the strength of the material.

Titanium disilicide containing up to 10 wt.% copper can be sintered at a maximum temperature of 1350°C for 60 minutes to provide samples with maximum surface porosity of 8 %. Such samples show no useful resistance to oxidation at temperatures as low as 1000°C due to the formation of a liquid oxidation product upon localized oxidation of one phase very high in copper content but very low in silicon content.

References

1. Schwettman, F.N., R.A. Graff, and M. Kolodney, *Journal of the Electrochemical Society*, 118 [12], 1973 (1971).
2. Wirkus, C.D., and D.R. Wilder, *Journal of The American Ceramic Society*, 49 [4], 173 (1966).
3. Berkowitz-Mattuck, J.B., P.E. Blackburn, and E.J. Felten, *Transactions of the Metallurgical Society of AIME*, 233, 1093 (1965).
4. Valyi, G., L. Zhaokang, A. Steffen, M. Maier, and P. Balk, *Thin Solid Films*, 116 [4], 383 (1984).
5. Yang, W.Y., H. Iwakuro, H. Yagi, T. Kuroda, and S. Nakamura, *Japanese Journal of Applied Physics*, 23 [12], 1560 (1984).
6. Lavendel, H.W., and A.G. Elliot, *Transactions of the Metallurgical Society of AIME*, 239, 143 (1967).
7. d'Heurle, F., E.A. Irene, and C.Y. Ting, *Applied Physics, Letters*, 42 [4], 361 (1983).
8. Stone, H.E.N., *Journal of Materials Science, Letters*, 2, 609 (1980).
9. Chen, J.R., M.P. Houng, S.K. Hsiung, and Y.C. Liu, *Applied Physics, Letters*, 37 [9], 824 (1980).
10. Baas, H., C.A. Pickles, and J.M. Toguri, "Recovery of Titanium Silicide Crystals from a Copper Melt", to be published.
11. Samsanov, G.V., "Silicides and Their Uses in Engineering", Translation from Russian FTD-TT-62 430 1&2 (1962).
12. Ricker, W., and F.A. Hummel, *Journal of The American Ceramic Society*, 34 [9], 271 (1951).
13. Searcy, A.W., *Journal of The American Ceramic Society*, 40 [12], 431 (1957).
14. Schlichting, J., *Ceramurgia International*, 4 [4], 162 (1978).
15. Berezhnoi, A.S., L.I. Karyakin, and I.F. Dudavskii, *Doklady Akad. Nauk S.S.S.R.*, 83 [3], 401 (1952).

Acknowledgements

This work was funded by the Department of Energy, Mines and Resources (Canada) through DSS Contract No. 55SS.23440-7-9161.